THE CHARACTERISATION OF CARBON FIBRE SURFACES BY ELECTROCHEMICAL METHODS

A Thesis

presented for the degree of

Master of Science

in the Faculty of Science of the

University of St Andrews

TO MY PARENTS

DECLARATION

I declare that this thesis is my own composition, that the work of which it is a record has been carried out by me, and that it has not been submitted in any previous application for a Higher Degree.

This thesis describes the results of research carried out in the Department of Chemistry, under the supervision of Dr C A Vincent since the 1st of October 1984.

October 1988 Colin J M Stewart

CERTIFICATE

I hereby certify that Colin J M Stewart, BSc, has spent eleven terms of research work under my supervision, has fulfilled the conditions of the Resolution of the University Court, 1974 No 2, and is qualified to submit the accompanying thesis in application for the Degree of Master of Science.

October 1988

C A Vincent

Director of Research

ACKNOWLEDGMENTS

I would like to thank Dr C A Vincent for his help and encouragement throughout this work, and the Science and Engineering Research Council and Ministry of Defence for a Research Studentship award.

In addition, I wish to thank Dr B A Boukamp for the use of his equivalent circuit fitting program.

Thanks are also due to Professor J R MacCallum for providing advice on certain aspects of this work.

I would finally like to thank various members of the Chemistry Department staff, particularly Mr J Bews, Mr D Wilkie and Mr J Rennie, for their technical assistance provided during the course of this research.

SUMMARY

The possibility of surface characterisation of carbon fibres by electrochemical methods is investigated. A three electrode cell set-up is used and the carbon fibre electrode/solution electrolyte interface is studied. The interface is represented as an equivalent circuit of electrical components and the variation in the nature and value of these components is investigated for various high modulus fibres.

Initial studies using non-sinusoidal techniques show that the simple equivalent circuit model, containing a solution resistance, a charge transfer resistance and a double layer capacitance, normally used for this type of cell is completely inadequate. It is not feasible to distinguish between fibres or even between different electrolyte solutions using these methods.

However, it is shown that by applying an a.c. impedance technique coupled with equivalent circuit analysis developed by Boukamp it is possible to generate a more accurate representation of the fibre/solution interface. The new circuit contains additional elements such as an interfacial inductance and a constant phase diffusional element.

By monitoring the d.c. polarisation potential dependence of these circuit components it is shown to be possible to distinguish between untreated and surface-treated fibres. However, it is not possible to distinguish between different batches of the same fibre.

It is shown that galvanic oxidation of untreated fibres can be monitored by this method. The effects of time on oxidised fibres is also investigated.

CONTENTS

CHAPTER 1

THE INTRODUCTION

1.1 The Development of Composite Science

With the technology explosion in recent years, there have been rapid advances in all spheres of science. This is particularly apparent in the field of materials science, where these technological advances have focused interest into the development of more efficient and convenient materials for engineering and other applications. These materials, such as plastics, are rapidly replacing the more traditional materials such as metals, wood and stone in all aspects of structural and mechanical engineering and construction. One group of materials which have been applied extensively is what are known as composite materials.

1.2 The Nature of Composite Materials

The definition of a composite material is one which consists of two or more physically distinct and mechanically separable components which can be mixed so that the dispersion of one material in the other can be controlled to achieve optimum properties, which are superior to that of the components taken singly. The field of composite materials is very diverse and an extensive discussion would encompass a wide range of materials, from naturally occurring solids such as bone and wood, macro-composites such as concrete and to microcomposites including metals, ceramics and polymers. Here we concentrate on the microcomposite engineering materials such as metallic alloys, toughened thermoplastics and

reinforced thermoplastics. These materials obtain their strength and toughness by amalgamating high strength phases with tough, ductile phases. For example, carbon steels when cooled slowly from 800°C, consist of alternative layers of a soft ductile phase, almost pure iron, and a brittle compound Fe_3C.

A comprehensive classification of microcomposites is based on the size, shape and distribution of the two or more phases in the composite material. This classification can be seen in Table 1.1.

Table 1.1 The Classification of Microcomposites[1]

1. Continuous fibres in the matrix (aligned, random)
2. Short fibres in the matrix (aligned, random)
3. Particulates (spheres, plates, ellipsoids, irregular, hollow or solid) in the matrix
4. Dispersion strengthened, as for 3, above, with particle size $< 10^{-8}$m.
5. Lamellar structures
6. Skeletal or interpenetrating networks
7. Multi-components, fibres, particles etc.

As can be seen, these classifications are not distinct and there will be considerable overlap in some cases.

This discussion is further limited to the particular area under study viz. fibre-reinforced composites. The advantages of such materials are based on their mechanical properties normalised to unit weight. Mechanical properties[1] such as specific strength

and specific modulus are much larger in fibre-reinforced composites than in other materials and hence the overall weight of the components can be reduced. Obviously, this is advantageous in construction, particularly types of transport, enabling a reduction in costs and an increase in efficiency with no loss of mechanical strength.

Fibre-reinforced composite materials usually consist of just two components, a fibrous material and an organic matrix. The fibres may have excellent mechanical properties but tend to be brittle, whereas the organic matrix may be either ductile or brittle but it generally has considerable resistance to chemical environments. Therefore the resultant composite has strength and stiffness similar to that of the fibre combined with the chemical resistance of the matrix. In addition, the composite material has certain synergistic features such as a degree of crack propagation resistance and an ability to absorb energy during deformation. The most common types of fibres used in composite manufacture are carbon, glass and organic fibres such as "Kevlar".

To obtain an understanding of the properties of carbon fibre-reinforced composites it is necessary to examine the individual components and in particular the nature of the interface between the fibre and the matrix.

1.2.1 Carbon Fibres

Extremely fine carbon fibres, usually about 10 μm in diameter, have superior specific strength and stiffness properties in comparison to glass and "Kevlar". However, these fibres are very brittle and tend to be anisotropic in structure and hence only have the

required mechanical properties if the stress is applied parallel to the fibre axis.

The internal structure of one of these carbon fibres may be separated into two distinct regions. Close to the fibre surface there is what is called the "sheath" region. Here is a series of highly orientated graphitic layer planes lying parallel to the fibre axis which are stacked together to form fibrils. These layers of planes are separated by a few long needle-like pores or voids, which also exhibit similar preferred orientation to the fibre axis. In addition, there is a small degree of interconnection normal to the axis. The inner region, known as the "core", contains similar fibrils, but the orientation of the layer planes is much more random and there is a higher degree of interconnection normal to the fibre axis. The voids present in this region are more numerous and tend to be irregularly shaped, unlike in the outer "sheath" region. This gives the cross section a net-like appearance whereas the outer region appears much more fibrillar.

However as far as production of the composite is concerned, the most important area of the carbon fibre is its surface. The surface of carbon fibres have a degree of surface roughness and tend to have a coverage of reactive chemical groups. These functional groups are acidic and basic oxides. The acidic surface oxides tend to be carboxyl, phenolic hydroxyl and carbonyl groups whereas the basic oxides are thought to be chromene-type structures. Both the degree of surface roughness and concentration and nature of the surface groups, which are highly dependent on the fibre processing, are considered to play an important role in the formation and properties of the fibre-matrix interface. However, it is

disputed which is the more important. The surface roughness of the fibre may provide sites for physical interlocking between the fibre and the organic matrix whereas the functional groups may form chemical bonds and interactions with surface groups present on the matrix.

1.2.2 The Organic Matrix

The organic matrix must combine acceptable processing characteristics with good chemical, physical and mechanical properties. There are two types of organic matrix used in carbon fibre-reinforced composite manufacture i.e. thermosetting resins and thermoplastics.

Thermosetting Resins

The two most common thermosetting resins used are epoxy- and polyester-based polymers.

The uncured liquid polymer is converted into hard, brittle solids by chemical cross-linking which generates the formation of tightly bound three-dimensional network of polymer chains. The final mechanical properties are dependent on the molecular components comprising the network and on the density and length of the cross-links. These resins are usually isotropic. Epoxy resins have superior mechanical properties and a lower coefficient of thermal expansion and hence tend to be used in preference to polyester resins. A typical epoxy resin used in composite manufacture can be seen in Fig. 1.1.

Fig. 1.1[2]

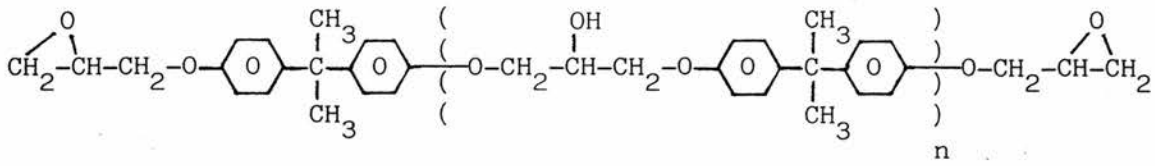

The structural formula of 828-resin (diglycidyl ester of bisphenol A).

Thermosetting resins offer the high modulus and strength of the cured polymer combined with the low molecular weight and easy handling characteristics of the uncured components. The cured resins, due to the high degree of cross-linking and polarity behave as glasses and are therefore brittle under stress. In addition, they generally have high heat ageing stability.

Thermoplastics

In contrast to the thermosetting resins, thermoplastics are not cross-linked. The stiffness and strength of the matrix, in this case, comes from the intrinsic properties of the monomer and the material's very high molecular weight. In amorphous thermo-plastics this guarantees that there is a high degree of molecular entanglements, which act as effective cross-links, whereas in crystalline materials there is a high proportion of molecular order and alignment.

All these thermoplastics yield and undergo large deformations before final fracture and their mechanical properties are highly dependent on the temperature and the applied strain rate. In addition, all thermoplastics under constant loading show increased strain with time i.e. the matrix "creeps" under load. This is important, since

during composite deformation there will be load redistribution between the resin and the fibre.

Thermoplastics are usually used with short fibre reinforcement for applications in materials manufactured by injection moulding.

1.2.3 Fibre-Matrix Interface

The structure of the fibre-matrix interface plays a major role in the properties, both physical and mechanical, of the subsequent composite. In particular, the major disparity between the elastic properties of the fibre and the matrix have to be passed through the interface i.e. stresses acting on the matrix must be transferred to the fibre. Transmission of stress between the matrix and fibre is reliant on a strong interfacial bond. Therefore, the degree of contact and the cohesive forces at the interface are of considerable importance. Intrinsic tangential stresses produced by thermal effects are present at the interface and are therefore an important factor in bond strength.

The interface must be able to withstand mechanical and thermal deformation in an approximately reversible manner. Therefore, it must combine acceptable strength characteristics with the ability to absorb mechanical energy. Due to unavoidable variation of certain properties, such as the coefficient of thermal expansion, moduli and Poisson ratio, of the two components tangential stresses are present at the interface which can generate de-wetting and/or crack formation. These interfacial defects will reduce the strength of the composite since they act as stress concentrators.

The nature of the interfacial bonding is dependent on the

atomic arrangement and chemical properties of the fibre and on the molecular conformation and chemical constitution of the polymer matrix. Therefore each interface is specific to a particular fibre-matrix system.

Herrick[3] first proposed that the bond between the fibre and matrix was both physical and chemical in nature. This proposal has been supported by various authors[4-8]. Drzal[4] stated that the number and types of each form of bonding strongly influence the interaction between the fibre and matrix. However, the relative importance of these two interactions has yet to be fully established and will probably vary with fibre pretreatment.

There are two major types of physical adhesion between the fibre and matrix. First there is the phenomenon known as "wetting". In this case, generating effective wetting of the fibre surface requires that the liquid resin closely fit the contours of the surface. The second type involves bonding by mechanical interlocking of the two surfaces. In both cases, the degree of physical bonding is highly dependent on the surface area of the fibre. In addition to the two bonding forms already mentioned there is also probably a very small degree of interdiffusion of the resin surface molecules into the bulk fibre.

Chemical bonding at the interface may be covalent and/or electrostatic. Horie[7] suggested that both covalent and hydrogen play a role in fibre-matrix adhesion, the balance between the two forms being dependent on the resin structure and thermal history, as well as fibre properties.

It is known that the good adhesion properties found with

epoxy resins are due to the presence of polar functional groups in their structure. The high reactivity of epoxy resins during hardening is determined by the number of epoxide (CH_2-CH-) and hydroxyl groups present in the resin. In the formation of the fibre-epoxy resin interface these groups in the resin react with acidic functional groups on the fibre surface forming chemical bonds. Possible reactions for the formation of covalent bonds are shown below:-

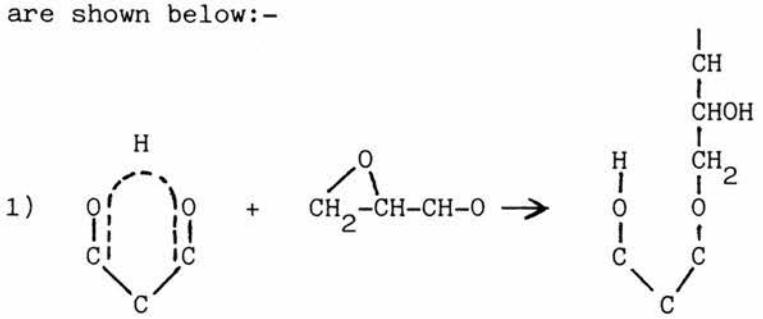

(1.1)

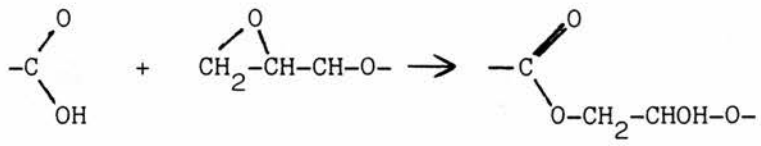

(1.2)

It can be seen that both these reactions are nucleophilic additions to the epoxide. From the evidence available[2] it seems that reaction (1.1) is most likely.

In addition to the epoxide groups forming covalent bonds with the fibre surface, it is thought that they form hydrogen bonds, such as ($-OH^{\delta+} \cdots\cdots -OH^{\delta-}$) and ($-OH^{\delta+} \cdots\cdots O{=}C{=}^{\delta-}$), at the interface.

Polyester resins, however, contain ($-\overset{\overset{O}{\|}}{C}-O-$) type polar groups and in this case can only form weak dipole bonds involving ($=C^{+}=O^{-}$) groups and Van der Waals bonds with the fibre. There is no covalent bond formation.

Increasing the surface functional group concentration on the fibre by surface treatments is known to have significant influence on the mechanical properties of the composite. However, the relationship between surface functional group concentration and composite strength properties has an optimum value of concentration, in the case of epoxy-based composites thought to be 1.5-2.0 μ moles/m^2[9]. Increasing the concentration beyond this value shows no significant increase in composite strength characteristics. Polyester-based carbon fibre composites however show only a slight and virtually linear increase in strength which is directly proportional to the increases in the fibre surface area.

The differing nature of the interfaces of epoxy- and polyester-based composites can be illustrated by considering the effect of water treatment on composite properties. The mechanical properties of epoxy-based composites are not affected appreciably whereas those of polyester-based decrease significantly. A major factor thought to be responsible for the weakening of interfacial bonding in polyester-based composites appears to be the penetration of water molecules to the interface with subsequent hydration and sheilding of the polar groups, and also a reduction in the strength of the hydrogen bonds. Whereas in epoxy-based composites it is thought[9] the strength remains relatively unchanged due to chemical bond formation at the interface. In carbon fibre-epoxy resin composites only 10-20% of the surface functional groups on the fibre can interact with the resin, the remaining groups seem to provide an additional source of active sites for sorption of water molecules. The surface of the fibre may be treated in order to enhance adhesion to the resin. If the interface is constructed successfully, then these interactions can be increased to a point where composite failure occurs in the resin and not at the interface.

1.3 Composite Properties

This discussion will concentrate on the properties relevant to this particular project viz. high modulus PAN-based carbon fibre-epoxy resin structural composites.

A property of major importance to these materials is their light weight compared to traditional materials, such as metals. The density of these composites is found to be approximately 1.6 g/cm^3[10,11].

Of equal importance are their mechanical properties. The Young's modulus of these materials tends to be reasonably large, ranging from 250-400 GNm^{-2}[12-14], but the Tensile strength is generally lower, ranging from 0.5-1.2 GNm^{-2}[1,15] than other types of carbon fibre composites. In addition, the compressive strength tends to be high, ranging from 0.7-0.9GNm^{-2}[1,16], but they normally exhibit poor flexibility; with strain failure occurring at values of only 0.5%[10]. The Interlaminar Shear Strength (ILSS) is approximately 60 MNm^{-2}[1,10,11].

These composite materials seems to have little advantage over the more traditional structural materials, in terms of their mechanical properties alone. However, when these properties are combined with the composite's light weight to give specific mechanical properties[1,17] i.e. values per unit weight, then they are much more effective. This is of particular importance in their application in the field of transport where reduced weight with no loss of mechanical strength improves efficiency and therefore reduces expenditure.

Several other physical properties are important in certain applications of these composites. They have good weathering properties and tend to have high chemical and corrosion resistance. These materials also have excellent thermal stability due to the low, practically zero, coefficient of thermal expansion of the carbon fibre component. This property has generated great interest in these materials for use in structures, such as high gain antennae and optical systems, where thermal distortion limits conventional materials.

The actual properties of a particular carbon fibre composite will be dependent on a large number of factors. These include component processing variables such as pre-treatment time, pressure, temperature, environment and the resultant nature of the fibre surface and the resin structure.

1.4 Applications[1,11,17-20]

In the early years of carbon fibre composite development, the application of these materials was greatly restricted by the cost of the raw materials i.e. fibres. However, with improvements in both the manufacturing process and composite material properties these costs have been reduced to a point where these materials are rapidly replacing traditional materials in many aspects of industry and commerce. Their applications can be seen in Table 1.2.

Table 1.2

INDUSTRY	EXAMPLES
Aircraft	Wings, fuselages, landing gear, control surfaces, helicopter rotor blades.
Automobile	Body parts, lamp housings, bumpers, seats.
Space	Heat resistant tiles for the shuttle and re-entry module.
Boat	Hulls, decks, masts, fittings.
Chemical	Pipes, tanks, pressure vessels.
Furniture and Equipment	Panels, chairs, tables, ladders.
Electrical	Panels, antennae.
Sport	Golf clubs, squash, tennis and badminton rackets, skis, canoes.

1.5 Project Aims

One particular field of application for carbon fibre composites is in aviation. It is hoped that in the future these materials can be used as primary engineering material. However, before this can be accomplished it is necessary to have better understanding of interface mechanics and property prediction. Surface treatments of carbon fibres are used to improve the mechanical properties of the composite but the actual effects of these surface treatments on the fibre surface are not fully understood. Therefore there is a need for surface characterisation techniques for the treated fibres which will lead to accurate prediction of composite properties.

Spectroscopic and physical-chemical are the two general types of methods presently employed in the characterisation of treated fibre surfaces. Spectroscopic techniques provide a wide range of information about these surfaces. X-Ray Photoelectron Spectroscopy (XPS)[2,4,21] provides information on the nature and concentration of the functional groups present on the fibre surface. Whereas Electron Microscopy[11,22] generally provides information about the surface topography. Other methods also used are Auger and Ion Scattering Spectroscopy[4]. These spectroscopic methods, although providing accurate information, tend to be relatively expensive and are not widely available. Physical-chemical techniques tend to be used to supplement the information generated by spectroscopic methods. Gas adsorption measurements[4,22] and base titration with dil. NaOH[8,9] provide information about the functional groups present on the fibre surface. Whereas contact angle measurements[4,22] produce information about the fibre's surface thermodynamic state. These

methods tend to be less expensive but they are also less accurate and tend to be time-consuming.

The aim of this project was to investigate the use of electrochemical and spectro-electrochemical methods to characterise carbon fibre surfaces which had been subjected to different forms of treatment. It was considered that fibres treated in a particular manner would be likely to have such a typical electrical fingerprint which might be easily recognisable. Such techniques might therefore provide a rapid and relatively inexpensive characterisation method.

CHAPTER 1

REFERENCES

1. D Hull: "An Introduction to Composite Materials". Pub. by Cambridge University Press (1981).

2. P M A Sherwood; C Kozlowski: Final Report May 1986 Ref. G-3819 Kansas State University, Manhattan, Kansas, USA.

3. J W Herrick: AFML-TR-66-178 Part II (1967).

4. L T Drzal: 28th National SAMPE Symposium April (1983); SAMPE Journal 19 7 (1983).

5. L T Drzal; M J Rich; J D Camping; W J Park: Proc. Conf. Annu. 35th Reinf. Plast./Composites Inst. Soc. Plast. Ind. (1980) 20-C, 1-20-C 7.

6. Y Suk Ko; W C Forsman; T S Dziemianowicz: Polym. Eng. Sci. (1982) 22 (13) 805.

7. K Horie; H Murai; I Mita: Fibre. Sci. Technol. 9 253 (1976).

8. P Ehruburger; J J Herque; J B Donnet: Proc. London Int. Carbon Graphite Conference 1 398 (1978).

9. B D Sokolov; E P smirnov; G P Markov; E I Belova; S I Kol'tsov: J. Appl. Chem. of the USSR 53 88 (1980).

10. C R Thomas; E J Walker; Proc. 5th Int. Conf. on Carbon/Graphite 520 (1978).

11. J B Donnet; P Ehruburger: Carbon 15 143 (1977).

12. A E Standage; R Prescott: Nature 211 169 (1966).

13. P Favre; J Perrin: J. of Mat. Sci. 7 1113 (1972).

14. W N Reynolds; N L Hancox: 7th Int. Reinf. Plast. Conf. Brit. Plast. Fed. Paper 12 1 (1970).

15. G T Merrall: 7th Int. Reinf. Plast. Conf. Brit. Plast. Fed. Paper 26 1 (1970).

16. I Petker: SAMPE Quart 3 7 (1972).

17. J Fray: 7th Int. Reinf. Plast. Conf. Brit. Plast. Fed. Paper 28 1 (1970).

18. J V Mullin; V F Mazzio: SAMPE Quart 3 (2) 22 (1972).

19. B Bongers; K Brunsch; W Jonda: 7th Int. Reinf. Plast. Conf. Brit. Plast. Fed. Paper 1 1 (1970).

20. R R June; J B Kelly: SAMPE Quart 3 (2) 58 (1972).

21. P Denison; F R Jones; J E Bailey: Final Progress Report July 1983-October 1985 MoD Ref: AT/2064/067 XRMat.

22. D W McKee; V J Mimeault: "The Chem. & Phys. of Carbon Vol. 8". Edited by Thrower and Walker. Pub. by Marcel Dekker (1973).

CHAPTER 2

CARBON FIBRES

Introduction

To obtain a more accurate understanding of the effects of electrochemical and chemical treatments on the surface of carbon fibres and their effect on the physical and mechanical properties of the subsequent fibre-epoxy resin composites; it is necessary to have a comprehensive knowledge of the structure, properties and chemical nature of the untreated carbon fibres. Suitable preliminary study for this is the physical, structural and chemical properties of other forms of carbon.

There are more compounds of carbon than of any other element except hydrogen, however the vast majority of these are best regarded as organic compounds.

2.1 Elemental Carbon

The electronic structure of the carbon atom in its ground state is $1s^2 2s^2 2p^{2(1)}$ with the two 2p electrons unpaired as expected from Hund's rule. Carbon normally has four-covalence which can be accounted for by considering that it is promoted to a valence state based on the $2s2p_x 2p_y 2p_z$ configuration. The ion C^{4+} does not arise in any normal chemical process: something approximating to the C^{4-} ion may possibly exist in some carbides. In general, however, carbon forms covalent bonds.

Some cations such as carbonium ions, anions such as carbanions and radicals of moderate stability can occur. There is abundant evidence from the study of organic reaction mechanisms for transient species of these types. In all three species their stability is usually dependent on their ability to effectively delocalise the additional charge throughout the molecule.

An important feature of carbon chemistry is the ability for catenation i.e. the formation of chains and rings of atoms, not only with single but also with multiple bonds. Clearly an element must have a valency of at least 2 and must form strong bonds with itself to accomplish catenation to any significant degree. Of all the elements, carbon is the most inclined to catenate due to the thermal stability of the C-C bond in relation to the C-O bond hence its insusceptibility to chain oxidation, unlike other catenating elements such as silicon and sulphur.

The element carbon can exist in many different forms, both natural and manufactured, but there are only three different allotropes of carbon. Two of these are types of graphite and the other is diamond.

2.2.1 Diamond

Diamond is one of the hardest known substances. This property can be explained by diamond's very robust three dimensional crystalline structure which is composed of single carbon-carbon bonds.

Each carbon atom exists in the hybridised state with one S state and three p states known as sp^3. This allows each atom to be bonded tetrahederally, at the optimum bond angle of $109^{o}28'$, to four other carbon atoms. The diamond structure shown below (Fig.2.1) is only one of the several structural possibilities that satisfy this bonding arrangment. The diamond crystalline structure is highly symmetrical and the overall symmetry is cubic.

Fig.2.1 Unit Cell Representation for Diamond

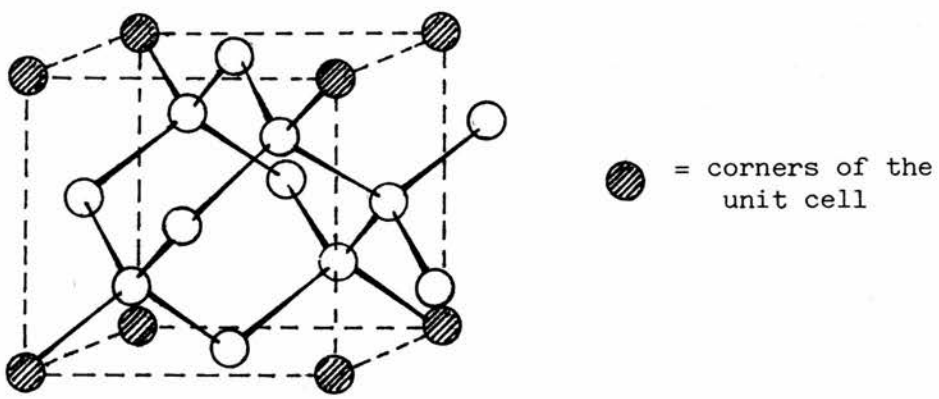

Unit Cell Representation for Diamond

Diamond, due to its symmetrical structure, has a high refractive index, which in turn produces its natural "brilliance" and hence diamond's suitability as a gemstone and optical component. Pure diamond is colourless and transparent but on addition of impurities, coloured diamonds may be produced.

Closely related to structure is the poor conductivity of heat, but more importantly electricity in diamond.

The possible electronic states of the sp^3 electrons in diamond can be divided into bonding and antibonding states with the latter having higher energies. At T = OK, all bonding electrons lie in the lowest possible energy states which are broadened into a band of levels. The bonding states are separated from the anti-bonding or conduction levels by a band gap of 5.3 eV[2] and hence diamond is a very good insulator.

For diamond to conduct, electrons must be excited across this gap which requires very high temperatures to achieve even a small density of electrons and holes for conduction. Introduction of small amounts of impurities or defects can lower the band gap and hence increase conductivity.

2.1.2 α-Graphite

A different hybridisation scheme for the bonding electrons to that of diamond occurs when the carbon atoms arrange themselves to form hexagonal rings. In graphite, orbitals composed of one S and two p , sp^2 bonds, are formed at 120° to each other in a plane producing strong covalent bonds, known as σ bonds. This generates the extended ring structure of the graphite layer which can be seen in Fig.2.2 a). The one remaining orbital has a p_z configuration, known as the π molecular orbital, and it provides the weak bonding between adjacent layers in the graphite structure. A system of completely delocalised overlapping π molecular orbitals allow the transport of electrons throughout the graphite crystal and therefore graphite is a good conductor and can be regarded as a semi-metal.

The structure of a graphite crystal is a set of graphite layers separated by $3.35A^{\circ}$ and stacked in a particular stacking pattern. The type of graphite is determined by the stacking pattern and in fact this is the major difference between α- and β-graphites. In α-graphite the layers are stacked in an ABAB pattern i.e. the carbon atoms of every second layer are vertically above each other, as shown in Fig. 2.2 b). The observed softness and particularly the lubricity of graphite can be attributed to the easy slippage of these layers over each other due to the weak interplanar bonding.

The surface of microcrystalline graphite can be considered as a collection of oxygen-containing organic functional groups[3]. These groups are either acidic or basic oxides. The acidic oxides consist of phenolic, carboxylic, lactone and ketonic groups with

the possibility of hydrogen bonding between C-O sites, whereas the basic oxides are probably chromene-like groups.

The graphite crystal is highly anisotropic and this is reflected in its mechanical properties e.g. The Young's modulus parallel to the basal plane is 1.02×10^3 GNm^{-2}[4] whereas normal to the basal plane it is only 36.5 GNm^{-2}[5].

2.1.3 β-Graphite

This is a very rare form of carbon. It differs structurally from the more abundant α-form in that instead of an ABAB layer stacking pattern, it has an ABC ABC pattern i.e. every third layer is vertically above each other, as shown in Fig. 2.2 c). The β-form or rhombahederal form can be artifically manufactured from the α- or hexagonal form by mechanical treatment such as grinding.

Fig. 2.2

a) Graphitic Layer Plane

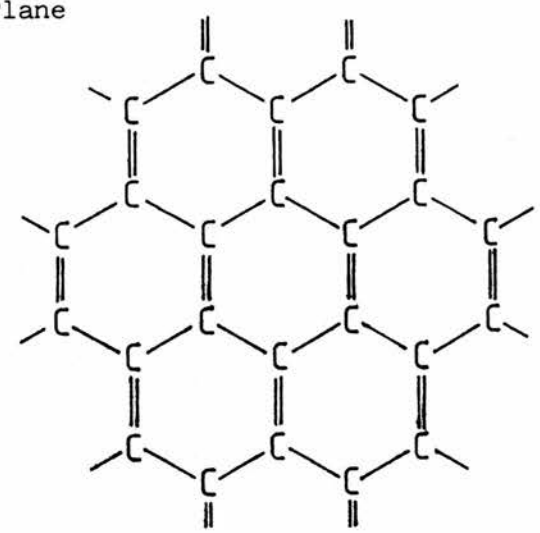

b) Layer Stacking Patterns

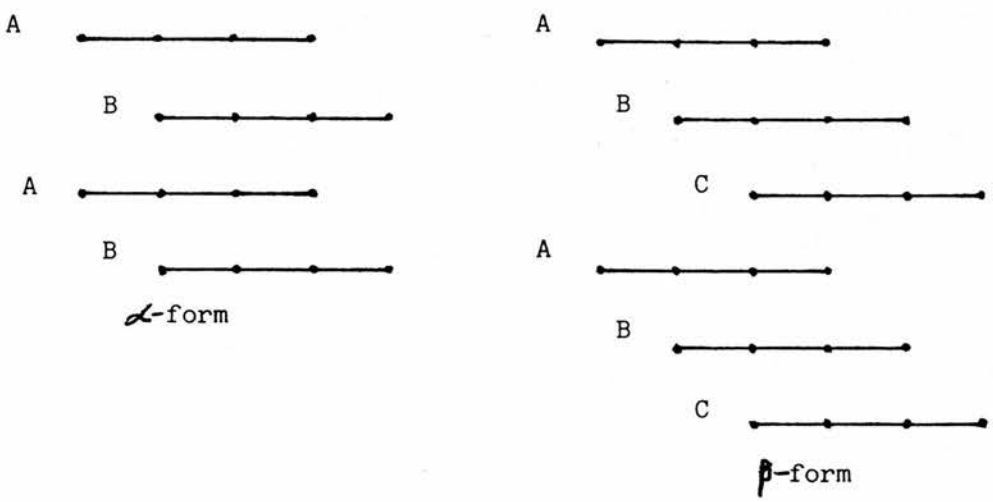

An important aspect of graphite technology is the production of very strong fibres of orientated organic polymer fibres which when harnessed in reinforced materials produce materials which are very light and strong.

2.2 Other Forms of Carbon

2.2.1 Pyrolytic Graphite

Pyrolytic graphite is produced by the deposition of carbon from the vapour phase, initially on the surface of a substrate. The resulting material is a polycrystalline form of carbon, which is characterised by a high degree of orientation and which exhibits metallic type behaviour in the plane parallel to the deposition surface and ceramic type of behaviour perpendicular to the surface. For example, it shows high electrical conductivity in the plane and low conductivity across the plane.

Pyrolytic graphite is impervious to all gases and Horton[6] noted that it has no appreciable pores. The structure of any given piece of pyrolytic graphite will be influenced by the substrate on which it is deposited. The deposited carbon tends to reproduce the small planes found on the substrate. The imperfections then act as nucleation sites for the growth of cones which are the chief structural feature of pyrolytic graphite[7]. Although pyrolytic graphites are turbostratic in the as-deposited state, they are fully graphitised after high temperature annealing or stress annealing.

The mechanical and physical properties have been shown to be closely related to the structure produced during deposition[8]. It would seem reasonable to include the chemical properties, since they are also energy dependent. The significance of preferred orientation in polycrystalline graphite can be illustrated by the extreme values of the mechanical properties, such as Young's modulus, found in some highly orientated pyrolytic graphite[9].

Pyrolytic graphites exhibit the low basal-plane shear strength and shear modulus[10] and the low c-axis strength and tensite modulus that are characteristic of the graphite crystal.

2.2.2 Amorphous Carbons

The many forms of so-called "amorphous" carbon, such as charcoals, soot and carbon black, are actually microcrystalline forms of graphite. "Amorphous" carbons consist of extremely small, possibly only a few unit cells, crystallites constructed, like graphite, of layers of six-membered carbon rings. These layers are turbostratically stacked in columns and hence they do not possess the mutual three-demensional orientation found in the graphite lattice. The layers are separated by 3.44-3.65A^{o}[11], which is slightly larger than graphite. Hofmann[12] et al showed that the layer diameter of typical active charcoal is approximately 30^{o}A and the average column height is 10-13A^{o}.

Both acidic and basic surface oxides are found on the surface of "amorphous" carbons. The acidic surface oxides are in the form of carboxyl, phenolic hydroxyl and carbonyl groups while the basic surface oxides are thought to be chromene-like structures[13]. In "amorphous" carbons e.g. carbon black, most of the free valencies at the edges of the carbon layers are saturated by hydrogen. Graphitised carbon blacks have a very homogeneous surface and have practically no acidic surface oxides.

The physical properties of such materials are mainly determined by the nature and magnitude of their surface areas.

2.2.3 Polymeric Carbons

These are single-phase materials and are manufactured by carbonising various resins of the non-graphitising variety. Unless

the starting material is in the fibre form then these polymer carbons are always isotropic i.e. they show no preferred orientation.

2.3 Carbon Fibre - History and Preparation

2.3.1 Historical Development

For a discussion of the historical development of fibre produced from cellulose, it is necessary to consult the patent literature. In the 1880's Edison's[14] carbonisation of natural cellulose filaments to produce an incandescent lamp filament was the first recognised use of cellulose in the production of carbon filaments. This application was made redundant in the 1900's with the development of the less fragile tungsten filaments.

Further development was suspended until the 1950's when Abbot[15] converted rayon, by carbonisation at 1000°C, into a fibrous carbon material. These materials had acceptable tensile strength and were applied in insulation, filtration and adsorption. In 1959 the Union Carbide Corporation commercially manufactured "graphite cloth" which was made by using a slow batch method[16]. In this process the fibres were heated to approximately 900°C in an inert atmosphere and then graphitised at temperatures above 2500°C. In addition to the production of graphite fibres, lower temperature carbon fibres, heated to approximately 1500°C, were also produced had a tensile strength which was a factor of 2 or 3 greater but a much lower Young's modulus than that of the graphite fibres. The primary application of these lower temperature carbon fibres was the reinforcement of phenolic resins to form composite materials for use in the aviation and aerospace industries.

The early development and applications of carbon fibres has been reviewed[17] and hence will not be discussed further in this report.

The production of carbon fibres has been improved by the use of chemical pretreatments. For example, in the case of rayon-based carbon fibres, these pre-treatments[18] have improved carbon yields and increased process rates since they facilitate the application of continuous-processing techniques.

The presence of strong and uniform carbon yarns produced by continuous processing allowed very high degrees of stretch to be applied during high temperature graphitisation. This development led to Union Carbide's production of high strength and high modulus graphite fibres (Thornel 25). This opened the way and since then many companies have produced quality fibres.

2.3.2 Carbon Fibre Preparation

Due to the vast diversity of carbon fibres available for various applications, this report will only describe production methods for high modulus carbon fibres and in particular it will concentrate on those fibres derived from rayon and polyacrylonitrile (PAN) precursors.

The production of high modulus carbon fibres generally involves three basic steps: 1) Heat treatment 2) Carbonisation 3) Graphitisation. These steps will now be discussed in detail.

High Modulus Carbon Fibres from Rayon

The purpose of the heat treatment stage is to completely destroy the cellulose structure of rayon to form a primary char suitable for rapid carbonisation. The rayon is heated to about

350°C and undergoes a 50% weight loss. The principal product evolved is water but complex tars are also produced. The prevention of excessive deposition of these tars onto the filament is probably the principal factor in the successful heat treatment of rayon. This may be accomplished in several ways: pyrolysis in an inert atmosphere[19] or in a reactive atmosphere such as air or O_2[20]. However, the most effective method is pyrolysis after chemical pre-treatment[18]. The heat treatment stage is the most important, as far as process control is concerned.

The fibres are then carbonised which is normally carried out in an inert atmosphere at a temperature between 1000 and 1500°C for about one minute. The introduction of stress at this stage increases the degree of preferred orientation and hence the fibre's mechanical properties and in addition, it reduces the level of fibre shrinkage[21].

The graphitisation step involves heating the carbonised fibres to temperatures above 2800°C for a few seconds. For the production of truly high modulus carbon fibres from rayon, it is necessary to apply significant degrees of tensile stress during graphitisation[22]. Graphitisation increases the strength of the fibres by a factor of about five, however the mechanical properties are highly dependent on the graphitisation temperature.

High Modulus Carbon Fibres from PAN

The polymer precursor PAN, shown in Fig.2.3, is very similar to polyethylene in molecular conformation but every alternate hydrogen side group is replaced by a nitrile group. An important

method for producing high modulus PAN-based carbon fibres is by orientation of the polymer precursor by stretching[21].

The bulk PAN is converted into fibre which is then stretched to produce the alignment of the molecular chains along the fibre axis. On heating the stretched fibre, the active nitrile groups interact to produce a ladder polymer consisting of a row of six-membered rings, as shown in Fig.2.3.

Fig.2.3[23]

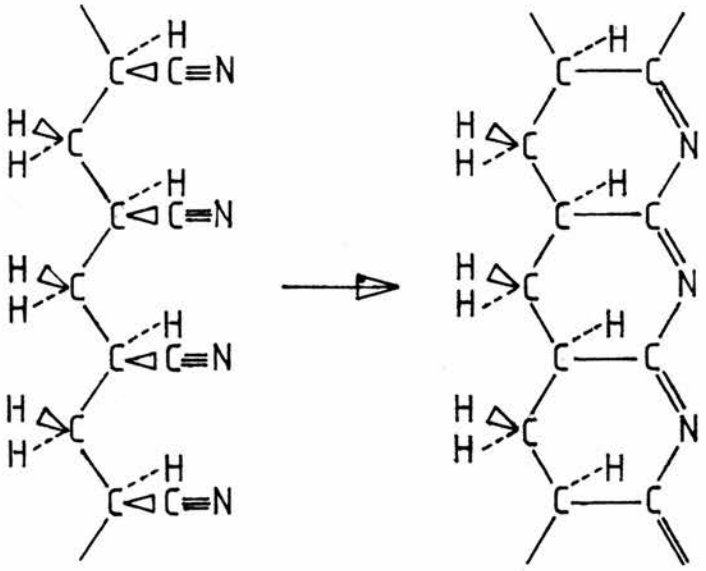

While the fibre is still under tension it is heated in an oxygen atmosphere, which leads to further chemical reaction and cross-link formation between the ladder molecules. The oxidised PAN is then reduced to give the carbon ring structure which is converted to "turbostratic" graphite by heating at higher temperatures. As was found with rayon-based fibres, the mechanical properties of PAN-based fibres are highly dependent on the final heat treatment temperatures.

The other major method for the production of high modulus PAN-based carbon fibres involves the application of tensile stress during the high temperature graphisation step[24]. The stretching causes an increase in preferred orientation and is accompanied by an increase in the crystal size in the direction of the c-axis. These stretched fibres have markedly different mechanical properties to the unstretched fibres.

It is also possible to produce high modulus fibres, with preferred orientation, from pitch[25]. The pitch is heated to above 350°C to give "mesophase" pitch, which contains both isotropic and anisotropic material. It is then spun through a multi-hole spinneret to produce "yarn". Hydrodynamic effects at the hole during spinning generate the preferred orientation of the planar molecules. The fibres are then carbonised at about 2000°C. During some stages, the application of tensile stress is required to prevent relaxation and loss of the preferred orientation.

2.4 The Internal Structure of Carbon Fibres

The internal structure of carbon fibres has been investigated by a variety of methods such as electron diffraction[26,27], X-ray diffraction[26,28-32] and various forms of electron microscopy[30,33-37]. These techniques provide information about structural features of carbon fibres which range from a few to thousands of A^{o} in size. As before, due to the diversity of carbon fibres available, this report will concentrate on the structure of high modulus fibres, with particular emphasis placed on those derived from rayon and PAN.

General Description

From X-ray diffraction evidence, both Ruland[32,38] and Johnson and Tyson[30] have suggested fundamental structural models for carbon fibres. X-ray diffraction methods provide information about the crystallite dimensions and most importantly about the degree of preferred orientation of the layer planes parallel to the fibre axis. Ruland proposes that all high modulus carbon fibres comprise of extended narrow fibrils separated by needle-like pores with diameters in the range of 10-20A^{o} and lengths of at least 200-300A^{o}. Both the fibrils and pores have preferred orientation parallel to the fibre axis. The structural model can be seen in Fig 2.4 a).

Johnson and Tyson, however, propose a model, seen in Fig.2.4 b), which consists of short turbostratic crystallites stacked roughly end to end but misorientated, generating twist and tilt boundaries, in the transverse direction, between crystallites in the columns. The average lengths of the crystallites is about 65 A^{o} and the widths

range from 20-110 A°. The columns are separated by intercrystalline boundaries but more importantly by sharp-edged voids generated by the imperfect crystallite stacking. These long, narrow sharp-edged voids generally extend for more than $200A^{\circ}$ and have mean width of less than $10A^{\circ}$. Both the crystallite columns and voids show preferred orientation parallel to the fibre axis.

Fig.2.4 Structural Models for Carbon Fibres

a) Ruland's Model

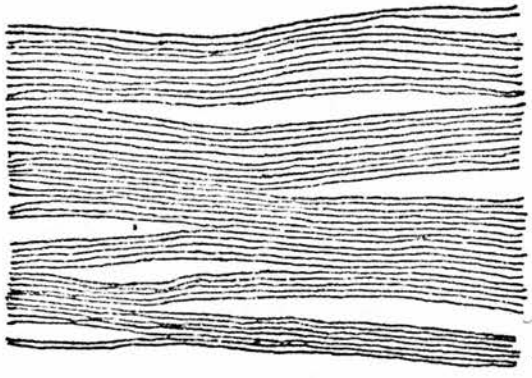

b) Johnson and Tyson's Model

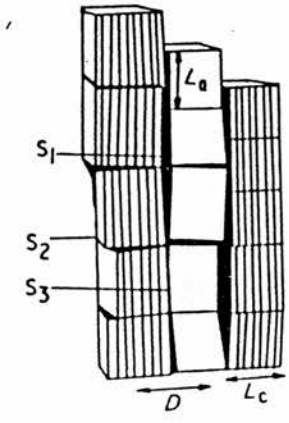

Schematic, idealized diagram summarizing x-ray diffraction evidence. S_1, void; S_2, subgrain twist boundary; S_3, intercrystallite boundary.

2.4.1 Internal Structure of Rayon-based High Modulus Carbon Fibres

Ruland[32] and Johnson and Watt[26] concluded, from X-ray diffraction studies, that rayon-based high modulus carbon fibres consist of long primary units lying parallel to the fibre axis, which are bonded together to form an extended network of branched fibrils that apparently run the whole length of the fibre. These fibrils are separated by needle-shaped pores which also show preferred orientation parallel to the fibre axis. These pores have diameters of only about 10A° but extend for at least 200-300A°. This description was given further support by the electron microscopy provided by Hugo et al[34], who also noted that the overall diameter of rayon-based fibres was about 5 μm. All this evidence suggests that high modulus rayon-based carbon fibres seem to fit the structural model proposed by Ruland.

However, in contrast, Mimeault and McKee[28] and others[4] found that these fibres consist of columns of crystallites which are separated by needle-like voids. Both crystallite columns and voids show preferred orientation parallel to the axis. The crystallite lengths were found to range from 30 to 125A° and the widths between 30 and 85A°. The crystallite dimensions are dependent on the treatment temperature, preferred orientation and to a lesser extent the nature of the precursor. These studies support the model proposed by Johnson and Tyson.

In conclusion, neither structural model can be said to be an accurate description of all types of rayon-based high modulus carbon fibres.

2.4.2 Internal Structure of High Modulus PAN-based Carbon Fibres

Johnson and Watt[26] found, from electron diffraction studies, that high modulus PAN-based fibres, consisted of long, narrow fibrils lying parallel to the fibre axis. The fibril width was about 100A° but the length was indefinable. These fibrils contained turbostratic stacks of graphitic layer planes, separated by 3.42A°, and hence there is little 3-D order to the internal structure. Separating the fibrils are long, narrow needle-like pores with a mean diameter of only 10A° . Both the fibrils and pores show a high degree of preferred orientation parallel to the fibre axis.

However, from X-ray diffraction[20,29] and electron microscopy[26], it was found that these fibrils consist of turbostratic crystallites, of length between 60-120A° and of average width 65A°, stacked end to end into columns parallel to the fibre axis. The imperfect stacking generates both tilt and twist components at sub-grain crystalline boundaries in the transverse direction. PAN-based carbon fibres have larger crystallite width but smaller lengths than rayon-based fibre, for a particular treatment temperature.

Johnson et al[37] have found, for highly graphitised PAN-based fibres, the existence of two types of structure in one particular fibre. The outer region possessed the normal fibrillar structure whereas the "core" was found to be sheet-like or graphitic structure surrounding a slit-like hole. It was shown that the area of the laurellar region, showing "tree-trunk" preferred orientation, could be increased by raising the graphitisation temperature. Similar features were seen by Johnson, Crawford and Jones[33] and by Bennet[39].

2.4.3 General Description of Carbon Fibre Structure

The fundamental structural unit of carbon fibres, comparable to the long chain molecule in polymers, is the graphitic layer. This layer probably extends for thousands of A°, although in reality its length is almost indefinable, and several hundred in the transverse direction. Ideally these layers are comparatively linear parallel to the fibre axis but highly curved and tortuous in the transverse direction, producing a corrugated-sheet like feature. These layer planes are stacked "turbostratically", separated by approximately $3.4A^{\circ}$, to produce a continuous branched network of microfibrils or crystallites. These microfibrils are aligned with preferred orientation parallel to the fibre axis and are separated by similarly orientated needle-like voids.

The crystallite dimensions are almost indefinable, since each microfibril connects smoothly with the next, through curving twisting and branching. These connections occur in both longitudinal and transverse directions with the transverse having greater branching and tortuosity.

This branching and tortuosity produces voids or micropores between the microfibrils. These voids are long, needle-like which extend for at least $200-300A^{\circ}$ in the longitudinal direction only $10A^{\circ}$ in the transverse direction.

The secondary structural unit of carbon fibre is a bundle of microfibrils with a diameter of $250-1000A^{\circ}$ and is known as a fibril. These fibrils have similar preferred orientation to that of the microfibrils. The lateral boundary between fibrils may be just

a surface composed of mostly graphitic layer faces and therefore few layer connections.

The overall fibre diameter for high modulus carbon fibres is about 7-8 μm.

2.5 Surface Structure of Carbon Fibres

2.5.1 Physical Surface Features

In general, rayon-based carbon fibres show an irregular fluted cross-section, when studied by electron microscopy, and their surfaces are characterised by longitudinal grooves and striations. In contrast, PAN-based fibres tend to show a circular cross-section with relatively smooth and featureless topography. However, not only the precursor affects the physical nature of the fibre surface, the heat treatment temperature applied in preparation is also an important factor. In the case of rayon-based fibres, those formed at low temperatures are highly porous and have rough surfaces whereas those graphitised at high temperatures are less porous and have lost most of their surface roughness. In addition, carbon fibres produced by different manufacturers often show distinct topographical features. For example, PAN-based high modulus fibres produced by Harwell have few surface pits whereas those from Rolls-Royce are heavily surface pitted[40].

Denison et al[41] suggest that the surface of carbon fi-bres may undulate and contain lattice vacancies, discontinuities and defects, at which chemical activity may occur. From X-ray studies, it was also shown that the surface contains micropores, with a diameter of about 10A^{o}.

2.5.2 Chemical Functional Groups on Carbon Fibre Surfaces

The surface properties of carbon fibres have often been explained by the presence of polar surface groups formed during

oxidative pretreatment. The functional groups produce hydrophilicity in the carbon surface, probably by supplying chemisorptive sites for water molecules. The functional groups found on carbon fibre surfaces are reasonably similar to those found on other forms of carbon, such as carbon black[11,42] and pyrolytic graphite[7]. These groups are produced at edge sites and plane defects and generally consist of "surface oxides".

In general, there are two types of "oxide" present on carbon fibre surfaces, acidic oxides and basic oxides. The relative proportions of these oxides can be controlled by the nature of the pretreatment.

The acidic surface oxides are thought to consist mainly of carboxylic, phenolic hydroxyl and carbonyl groups, however more complex groups have been identified, such as lactones[43], esters and quinoid structures. Denison et al[41] suggests that in PAN-based carbon fibres the carboxylic groups, due to steric considerations, are probably located at surface sites rather than at sites in the surface micropores themselves where the relatively smaller -OH groups or water molecules, could bind.

A lot less is known about the nature of the basic surface oxides present on carbon fibres but Garten and Weiss[13] suggested that they have a chromene-type structure.

Obviously the surface functionality present will differ according to the nature of the particular fibre. The most important factor affecting the surface functionality is the nature of the fibre pretreatment. For example, type I PAN-based carbon fibres have significantly less surface oxygen concentration than type

II and hence have a lower concentration of acidic groups. This may be explained by the higher pretreatment temperature used to produce type I fibres, which removes much of the surface functionality.

2.5.3 A General Description of Carbon Fibre Surfaces

Carbon fibre surfaces show a great diversity of physical and chemical features, depending on the nature of pretreatment and on the precursor. Rayon-based fibres tend to have surfaces which are characterised by grooves and striations whereas PAN-based are much more smooth and featureless. The pretreatment temperature is most important, those fibres prepared at high temperatures tend to exhibit a lot less porosity and surface roughness compared with those manufactured at lower temperatures.

The chemical nature of the fibre surface is characterised by the presence of various functional groups. These groups consist of both acidic and basic surface oxides. The acidic oxides are mainly carboxylic, phenolic hydroxyl and carbonyl groups whereas the basic oxides are thought to be chromene-type structures. As with the physical nature of the surface, chemical functionality is highly dependent on the nature of the pretreatment and in particular on the pretreatment temperature. Fibres produced at high temperatures exhibit much less surface functionality than those manufactured at lower temperatures.

Considerations of both the physical and chemical features allows one to accept the model proposed by Denison et al[41], shown in Fig.2.5, as a reasonable representation of carbon fibre surface structure.

Fig.2.5[41] Denison's Model of Carbon Fibre Surface Structure

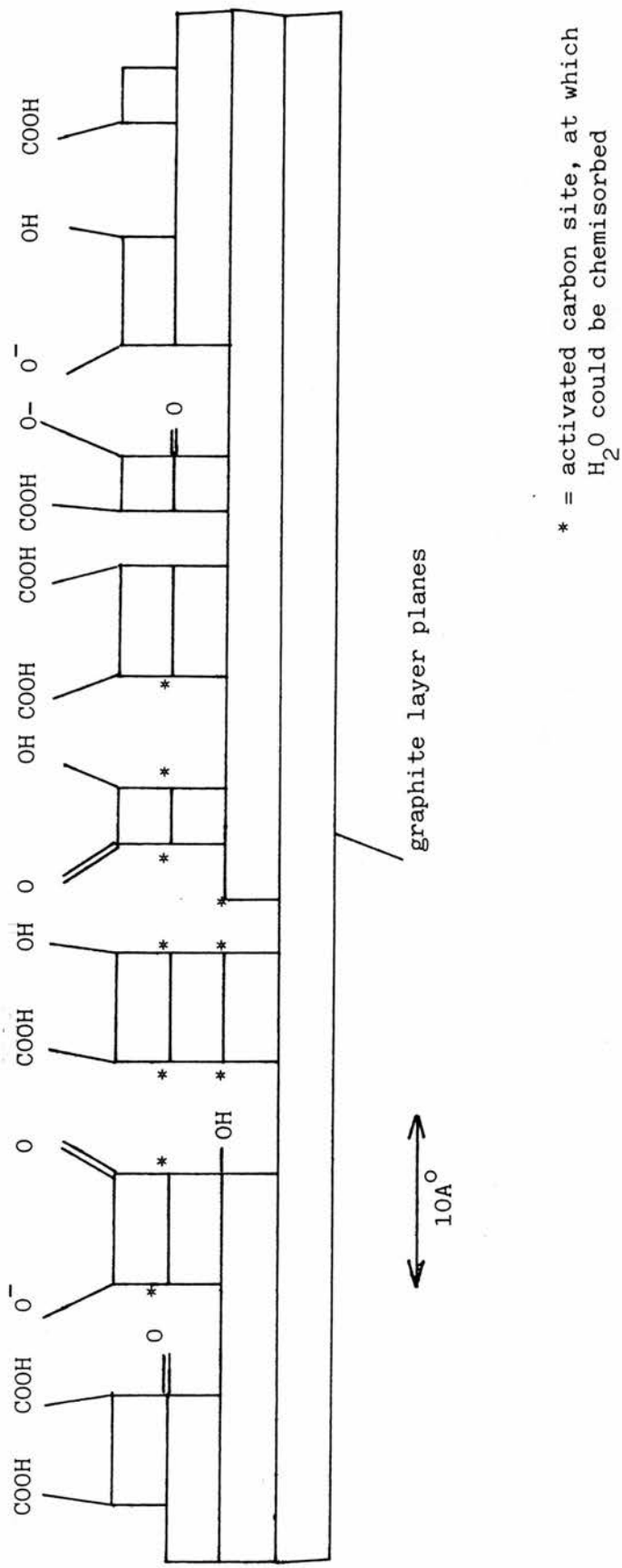

As has already been discussed in Chapter 1, the physical and chemical nature of the carbon fibre surface is very important in determining the mechanical properties of the subsequent carbon fibre composite material. The mechanical properties of the composite are generally dependent on the nature and therefore properties of the fibre-resin interface. The properties of the interface are thought to be related to the combination of physical interlocking and chemical interbonding between the two surfaces.

2.6 Physical and Mechanical Properties of Carbon Fibres

The physical and mechanical properties of carbon fibres are highly dependent on their structure and hence the nature of the pretreatment applied in manufacturing these fibres. They are also dependent, to a lesser extent, on the nature of the precursor material.

2.6.1 Density, Surface Area and Porosity of Carbon Fibres

The densities of carbon fibres are less than pure graphite and range from 1.5-1.6 g/cm^3[44] for low temperature fibres to 1.9-2.1 g/cm^3[4,45,46] for highly graphitised fibres. In general, fibres manufactured from pitch tend to be more dense than those from PAN and rayon. However, the most important factor affecting density in the case of highly graphitised fibres is the degree of stretching applied in manufacture, since this collapses the pores between the microfibrils and increases the density.

The surface areas of untreated PAN-based carbon fibres range from 0.1-0.45 m^2/g[47,48] whereas those based on rayon tend to have

larger surface areas due to their increased surface roughness and porosity, ranging from 0.5-1.8 m^2/g[4]. The actual value of surface area for a particular precursor is mainly dependent on the heat treatment temperature used in preparation i.e. high temperature graphitised fibres have much lower surface areas than those prepared at low temperatures.

The porosity of carbon fibres shows similar trends and is dependent on similar factors as the surface area i.e. porosity and surface area are closely related properties. In addition, the degree of stretching applied in preparation of the fibre is an important factor in the porosity of carbon fibres, since stretching collapses the pores separating the microfibrils and hence reduces the porosity.

2.6.2 Young's Modulus

When a material is subjected to simple tension or compression, then the Young's modulus, or modulus of elasticity, is defined as:-

$$Y = \frac{\text{tensile or compressive stress}}{\text{tensile or compressive strain}}$$

and has units of stress, usually Nm^{-2}.

The Young's modulus of carbon fibres is dependent on the processing variables such as the amount of stretch applied during carbonisation and/or graphitisation and the degree of heat treatment in the graphitisation i.e. the maximum temperature and its duration.

It is also dependent on structural features such as the degree of preferred orientation.

In general[45,49,50], non-graphitised low temperature fibres have Young's moduli ranging from 30-250GNm^{-2} whereas high temperature graphitised fibres tend to have larger Young's moduli ranging from 350-750GNm^{-2}. The variation of Young's modulus between fibres produced from different precursors, at a particular heat treatment temperature, can be explained by considering the porosity of the fibres involved. It must be noted that the value for the Young's modulus quoted for carbon fibres are measured in the direction parallel to the fibre axis.

2.6.3 Longitudinal Shear Modulus

Shear stress exists on a material if on opposite faces of the section, equal and opposite parallel forces exist. If a body is subjected to pure shear then the shear modulus, or modulus of rigidity, is defined as

$$G = \frac{\text{shear stress}}{\text{shear strain}}$$

and has units of shear stress, usually Nm^{-2}.

The shear modulus of carbon fibres is independent of both the Young's modulus and the nature of the fibre precursor and has a value between 15-30GNm^{-2} for all fibres.

2.6.4 The Strength of Carbon Fibres

The strength of carbon fibres is usually dependent on the nature and quantity of the structural imperfections; such as discrete flaws, fibril and microfibril boundaries, kinks and dislocations, present. Discrete flaws, like voids and surface pits, generally control the tensile strengths of low temperature carbon fibres but have less effect on the highly graphitised fibres. The fibrils and microfibril boundaries provide avenues for fracture propagation and the kinks and dislocations are points of localised weakness. Hence, all these structural imperfections are factors which affect the overall strength of the fibres.

When considering the strength of carbon fibres, the property most often quoted is the tensile strength. As was found with the Young's modulus, the most important factor affecting tensile strength is the degree of stretch applied in graphitisation. Hence, as the degree of fibrillar structure, present in the fibre, increases the tensile strength decreases. A similar relationship exists between the fibre diameter and the tensile strength. Therefore high stength fibres tend to be narrow fibres prepared at low temperatures with no application of stretch. The tensile strength of carbon fibres[51,52] range from 1.5-2.4GNm^{-2} for the highly graphitised HM fibres to 2.4-4.0GNm^{-2} for the low temperature, non-stressed HT fibres. In general, the nature of the fibre precursor has little effect.

The compressive strength of carbon fibres is only dependent on the processing time and temperature during graphitisation. As these parameters increase there is a corresponding reduction

in the compressive strength, hence HM graphitised fibres have the lowest compressive strength.

2.6.5 Flexibility

Carbon fibres are almost completely brittle and show 100% elastic recovery when loaded to stresses below the fracture strength. The high modulus fibres have considerably lower value for strain to failure, 0.5%, compared with 1.0% for high strength fibres. Beyond this value, known as the "yield point", the HM fibres exhibit non-linear stress-strain behaviour in bending, probably due to their fibrillar structure. At high stress levels, bond failure between adjacent fibrils occurs enabling the fibrils to separate and deform, probably by buckling, independently. However, this does not initiate total fibre failure.

2.6.6 Electrical Properties

When talking about the electrical properties of carbon fibres, one usually considers the electrical resistivity (ρ) rather than the more normal electrical conductivity. In general, the electrical resistivity of carbon fibres is about 10^2-10^3 higher than that of metals such as iron and aluminium and ranges from 2×10^2-3×10^3 $\mu\Omega$ cm[45,53]. The electrical resistivity of carbon fibres increases as the graphisation temperature used in preparation decreases and therefore generally high modulus fibres have low resistivity compared to high strength and low temperature fibres.

Johnson and Watt[26] suggested that the high electrical resistivity of carbon fibres compared to highly-orientated pyrolytic

graphite was due to the small crystallite size but Watt later indicated that it was probably caused by the effect of crystallite boundaries on the predominant scattering effect of these boundaries.

Several authors[53-55] have noted that there seems to be close correlation between the variation in electrical resistivity and the variation in the Young's modulus. In addition, it has been observed that the electrical resistance of carbon fibres increases with the degree of strain applied to the fibre.

Owston[53] stated that carbon fibres can be considered as conducting particles which are bonded together at certain points and which may just be in contact, but not bonded, at others. He proposed an idealized model, shown in Fig.2.6, for the electrical conduction paths in carbon fibres, assuming that, for both the fibrillar and crystallite structural models, the particles were roughly rectangular.

Fig.2.6 Model for the Electrical Conduction Through Carbon Fibres

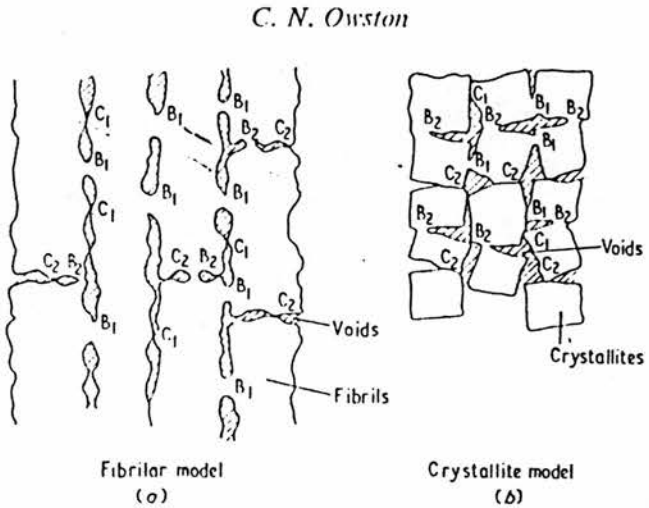

B_1C_1 bonded regions or interfacial contacts in the transverse direction. B_2C_2 bonded regions or interfacial contacts in the axial direction.

Owston suggests two possible conduction paths.

1. Direct path in which the current flows along each fibril or crystallite and jumps to the next one in line via B_2 bonds and C_2 contacts.

2. Indirect path involving many transverse jumps via B_1 bonds and C_1 contacts.

Electrical resistivity in the transverse direction will be much greater than that in the axial direction. Current

flow by path 2) will involve a much greater path length than by path 1).

Both these effects Owston suggests, indicate that path 1) will have the lowest resistance and that the electrical behaviour of the fibres will probably be more dependent on bonds B_2 and contacts C_2 than on bonds B_1 and contacts C_1.

2.6.7 Thermal Expansion and Conductivity

Due to the highly anisotropic nature of carbon fibres, the thermal expansion is highly dependent on the direction of measurement. The thermal expansion parallel to the fibres axis tends to be much lower than that in the normal direction. This is illustrated by high modulus PAN-based fibres where the co-efficient of thermal expansion is negative parallel to the axis and 7-12 x $10^{-6}{}^{o}C^{-1}$ in the transverse direction. At low temperatures, high modulus fibres tend to have lower co-efficients of thermal expansion, especially in the axial direction, than high strength fibres.

The intrinsic thermal conductivity of carbon fibres is difficult to determine but since the axial thermal conductivity of these fibres is much higher than that of organic resins, it may be estimated by measuring the fibre-resin composite. The thermal conductivity of high modulus fibres was found to be much larger than those of high strength. The values ranged from 20-30 to $\approx$ $100 Wm^{-1}{}^{o}C^{-1}$ (23).

As has been seen the physical and mechanical properties of manufactured carbon fibres are very different depending on the structure and hence the preparation parameters applied. Therefore a discussion of these properties in general terms is very difficult.

In addition, these properties can be altered significantly by the use of surface treatment methods and processing techniques, such as whiskering, after the fibre has been prepared. There is even a diversity of properties in one particular fibre due to the non-uniformity of structure produced.

2.7 Surface Treatments

The aim of commercial and laboratory surface treatments on carbon fibres is to improve the strength of the fibre-resin interface in the composite and hence the mechanical properties of the composite material. There are three types of surface treatments used:-

1) Whiskering
2) Polymer Coating
3) Oxidation

Whiskering[56] is a process which involves the growth of silicon carbide on the fibre surface, perpendicular to the fibre axis, at high temperatures. It generates a threefold increase in the shear strength of rayon-based and a fivefold for PAN-based fibres. Polymer Coatings tend to be added to improve the handling properties of the fibres but they have little overall effect on the mechanical properties. By far the most important type of surface treatment is oxidation. There are three types of oxidation generally used.

1) Dry Methods
2) Chemical Oxidation
3) Electrochemical Oxidation

2.7.1 Dry Methods

The four main reagents used in dry oxidation of carbon fibres are vacuum desorption, air oxidation, O_2 and/or ozone and metal oxide

catalysts. Vacuum desorption, at 300°C and 1 torr, only removes surface impurities but has little effect on the mechanical properties. Air and particular oxygen/ozone oxidation methods are difficult to control and are generally non-reproducible. In the case of rayon-based Thornel 40 fibres, air oxidation at 400°C for 16-30 hours was found by Goan and Prosen [57] to increase the surface area and the concentration of -COOH groups on the surface of the fibre. In PAN-based fibres[58], a mild form of air oxidation is important in the removal of structural flaws whereas excessive oxidation causes marked pitting. Metal oxides such as Cu,Pb and V oxides, at 300-700°C, can act as catalysts to improve surface roughness.

2.7.2 Chemical Methods[59-63]

Several concentrated chemical reagents are used as oxidative surface treatments, however by far the most common is concentrated nitric acid.

Herrick et al[64] found that high strength rayon-based fibres treated in 60% HNO_3 for 24 hours showed a 12% weight loss and an increase in surface area. In addition, there was an increase in carboxyl groups and a significant increase in the concentration of phenolic hydroxyl functionality on the surface.

PAN-based fibres, in general, are more easily oxidised than rayon-based but their susceptibility to surface activation is highly dependent on the preparation temperature. Type I fibres show little effect of surface topography alterations and there is very little weight loss on oxidation but form a graphitic surface oxide layer whereas type II show a 50% weight loss and

severe pitting and surface degradation[59]. In general, concentrated nitric acid and oxidation increases the tensile strength of the fibre but decreases the Young's modulus due to the removal of the better aligned outer sheath, along with the surface irregularities[63]. Also the increase in functionality results in carbon-carbon surface interactions which cause misorientation of the aligned regions decreasing the Young's modulus.

Concentrated $KMnO_4$ increases the surface area and compressive strength but decreases the flexural strength of carbon fibres. H_2SO_4 may also be used, as in the case of pitch-based fibres treated with 98% H_2SO_4. Maeda et al[60] found the formation of a graphitic surface oxide layer and found evidence of interaction, unlike nitric acid. Other reagents used include H_2O_2, NaOCl and HOCl.

However not all strong oxidising agents improve the properties of the fibres after treatment. Concentrated $K_2Cr_2O_7$ was found to produce a reduction in surface area and pores with a large diameter.

2.7.3 Electrochemical Methods[41,59,63,65-71]

Electrochemical oxidation methods are highly suited to both a laboratory and commercial application for surface treatments of carbon fibres because they can be performed at about room temperature and for a relatively short time span of a few minutes to produce a significant degree of oxidation and mechanical property improvement. The degree of oxidation is influenced by the nature of the electrolyte, its concentration, oxidation time, current density and temperature. A large variety of electrolytes are used in electrochemical anodic oxidation, ranging from bases,

such as NaOH, KOH, NaOCl, to highly acidic electrolyte solutions of strong acids, such as H_2SO_4, H_3PO_4 and HNO_3. The variety of electrolytes available allows manufacturers to select reagents to generate the properties required. All electrochemical treatments, current densities ranging from 0.5-4.0mA/cm^2, increase the concentrations of surface oxides present on the fibre.

In general, high modulus fibres, type I, oxidised in acidic electrolytes, such as HNO_3 and H_2SO_4, tend to form graphitic oxide layers on the fibre surface. In addition, type I form significantly less surface oxides, chemisorptive sites and micropores than the more reactive type II high strength fibres. Denison et al[41] suggest that type II fibres have a more preferential surface structure for acidic group formation. After initial oxidation, the edge sites in type II fibres can be further oxidised to carboxyl functional groups and/or CO_2. Fitzer et al[67] found that at very large anodic oxidation potentials, even high modulus fibres show degradation.

Theodoridou et. al.[70] found that PAN-based high modulus fibres oxidised in 97% H_2SO_4 and then reduced showed a high concentration of defects in the crystal lattice, situated in the bulk store as well as the surface. These defects can be oxidised to give bulk functional groups and generate a material with high strength, surface area and electrical conductivity, which is highly suitable for use as a bulk-modified electrode.

Generally, fibres treated in acidic elctrolytes have reduced tensile strength whereas the Young's modulus is unaffected.

Kozlowski and Sherwood[65] found that PAN-based type II fibres largely retained the graphitic nature of their surface, even after rigorous oxidation, 2.5V, in NaOH electrolyte. The carboxyl-type group predominated at high potentials, unlike HNO_3. Increasing the potential increases the phenolic hydroxyl content of the surface and there was also low levels of intercalation. The tensile strength of the resultant composite tends to increase with oxidation but the Young's modulus is unaltered, due to the loss of the outer sheath being compensated by the passage of current through the fibre during oxidation.

The physical mechanism of oxidation for basic electrolytes seems to be different to that of acidic electrolyte solutions. Circular holes are formed at edge sites on the fibre surface and these appear to be areas of localised attack and they may provide keying points to which the resin can adhere in composite production. Unlike acidically treated carbon fibres, there is no evidence of graphitic surface oxide layer formation in the basically oxidised fibres.

CHAPTER 2

REFERENCES

1. F A Cotton; G Wilkinson: "Advanced Inorganic Chemistry" 4th Ed. Pub. by J Wiley and Sons (1980).

2. I L Spain: "The Chemistry and Physics of Carbon. Vol 16" by Walker and Thrower. Pub. by Dekker Inc. (1981).

3. K F Blurton: Electrochimia Acta 18 869 (1973).

4. R Bacon: "The Chemistry and Physics of Carbon. Vol.9" by Walker and Thrower. Pub. by Dekker Inc. (1973).

5. O L Blakslee; D G Proctor; E J Sedlin; G B Spence; T Weng: J. Appl.Phys. 41 3373 (1970).

6. W S Horton: Proc. Conf. Carbon (1961) 5 Vol.2. 233 (1963).

7. R E Panzer; P J Elving: Electrochimia Acta. 20 635 (1975).

8. L F Coffin: J.Amer.Ceram.Soc. 47 473 (1964).

9. A R Ubbelohde; D A Young; A W Moore: Nature 198 1192 (1963).

10. D E Soule; C W Nezbeda: J.Appl.Phys. 39 5122 (1968).

11. H P Boehm; E Diehl; W Heck; R Sappok: Angew.Chem.Int.Ed. 3 (10) 669 (1964).

12. K Biastoch; U Hofmann: Angew.Chem. 53 327 (1940).

13. V A Garten; D E Weiss: Austral.J.Chem. 10 309 (1957).

14. T A Edison: U.S. Pat. 223, 898 (1880).

15. W F Abott: U.S. Pat. 3, 053, 775. (1962).

16. C E Ford; C V Mitchell: U.S.Pat. 3, 107, 152 (1963).

17. D L Schmidt; H T Hawkins: Reinf.Plast. '65 Soc.Plast. Engineers Regional Techn.Conf. Seattle, p111 (1965).

18. E M Peters: U.S.Pat. 3, 235, 323 (1966).

19. Basic Carbon Corp: Brit.Pat. 1, 071, 394 (1967).

20. S L Strong: ACS Div. of Organic Coatings and Plastics.Chem. Reprints 31 426 (1971).

21. E Fitzer; M Heym: Chemistry and Industry 21 663 (1976).

22. W J Spry: Brit.Pat. 1, 093, 084 (1967).

23. D Hull: "An Introduction to Composites Materials". Pub. by Cambridge Univ. Press. (1981).

24. J W Johnson; J R Marjoram; P G Rose: Nature 221 357 (1969).

25. S Otani; Y Kokubo; T Koitabashi: Bull.Chem.Soc.Jpn. 43 3291 (1970).

26. W Johnson; W Watt: Nature 215 384 (1967).

27. B J Wicks: J.Mat.Sci. 6 173 (1971).

28. V J Mimeault; D W McKee: Nature 224 793 (1969).

29. D J Johnson: Nature 226 750 (1970).

30. D J Johnson; C N Tyson: J.App.Phys. (J.Phys.D.) 2 787 (1969).

31. R Perret; W Ruland: J.App.Cryst. 2 209 (1969).

32. W Ruland: J.App.Phys. 38 3585 (1967).

33. D J Johnson; D Crawford; B F Jones: J.Mat.Sci. 8 286 (1973).

34. J A Hugo; V A Phillips; B W Roberts: Nature 226 144 (1970).

35. H M Hawthorne; C Baker; R H Bentall; K R Linger: Nature 227 946 (1970).

36. R Bacon; A F Silvaggi: Carbon 9 321 (1971).

37. J W Johnson; P G Rose; G Scott: 3rd Conf. on Industrial Carbon and Graphite, 1970, Soc. of Chem.Ind., London (1971).

38. W Ruland: "Chemistry an Physics of Carbon. Vol 4". Pub. by Dekker Inc. (1969).

39. S C Bennet; D J Johnson: Carbon 17 25 (1979).

40. R Dietz; M E Peover: J.Mat.Sci. 6 1441 (1971).

41. P Denison; F R Jones; J E Bailey: Final Progress Report July 83-Oct 85, Univ. of Surrey. MOD Ref - AT/2064/067 XRMat.

42. H P Boehm: Angew.Chemie.Int. 5 (6) 533 (1966).

43. V A Garten; D E Weiss: Austral.J.Chem. 8 68 (1955).

44. H M Hawthorne; G Baker; R H Bentall; H R Linger: Nature 227 946 (1970).

45. J S Murday; D D Dominguez: Proc. Electrochem.Soc. 1983 83-3 359.

46. W Watt: Carbon 10 121 (1972).

47. B Rand; R Robinson: Carbon 15 257 (1977).

48. K Wolf; R E Fornes; J D Memory; R D Gilbert: "Chemistry and Physics of Carbon Vol. 18", p 93. Pub. by Dekker Inc. (1982).

49. B F Jones: J.Mat.Sci. 6 1225 (1971).

50. J D Besenhard; H Mohwald; J J Nickl: Rev.Chim.Miner. 19 (4-5) 588 (1982).

51. E Fitzer; M Heymn: Chem.Ind. 21 663 (1976).

52. D J Johnson; G N Tyson: J.Phy.D.: Appl.Phys. 3 526 (1970).

53. C N Owston: J.Phys.D.: Appl.Phys. 3 1615 (1970).

54. H M Ezekiel: J.Appl.Phys. 41 5351 (1970).

55. P C Conor; C N Owston: Nature 223 1146 (1969).

56. R A Simon; S P Prosen: 23rd Ann.Tech.Conf., Soc. Plastics Ind., Reinf. Plast. Div., Section 16B (February 1968).

57. J C Goan; S P Prosen: in Interfaces in Composites, ASTM Special Tech.Publ. No 452, p3.

58. B Harris; P W R Beaumont; A Rosen: J.Mat.Sci. 4 432 (1969).

59. P M A Sherwood; C Kozlowski: "Studies on the Surfaces of Carbon Fibres" May 1986 Ref G-3819 Kansas Stat Univ.

60. Y Maeda; Y Okemoto; M Inagaki: J.Electrochem.Soc. 132 2369 (1985).

61. R C Bansal; P.Chhabra; B R Puri: Indian.J. of Chem. 19A 1149 (1980).

62. B D Sokolov; E P Smirnov; G P Markov; E I Belova; S.I. Kol'tsov: J. of App.Chem. of USSR 53 103 (1980).

63. O P Bahl; R B Mathur; T L Dhami: Proc. IUPAC, IUPAC Macromol. Symp. 28th 461 (1982).

64. J W Herrick; P E Gruber Jnr; F T Mansur: "Surface Treatments fo Fibr-ous Carbon Reinforcements" AFML-TR-66-178, Part I Air Force Mat.Lab. (July 1966).

65. C Kozlowski; P M A Sherwood: J.Chem.Soc. Faraday.Trans. 1 81 2745 (1985).

66. S Subbaro; P Vishnu Sharma; M K Mukherjee: Fundam.Appl.Electro-chem. Proc. Symp. 168 (1982).

67. E Fitzer; F V Sturm; R Weiss: Ext.Abstr.Prog-Bienn. Conf. Carbon 16th 494 (1983).

68. A Proctor; P M A Sherwood: Carbon 21 53 (1983).

69. P Ehrburger; J J Herque; J B Donnet: London Int. Conf. Carbon Graphite 4th 201 (1974).

70. E Theodoridou; J O Besenhard; H P Fritz: J.Electroanal.Chem. 122 67 (1981).

71. E Fitzer; R Weiss: Process Uses Carbon Fibre Reinf. Plast. 45 (1981).

CHAPTER 3

ELECTROCHEMICAL THEORY AND METHODS

Introduction

As has been previously mentioned, there are many different techniques which may be applied to provide information about the nature of the material under study. In the case of carbon fibre, these methods may be chemical, physical and/or spectroscopic but all provide valuable information and each has advantages and drawbacks over the others. However, since the purpose of this research is to investigate the nature of carbon fibre by electrochemical methods, no further discussion of other techniques will be entertained unless they can be applied in the electrochemical study undertaken.

Electrochemical techniques generally applied in the characterisation of materials, mainly provide information on the nature of the surface of the material. In the case of carbon fibre, it tends to be about the physical and chemical nature of the surface and the material's structural properties.

Electrochemical reactions involving the transfer of charge at an electrode/solution interface, such is the case with carbon fibre electrodes, fall into the general class of reactions known as heterogeneous processes. The kinetics of heterogeneous reactions are usually determined by a series of steps involving both transport through the solution and the transfer of charge at the interface.

Consider the simple electrochemical reaction shown below:-

$$O + Ne^{\ominus} \rightleftharpoons R \qquad (3.1)$$

This overall reaction involves several separate steps:

1. Transport of O from the bulk solution to the interface
2. Adsorption of O onto the surface
3. Charge transfer at the electrode to form R
4. Desportion of R from the surface
5. Transport of R from the interface to the bulk solution.

The reactions in steps 2 - 4 are generally known as the "activation" process whereas 1 and 5 are referred to as "mass transport" processes. As these reactions are sequential, the overall reaction rate is equal to the rates of the individual steps. In addition, under non-steady state or transient conditions the individual process rates are time-dependent. Analysis of this time dependence forms the foundation of transient electrochemical methods.

The time dependence can best be seen by examining a particular example. Consider reaction (3.1) under potentiostatic control. Initially the system is at equilibrium and the concentrations of O and R are uniform up to the interface, providing that double layer effects are ignored. Immediately on altering the potential from E_{eq} to a more negative value, by imposition of a potential step, the concentrations of O and R at the interface begin to decrease and increase respectively. This initiates the production of diffusion gradients in the solution close to the surface for both O and R as shown schematically in Fig.3.1 a).

Fig. 3.1

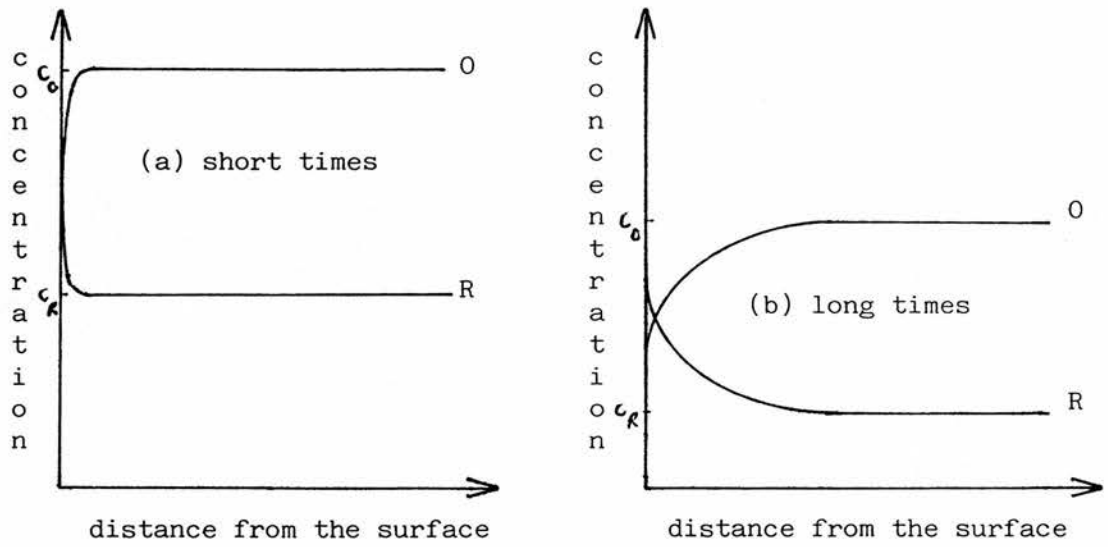

As time passes the concentration profiles extend further into the solution and the concentrations of O and R alter towards their steady state values (Fig.3.1 b).

On assumption that mass transport only occurs by semi-infinite linear diffusion, then the rates of the mass transport steps are dependent on the concentration gradients at the interface, in accordance with Fick's first law:

$$-\frac{i}{NFA} = J_O = -D_O \left(\frac{\partial C_O}{\partial x}\right)_{x=o} \qquad (3.2)$$

$$\frac{i}{NFA} = J_R = -D_R \left(\frac{\partial C_R}{\partial x} \right)_{x = o} \qquad (3.3)$$

where J is the flux normal to the surface in $mols^{-1}m^{-2}$, A the surface area and D the diffusion coefficient in m^2s^{-1}.

It can be seen from correlating Fig.3.1 and equations (3.2) and (3.3) that the rate of the mass transport steps, and therefore the current, decrease with them.

However, the rate of the reaction at the surface is given by

$$\frac{i}{NFA} = k_f C_{o(x = o)} \qquad (3.4)$$

where k_f is the potential-dependent rate constant and $C_{o(x = o)}$ the concentration of O at the interface.

Since k_f responds instantaneously to potential, unlike concentration, then the rate at t = o can be written:-

$$\left(\frac{i}{NFA} \right)_{t = o} = k_f C_o^{\,b} \qquad (3.5)$$

where $C_o^{\,b}$ is the bulk concentration of O.

Hence the rate constant k_f can be found, knowing the rate at t = o.

However, at longer duration the reaction rate is given by equation (3.4) where $C_{o(x = o)} < C_o^b$ and therefore, since the surface concentration cannot be directly measured, k_f cannot be determined.

This stated analysis shows that only at t = o are there no mass transfer effects present in the system. The goal of electrochemical transient methods is to produce theoretical expressions relating rate, current, to time to facilitate the removal of diffusion effects.

It is assumed for all these transient methods that the electrochemical cell dimensions are sufficiently large that the concentrations of the electroactive species at the electrode/electrolyte boundary remain constant throughout the duration of the experiment.

3.1 The Electrical Double Layer

The processes occurring at electrodes are closely related to the structure of the region generally known as the "double layer". This region is located in the electrolyte solution in close proximity to the electrode. As has been previously mentioned, the presence of the reactants is required in this region for the rate-determining step in an electrode process. The development of theoretical models representing the structure of the double layer has progressed steadily during the past century. Progression has been closely associated to advances in other disciplines, such as the Debye-Huckel[1] treatment of ionic atmospheres.

The first and most basic theoretical model for the electrical double layer was proposed by Helmholtz[2]. It suggested that at the surface there is simply a unimolecular layer of ions of opposite sign to the charge existing on the electrode, as shown in Fig.3.2 a). The electrical potential changes sharply from the surface of the electrode to the centre of the ionic layer. Gouy[3] and Chapman[4] both stated that the Holmholtz model was inaccurate since it neglected the Boltzman distribution of the ions in a varying potential field. The Gouy-Chapman treatment led to production of a model where there is an ionic-atmosphere type distribution with the potential decreasing more gradually through the diffuse layer formed.

Stern[5] further refined the double layer model by combining both the Helmholtz and the Gouy-Chapman models to consider the finite size of the ions present and the specific chemisorptive interactions between the ions and the electrode surface. The resultant model is shown schematically in Fig.3.2 b). The layer of positive ions is held at the surface by chemisorptive and electrostatic interactions. From the surface to the centre of this layer of ions is known as the Helmholtz layer; within this region there is a sharp drop in potential from ϕ_{su} to ϕ_1. Whereas in the region beyond the Helmholtz layer, known as the Gouy-Chapman or diffuse layer, there is a more gradual potential drop from ϕ_1 to ϕ_s, the potential in the bulk electrolyte solution.

Various additional refinements of the Stern model have been carried out to explain experimental deviations. In particular, Grahame[6] found that the effects of adsorbed anions on the potentials of mercury electrodes could not be adequately explained by using the Stern model. He therefore proposed the expanded model shown in Fig.3.2 c).

A potential drop from ϕ_{su} to ϕ_2 exists from the surface of the electrode to the centre of the layer of specifically adsorbed ions. In addition, there is a further drop to ϕ_1 at the inner boundary of the diffuse layer, where a layer of ions are separated from the surface by a layer of solvent molecules and are held not by chemisorption but by electrostatic forces. Lastly there is a potential drop over the diffuse layer from ϕ_1 to ϕ_s. The boundary at ϕ_2 occurs is known as the inner Helmholtz layer and where the potential is ϕ_1 is known as the outer Helmholtz layer.

Fig.3.2 Double Layer Models

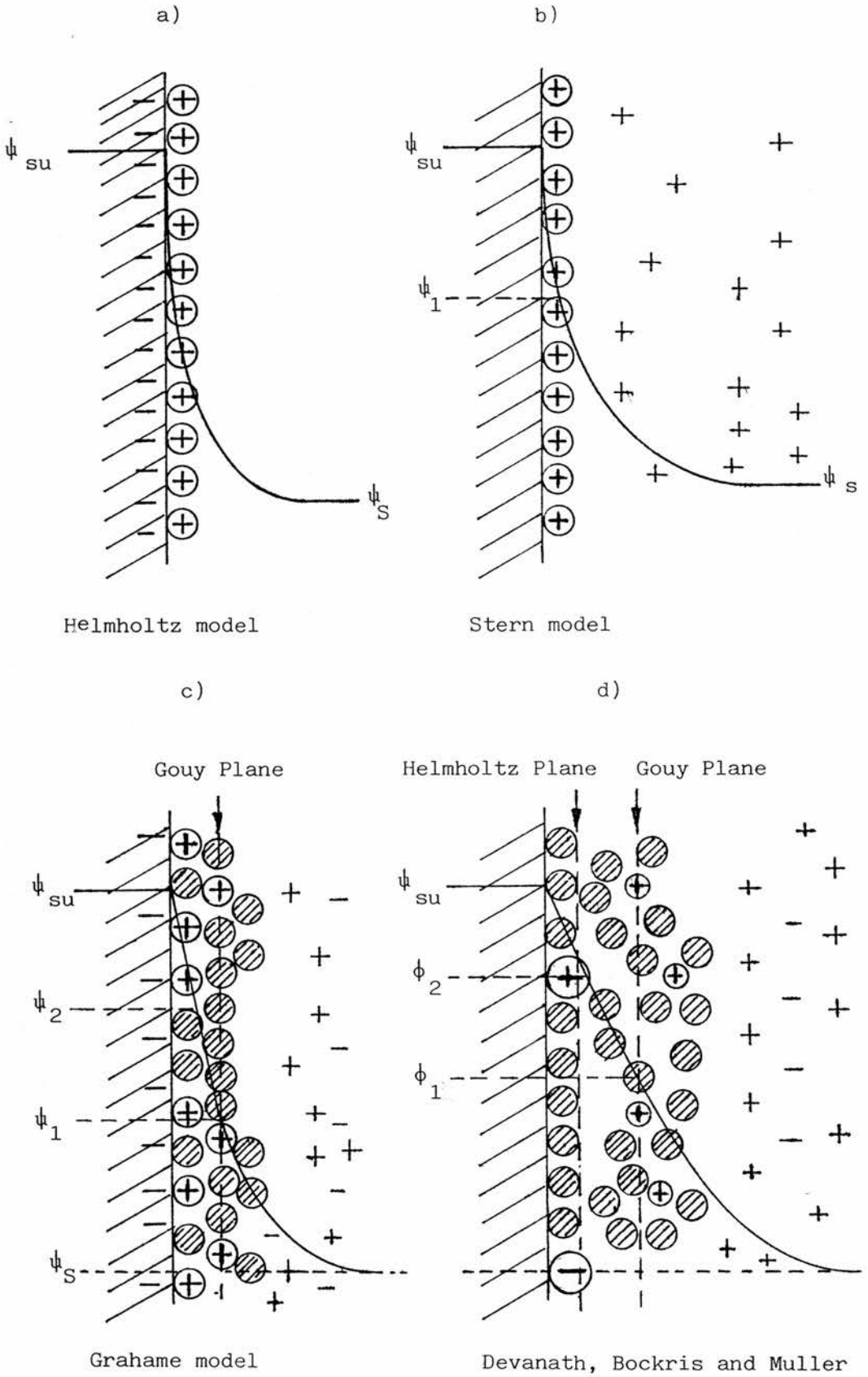

However even these modifications to the theoretical model were not adequate to explain all experimental results. Grahame[7] found that the double layer capacitance at mercury electrodes was generally independent of cation size, which is in conflict with the new model. In addition, the anion adsorption results indicated that the observed effects were related to the anion's degree of hydration instead of the bond strengths between anion and surface, as would be expected from the model.

A further modification to the model, shown in Fig.3.2 d), was introduced by Devenathan, Bockvis and Muller[8], to account for these and other discrepancies, which considered the adsorption of solvent molecules. It suggests that there is a layer of strongly adsorbed solvent molecules at the surface, which are held by charge-dipole interactions. It is thought that the specifically adsorbed anions are able to penetrate this solvent layer. The outer plane of of this solvent layer, at potential ϕ_2, is known as the Helmholtz plane. Adsorbed cations with their primary hydration shells are thought to remain outside this solvent plane; the plane through the centre of this layer of cations, at potential ϕ_1, is known as the Gouy plane. There is a further potential drop outside this Gouy plane from ϕ_1 to ψ_s over the diffuse layer. In the diffuse layer the population of ions of a given charge at any point from the surface is determined by the opposing effects of the electric field and thermal agitation.

As can be seen, the double layer model has already become reasonably complex however even this model has disregarded such effects as electrokinetics and electrode features such as porosity[12] and surface roughness[12]. Therefore should a more detailed treatment

of the double layer be required, it is suggested that the reader consult other works such as those of Delahay[19], Parsons[10] and Barlow[11].

Those factors which concern carbon fibre electrodes will be discussed later.

3.1.1 The Double Layer Capacitance

From a consideration of Fig.3.2 d), the double layer can be said to be made up of three distinct regions. The potential drop across the two inner regions closest to the electrode surface, known as the compact layer, is approximately linear whereas across the diffuse layer it tends to decay approximately exponentially with distance. The total potential drop across the interface can be written:-

$$\Delta_s^{su}\phi = (\psi_{su} - \phi_1) + (\phi_1 - \phi_2) + (\phi_2 - \psi_s) \qquad (3.21)$$

Differentiation of equation (3.21) with respect to the change on the electrode (q_{su}) and considering the definition of differential capacitance

$$C = \frac{dq}{d\phi} \qquad (3.22)$$

gives an equation for the total double layer capacitance in terms of the three contributing double layer regions.

$$\frac{1}{C_{dl}} = \frac{1}{C_{HP}} + \frac{1}{C_{GP}} + \frac{1}{C_{diff}} \qquad (3.23)$$

The above analysis suggests that the electrical double layer can be considered as a series combination of three capacitances and also that the value of C_{dl} is principally determined by the value of the smallest of the three double layer capacitances. However, this electrical representation of the electrolyte-electrode interface can only be applied accurately up to a point, since

the double layer capacitance is in general dependent on the potential drop across the interface. In spite of this, the analogy can be productive in the analysis of the electrode's response to various perturbations.

3.2 Kinetics of Charge Transfer in the Steady State

3.2.1 Simple Charge Transfer Reactions

The activated complex theory[13,14] states that for a simple charge transfer process the forward and reverse rate constants are of the form

$$k_f = k_f^o \exp\left(\frac{-\beta nFE}{RT}\right) \tag{3.6}$$

$$k_b = k_b^o \exp\left(\frac{(1-\beta)nFE}{RT}\right) \tag{3.7}$$

where β is the cathodic transfer co-efficient.

k_f^o and k_b^o are not directly dependent on E but are functions of the standard Gibbs activation energies and the electrical potentials at the initial states.

The net current passing through an external circuit is

$$i = i_f - i_b \tag{3.8}$$

which apon substitution of (3.4) gives

$$i = nFA\left(k_f C_{o(x=o)} - k_b C_{R(x=o)}\right) \tag{3.9}$$

which yields:-

$$i = nFA\left(C_{o(x=o)}k_f^o \exp\left(\frac{-\beta nFE}{RT}\right) - C_{R(x=o)}k_b^o \exp\left(\frac{(1-\beta)nFE}{RT}\right)\right) \qquad (3.10)$$

At equilibrium ($E = E_e$), the total current is zero and hence no concentration gradient exists at the interface:-

$$C_o^b k_f^o \exp\left(\frac{-\beta nFE_e}{RT}\right) = C_R^b k_b^o \exp\frac{(1-\beta)nFE_e}{RT} = \frac{i_o}{NFA} \qquad (3.11)$$

where i_o is the exchange current

$\therefore$

$$i = i_o\left(\left(C_{o(x=o)}/C_o^b\right) \exp\left(\frac{-\beta nF\eta}{RT}\right) - \left(\frac{C_{R(x=o)}}{C_R^b}\right)\exp\left(\frac{(1-\beta)nF\eta}{RT}\right)\right) \qquad (3.12)$$

---

where $\eta = E-E_e$ and is known as the overpotential.

Equation (3.12) is particularly important, since it relates the current to both the surface concentrations and the overpotential.

A simplified form can be produced, if k^o is sufficiently small that no appreciable concentration gradients are present at the surface, then $C_{o(x=o)} \approx C_o^b$ and $C_{R(x=o)} \approx C_R^b$.

$$\therefore$$

$$i = i_o \left(\exp\left(\frac{-\beta nF\eta}{RT} \right) - \exp\left(\left(\frac{(1-\beta)nF\eta}{RT} \right) \right) \right) \qquad (3.13)$$

This expression is frequently applied in the analysis of surface-controlled reactions under transient conditions and is generally known as the Bulter-Volmer equation.

3.2.2 Complex Charge Transfer Reactions

A comprehensive discussion of the kinetics of complex charge transfer processes is not possible within the restrictions of this present work. However, it is necessary to discuss the techniques applied in the analysis of complex process kinetics to allow familiarisation with the basic principles before trying to explain the the transient responses of electrochemical cells. Much more detailed discussions of the field are given by Parsons[15], Laidler[16] and Vetter[17].

The kinetics of complex reactions can be adequately investigated by applying one of two closely related methods: the pre-equilibrium technique or the steady-state method. In the pre-equilibrium method the assumption made is that all the steps before the rate-determining step are said to be in equilibrium. Hence the concentrations of reactants and products for each of these preceding steps are related by equilibrium expressions which are independent of the kinetic reaction parameters. Therefore, it is possible to deduce an equation for the reactant concentration in the rate-determining step in terms of the equilibrium constants of the previous reactions. The differential rate law is then easily established.

The steady-state theory suggests that the concentrations of all intermediates in the reaction scheme are not dependent on time. From this supposition, it is possible to produce applicable expressions for the intermediate concentrations in terms of the kinetic parameters involved in their formation and destruction. The steady-state theory is the more general and therefore its use in complex reaction mechanism analysis will be illustrated.

In the illustrated example it is assumed that the process is a two-step reaction where, firstly, a reactant in the solution is reversibly adsorbed onto the electrode surface and then it reacts with another solution-transported species in an irreversible electrochemical reaction to form the products of the reaction.

$$O + e^{\ominus} \underset{k_b}{\overset{k_f}{\rightleftharpoons}} I \qquad (3.14)$$

$$I + X + e^{\ominus} \xrightarrow[k_{f'}]{} R \text{ (rate-determining)} \qquad (3.15)$$

If θ is the degree of adsorption coverage of the active sites on the surface then:-

$$\frac{d\theta}{dt} = k_f C_{o(x = o)} (1-\theta) - k_b \theta - k_{f'} \theta C_{X(x = o)} \qquad (3.16)$$

But at the steady state $\frac{d\theta}{dt} = 0$

$$\therefore \quad \theta = \frac{k_f C_{o(x = o)}}{k_f C_{o(x = o)} + k_b + k_f' C_{x(x = o)}} \qquad (3.17)$$

The total current across the interface is

$$i = \sum_j i_{f,j} - \sum_j i_{b,j} \qquad (3.18)$$

$$\therefore \quad i = AF (k_f C_{o(x = o)}(1-\theta) + k_{f'} C_{X(x = o)}\theta - k_b\theta) \qquad (3.19)$$

On substitution of (3.17) for θ, the required equation for current under steady-state conditions is generated:-

$$i = \frac{2AFk_f k_{f'} C_{o(x = o)}}{\left(k_f + k_b + k_{f'} C_{X(x = o)} \right)} \qquad (3.20)$$

It should be noted that equation (3.19) is the general form and it does not require the steady-state assumption. Therefore equation (3.16) can be solved for θ as a function of time for the appropriate boundary conditions and replaced in (3.19) to produce the transient response of the system.

3.3 Electrode Surface Heterogeneity

The expressions, (3.6) and (3.7), for the rate constants in simple charge transfer reactions only hold for the adsorption/desorption reaction

$$M + A^{\ominus} \underset{k_b}{\overset{k_f}{\rightleftharpoons}} MA_{ads} + e^{\ominus} \qquad (3.24)$$

when the Gibbs activation energy is said to be independent of the fraction (θ) of discharged sites covered by A_{ads}. This is the assumption made when applying Langmuir adsorption statistics[13].

However, a more exact model for electrochemical adsorption may be produced by assuming that the Gibbs activation energy for forward and reverse processes is dependent on the coverage θ[13]. Numerous factors are responsible for the generation of this dependence, including the presence of a distribution of adsorption sites of different energies over the electrode surface and lateral interaction between adsorbed elements. If it is assumed that the dependence is linear then equations (3.6) and (3.7) can be modified to:-

$$k_f = k_f^o \exp\left(\left(\frac{(1-\beta)nFE}{RT} \right) - g_f \theta \right) \qquad (3.25)$$

$$k_b = k_b^o \exp\left(\frac{-\beta nFE}{RT} + g_b \theta \right) \qquad (3.26)$$

---

where g_f and g_b are the heterogeneity constants.

3.4 Electrochemical Adsorption and Pseudocapacitance

For an electrochemical adsorption process such as that shown in equation (3.24), the charge connected with the deposited phase is

$$q = \gamma \theta \tag{3.27}$$

where γ is the charge relating to a complete monolayer.

The variation of charge with potential produces what is known as a pseudocapacitance

$$C_\phi = \gamma \left(\frac{d\theta}{dE} \right) \tag{3.28}$$

The pseudocapacitance is generated actually on the electrode surface whereas the double layer capacitance is related to space charge due to ion movements in the electrolyte near to be electrode surface.

Again consider the reaction (3.24)

$$\frac{d\theta}{dt} = k_f \ (A) \ (1-\theta) - k_b \theta \tag{3.29}$$

but at equilibrium

$$\frac{\theta}{1 - \theta} = \left(\frac{k_f}{k_b} \right) \left(A^{\theta} \right) \tag{3.30}$$

on introduction of the rate constant expressions for heterogeneity:-

$$\frac{\theta}{1-\theta}\exp(g\theta) = K^{o}\exp\left(\frac{nFE}{RT}\right)(A^{\theta}) \qquad (3.31)$$

where $g = g_f + g_b$ and $K^{o} = k_f^{o}/k_b^{o}$

Therefore the pseudocapacitance in terms of θ is

$$C_\phi = \nu\left(\frac{nF}{RT}\right)\left(\frac{\theta(1-\theta)}{(1+g\theta(1-\theta))}\right) \qquad (3.32)$$

However, for the Langmuir model $g_f = o$ and $g_b = o$

$$\therefore\ C_\phi^{L} = \nu\left(\frac{nF}{RT}\right)\theta(1-\theta) \qquad (3.33)$$

by comparing the last two expressions:-

$$\frac{1}{C_\phi} = \frac{1}{C_\phi^{L}} + \frac{RT\,\eta}{\nu\,nF} \qquad (3.34)$$

As can be seen from above, the pseudocapacitance in general terms can be represented by a series combination of two capacitances. As $g \longrightarrow \infty$ then C_ϕ is determined by the heterogeneity of the electrode surface. A comprehensive discussion of pseudocapacitance can be found in the literature[13,18].

3.5 3-Electrode Cell Theory

In all electrochemical characterisation experiments performed a three-electrode cell, similar to that shown in Fig.4.1, was used. The three-electrode cell was preferred to the normal two-electrode cell because the ohmic potential drop generated across the electrolyte solution between the reference and working electrodes was known to be high. This potential drop may be minimised by addition to the cell of a third electrode, known as a counter electrode. The nature of the counter electrode is unimportant since its electrochemical properties do not affect the behaviour of the working electrode. However addition of the third electrode does not remove the potential drop completely since this may only be accomplished by placing the reference electrode exactly at the surface of the working electrode. The remaining potential drop is known as the "uncompensated solution resistance potential drop (iR_u)".

Luggin Capillary

This may be reduced, but not removed completely, by use of a modified reference electrode which contains a Luggin capillary. The Luggin allows close placement of the reference electrode to the working, as shown in Fig.4.1. When the Luggin capillary is placed in the potential gradient generated by current flowing between the counter and working electrodes, it behaves like the contact in a slide wire potentiostat. Then as the potentiostat maintains a constant potential (E) between the Luggin and working, the actual E across the interface is in error by the new $I - R_u$.

The optimum distance between the Luggin and the working electrode was shown by Barnatt[19] to be approximately 2d, where d is the outside diameter of the Luggin. The dependence of iR_u on distance can be calculated for simple electrode geometries if it is assumed that the specific conductivity, κ, is constant.

In all cases, the potential drop is proportional to i_{cd} so the correction will be the dominant effect in transients with short times when there is large instantaneous current flow. If the Luggin is placed too close then observed transient, following the potential step, will display severe imaging (i.e. it will oscillate). Transients should not be analysed in this region. Other sources of errors at short time scales are double layer charging, $R_u C_{dl}$, and stray capacitances to ground. Further discussion of iR drop in relation to Luggin capillaries can be found in the literature[20,21].

3.6 Cyclic Voltammetry

The complete electrochemical behaviour of a system may be obtained by recording the individual current-time plots for a series of different potentials. This produces the three-dimensional i-t-E surface but it is extremely time-consuming and relatively unproductive. Much more information can be obtained from a single experiment, by sweeping the potential with time and recording the resultant i-E curves. In essence, this is a qualitative method for traversing the i-t-E surface. The Normal procedure is for the potential to be linearly varied with time, by using a function generator to ramp the potential at a particular scan rate. Convention is to record the current as a function of potential. The technical name for this technique is Linear Sweep Voltammetry (LSV). A typical LSV curve is shown in Fig.3.3 a) for a simple redox species A.

If the scan is begun at a potential well positive of the standard electrode potential, E^{o}, for the reduction, then initially only non-faradaic currents flow. When the electrode potential approaches the region of E^{o} the reduction of species A to $A^{\ominus}$ begins and faradaic current starts to flow. As the potential of the system continues to become more negative, the surface concentration of A decreases and the current increases to keep the surface concentration "correct" for the Nernst equation[1].

$$E = E^{o} + \frac{RT}{nF} \ln \left(\frac{(A)}{(A^{\ominus})} \right) \qquad (3.35)$$

As the potential moves past E^{o}, the surface concentration of A falls too close to zero, mass transfer of A to the surface reaches a maximum rate and then declines as the depletion effect is seen. This series of steps is observed as a peak on the i-E curve.

Cyclic Voltammetry is what is known as a reversal technique for LSV. In this case, instead of only sweeping the potential in one direction, the potential is swept between two limits, in both the cathodic and anodic directions producing an i-E curve such as that shown in Fig.3.3 b). The waveform produced by the function generator in this instance is triangular instead of a ramp.

Again consider the simple redox species A. On reaching the cathodic potential sweep limit, suddenly the scan direction is reversed and is now in a positive potential direction. In the vicinity of the electrode there is now a large concentration of oxidisable $A^{\ominus}$ anion. As the potential approaches then passes E^{o}, the chemical gradient at the electrode surface grows more and more favourable to the neutral species A. Therefore the abundant $A^{\ominus}$ is oxidised to A and an anodic current flows producing the observed peak on the i-E curve in Fig.3.3 b).

Fig.3.3 a) i-E Curves for Sweep Voltammetry

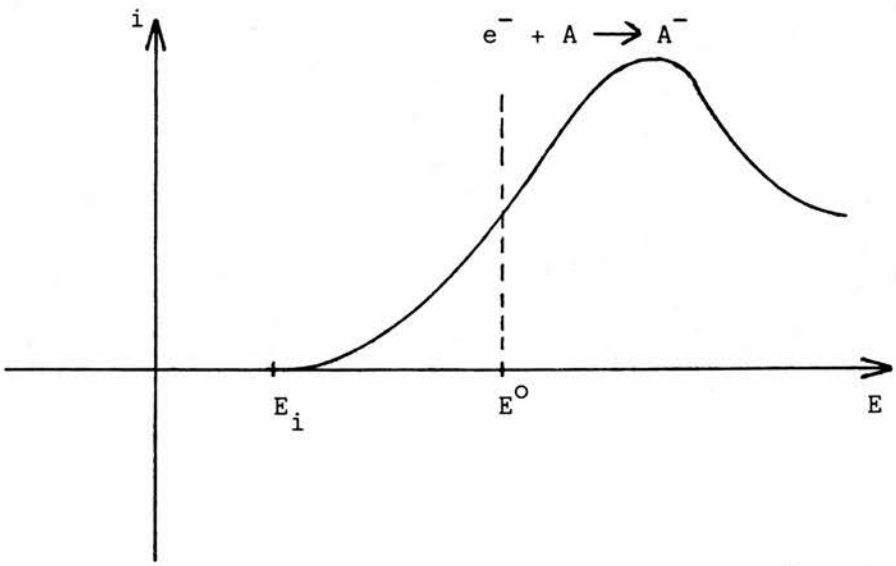

LSV

Fig.3.3 b)

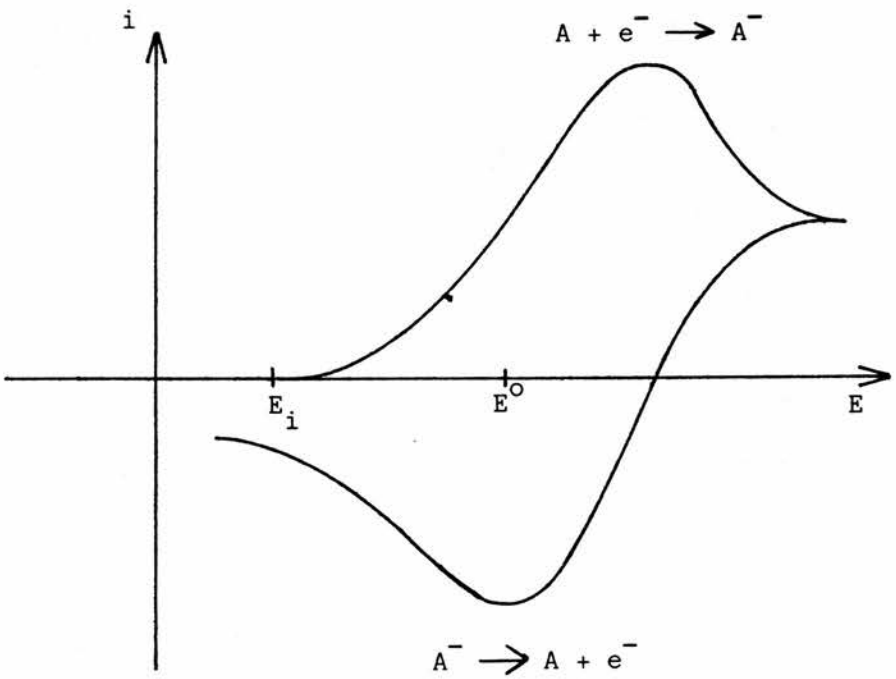

Cyclic

3.7 Galvanostatic Techniques

Galvanostatic techniques essentially involve passing a constant current and measuring the potential as a function of time. In these experiments, it was assumed that the electrode area to solution volume ratio was small and that semi-infinite diffusion theory could be applied. The experimental method is carried out by applying the controlled current between the working and counter electrodes with a constant current source, known as a galvanostat, and determining the potential between the working electrode and the reference electrode, which is usually recorded using a chart recorder as shown in Fig.3.4 below.

Fig.3.4

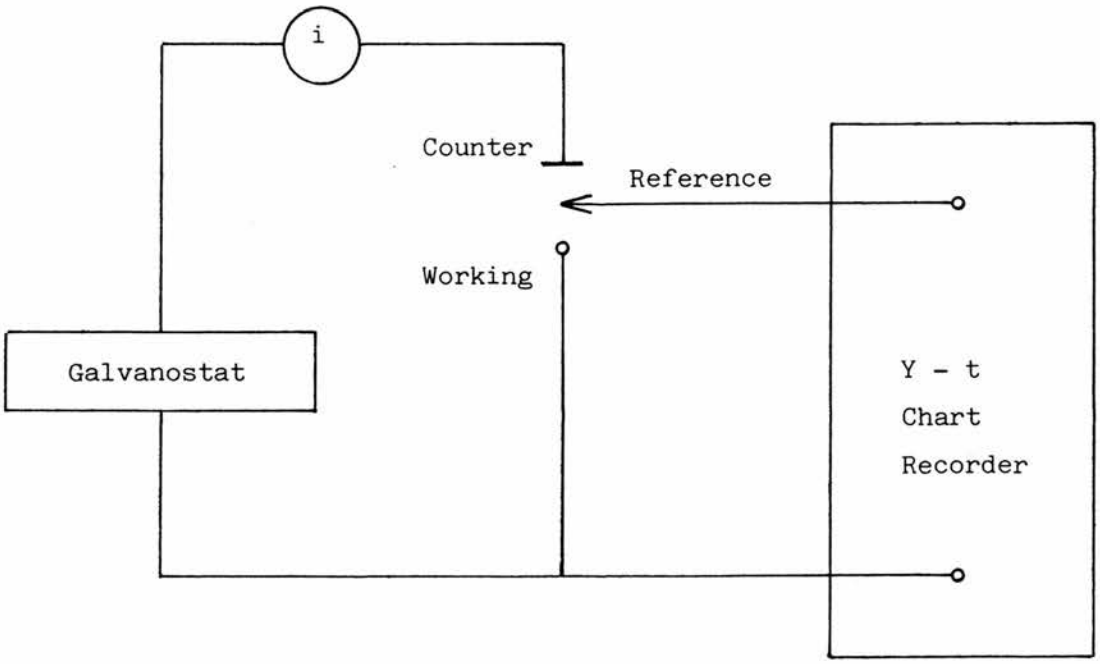

These electrochemical techniques are also known as chronopotentiometric methods, due to the potential being recorded as a function of time.

3.7.1 Galvanostatic Capacitance Measurement Method

Consider the electrochemical cell to be represented electrically by an equivalent circuit containing a resistor and capacitor in parallel, in series with a resistor as is shown in Fig.3.5 below:-

Fig.3.5

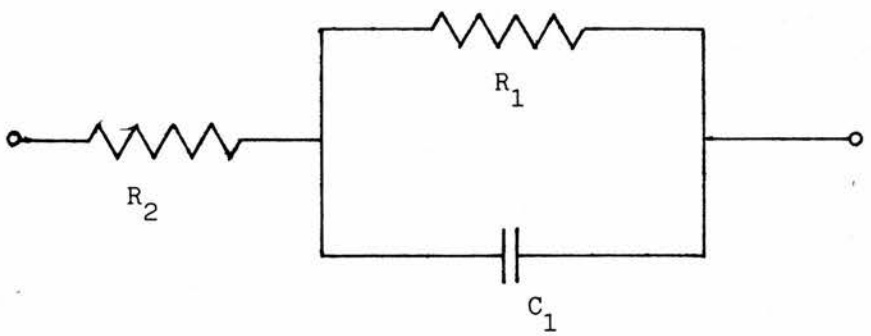

where

R_2 is the solution resistance

R_1 is the charge transfer resistance

C_1 is the double layer capacitance

Since addition of the series resistor R_2 does not significantly affect the circuit, only adding an additional constant voltage step, it can be simplified to just the parallel unit.

Consider the simplified circuit in more detail with respect to a galvanostatic experiment.

Fig.3.6

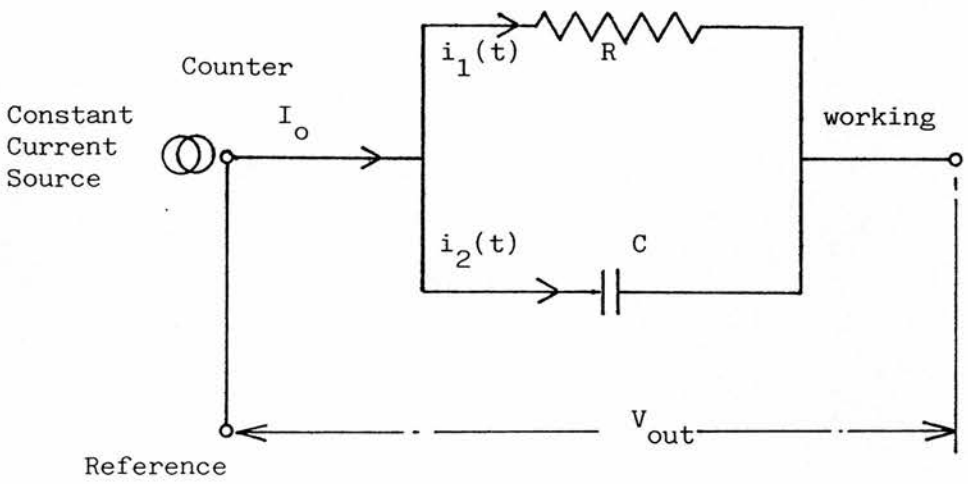

I_o = initial current applied

$$\therefore \quad I_o = i_1(t) + i_2(t) = I_C + I_R \tag{3.36}$$

where

$i_1(t)$ = current flowing across the resistor

$i_2(t)$ = current flowing through the capacitor

$$\therefore \quad i_1(t) = \frac{E(t)}{R} \quad \text{and} \quad i_2(t) = \frac{dq}{dt} = C.\frac{dE}{dt} \tag{3.37}$$

$$\therefore \quad I_o = \frac{E(t)}{R} + C.\frac{dE}{dt} = \frac{E(t)}{R} + C.\frac{dE}{dt} \tag{3.38}$$

$$\therefore \quad E(t) = I_o R \left(1 - \exp\left(-t/RC\right)\right) \tag{3.39}$$

Equation (3.39) must be rearranged to produce a linear equation with the gradient terms containing the capacitance.

$$\therefore \quad \ln\left(1 - \frac{E}{I_o R}\right) = -\frac{1}{RC}.t \tag{3.40}$$

But since the value R is unknown, it must be replaced by E_{max}/I_o.

$$\therefore \quad \ln\left(1 - \frac{E(t)}{E_{max}}\right) = -\frac{I_o}{E_{max}.\ C}.\ t \tag{3.41}$$

The equation (3.41) is now in the form $y = mx + c$. Hence, if a plot of $\ln\left(1 - \frac{E(t)}{E_{max}}\right)$ versus t is done, then the double layer capacitance can be calculated from the gradient.

3.8 A.C. Impedance Techniques

3.8.1 Introduction

The reactions occurring at electrodes are heterogeneous chemical processes, their rates being controllable by altering the electrical potential of the electrode. On application of Faraday's Law, the electrode reaction rate can be simply measured as a current density and therefore electrode reaction's rate constants are more easily obtainable than those for common heterogeneous chemical processes.

The chemistry of electrode surfaces and hence an understanding of why differing reactions have different rates requires study. However, in fact most efforts have concentrated on the development of techniques for the measurement of kinetic parameters. These techniques have been refined to a high degree of perfection but the correlation of results from different methods has sometimes proved unsatisfactory due to the great difficulty of bringing an electrode surface to a well-defined state.

For the study of simple processes one only requires to use steady-state techniques but for more complex electrochemical systems, it is necessary to apply non-steady state methods. Application of these techniques depends on principles similar to those which warrant relaxation methods used at the equilibrium state in kinetic studies. By disturbing the reaction from the steady-state, on application of a perturbation to the electrochemical system, this enables the system to relax to a different steady state. Since

the various fundamental processes alter at different rates, the overall process may be dissected by analysing the system's response to the perturbation.

Certain transient methods are widely applied because they are expedient for producing kinetic parameters when the mass transport is tedious. However on interaction of complex heterogenerous reactions with mass transport, time analysis of the transients produces very inaccurate results when attempting to obtain a reaction mechanism, and analysis by frequency is more efficient.

In recent years there has been much effort to measure the rate constants of fast electrode processes, applying shorter and steeper pulses or sine waves of high frequency in order to suppress diffusion polarisation. On comparison, accounting for any pulse being described as a sum of sine waves in a Fourier integral, the problems due to the pulse method, both mathematical and instrumental, can be avoided by using a high frequency sine wave which eliminates all the lower frequency components associated with pulses.

Sine wave methods have an additional advantage of obtaining information from the phase angle as well as the amplitude therefore allowing an internal check or consideration of an additional parameter as unknown. These methods are also preferable experimentally since signal generation and response detection, by a tuned amplifier, are relatively simple due to advances made in instrumentation in recent years.

There are several main a.c. techniques which may be applied in the impedance measurement of electrochemical cells. Although these methods differ markedly in their instrumentation and method of data collection, they are similar in one respect; in that the components of the impedance are determined and then applied to give information about the electrochemical processes involved. Before the mechanics of these methods can be discussed, it is necessary that one has an accurate description of the kinetic and electrical laws which govern the interface. Therefore an understanding of basic a.c. theory and the general concepts of electrochemical impedance is required.

3.8.2 Simple A.C. Theory and its Application to Circuits

A completely sinusoidal voltage can be expressed as

$$E = E_o \sin(wt) \qquad (3.42)$$

where E is the observed voltage

w = angular frequency = $2\pi f$

E_o = amplitude of the voltage

Consider E as a rotating vector or phasor quantity, as shown in Fig.3.7 a), E is the component of the phasor projected on some particular axis at any time.

Fig.3.7 a)

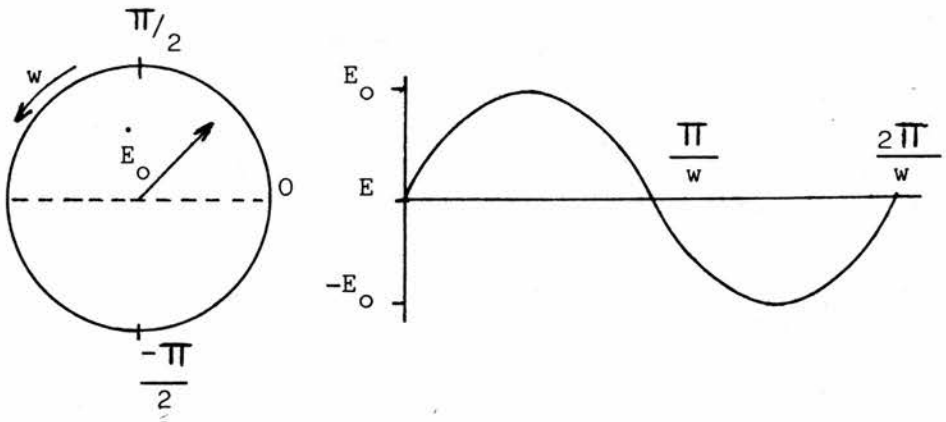

It is often required that the relationship between two related sinusoidal signals, such as current I and voltage E, is considered. Each signal is represented as a separate phasor, $\dot{I}_o$ or $\dot{E}_o$, rotating at the same frequency. These will generally not be in phase and the phasors will be separated by a phase angle ϕ, as can be seen in Fig.3.7 b).

Fig.3.7 b)

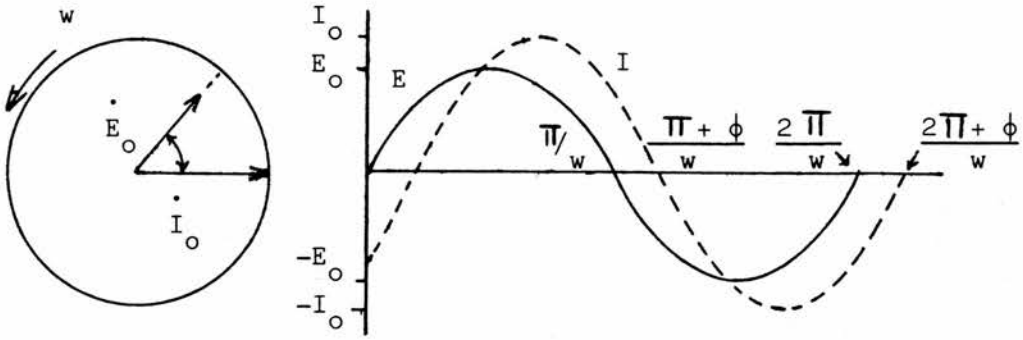

One of the phasors is taken as a reference signal, often $\dot{E}_o$, and ϕ is measured with respect to it. It can be seen that the current lags the voltage. This may be expressed generally as

$$I = I_o \sin (wt + \phi) \qquad (3.43)$$

Since the relationship between the two phasors at the same frequency is constant then the phase angle is also constant. Hence the phasor representation may be disregarded and the quantities plotted as vectors having a common origin and separated by the appropriate phase angle.

Let us consider the application of a.c. theory to several simple electrical circuits.

1. A Resistor

Ohm's Law holds in a.c. theory as it does in d.c. theory

$$\therefore \quad \dot{I}_o = \frac{\dot{E}_o}{R} \quad \text{and} \quad \phi = o$$

$\dot{E}_o \longrightarrow \quad \dot{I}_o \longrightarrow$ and

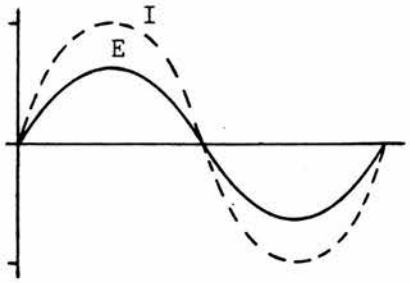

$$I = {}^{E}/_{R} \sin(wt) \tag{3.44}$$

2. A Capacitor

$$I_c = C\left(\frac{dE}{dt}\right) \qquad I = wCE\cos(wt) \tag{3.45}$$

$$I = \frac{E}{X_c} \sin(wt + \pi/2) \tag{3.46}$$

where $X_C = \frac{1}{wC}$ and is known as the capacitive reactance

The phase angle in this case is $\pi/2$

Now the vector diagram may be expanded, as shown in Fig.3.8, into a plane, since I leads E by $\pi/2$. It is now necessary to introduce complex number notation to maintain the linearity of the vector components

Fig.3.8

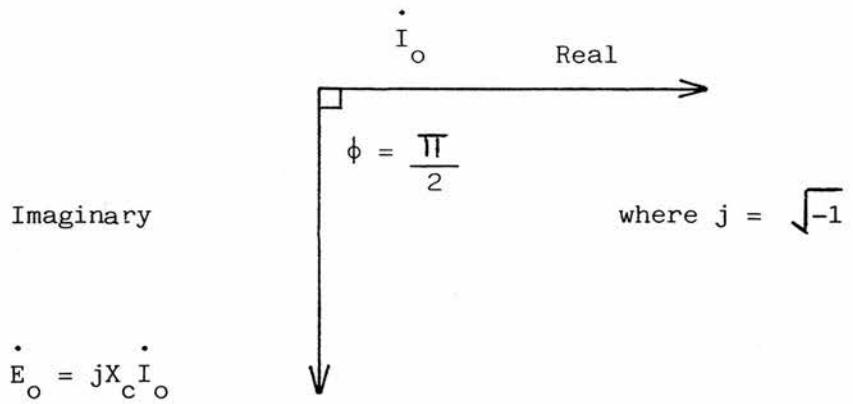

The capacitive reactance, in this case, is frequency dependent, unlike the resistance. Both the "Imaginary" and "Real" components are real, in the sense that they are measurable by the phase angle.

In all circuit analysis, it is advantageous to plot the vectors $\dot{I}_o$ and $\dot{E}_o$ as is shown above.

3. A Resistor and Capacitor in Series

According to Kirchoff's Laws, the total voltage E applied across the components is the sum of the individual component voltages.

$$\therefore \quad E_T = E_R + E_c \tag{3.47}$$

$\therefore$ In vector terms:-

$$\dot{E}_{oT} = \dot{E}_{oR} + \dot{E}_{oc} = \dot{I}_o R - jX_c\dot{I}_o \tag{3.48}$$

$$\therefore \dot{E}_{oT} = \dot{I}_o (R - jX_c) = \dot{I}_o \dot{Z} \tag{3.49}$$

where $\dot{Z}$ = total impedance of the circuit

This impedance vector has a modulus $|Z|$ and a phase angle ϕ, as shown in Fig.3.9.

$$|z| = (R^2 + X_c^2)^{\frac{1}{2}} \quad \text{and} \quad \tan \phi = \frac{1}{wRC} \tag{3.50}$$

Fig.3.9

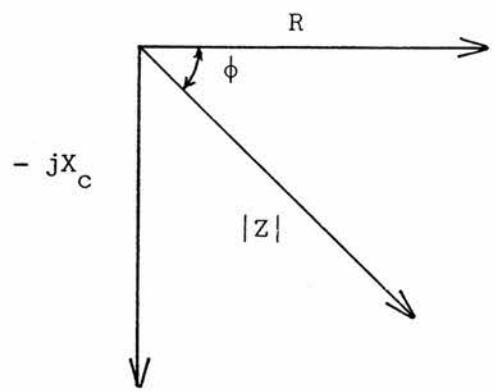

The total impedance can be represented by a combination of the "real" (Z') and the "Imaginary" (Z") components.

$$\therefore Z_T = Z' - jZ'' \tag{3.51}$$

where $Z' = R$ and $Z'' = \frac{1}{wC}$, in this case.

This new definition of impedance gives rise to a graphical representation, as is shown in Fig.3.10, which is often useful for gaining insight into the behaviour of the circuit with respect to a varied parameter, such as frequency. The components Z" and Z' are plotted against each other for differing values of the parameter.

Fig.3.10

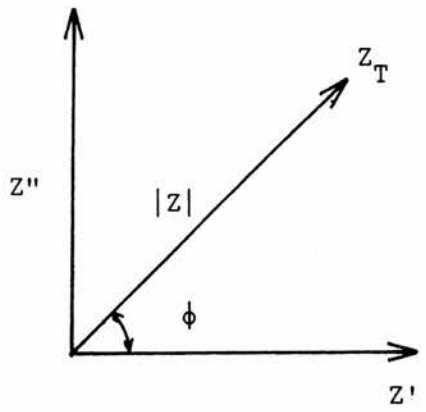

This type of diagram is often known as an Argand diagram.

More complex circuits may be analysed using this method by combining the electrical components according to the electrical suming rules. Note that impedances are combined in a similar fashion to resistances.

i.e. $R_T = R_1 + R_2 + \ldots\ldots\ldots\ldots$) Elements in Series

$$\frac{1}{C_T} = \frac{1}{C_1} + \frac{1}{C_2} + \ldots\ldots\ldots\ldots$$) Elements in Series

$$\frac{1}{R_T} = \frac{1}{R_1} + \frac{1}{R_2} + \ldots\ldots\ldots\ldots$$) Elements in Parallel

$C_T = C_1 + C_2 + \ldots\ldots\ldots\ldots$) Elements in Parallel

For example, consider the case of a resistor in parallel with a capacitor.

$$\therefore \quad \frac{1}{Z_T} = \frac{1}{Z_1} + \frac{1}{Z_2} \qquad (3.52)$$

where

$$Z_1 = R \text{ and } Z_2 = -j \cdot \frac{1}{wC}$$

$$\therefore \quad \frac{1}{Z_T} = \frac{1}{R} + jwC = \frac{1 + jRwC}{R} \tag{3.53}$$

$$Z_T = \frac{R}{1 + jwRC} \tag{3.54}$$

$$\therefore \quad Z_T = \frac{R - jwR^2C}{1 + R^2w^2C^2} \tag{3.55}$$

$$\therefore \quad Z_T = \frac{R}{1 + R^2w^2C^2} - j\,\frac{R^2wC}{1 + R^2w^2C^2} \tag{3.56}$$

Real Z' Imag. Z"

where

$$Z' = \frac{R}{1 + R^2w^2C^2} \quad \text{and} \quad Z'' \; \frac{R^2wC}{1 + R^2w^2C^2} \tag{3.57}$$

These quantities can then be plotted to show the impedance response to the variation of frequency of the circuit under study.

3.8.3 General Concepts of Electrochemical Impedance

The response of an electrochemical system to a perturbation from the steady state can be described in two distinct ways depending on whether the system exhibits linear or non-linear behaviour.

Linear System Analysis[22]

The response y(t) of a linear system to a perturbation x(t) is determined by

$$b_o \frac{d^n y(t)}{dt^n} + b_1 \frac{d^{n-1} y(t)}{dt^{n-1}} + \ldots\ldots b_n y(t) =$$

$$a_o \frac{d^m x(t)}{dt^m} + a_1 \frac{d^{m-1} x(t)}{dt^{m-1}} + \ldots\ldots a_m x \qquad (3.58)$$

$\therefore$ if $x(t) = A \sin(wt)$ (3,59)

then the response, $y(t) = B\sin(wt + \phi)$ (3.60)

and therefore a transfer function can be defined

$$H(w) = |H(w)|e^{j\phi} \qquad (3.61)$$

where

$|H(w)| = B/A$ and $|H|$ and ϕ are the modulus and phase angle of the transfer function.

Now if x(t) is the current and y(t) the voltage, then H(w) is the impedance. However if these are reversed then H(w) will be the inverse impedence, known as Admittance (Y).

$\therefore$ If the inverse Fourier transform, h(t) is considered

$$h(t) = \mathcal{F}^{-1}(H(w)) \tag{3.62}$$

then

$$y(t) = \int_{-\infty}^{+\infty} h(\theta)x(\theta-t)d\theta \tag{3.63}$$

In the case where x(t) is a Dirac impulse i.e. a Fourier transform of white noise

$$y(t) = \int_{-\infty}^{+\infty} h(\theta)\,\delta(\theta-t)d\theta \equiv h(t) \tag{3.64}$$

hence h(t) is known as the impulse response and may be measured using white noise, as in the case of impedance determination by computer methods[23].

In theory, any kind of perturbing signal x(t); whether it be white noise, step, impulse or sine wave, can be used to determine the value of H(w) and hence the impedance since equation (3.63) is equivalent to

$$Y(w) = H(w)\,X(w) \tag{3.65}$$

in the frequency domain.

The impedance Z(w) of an electrochemical interface, as has been previously stated, is a combination of the "real" and "imaginery" parts of the total impedance.

$$\therefore \quad Z(w) = ReZ + jImZ \qquad (3.66)$$

Non-Linear System Analysis

When an external energy source is used to perturb the interface from equilibrium, a flow of charge and matter occurs at the interface. This is caused by

1. Electrochemical reactions, which allow charge transfer between the electrolyte and the electrode.

2. The electric and chemical potential gradients which allow mass transport to and from the interface.

The laws which control these processes assign to the system a non-linear behaviour which in some cases can be very pronounced[24,25].

The behaviour of a non-linear system can be completely described in linear terms if for every point of the steady-state profile the equivalent linear expressions are known.

Experimentally, the impedance of an electrochemical cell can be measured about a given polarisation potential by using a very small amplitude perturbing signal.

Therefore superimposition of a small amplitude sine wave $\Delta E \sin(wt)$ on a d.c. polarisation potential E_o and measurement of the system's impedance response will produce an accurate picture of the electrochemical interface of the cell. This idea is the basis of impedance studies using a Frequency Response Analyser combined with an Electrochemical Interface, which are carried out in this project.

3.8.4 Historical Development

In general terms an electrochemical cell is basically an impedance to a small sinusoidal signal and therefore it should be possible to represent its behaviour by an equivalent circuit of electrical components that pass current with the same amplitude and phase angle as the cell, for a given perturbation.

Sluyters[26] was first to introduce the use of complex impedance plane for the analysis of electrochemical reactions. However, initial investigations of complex electrochemical processes were carried out by Dolin and Erschler[27] on the adsorption of hydrogen on a platinum electrode and the equations derived describe the electrode impedance in terms of a resistance and a capacitance in parallel. Randles[28], however, examined fast metal/metal ion and redox reactions where the time-arranged concentrations at the electrode surface obeyed the Nernst equation. Using the above assumptions it was determined that the impedance can be represented by a capacitance (C_s) and resistance (R_s) in series, where:-

$$R_s = \frac{RT}{n^2F^2c}\left\{\left(\frac{2}{wD}\right)^{\frac{1}{2}} + \frac{1}{k}\right\} \qquad (3.67)$$

$$C_s = \frac{n^2F^2c}{RT}\left(\frac{D}{2w}\right)^{\frac{1}{2}} \qquad (3.68)$$

where

c = concentration

D = diffusion co-efficient

k = rate constant

This network can be represented, Fig.3.11, by what is known as the Randles' equivalent circuit.

Fig.3.11

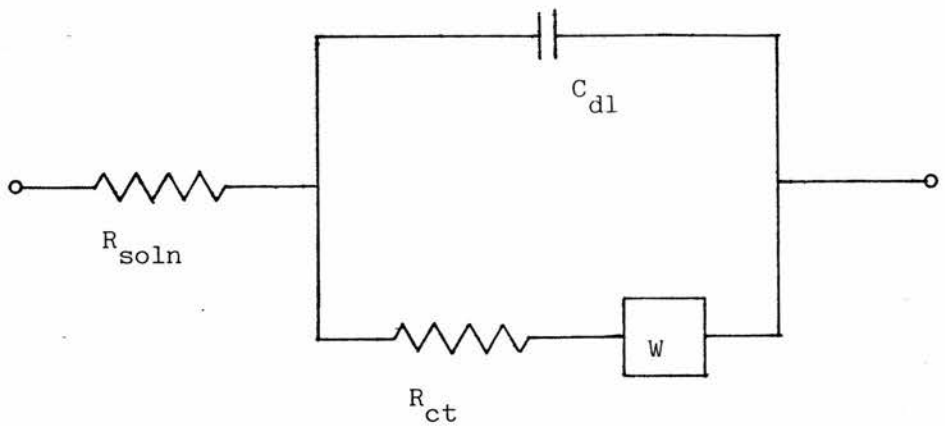

where

R_{soln} = Solution Resistance W = Warburg Impedance

C_{dl} = Double Layer Capacitance

R_{ct} = Charge Transfer Resistance

This method, however, relies on the ability to separately measure the double layer capacitance and the solution resistance. The separation of the faradaic impedance i.e. the total impedance from summing the charge transfer resistance and the warburg impedance; and the double layer capacitance is suggested[29] to be invalid in most cases, particularly where there is adsorption of electroactive species.

Efforts have been made, particularly by Gerischer[30], Grahame[31] and Delahay[29], to derive equations that also consider potentials apart from the equilibrium value. The time-averaged concentration at the electrode surface had to be defined and attempt to accomplish

this was Delahay's development of the semi-infinite linear diffusion theory.

On application of this theory, it was possible to derive expressions, shown below, for the R_{ct} and the W , from the rate expression for a one-step reaction and solution of Fick's law of diffusion, on application of the correct boundary conditions.

$$R_{CT} = \frac{RT}{n^2F^2k_s} (C_o^s)^{\alpha} (C_R^s)^{1-\alpha} \qquad (3.69)$$

$$W = \sigma w^{-1/2} - j\sigma w^{-1/2} \qquad (3.70)$$

where

$$\sigma = \text{diffusion coefficient} = \frac{RT}{n^2F^2\sqrt{2}} \left(\frac{1}{C_o^s D_o^{1/2}} + \frac{1}{C_R^s D_R^{1/2}} \right)$$

and

D_R and D_o = diffusion coefficient of the reduced and oxidised species respectively.

The faradaic impedance $Z_f = R_{CT} + W$

$$\therefore \quad Z_f = R_S + \left(\frac{1}{jwC_s} \right) \qquad (3.71)$$

where

$$R_s = R_{CT} + \sigma w^{-1/2} \text{ and } \frac{1}{wC_s} = \sigma w^{-1/2}$$

The Randles method of a.c. impedance analysis requires the plotting of R_s and $^1/wC_s$ against $w^{-½}$ as shown in Fig.3.12.

Fig.3.12

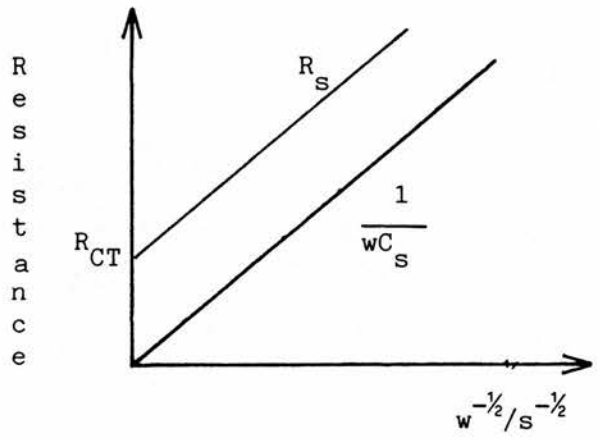

This enables the effects of diffusion to be extrapolated out.

Sluyters[26] and Sluyters-Rehbach[32] developed a method, however, which is much more suited to experimental analysis since R_{CT} can be calculated without any knowledge of the value of C_{dl} whereas with the Randles method this knowledge is a necessary requirement.

From the Randles' circuit, shown in Fig.3.11, it can be seen that

$$Z_T = R_{so} + \left(\frac{1}{jWC_{dl}} + \left(\frac{1}{R_{CT}} + \sigma w^{-\frac{1}{2}} - j\sigma w^{-\frac{1}{2}} \right) \right) \qquad (3.72)$$

However from this complex equation two limiting cases can be considered.

Firstly, where charge transfer is important, at high frequencies or when diffusion is not significant, and where the electroactive species at the electrode surface are always maintained at their Nernstian concentration. Equation (3.72) now simplifies to:-

$$Z_T = R_{SO} + \frac{R_{CT}}{1 + w^2 C_{dl}^2 R_{CT}^2} - \frac{jwC_{dl}R_{CT}^2}{1 + w^2 C_{dl}^2 R_{CT}^2} \qquad (3.73)$$

NOTE: that this is similar to equation (3.56), produced for a parallel network of R and C equivalent circuit, but with an additional resistor added in series.

Should impedance be plotted in the complex plane as a function of frequency then the resultant single semi-circle, as shown in Fig.3.13, has a diameter of the value of R_{CT} in ohms. In addition,

$R_{CT} = \frac{1}{w^* C_{dl}}$ where w* is the angular frequency at the maximum value of the semi-circle.

Fig. 3.13

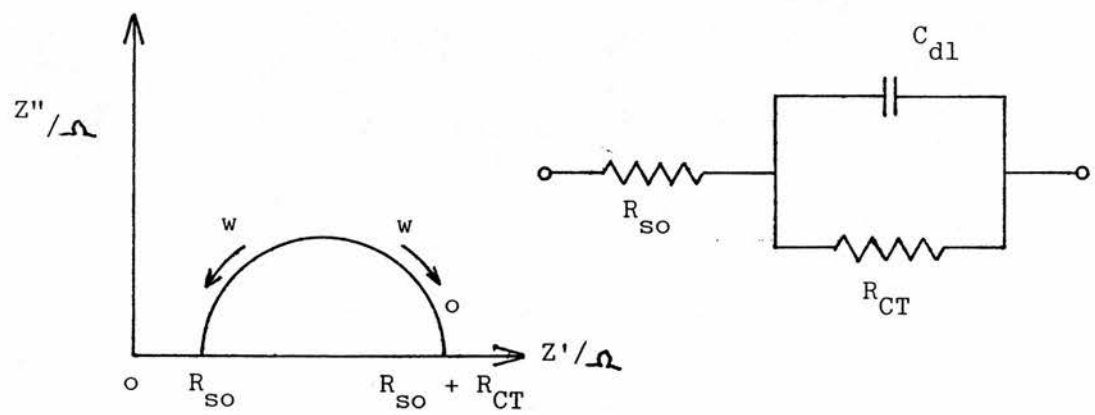

In the other limiting case, diffusion is predominant and charge transfer is small. Therefore equation (3.72) simplifies to:-

$$Z_T = R_{so} + R_{CT} + \sigma w^{-\frac{1}{2}} - j(\sigma w^{-\frac{1}{2}}) - 2\sigma^2 C_{dl} \qquad (3.74)$$

On plotting the Argand diagram, a straight line with a slope of 45^o is observed, as shown in Fig.3.14.

Fig.3.14

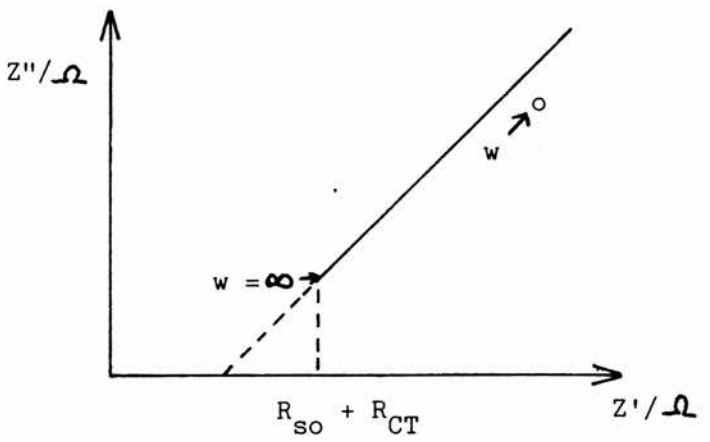

Derivation of equation (3.74) assumed that the a.c. diffusion layer is made thinner than the Nernstian layer. For a more exact consideration of diffusion effects, the review by Armstrong[33] is suggested.

However in most cases neither charge transfer nor diffusion predominates and hence there will be interaction between the interfacial impedance and the Warburg impedance, which can be written:-

$$Z_T = Z_f + Z_d \qquad (3.75)$$

The form of the Argand diagram observed will be highly dependent on the respective values of R_{CT}, σ and C_{dl}. Typical spectra can be seen in Fig.3.15.

Fig.3.15

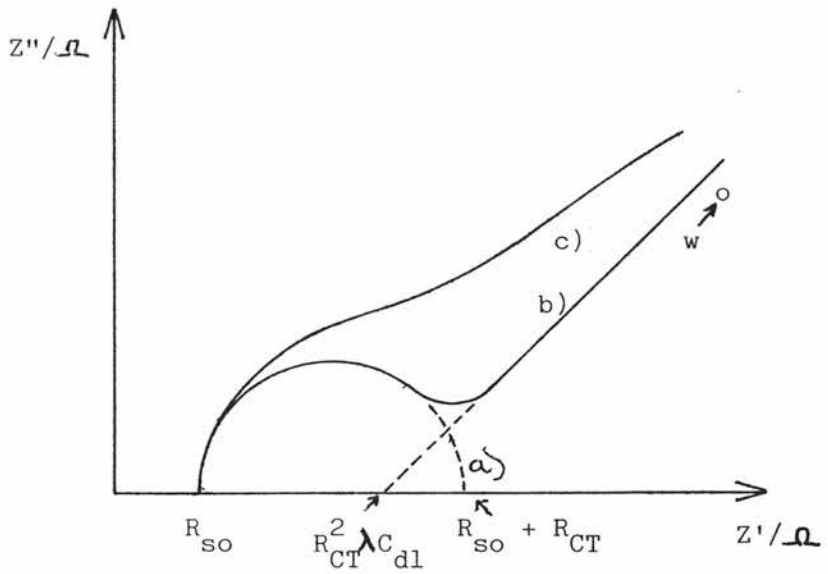

where

$$\lambda = \frac{k_R}{\sqrt{D_o}} + \frac{k_o}{\sqrt{D_R}}$$

As diffusion becomes more important

a) < b) < c)

3.8.5 A.C. Impedance Measurement Methods

The impedance response of an electrochemical cell can be measured using various different techniques. These methods can be classified into three general types: 1) a.c. bridge methods 2) "direct" methods 3) phase sensitive detection techniques. These technique types are markedly different in instrumentation and methods of data collection but they are similar in the fact that firstly the elements of the impedance are found and then these are utilised to generate information about the electrochemical reactions involved.

Initial a.c. impedance measurements were done by applying a.c. bridge methods[34] but these, although very accurate, were found to be very time-consuming and to have too limited an operational frequency range. "Direct" methods[22] simultaneously display the input and output signals on a suitable recording device, usually an XY oscilloscope or sometimes an XY chart recorder, and then the impedance is calculated directly from the dimensions of the figures, known as Lissajous Figures, displayed. These "direct" methods increase the frequency range that can be studied.

Due to advances in instrumentation in the last twenty years, phase sensitive detection is a method which is becoming increasingly popular due to its simplicity in the definition of the impedance of the system. Therefore it will be discussed in greater detail. Particular emphasis will be placed on a refinement of this method, known as digital frequency response analysis, since this was the technique applied in all experimental a.c. impedance studies discussed in this project.

Phase Sensitive Detection[35]

A phase sensitive detector, or lock-in amplifier, is an instrument which compares two sinusoidal signals to give an output that can be applied to produce the phase difference between the signals and the peak amplitude ratios. A typical circuit for phase sensitive detection can be seen in Fig.3.16.

Fig.3.16

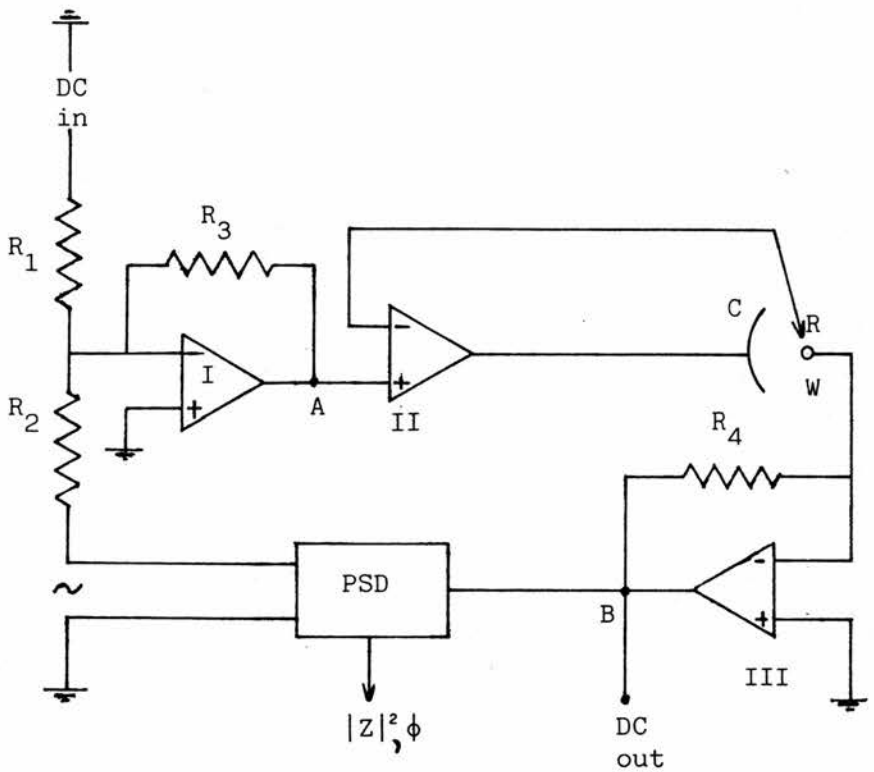

I = voltage adder, II = potentiostat control amplifier

III = current follower amplifier

Automatic variation of the current between the counter and working electrodes allows "potentiostatic" control of the voltage between the working and the reference electrodes in the three-electrode cell. Addition of two or more input voltages, one being

a small amplitude, < 10mV peak to peak, sinusoidal signal is accomplished by the operational amplifier labelled I. The signal detected at point A is, a weighted addition of the two inputs. The required current output is generated by the potentiostatic control amplifier, II, and it is detected at point B as a potential output of the current follower amplifier, III. Where the impedance is not purely resistive in nature then the a.c. part of the current will be out of phase with the potential input. The PSD calculates the phase angle and the ratio of the peak values.

Since only the impedance of the working electrode and the solution between it and the reference electrode is measured therefore this is a major advantage compared with a.c. bridge methods, which require a large counter electrode. In addition, the uncompensated solution resistance may be removed by use of positive feedback circuits. Hence the conrol amplifier accurately superimposes the total input signal, including both a.c. and d.c. elements, across the working electrode/solution interface whereas in a.c. bridges techniques both components of the signal are applied across the cell, which causes drastic distortion, due to the cell resistance, of the d.c. signal applied across the interface.

Advances in instrumentation have produced phase sensitive detectors which can supply continuous output signals which are proportional to the real and complex components of the impedance. This type of output makes phase sensitive detection perfect for interfacing with computers for data evaluation, often using Fourier transform methods for collection and processing of the data. The limitations of this technique, like the high frequency limit being restricted by the transient response of the circuit and

by the amplifier bandwidths, have been minimised by advances in component design. These advances have led to requirements of the method such as digital frequency response analysis.

Digital Frequency Response Analysis

As has been already mentioned, in section 3.8.3, transfer functions can be used to represent the impedance.

The principle of transfer function measured can be seen illustrated in Fig.3.17.

Fig.3.17

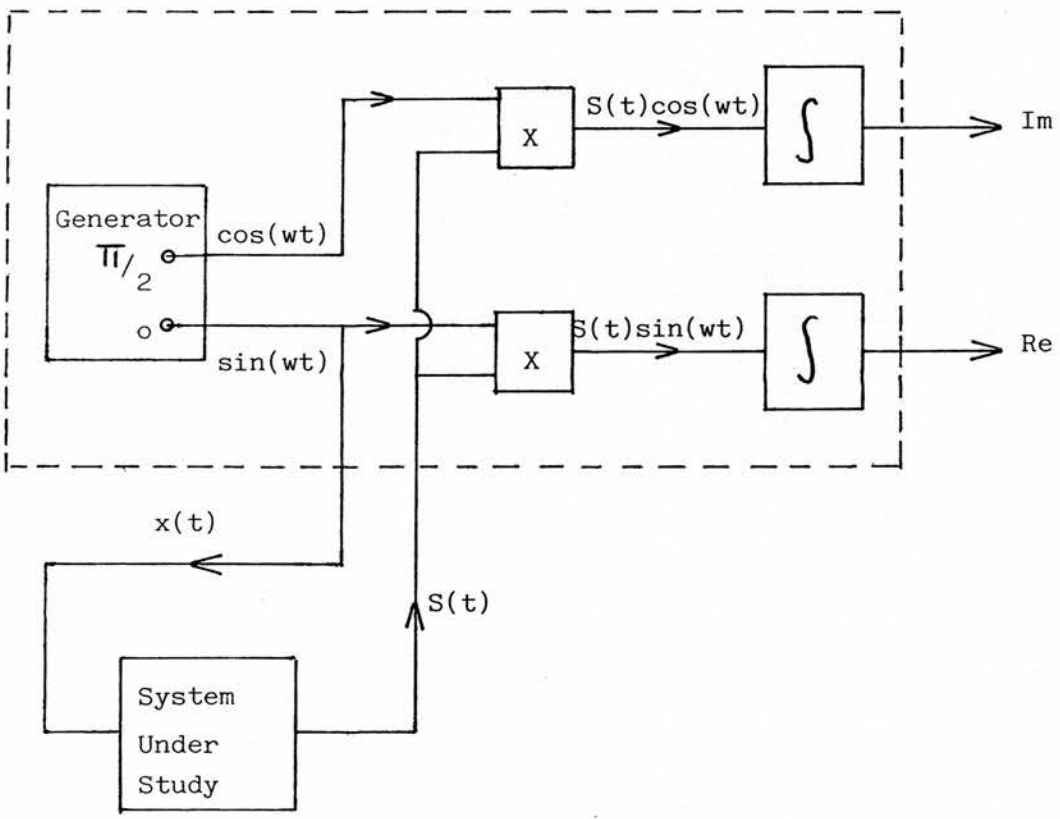

x(t) = perturbating signal S(t) = cell response signal

The cell's response, to $x(t) = X_o \sin(wt)$, is correlated with two synchronous reference signals, one of which is in phase with $x(t)$ and the other $\pi/2$ out of phase, i.e. $\sin(wt)$ and $\cos(wt)$, since:-

$$\left.\begin{aligned} Re &= \frac{1}{T}\int_o^T S(t)\sin(wt)dt \\ Im &= \frac{1}{T}\int_o^T S(t)\cos(wt)dt \end{aligned}\right\} \qquad (3.76)$$

where

$$S(t) = X_o K(w)\sin(wt + \phi(w)) + \sum_m A_m \sin(wtm - \phi_m) + n(t) \qquad (3.77)$$

and is the sum of the various harmonics and parasitic noise for a cell with a transfer function

$$K(w) = e^{j\phi(w)} \qquad (3.78)$$

T = the integration time

Consider the harmonies, only the fundamental signal has aa non-zero integral and hence all others will be neglected. However, allowing for noise, total rejection is only possible where $T = \infty$. Therefore the equivalent filter would have to have an infinitely narrow bandwidth, centred on the generator frequency.

$$\therefore \quad Re = \lim_{T \to \infty} \frac{1}{T}\int_o^T S(t)\sin(wt)dt = X_o K(w)\cos\phi(w) \qquad (3.79)$$

$$Im = \underset{T \to \infty}{\text{limit}} \frac{1}{T}\int_{o}^{T} S(t)\cos(wt)dt = X_o K(w)\sin\phi(w) \qquad (3.80)$$

One can therefore obtain these two components of the impedance and describe the electrochemical processes occurring in the cell.

However, the measurement time T cannot, experimentally, be infinite and therefore the filter bandwidth is dependent on T. The signal-to-noise ratio can be improved and the noise bandwidth can be reduced to

$$\Delta f = \frac{1}{T}$$

Experimentally the Solartron two channel 1250 F.R.A. can automatically and simultaneously record the real and imaginery components, with correlation to x(t). The transfer function, H_{12}, can then be calculated:-

$$H_{12}(w) = \frac{S_2(w)}{S_1(w)} = \frac{A_2 + jB_2}{A_1 + jB_1} \qquad (3.81)$$

where

A and jB are the real and imaginery components.

$H_{12}(w)$ is directly related to the impedance of the cell without any influence of the regulating element.

Since all experiments were conducted using the F.R.A. in a potentiostatic mode, then only this mode will be illustrated:-

$$S_1(w) = G_I R \frac{K_1 X_o}{Z} \tag{3.82}$$

$$S_2(w) = G_V K_1 X_o \tag{3.83}$$

where $S_1(t)$ and $S_2(t)$ are current and voltage respectively

$$\therefore \quad H_{12}(w) = \frac{G_V}{G_I} \cdot \frac{Z}{R} \tag{3.84}$$

where K_1 = transfer function of the potentiostat

R = standard resistor used for measuring current

G_V, G_I = voltage and current amplifier gains.

If there are no inductive or capacitive elements present over the frequired frequency range, then $G_I = G_V$.

$$\therefore \quad Z(w) = RH_{12}(w) \tag{3.85}$$

At the present level of instrumentation, one can measure and plot the electrochemical impedance automatically by using computer control. The generator can be programmed to scan from a maximum frequency to a minimum frequency using a series of steps, Δf. The measurement frequency is altered automatically and hence the measurement time for the a.c. impedance can greatly be reduced. In addition, the digital data collected can be recorded in the computer's memory and then it may be plotted or undergo further analysis at one's leisure. This is the case with the automated system, shown in Fig.4.7, used in all experimental a.c. impedance studies in this project.

3.8.6 The Analysis of A.C. Impedance Data

The analysis of a.c. impedance data is usually accomplished by applying graphical methods, such as Argand diagrams and Bode plots. These plots tend to provide the required equivalent circuit parameters. However in more complex circuits, if the time constants of the respective subcircuits are similar, then the frequency dispersion cannot be separated into distinct regions. This also occurs when there are components, such as Warburg and Constant Phase Elements (CPE), present that have a fractional power dependence on frequency; because the modulus of these elements varies sub-linearly with frequency, producing an extension of its influence over a large frequency range in the dispersion. The circuit parameters must be adjusted simultaneously to allow the experimental data to be fitted to these complex equivalent circuits.

The frequency dispersion data of an electrochemical system can be analysed by using a non-linear least squares fit (NLLSF), known as program "EQIVCT" devised by Boukamp[36]. This program, which uses the above principle, has been harnessed to analyse a.c. impedance data produced by F.R.A. methods. The program uses a combination of an analytical and gradient search according to the Marquardt algorithin. Through application of a unique method of equivalent circuit description, known as the Circuit Description Code (CDC), it is possible to apply any particular circuit as input and obtain the optimum fit and the subsequent circuit parameters. Details of the operation of this program can be found in literature[36].

3.9 Aims

It is hoped that by monitoring changes in the double layer capacitance and the other electrical surface parameters, by electrochemical methods, that an inexpensive, rapid and reliable surface characterisation method can be found for surface modified carbon fibres.

Chapter 3 References

(1) P Debye; E Huckel: Physik. Z. 24 185,305 (1923).

(2) H L Von Helmholtz: Wiss. Abhandl. Physik-Tech.Reichsanstalt 1 925 (1879).

(3) G Gouy: J.Phys. 9 457 (1910).

(4) D L Chapman: Phil.Mag. 25 475 (1913).

(5) D Stern: Z. Electrochem. 30 508 (1924).

(6) D C Grahame: J.Chem.Phys. 18 903 (1950).

(7) D C Grahame: J.Electrochem.Soc. 98 343 (1951).

(8) M.A. Devanathan; J O'M.Bockris; K Muller: Proc. Royal. Soc. A274 55 (1963).

(9) P Delahay: "Double Layer and Electrode Processes". Pub. by J Wiley and Sons (1965).

(10) R Parsons: "Advances in Electrochem. and Electrochemical Eng. Vol. 1" by P Delahay, p1. Pub. by Intersci. N.Y. (1961).

(11) C A Barlow, Jnr.; J R Macdonald: "Advances in Electrochem. and Electrochemical Eng. Vol. 6" by P Delahay, p1. Pub. by Intersci. N.Y. (1970).

(12) R De Levie: "Advances in Electrochem. and Electrochemical Eng. Vol. 6" by P Delahay and C W Tobias, p329. Pub. by Intersci. N.Y. (1970).

(13) B E Conway: "Theory and Principles of Electrode Processes". Pub. by Ronald Press N.Y. (1965).

(14) J O'M.Bockris; A K N Reddy: "Modern Electrochemistry". Pub. by Plenum Press N.Y. (1970).

(15) R Parsons: Surf. Sci. 2 418 (1964).

(16) K J Laidler: J.Chem.Educ. 47 600 (1970).

(17) K J Vetter: "Electrochemical Kinetics". Pub. by Acad. Press N.Y. (1967).

(18) B E Conway; E Gileadi: Trans. Faraday Soc. 58 2493 (1962).

(19) S Barnatt: J.Electrochem.Soc. 99 549 (1952).

(20) K Tokuda; T Gueshi; K Aoki; H Matsuda: J.Electrochem.Soc. 132 (10) 2390 (1985).

(21) D T Sawyer; J L Roberts, Jnr: "Experimental Electrochemistry for Chemists". Pub. by Wiley (Intersci.) N.Y. (1974).

(22) C Gabrielli: "Identification of Electrochemical Processes by Frequency Response Analysis" Tech. Report No 004/83. Pub. by Solantron Instruments (1984).

(23) S C Greason; D E Smith: J.Electroanal.Chem. 36 App 1 (1972).

(24) I Epelboin; C Gabrielli; M Keddam; H Takenouti: "Comprehensive Treatise on Electrochem. Vol.4", p151. Pub. by Plenum Press N.Y. (1981).

(25) I Epelboin; C Gabrielli; M Keddam: Corrosion Sci. 15 155 (1975).

(26) J H Sluyters: Recuil.Trav.Chim. Pays-Bas 79 1092 (1960).

(27) P Dolin; D Erschler: Acta Physicochim. U.R.S.S. 13 747 (1940).

(28) J E B Randles: Discuss. Faraday. Soc. 1 11 (1947).

(29) P Delahay: "New Instrumental Methods in Electrochem.". Pub. by Intersci. N.Y. (1954).

(30) H Gerischer: Z.Phys.Chem. 198 268 (1951).

(31) D C Grahame: J.Electrochem.Soc. 99 370C (1952).

(32) M Sluyters-Rehbach: Thesis (1963) Utrecht.

(33) R D Armstrong; M F Bell; A A Metcalfe: "Specialist Periodical Report - Electrochemistry Vol 7" by H R Thirsk. Pub. by The Chemical Soc. (1980).

(34) R D Armstrong; W P Race; H R Thirsk: Electrochemica Acta 13 215 (1968).

(35) R D Armstrong; M Henderson: J.Electroanal.Chem. 40 121 (1972).

(36) B A Boukamp: Solid State Ionics 20 31 (1986).

CHAPTER 4

EXPERIMENTAL DETAILS

4.1 3-Electrode Cell

The overall design of the actual 3-electrode cell, used in all electrochemical experiments, can be seen in Fig.4.1 however it must be noted that the cell's de-gassing elements, i.e. the gas inlet and outlets, have been omitted to improve the clarity of the diagram. The individual components which comprise the cell will now be described.

The counter electrode consisted of a coiled platinum wire electrode, with a braided copper wire connection, combined inside a glass tube with a sintered glass tip. The glass tube had a small hole in it near the top to allow the release of pressure build-up generated during de-gassing of the cell.

A Standard Calomel Electrode (S.C.E.) from Russell Electrodes, was used as a reference electrode. This electrode was placed in a glass Luggin capillary to reduce the overall solution resistance of the cell. The Luggin contained two different electrolytes; below the top of the tap there was the electrolyte contained in the cell but above the tap was the standard 3.0M KCl electrolyte required for operation of the S.C.E.

In cases where a platinum working electrode was required then a platinum-wire electrode, with a mercury junction and a tinned-copper wire connection, was used. However in all other cases

a carbon fibre working electrode was used. Detailed discussion of the nature and construction of these carbon fibre electrodes will be given in later sections (see 4.4).

The de-gassing elements of the cell consisted of a glass tube with a sintered joint tip for the gas inlet and a glass, paraffin-filled, bubbler for the outlet. Under experimental conditions the atmosphere of the cell required to be inert to remove any interactions occurring between the atmosphere of the cell and the electrodes and or electrolyte which might allow the electrochemical response of the cell. Since this is a particular problem where oxygen gas is present, the cell was de-gassed for approximately 20 minutes with an oxygen-free nitrogen gas before any experimental work was initiated. Details about the preparation of the oxygen-free nitrogen gas will be discussed in the next section.

Fig.4.1 The Three Electrode Cell

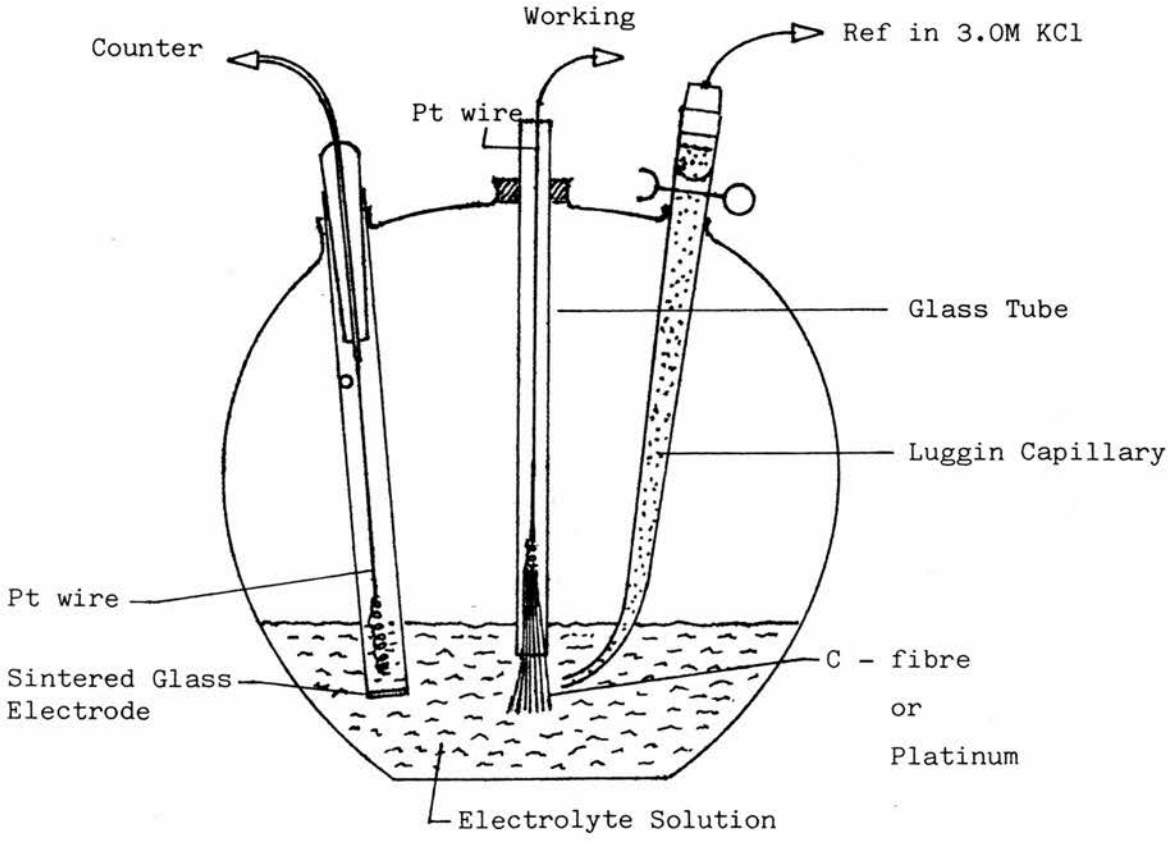

4.2 Gas De-oxygenating System

The gas preparation system consisted of a series of three dreschel bottle traps placed between the nitrogen gas supply (B.O.C.) and the 3-electrode cell. The purpose of these traps was to ensure that the nitrogen entering the cell was both "dry", i.e. contained very little water vapour, but more importantly de-oxygenated.

The middle trap is the most important since it is the de-oxygenating section of the system. It contains Zn/Hg amalgam in an acidified ammonium metavanadate solution which acts to remove any oxygen present. The other two traps contain liquid paraffin and sulphuric acid ensuring that the gas is "dry" as well as de-oxygenated.

A detailed description for the preparation of the middle trap can be found in Mietes[1] and the reactions occurring during that preparation may be seen in Appendix 1. The efficiency of this trap is reduced over long time periods and can be seen by loss of the deep violet colour of the solution. However its efficiency may be renewed by addition of a few more drops of conc. HCl and a further period of bubbling N_2 through it.

4.3 Electrolyte Preparation

In all electrochemical experiments the purity of the electrolyte solutions and the cleanliness of the glassware is paramount since the pressure of any impurity, even in small concentrations, may drastically affect the electrochemical response of the cell.

The glassware was scrupulously cleaned using a strong industrial detergent called Micro and in some cases it was cleaned using an ultrasonic bath. These methods were preferred to using strong inorganic agents such as chromic acid due to the ease of handling and removal of cleaning agents.

It was necessary, when dealing with aqueous electrolytes, that the distilled water used in the preparation of these solutions was particularly pure. This was accomplished by use of what is known as "triply" distilled water. "Triply" distilled water may be prepared by re-distilling distilled water over several crystals of $KMnO_4$.

The chemicals used in the preparation of the electrolyte solutions are listed in Table 4.1 below:-

Table 4.1

ELECTROLYTE	MANUFACTURER	MOLECULAR WEIGHT
$NaCl_4$	BDH Analar	140.46 g
$FeCl_2$	Fisons	198.81 g
$FeCl_3$	Fisons	270.30 g
KCl	BDH Analar	74.56 g
KBr	BDH Analar	119.01 g
KI	BDH Analar	166.01 g
KOH	BDH Analar	56.11 g

conc. HNO_3 = 70% w/w $\approx$ 15.78 M

conc. H_3PO_4 = 88% w/w $\approx$ 15.72 M

The required concentrations were produced by addition of "triply" distilled water. The volume of electrolyte used in the 3-electrode cell was approximately 150 mls.

4.4 Construction of Carbon Fibre Working Electrode

In the case of all carbon fibre experiments the platinum working electrode, shown in Fig.4.1 was replaced by an electrode similar to that shown in Fig.4.2 b).

Problems were encountered with the initial electrode design, shown in Fig.4.2 a), when a series of experiments were performed

using these unsealed carbon fibre electrodes. Cyclic voltammetric experiments were conducted using dilute acid electrolytes, such as HNO_3 and H_3PO_4, at varying concentrations and it was observed that all showed a continual increase in the current response as the potential sweep progressed. This was thought to be due to a combined increase in the active surface area of the carbon fibre electrode due to "wetting".

Obviously the electrode had to be re-designed to remove this factor and this was accomplished by sealing the fibre electrode into the quartz glass tube using Trylon Epoxy Embedding Resin as shown in Fig.4.2 b). The electrode now has a constant active surface area and therefore is suitable for use in future experiments.

Fig.4.2 Carbon Fibre Electrode Designs

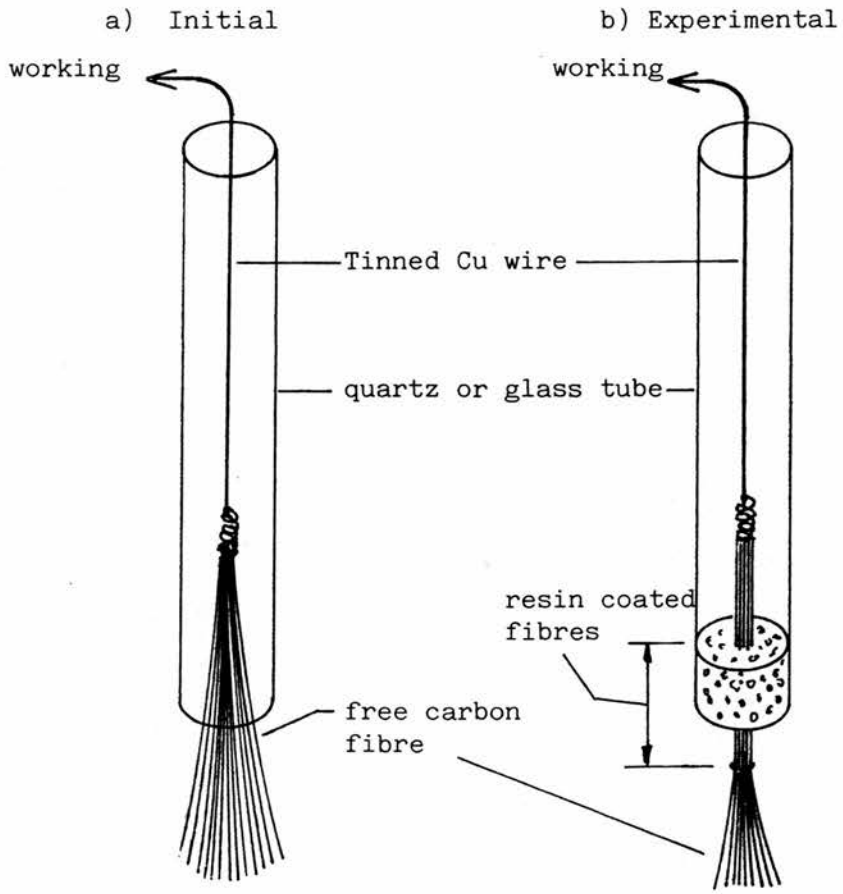

4.5 Experimental Equipment and Procedure

Cyclic Voltammetry

All cyclic voltammetric experiments carried out used the same basic experimental set-up. Its design can be seen in Fig.4.3 and the actual components used listed below:-

AMEL 567 Function Generator

AMEL 553 Potentiostat

HEWLET PACKARD 7007 X-Y Chart Recorder

Initially a few simple test cells, comprising actual electrical components, were run and their results at various potential scan rates provided a guideline for the limitations of the chart recorder as a useful data collection device.

4.5.1 C.V. on Platinum Wire

After these preliminary experiments were completed, a series of experiments were done, using a platinum wire working electrode, to facilitate familiarisation with the technique and define suitable operating parameters for future work on carbon fibre responses in aqueous electrolytes.

Fig.4.3 Experimental Equipment for Cyclic Voltammetric Studies

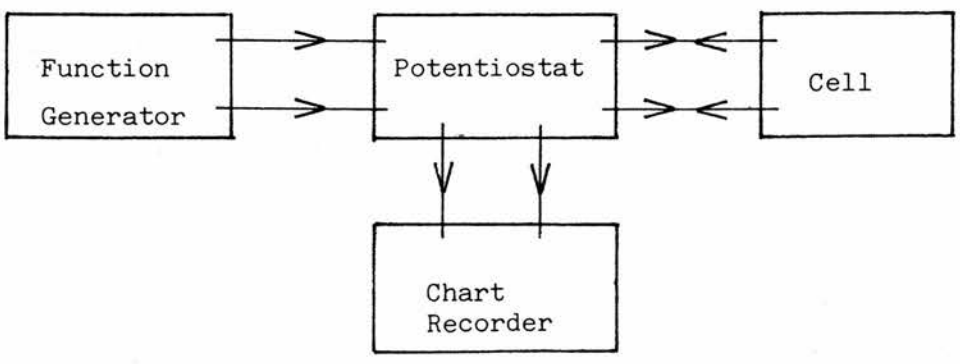

These experiments were carried out using various electrolytes and in the case of each electrolyte the potential sweep limits, both anodic and cathodic, and the optimum sweep rates were determined. Obviously, since one is dealing with aqueous electrolytes, these potential limits will lie between the potential values for the standard electrode half reactions of water i.e. the reduction of water to give hydrogen gas and the oxidation of water to produce oxygen. The half reactions and their standard reduction potentials are shown below, with all potentials with respect to S.C.E.

	$E^{o}(V)$
$2H_2O + 2e^{\ominus} \rightleftharpoons 2OH^{\ominus} + H_2$	- 0.85
$O_2 + 4H^{\oplus} + 4e^{\ominus} \rightleftharpoons 2H_2O$	+ 1.45

Within these potential limits it was possible to investigate the reactions occurring at the working electrode. All potentials mentioned are with respect to S.C.E. unless stated otherwise.

In addition to determining potential limits and optimum sweep rates, a series of runs were carried out that enabled values for the redox couple and the diffusion co-efficient, with a platinum wire working electrode, to be determined. By using a 1 : 1 mixture of 2.0 molal $FeCl_2$ and $FeCl_3$ electrolyte solution and several different potential sweep rates, it was possible to measure the Fe^{3+}/Fe^{2+} redox couple and calculate the diffusion co-efficient. These values were then compared with the literature[2] values.

4.5.2 C.V. on Carbon Fibre

pH Dependence

It was thought that the electrochemical behaviour of carbon fibre would correspond, in certain aspects, to that of platinum. Therefore most of the experiments carried out with platinum were repeated using the carbon fibre electrode. However an additional experiment was devised to investigate the effect of pH on the shape and on the potential limits of the voltammogram. In this case the 3-electrode cell was altered by replacing the gas inlet tube by a pH electrode. A range of pH's was established from pH 2 to 14 and the voltammograms for each were recorded on the same set of axes. This gave a visual method for assessing the effects of pH. The resulting trends were then compared to the cited literature[3] for other electrodes.

The results and conclusions of all experiments are discussed in Chapter 5.

Double Layer Capacitance Determination

As has been previously mentioned, it was thought that cyclic voltammetry could be applied to characterise the carbon fibre electrochemically by determining certain physical and electrical properties of the carbon fibre electrode surface. In particular the double layer capacitance could be found from the voltammograms by varying the potential sweep rates and recording the changing current values. This was done using 2.0M HNO_3 electrolyte and the double layer capacitance was calculated.

The double layer capacitance is normally recorded as a value per cm^2 i.e. in relation to the electrode surface area. However, in preliminary experiments, it was found that the value supplied[4] for the weight of the fibre to surface area ratio of 1 mg $\equiv$ 4 cm^2 was inaccurate for the fibres used.

This may be adequately seen in the result for the double layer capacitance produced from a series of experiments using a single carbon fibre electrode and various surface area values. The electrode was reduced in weight by a known amount after each capacitance reading. The surface areas were calculated by weighing the electrode and then using the conversion ratio above. A plot of capacitance versus surface area was done and the gradient gave a value for the double layer capacitance per cm^2 of electrode surface. The value produced was 7.8 $\mu F/cm^2$ which is quite low when compared to previous C.V. studies on solid carbon electrodes[6,7].

Therefore it was decided to record the double layer capacitance as a value per mg of fibre in all fibre experiments.

4.6 Galvanostatic Methods

4.6.1 Long-Duration Galvanostatic Methods

Galvanostatic experiments were initially conducted using the experimental set-up shown in Fig.4.4 and the components used listed below:-

Fig.4.4 Experimental Equipment for Long Duration Galvanostatic Studies

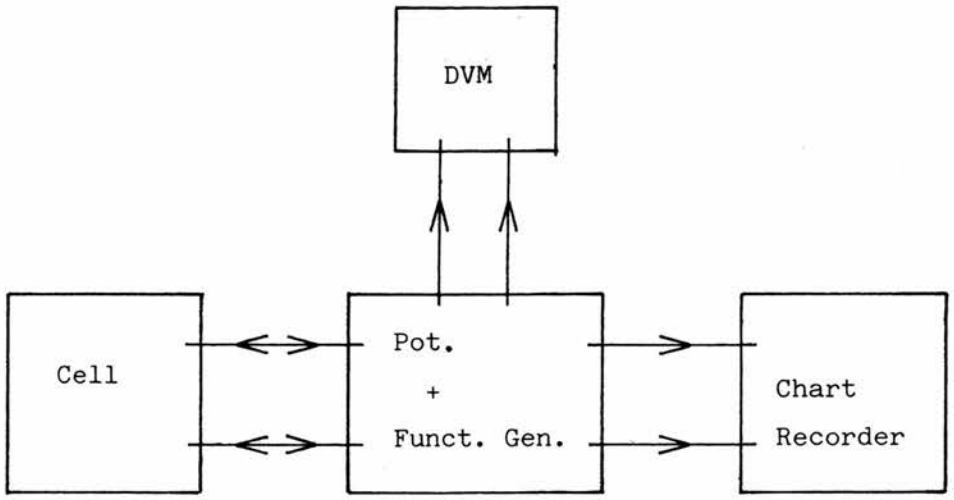

AMEL 553 Potentiostat

AMEL 567 Function Generator

HEWLET PACKARD 7007 Y-t Chart Recorder

SOLARTRON Digital Volt Meter

Firstly, a series of experiments were completed where several constant currents were passed through actual electrical component

circuits representing the cell to enable familiarisation with the technique and to check system operation. The resistor component representing the charge transfer resistance was kept at a constant value 1MΩ, and the capacitance was varied. For each value of capacitance a potential response with time was recorded. The values produced for the capacitance by analysis were then compared to the actual component values used in the circuit. The connection between these values was reasonably good but the experimental values were very dependent on the E_{max} value (see Chapter 3), which was difficult to determine and occurred at large time values.

A similar experiment was conducted using the 3-electrode cell with a carbon fibre electrode and 2.0M HNO_3 electrolyte. Several constant currents were applied and potential-time traces were recorded for each. Subsequent analysis produced similar problems in the determination and the time duration of E_{max}.

4.6.2 Short-Duration Galvanostatic Methods

Due to the problem found with determining E_{max} a new method had to be designed for accurate calculation of the double layer capacitance. It can be seen from the theory, shown in Chapter 5, that if the duration of the constant current is reduced then the potential-time traces become linear and the requirement of E_{max} is removed from the analysis. Therefore it was decided to reduce the overall duration of the experiment to less than 10 seconds.

However reducing the overall duration generated a new problem in that the chart recorder method of data collection was not accurate enough over these time spans and hence a more automated data collection

system must be employed. The revised experimental set-up is illustrated in Fig.4.5 and will be used in all further non-sinusoidal galvanostatic experiments. The actual components used are listed below:-

AMEL 553 Potentiostat

AMEL 567 Function Generator

STARDEL Data Recorder

B.B.C. Microcomputer

DEC VAX - 11/78 Mainframe Computer

TEXTRONIX 4052 Tape-Loading Micro

TEXTRONIX 4662 Plotter

KODE 43 Printer

Fig.4.5 Galvanostatic Experimental Set-Up

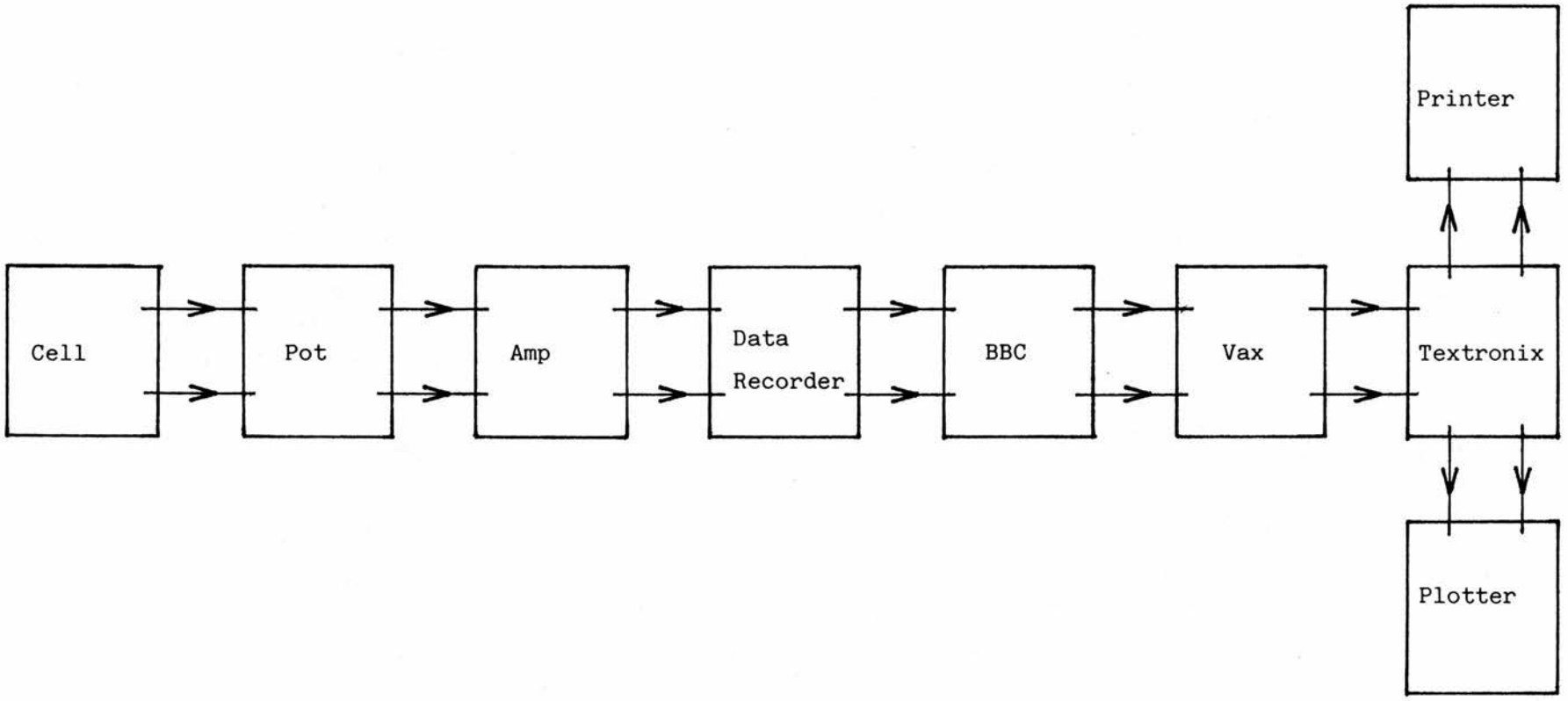

This set-up enabled the data to be recorded digitally using a small sampling interval and sampling 2000 points over the time span required. The information then went directly from the data recorder, via the B.B.C., to the VAX mainframe computer where it was transformed, using a series of command files, into the form required to produce the E-t plot and also to produce a value for the double layer capacitance of the carbon fibre electrode.

It was found through a series of preliminary experiments that the change in potential was best kept below 0.1 V and the time-span less than 5 seconds. In addition the optimum current range, for production of a linear plot within these limits, was found to be between 0.1 and 2.0 μA. Above this value the plots became non-linear and hence no longer fitted the simplified theory. In addition these plots did not fit the more complex analysis used previously.

This experimental set-up and these operational parameters form the basis for a series of galvanostatic experiments designed to determine the double layer capacitance of carbon fibre electrodes.

Therefore four currents were chosen which lay within the current range and each of these were passed through the cell. The response of the cell in terms of potential was recorded against time for a total duration of four seconds. Again the electrolyte chosen was 2.0M HNO_3 and the particular constant currents were 0.2, 0.5, 1.0 and 2.0 μA.

Determination of Capacitance to Weight Relationship

Due to the inaccuracies in the values produced for the double layer capacitance in preliminary experiments, it was decided to confirm the existence of a linear relationship between the capacitance and the weight of active electrode.

If an extremely long fibre electrode is used then this allows numerous measurements of capacitance versus weight, from the same electrode, to the mode. Initially the capacitance of the whole electrode was found and then the electrode was reduced in length by a constant value, 0.5 cm, each time and the capacitance calculated from the potential-time plots. The removed section was washed and weighed and hence it was possible, by difference measurements of weight, to produce a series of capacitance versus weight values. These were then plotted and the relationship was determined.

In this case only one constant current, 1 μA, was used and the same 2.0M HNO_3 electrolyte solution. The results can be seen in Table 4.2 and the subsequent plot in Fig.4.6.

Table 4.2

SECTION NO.	HNO_3		KOH	
	WEIGHT/mg	CAPACITANCE/ μF	WEIGHT/mg	CAPACITANCE/ μF
1	15.7	1180	15.2	1007
2	13.5	1000	13.2	896
3	11.8	926	11.7	838
4	11.0	801	11.1	775
5	9.9	787	9.7	736
6	8.5	600	8.6	716
7	7.0	554	6.1	605
8	5.9	419	5.7	530
9	4.3	317	4.1	424
10	2.1	190	2	283
11	0	0	0	0

Fig.4.6 The Double Layer Capacitance to Fibre Weight Relationship

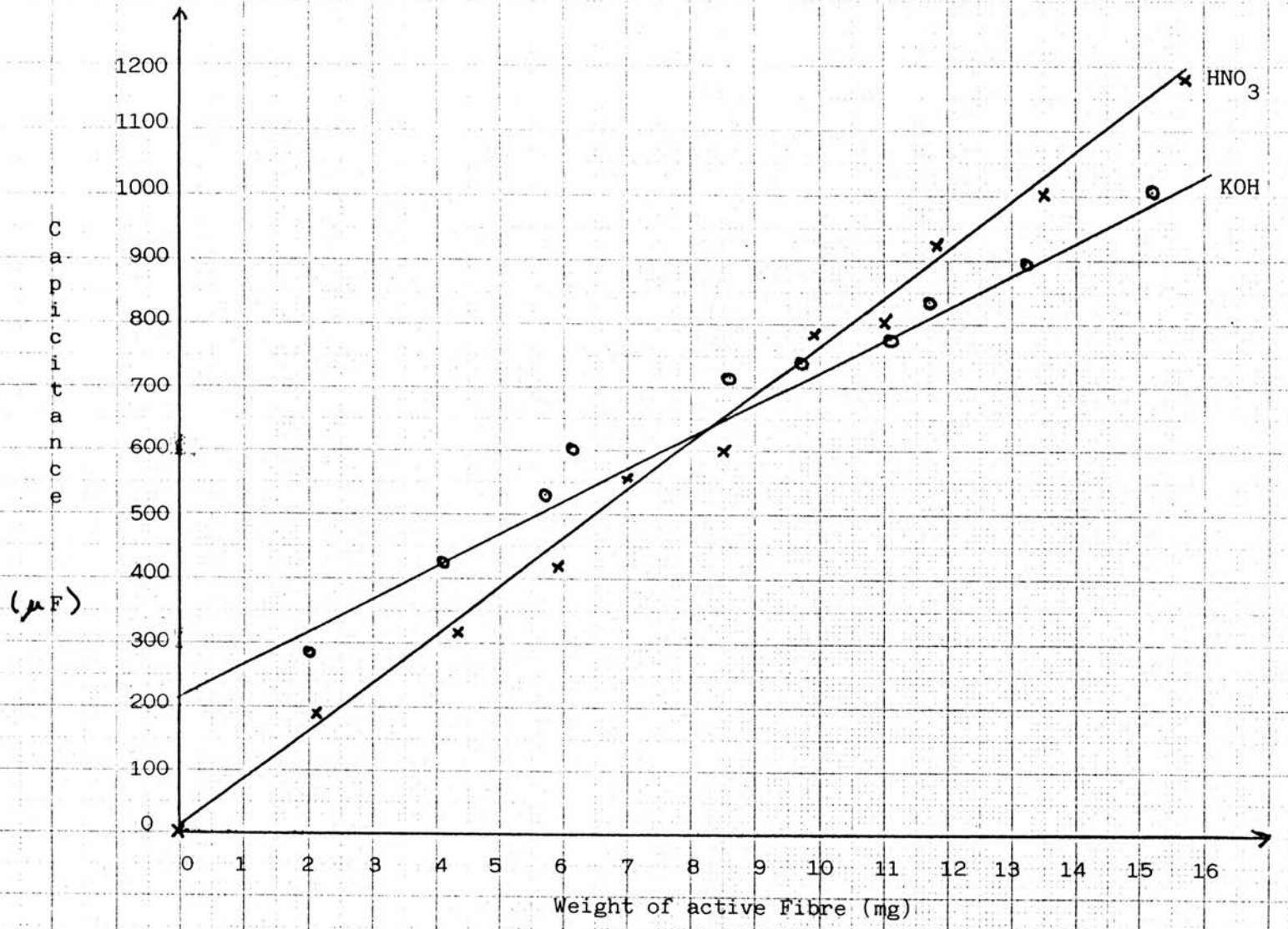

Fig.4.6 shows the expected linear plot going approximately through the origin for HNO_3. The gradient gives the value for the double layer capacitance per mg.

Double Layer Capacitance/mg = 75 μF
for 2.0M HNO_3

The second electrolyte, 2.0M KOH, was used to indicate whether the linear relationship was independent of electrolyte nature. The plot for 2.0M KOH solution can be seen in Fig.4.6 but in this case the linear relationship still exists but the graph does not pass through the origin as was expected. The discrepancy cannot be accounted for.

Double Layer Capacitance/mg = 54.8 μF
for 2.0M KOH

This difference in the value of capacitance/mg between the two electrolytes, is as expected, can be explained by the differing nature of the electrode/electrolyte interface generated by the differing electrolytes.

It can be concluded that the expected linear relationship does not exist between the double layer capacitance and the active fibre weight.

Electrode Reproducibility

For any meaningful conclusions to be drawn about the double layer capacitance of carbon fibre electrodes, it is necessary to demonstrate the reproducibility of these electrodes. Therefore a series of experiments were carried out using three different batches of the same type of fibre in each of the three electrolytes. Each fibre batch was run using several different constant currents but again all were within the specified current range. The electrolyte solutions, KOH, H_3PO_4 and HNO_3, used were all of the same concentration i.e. 2.0M. In each case the average capacitance value was found and they were then compared with the corresponding values for the other fibre batches.

Batch 1 = 6 month old HM-U fibres 2M207 B/10

Batch 2 = new batch HM-U fibres 2M307 D/10

Batch 3 = new batch HM-U fibres 2M371 E/10

HM-U represented high modulus PAN-based fibres produced by Courtaulds which are untreated by R.A.E.

Effect of the Nature of Electrolyte on Capacitance

A series of experiments were carried out using six different electrolytes and four constant currents for each. In all cases the molarity of the electrolytes was kept constant at 2.0M. The double layer capacitance was calculated from the limited duration potential-time plots as before. The electrolytes chosen were HNO_3, H_3PO_4, KOH, KCl, KBr and KI.

The results and discussion of all experiments using non-sinusoidal techniques can be found in Chapter 5.

4.7 A.C. Impedance Methods

A.C. theory and the operating principles of a.c. impedance techniques have already been discussed in section 3.4 and therefore only the equipment set-up and experimental procedure will be described in this section. All the results, tables and graphs will be presented and discussed in Chapter 6.

It was hoped that these methods would provide a more accurate determination of the cell's electrical components than has previously been achieved. It is hoped that these methods could be harnessed as an accurate, rapid and relatively inexpensive characterisation technique for manufactured carbon fibres.

4.7.1 Potentiostatic A.C. Impedance Studies

The experimental set-up used for all potentiostatic a.c. impedance studies can be seen in Fig.4.7. All connections between the components are BNC coaxial cables since they supply the required shielding from electrical interference.

The general experimental procedure remained unaltered throughout the application of this technique. The Frequency Response Analyser (F.R.A.) runs were controlled automatically using a control programme on the Textronix microcomputer. The preparation of the 3-electrode cell, i.e. de-gassing, etc. remained as for non-sinusoidal methods.

Fig.4.7 Experimental Equipment for Potentiostatic A.C. Impedance Studies

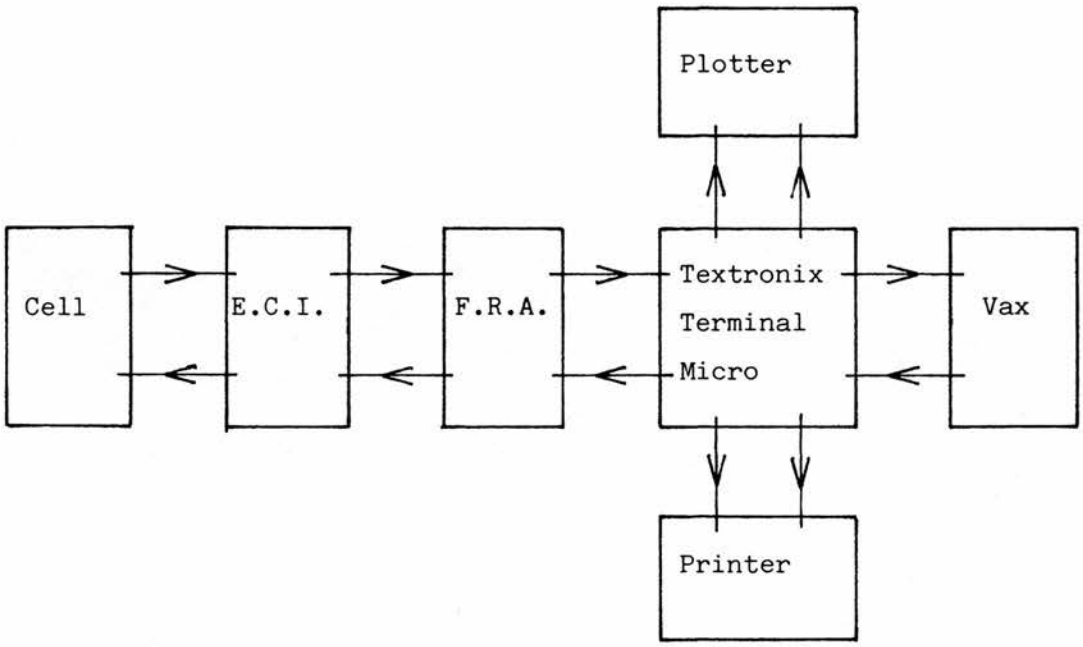

SOLARTRON SCHLUMBERGER 1186 Electrochemical Interface (E.C.I.)

SOLARTRON SCHLUMBERGER 1170 Frequency Response Analyser (F.R.A.)

TEXTRONIX 4052 Tape Loading Microcomputer

TEXTRONIX 4662 Digital Interactive Plotter

KODE 43 Printer

DEC VAX 11/78 Mainframe Computer

Initially the constant d.c. polarisation potential, over which the perturbing small a.c. signal will be applied, was set on the E.C.I. The details of th F.R.A. control program parameters were then put into the Textronix. The cell was then left to equilibrate before its impedance response was recorded over the required frequency range.

F.R.A. Control Parameters

A.C. Voltage signal = 10 mV

Cell Constant = 1

Integration Time = 10

Delay = 0.1 secs

Delta -F = 10

Frequency Range = 100 KHz $\longrightarrow$ 0.1 Hz

The cell constant parameter has no relevance in this experiment situation, since it refers to parameters which only have relevance in solid state cells, therefore it was valued at unity to remove its influence on the impedance response. The delta -F value is the number of points sampled per decade of frequency scanned.

Initially, to allow familiarisation with operational procedure and analysis methods of the subsequent complex impedance plots, it was felt necessary to run a series of simple electrical component circuits. To check the plotting program and the graphical analysis method, the resultant complex impedance plots, known as Argand diagrams, were compared to the theoretical impedance diagrams[5].

Several discrepancies were found in the shapes of these plots and in some cases the graphical analysis could not be performed. These discrepancies were thought to be due to the fact that the values chosen for the individual components in the circuit were affecting the shape of the overall plots. Therefore several sets of values for each circuit were tried but still the theoretical plots could not be obtained.

It was decided to generate, by use of a computer program, the values of the real (Z') and complex (Z'') parts of the circuit impedance from equivalent circuit theory. Computer programs produced these values, for the frequency range under study, they were then plotted in an Argand diagram and the graphical analysis method was carried out to give the component values of the original circuit. The values produced were then compared to the actual input values to assess the validity of the analysis method in an experimental situation.

Several different simple equivalent circuits were tried and for each various component values were used. This method may only be applied to simple circuits because beyond this the mathematical expressions for Z' and Z'' become too complex.

Having established that this technique and method of analysis are applicable in this experimental situation, several sets of experiments were conducted on carbon fibre electrodes in the 3-electrode cell. These experiments were designed to determine the value of the electrical elements present in the cell. In most cases the electrolyte used was 2.0M HNO_3.

Effect of Polarisation Potential on Untreated Fibres

For all potential variation experiments the general procedure remained constant. In the first run, the E.C.I. was set at the cell's open circuit potential and the cell's impedance was recorded. The d.c. potential, on the E.C.I., was then altered, by 0.1V each time, to produce a series of impedance responses across the cell's operational potential range. The potential was swept in both directions, anodic and cathodic, up to the limiting potentials. Obviously a different carbon fibre electrode was used in the anodic and the cathodic sweeps since approaching the potential limits will alter the electrode surface. The variation in shape of plots and value of components with potential was then determined. After use the electrode was washed in "triply" distilled water and dried in an oven. It was then weighed to give the active weight of the carbon fibre electrode.

Initial experiments with untreated carbon fibres were conducted using 6 month old fibres, Batch number HM-U 2M207 B/10. These fibres had been exposed to the atmosphere for a prolonged time period after their manufacture. It was expected that variation of potential would affect the impedance plots but was not known how.

OCV = + 0.70V Anodic Scan Range = + 0.70 ⟶ + 1.70V

Cathodic Scan Range = + 0.70 ⟶ - 0.30V

There was thought that there could be differences in the untreated fibres and therefore several different batches of the same manufactured fibre were examined, using this technique, to assess the lack of reproducibility of the carbon fibres production method.

1. HM-U 2M207 B/10 ,as above

2. HM-U 2M371 E/10

OCV = + 0.70V Anodic Scan Range = + 0.70 ⟶ + 1.70V

Cathodic Scan Range = + 0.70 ⟶ - 0.20V

3. HM-U 2M307 D/10

OCV = + 0.70V Anodic Scan Range = + 0.70 ⟶ + 1.60V

Cathodic Scan Range = + 0.70 ⟶ - 0.20V

Batches D and E were produced within several days of one another and hence should have similar surface properties and show similar behaviour.

Effect of Potential on R.A.E.-Treated Fibres

It was thought that these a.c. impedance methods could distinguish between untreated and surface treated carbon fibres. Therefore a series of potential dependance experiments were conducted on both types of fibres. In addition, both types of fibres were from the same manufacturing batch, the only difference being that the HM-S fibres were surface treated at R.A.E. after manufacture.

The actual fibres used were:-

1. HM-U Untreated Batch no. 2M307 D/10

OCV = + 0.70V Anodic Scan Range = + 0.70 $\longrightarrow$ + 1.70V

Cathodic Scan Range = + 0.70 $\longrightarrow$ - 0.20V

2. Treated HM-S Batch no. 2M307 F/10

OCV = + 0.70V Anodic Scan Range = + 0.70 $\longrightarrow$ + 1.50V

Cathodic Scan Range = + 0.70 $\longrightarrow$ - 0.10V

The two sets of Argand diagrams were then composed.

All potential dependence experiments were repeated several times to check reproducibility.

4.7.2 Galvanostatic Charging A.C. Impedance Studies

It was hoped that the untreated HM-U carbon fibres could be electrochemically surface-treated, in the laboratory, to resemble

R.A.E. surface-treated HM-S fibres and that these alterations could be monitored using a.c. impedance. These surface changes could be accomplished by galvanically charging the carbon fibre electrode i.e. passing a constant current through the electrode for a specified time period.

The experimental set-up for galvanic charging a.c. impedance experiments can be separated into two distinct stages, the actual charging process and the characterisation process. The charging process was accomplished using a laboratory-manufactured galvanostat to supply the constant current required for the fibre oxidation. After oxidation, the fibre was removed from the cell and washed in "triply" distilled water then dried in an oven. This was necessary to remove any microbubbles of gas, evolved in the oxidation process, present on the electrode which could affect the subsequent a.c. impedance response of the cell. The characterisation process employed an identical set-up to that used in previous a.c. impedance studies. In all cases the electrolyte used was 2.0M HNO_3 and the untreated fibre was HM-U 2M307 D/10.

Initial experiments were conducted on the untreated fibre to establish suitable operating parameter, such as the constant current value and the charging duration, for the galvanic oxidation. It was found that the optimum constant current was 10mA and therefore a series of different charging durations between 10 an 200s were tried with this value. The resultant a.c. impedance runs were carried out using only one d.c. potential value, + 1.30V, and the same F.R.A. parameters as used previously in the potentiostatic experiments. The effects of various galvanic oxidations on the Argand diagrams were then observed. For these charging durations

the effects of increased oxidation were not particularly apparent and certainly did not approach the required HM-S plot for this d.c. potential. The effect of increased oxidation can be much more satisfactorily observed with greater charging durations (t_c).

Effect of d.c. Potential Value on Increased Oxidation Plots

This experiment was designed to indicate the effect of anodic d.c. potential value on the analysis of the effects of increased galvanic oxidation.

In this case three anodic d.c. potentials were selected, one from each region of the anodic potential range i.e. the OCV + 0.70V, + 1.00V a mid range value and + 1.30V a potential approaching the anodic limiting potential. For each potential value a series of increased oxidations were carried out, with t_c values from 0 to 500s, and for each the impedance response was recorded.

Effect of Increased Galvanic Oxidation

It was thought that, although t_c = 500s produced significant changes towards the R.A.E.-treated HM-S fibres, the carbon fibre electrode was not fully charged. This conclusion was tested by supplying additional charge to the charged electrode to generate values for t_c = 1000s and t_c = 2000s.

Due to inconclusive results, the experiment investigating the effects of increased charging was repeated but using a greater range of t_c values, t_c from 0 to 3000s. In addition, the experiment incorporated the effect of analysis in both the anodic and cathodic potential regions by using + 1.30V and + 0.00V for the d.c. potential. This experiment consisted of four HM-U electrodes, two of which were analysed at + 1.30V and two at + 0.00V.

Effect of Time on the Impedance Response of Charged HM-U Fibres

During the course of conducting the previous experiments, it was found that there was significant alteration in the impedance response of the charged fibres over a period of time. This discovery initiated an investigation into the effects of time on variously charged electrodes.

Five electrodes were given different total charge values, varying from t_c = 0s to 5000s, and then their impedance response with respect to time was monitored over a period of two weeks. The impedance response was recorded at + 1.30V since this potential best indicated the effects of increased galvanic oxidation.

Chapter 4 References

(1) Mietes: "Polarographic Techniques", p89 (1970). Pub. by Wiley and Sons.

(2) A J Bard; L A Faulkner: "Electrochemical Methods". Pub. by J Wiley and Sons (1980).

(3) G Charlot; J Badoz-Lambling; B Tremillon: "Electrochemical Reactions". Pub. by Elsevier Pub. Co. (1962).

(4) M.O.D. R.A.E. Private Communication (1984).

(5) W I Archer; R D Armstrong: "Specialist Periodical Report - Electrochemistry, Vol 6" by H R Thirsk, p159. Pub. by The Chemical Society (1978).

(6) I Morcos; E Yeager: Electrochimica Acta 15, 953 (1970).

(7) S Kapusta; N Hackerman: J. Electrochem. Soc 131 (7) 1511 (1984).

CHAPTER 5

RESULTS AND DISCUSSION OF NON-SINUSOIDAL METHODS

5.1 Cyclic Voltammetry

5.1.1 Cyclic Voltammetry Using a Platinum Wire Electrode

The preliminary experiments carried out with various electrolytes to determine operational parameters and check the operation of the experimental set-up was reasonably successful. In the case of 0.1 molal $NaClO_4$ electrolyte, the only reactions found to be occurring were the various electrode half-reactions of platinum. The peak values of potential were found to be in reasonable agreement with those cited in the literature for platinum[1].

Fe^{3+}/Fe^{2+} Redox Couple

On carrying out a similar experiment to the preliminary runs but using a 1 : 1 mixture of 2.0 molal $Fe(Cl_3)$ and $Fe(Cl_2)$ electrolyte solution, it was found that the i-E curves were very similar to that of $NaClO_4$ although certain platinum peaks were absent. In addition, however, there was a distinct pair of peaks, one cathodic and one anodic, at approximately + 0.50V. These peak values were separated (ΔE_p) by a value of 40mV and therefore it can be reasonably assumed that they represent the Fe^{3+}/Fe^{2+} redox couple. The values of E_p and ΔE_p are consistent with those quoted in the literature[2] for this reversible couple.

By repeating this experiment for a series of different sweep rates, it is possible to produce a value for the redox diffusion co-efficients of this couple. If a plot of peak current (i_p) value versus the square root of the potential sweep rate (V) is done, then the diffusion co-efficient can be found from the gradient of the linear plot, since:-

$$D^{\frac{1}{2}} = \frac{i_p}{kn^{3/2}AC_oV^{\frac{1}{2}}} \qquad (5.1)$$

where

D = diffusion co-efficient k = Randles-Sevick Constant

n = no. of electrons A = Surface area C_o = concentrations

The values found for D_R and D_o were 3.39×10^{-2} cms^{-1} and 4.14×10^{-2} cms^{-1} respectively, these values seem extremely large compared to those found previously[3]. However this could be explained in the uncertainty of the value used for the Randles-Sevick constant k and the difficulty of accurately measuring the surface area of a pitted platinum electrode.

Fig.5.1 The Effect of pH on the C.V. Plots

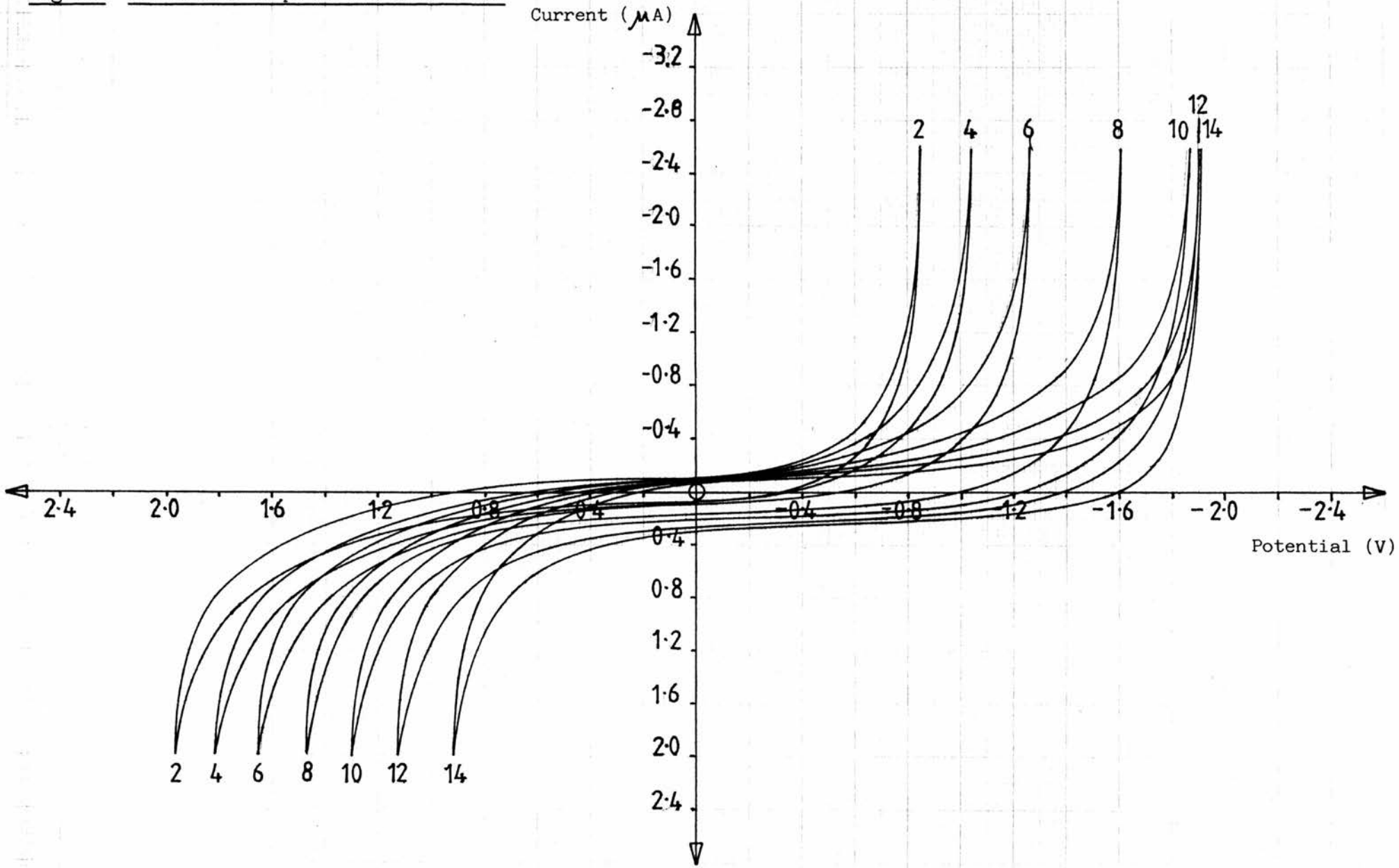

5.1.2 Cyclic Voltammetry on Carbon Fibre Electrodes

The initial experiments conducted on the platinum wire were repeated with carbon fibre electrodes. The results were, as expected, similar to the platinum responses. In the redox couple experiment the values of E_p and ΔE_p were found to be similar however, the diffusion co-efficients could not be calculated since no value for the Randles-Sevick constant could not be found in the literature.

pH Dependence of the Voltammogram

It was thought that carbon fibre electrodes would exhibit the expected pH dependence of the cyclic voltammograms shown by other solid electrodes[4]. Therefore the cyclic voltammograms for range of pH values were recorded on the same set of axes. This provided a visual method for assessing the effect of pH on the anodic and cathodic potential limits of the voltammograms. The results and plot can be seen in Table 5.1 and Fig.5.1 respectively.

Table 5.1

pH VALUE	ANODIC POTENTIAL LIMIT (V)	CATHODIC POTENTIAL LIMIT (V)
2	+ 1.96	- 0.85
4	+ 1.81	- 1.04
6	+ 1.65	- 1.26
8	+ 1.47	- 1.61
10	+ 1.30	- 1.87
12	+ 1.12	- 1.90
14	+ 0.91	- 1.91

The resultant i-E plots were similar to those found by Lipka et. al.[7], who used carbon fibre composite electrodes in IN H_2SO_4.

It was found that as the pH increased in value, the anodic potential limit decreased and the cathodic increased, producing a shift of the whole i-E curve to more negative potentials. The relative movements of the potential limits does not suggest that the pH and the E^o limits are linearly related, but the general trend is in good agreement with the cited literature[4] for other solid electrodes. It must be noted that there is little or no shift in the cathodic limit above pH 10, which suggests a cathodic limiting value for pH dependence.

In addition to the pH dependence of the potential limits, the intermediate section of the i-E curves for HNO_3 and H_3PO_4 electrolytes were analysed to determine the effect of pH on the intermediate peak positions and magnitude. This was accomplished by taking a strong acid and successively diluting it with triply distilled water and therefore decreasing the electrolyte concentrations and hence increasing the pH. It must be noted that the total volume of electrolyte in the cell remained constant for each pH reading.

It was seen that peak magnitude decreased until at approximately pH where only the charging currents seemed to remain. This result was as expected from the previously stated linear relationship, equation (3.5), between peak current size and electrolyte concentration. The peak positions shifted to a more negative value with increasing pH. This correlated with the behaviour of the potential limits and hence was expected.

Double Layer Capacitance Determination

The double layer capacitance can be calculated from normal potentiostatic i-E curves by varying the potential scan rate of the potentiostat and recording the charging current values, since:-

$$\text{Capacitance} = \frac{dq}{dE} = \frac{dt}{dE} \cdot \frac{dq}{dt} \qquad (5.2)$$

However

$$\frac{dq}{dt} = i \quad \text{and} \quad \frac{dt}{dE} = \frac{1}{V} \qquad (5.3)$$

where V = the potential scan rate

Hence (5.2) becomes:-

$$C = \left(\frac{1}{V}\right) . i \qquad (5.4)$$

$$\therefore \quad i = C.V \qquad (5.5)$$

Therefore, if a plot of charging current (i) versus potential scan rate (V) is carried out then the double layer capacitance (C) of the electrode surface is the gradient of the linear plot.

The electrolyte used for the above experiment was 2.0M HNO_3 and the results can be seen in Table 5.2.

Table 5.2

POTENTIAL SCAN RATE (Vs^{-1})	CHARGING CURRENT (A)
0.01	1×10^{-5}
0.02	2×10^{-5}
0.05	5×10^{-5}
0.10	9×10^{-5}
0.20	2×10^{-4}
0.30	3×10^{-4}
0.40	3.7×10^{-4}

Gradient = 1×10^{-3}

Double layer capacitance of the whole electrode = 1mF

However it is the usual convention to present the double layer capacitance as a value per cm^2, in this case a value per mg, and the weight of the active section of the fibre must be found.

Weight of the fibre used = 6.00 mg

The capacitance of the double layer = 167 μF/mg

This value for the double layer capacitance is in reasonable agreement with that found by Lipka et. al.[7], taking into account the adjustment for the different units.

5.2 Galvanostatic Capacitive Measurements

5.2.1 Long-Duration Galvanostatic Methods

Experiments were conducted using 2.0M HNO_3 electrolyte and carbon fibre electrodes. Several constant currents were applied and the potential-time plots were recorded for each. The theory behind this method is discussed in section (3.7.1). The results of these experiments were analysed using a linear regression programme called MINITAB but, as with preliminary experiments conducted on electrical component circuits, the accurate determination of E_{max} was a problem. Therefore the value for the capacitance could be suspect.

$$\text{Since:-}\quad \ln\left(1 - \frac{E_o(t)}{E_{max}}\right) = -I_o E_{max} C \cdot t \qquad (5.6)$$

Then the gradient provides the double layer capacitance.

Then the average value for the double layer capacitance was found to be 254 μF/mg.

From this value it is possible to calculate the charge transfer resistance value, since:-

$$\ln\left(1 - \frac{E_o(t)}{E_{max}}\right) = -\frac{1}{RC} \cdot t \qquad (5.7)$$

$$\text{then the gradient, } m = -\frac{1}{RC}$$

$$\therefore \qquad R = -\frac{1}{m.C.} \qquad (5.8)$$

The average value for the charge transfer resistance was 33.94 KΩ/mg.

It was found that for large constant currents, the potential-time plots were non-linear at large t values. This was thought to be due to the fact that the electrode process occurring was diffusion controlled. However, on attempting the plots associated with semi-infinite linear diffusion, such as overpotential η v $t^{\frac{1}{2}}$ and $\exp\left(\frac{\eta nF}{RT}\right) - 1$ versus $t^{\frac{1}{2}}$, it was found that neither produced the linear plots expected from diffusion theory[5]. It was concluded that the process under study was not controlled by semi-infinite linear diffusion but by a more complex form, possibly due to electrode surface roughness and porosity effects[6].

It was noted that if the resistance component R_1 was infinite then theoretically the expression for I_o can be simplified to:-

$$I_o = C \cdot \frac{dE_o(t)}{dt} \qquad (5.9)$$

$$E_o(t) = \frac{I_o}{C} \cdot t \qquad (5.10)$$

It was therefore decided to investigate the influence of R_1, by using a set of parallel RC circuits where the capacitance

remained constant and the resistance was varied. The potential-time plots were recorded for each value of R , from infinity down to a value approximating the carbon fibre electrode value.

It was shown that the effects of resistance on the plots can only be observed at times greater than 30 secs and hence for large changes in potential.

As already stated, should the experimental duration be reduced to less than 10 secs then the potential-time plots become linear and the requirement of E_{max} is removed from the analysis. In addition, the simplified circuit theory, of a series capacitor, can be applied to represent the cell in future galvanostatic experiments.

5.2.2 Short-Duration Galvanostatic Methods

The double layer capacitance of carbon fibre electrodes were determined using the method discussed in section 4.6.2. The results of experiments carried out in 2.0M HNO_3 electrolyte and using four constant currents can be seen in Table 5.3 below:-

Table 5.3

CONSTANT CURRENT (μA)	AVERAGE DOUBLE LAYER CAPACITANCE (μF/mg)
0.2	24.4
0.5	25.4
1.0	28.0
2.0	31.0

The values found for the double layer capacitance seem low, one would expect from previous results that it would be approximately 100 μF/mg, but at least they are of the correct order of magnitude. This discrepancy may be accounted for the difficulty of establishing the weight of the active electrode.

Electrode Reproducibility

As has already been mentioned, for any practical conclusions to be drawn about the double layer capacitance of carbon fibre electrodes, it is necessary to show their reproducibility. Hence, several different batches of fibres were measured in various electrolytes and their average double layer capacitances calculated. The results of these studies can be seen in Tables 5.4 to 5.6.

Table 5.4

2.0M HNO_3

BATCH NO	AVERAGE C_{total} (μF)	WEIGHT (mg)	CAPACITANCE/mg (μF)
1	119.1	3.1	35.2
2	93.9	3.4	30.4
3	161.9	5.4	30.0

Table 5.5

2.0M H_3PO_4

BATCH NO	AVERAGE C_{total} (μF)	WEIGHT (mg)	CAPACITANCE/mg (μF)
1	117.0	4.0	29.3
2	87.4	3.8	23.0
3	199.9	9.0	22.2

Table 5.6

2.0M KOH

BATCH NO	AVERAGE C_{total} (μF)	WEIGHT (mg)	CAPACITANCE/mg (μF)
1	185.7	8.1	22.9
2	145.9	4.9	29.8
3	336.9	11.3	29.8

Batch number 1 seems to have different electrical characteristics from batches 2 and 3 in all three electrolyte solutions. This can be explained by the fact that batch 1 are six-month old fibres and they seem to have undergone surface modification on exposure to laboratory conditions for a prolonged period of time.

In addition, there is a possibility the surface modifications produced surface treatments are time-dependent. Batches 2 and 3 were new fibres but from different manufacturing batches.

It was concluded that only new fibres would be used in all future galvanostatic experiments and that these fibres must be kept in an inert atmosphere to prevent surface modification.

Effect of the Electrolyte on the Double Layer Capacitance at the Electrode/Electrolyte Interface

The effect of electrolyte on the double layer capacitance value was investigated using six different electrolyte and four constant currents for each. The results of this study can be seen in Table 5.7 below:-

Table 5.7

2.OM ELECTROLYTE	AVERAGE CAPACITANCE/mg (μF)
HNO_3	30.5
H_3PO_4	22.6
KOH	30.0
KCl	21.4
KBr	21.8
KI	31.8

These results show only slight differences in the value for the double layer capacitances for the different electrolytes. Therefore, there are no major trends which can be implied to the effects of electrolyte on the double layer capacitance of carbon fibre electrodes.

CHAPTER 5

REFERENCES

1. J J Lingane: "Electrochemical Methods". Pub. by J Wiley and Sons (1980).

2. A J Bard; L A Faulkner: "Electrochemical Methods". Pub. by J Wiley and Sons (1980).

3. R N Adams: "Electrochemistry at Solid Electrodes". Pub. by Marcel Dekker Inc. (1969).

4. G Charlot; J Badoz-Lambling; B Tremillion: "Electrochemical Reactions". Pub. by Elsevier Pub. Co. (1962).

5. I Nairn: Ph.D. Thesis St Andrews Univ. (1984).

6. R De Levie: "Adv. in Electrochem. and Electrochemical Eng. Vol. 6" by P Delahay; C W Tobias, p329. Pub. by J Wiley and Sons (1970).

7. S M Lipka; G L Cahen Jnr; G E Stoner; L L Scribner Jnr; E Gileadi: Electrochimia Acta 33 753 (1988).

CHAPTER 6

RESULTS AND DISCUSSIONS OF A.C. IMPEDANCE STUDIES

6.1 Introduction

The conclusion drawn from the non-sinusoidal studies was that the carbon fibre electrode/electrolyte interface is much more complex than was first proposed. The simple equivalent circuit representation shown in Figure 3.13 is therefore insufficient for adequate characterisation of carbon fibre surfaces. It was thought that a more accurate equivalent circuit for the interface could be produced by application of spectro-electrochemical a.c. impedance techniques. It was hoped that these techniques could be harnessed to provide accurate monitoring of the effects of polarisation potential, time and chemical and electrochemical treatments on the carbon fibre surfaces. This could possibly lead to property prediction in the subsequent composite material.

6.2 A.C. Impedance Diagrams

The theory behind and experimental details of these a.c. studies can be seen in Chapters 3 and 4 respectively.

As discussed in Chapter 4, preliminary experiments conducted on electrical component circuits and computer generated a.c. impedance data from theoretical expressions for Z' and Z", established that the technique and analysis method were viable.

6.2.1 Polarisation Potential Dependence of Untreated Fibres

Initial a.c. impedance experiments carried out on HM-U 2M207 B/10 fibre into the effects of polarisation potential on the fibre electrode/ electrolyte interface produced argand diagrams similar to those shown in Fig. 6.1 and 6.2. These plots were thought to contain two distinct semi-circular features and a high frequency element which was not discernible. The high frequency element was therefore ignored in the subsequent graphical analysis since it could not be attributed to any recognisable electrical component.

A more detailed investigation of the effects of polarisation potential on HM-U 2M207 B/10 fibres was carried out using a potential variation of 0.1 V. In addition, the three electrode cell was de-gassed more thoroughly before these experiments were conducted. The argand diagrams produced are shown in Fig. 6.3 and 6.4.

It can be seen that these diagrams do not show the undiscernible element present in the previous figures.

These experiments were repeated for various batches of HM-U fibres, for details see Section 4.7.1, to investigate the variation of fibre surface between the different batches. The argand diagrams for these can be seen in Fig. 6.5-6.8.

6.2.2 Comparison of the Polarisation Potential Dependence of R.A.E. Treated Fibres and Untreated Fibres

As mentioned in Chapter 4, it was thought that the polarisation potential limits and dependence would be different for the treated and untreated fibres. Therefore this was investigated in both the anodic

Fig.6.1 Preliminary Study into the Potential Dependence of HM-U 2M207 B/10 Fibres. Anodic Region

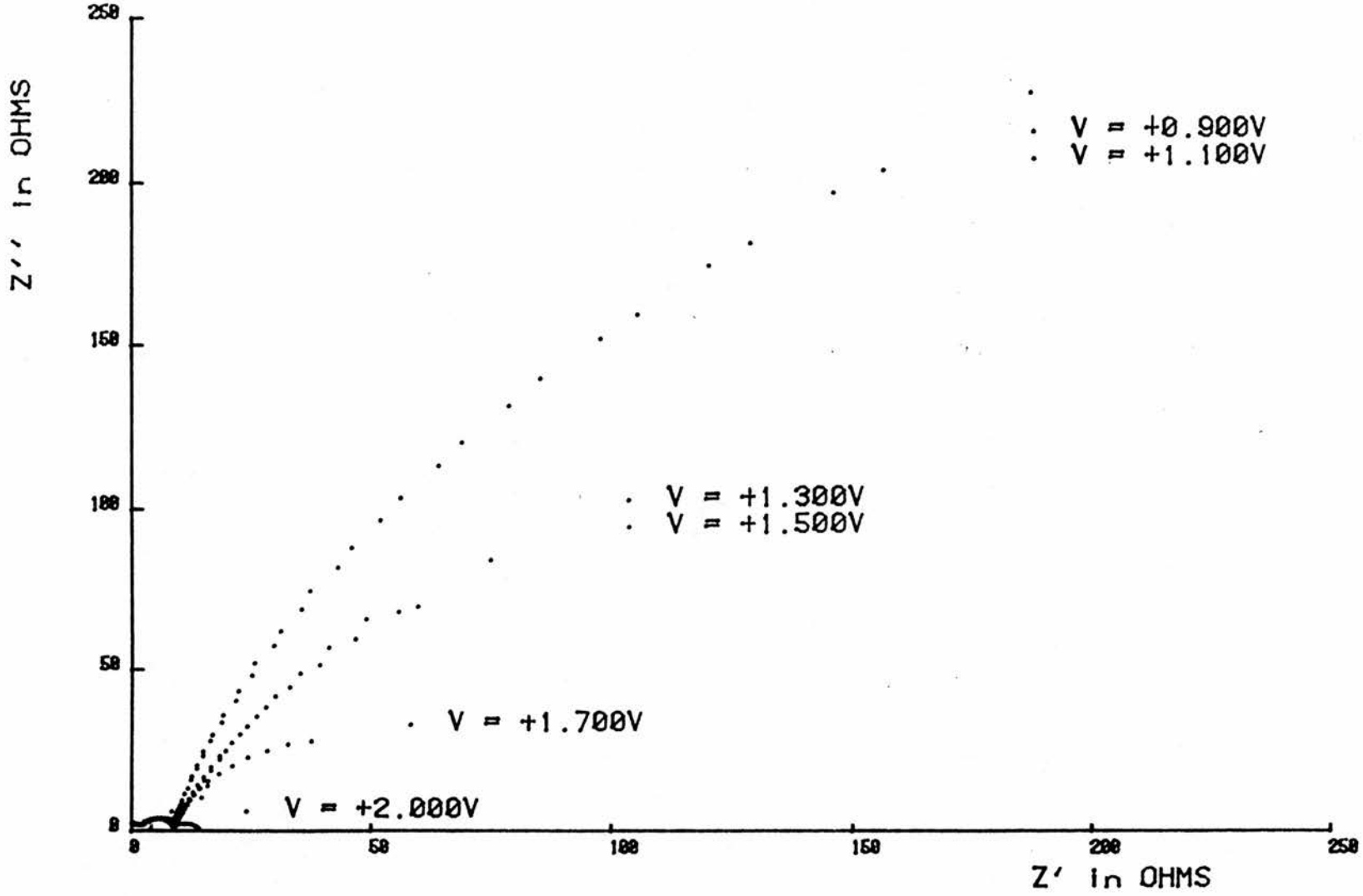

Fig.6.2 Preliminary Study into the Potential Dependence of HM-U 2M207 B/10 Fibres. Cathodic Region

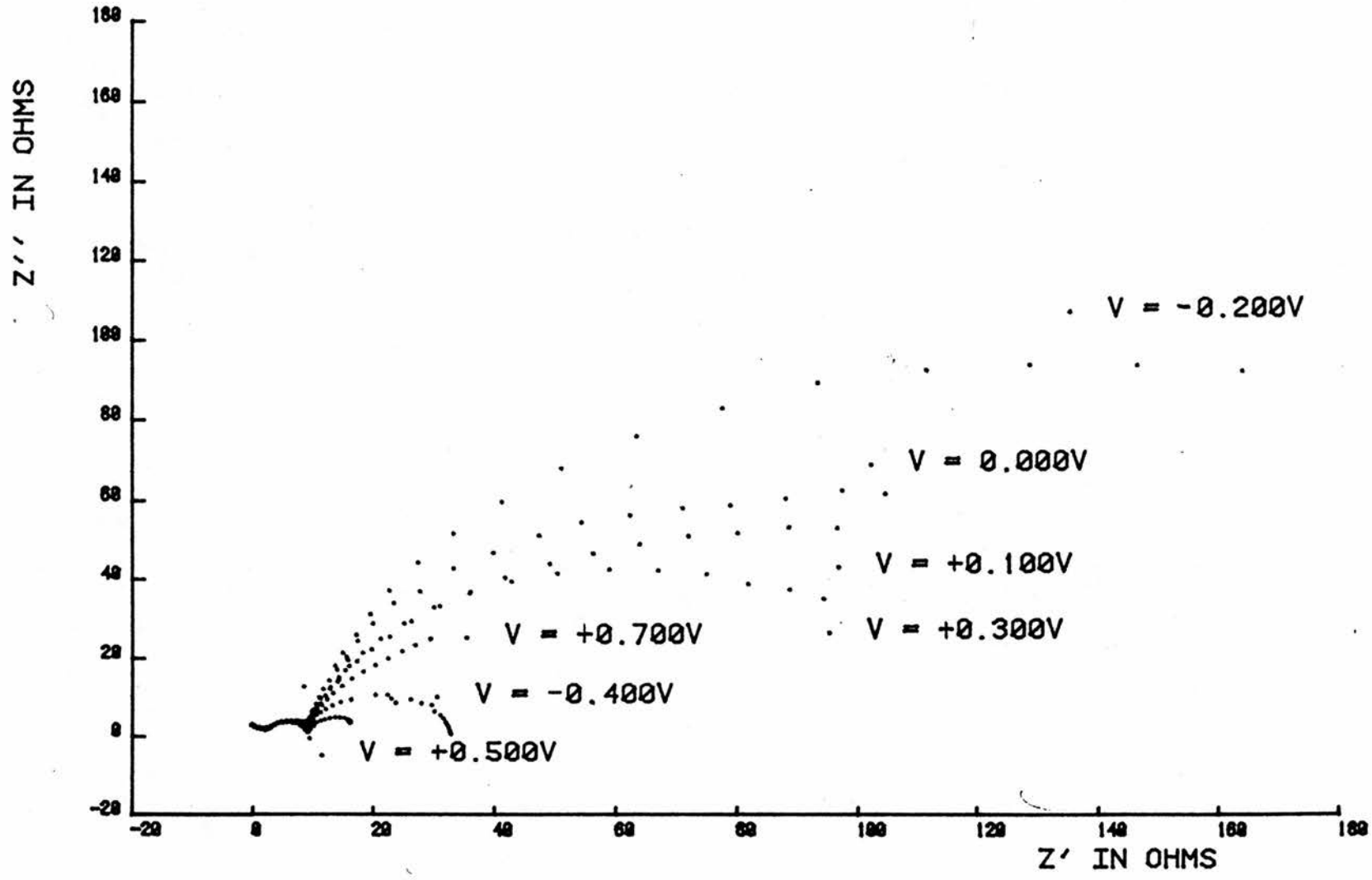

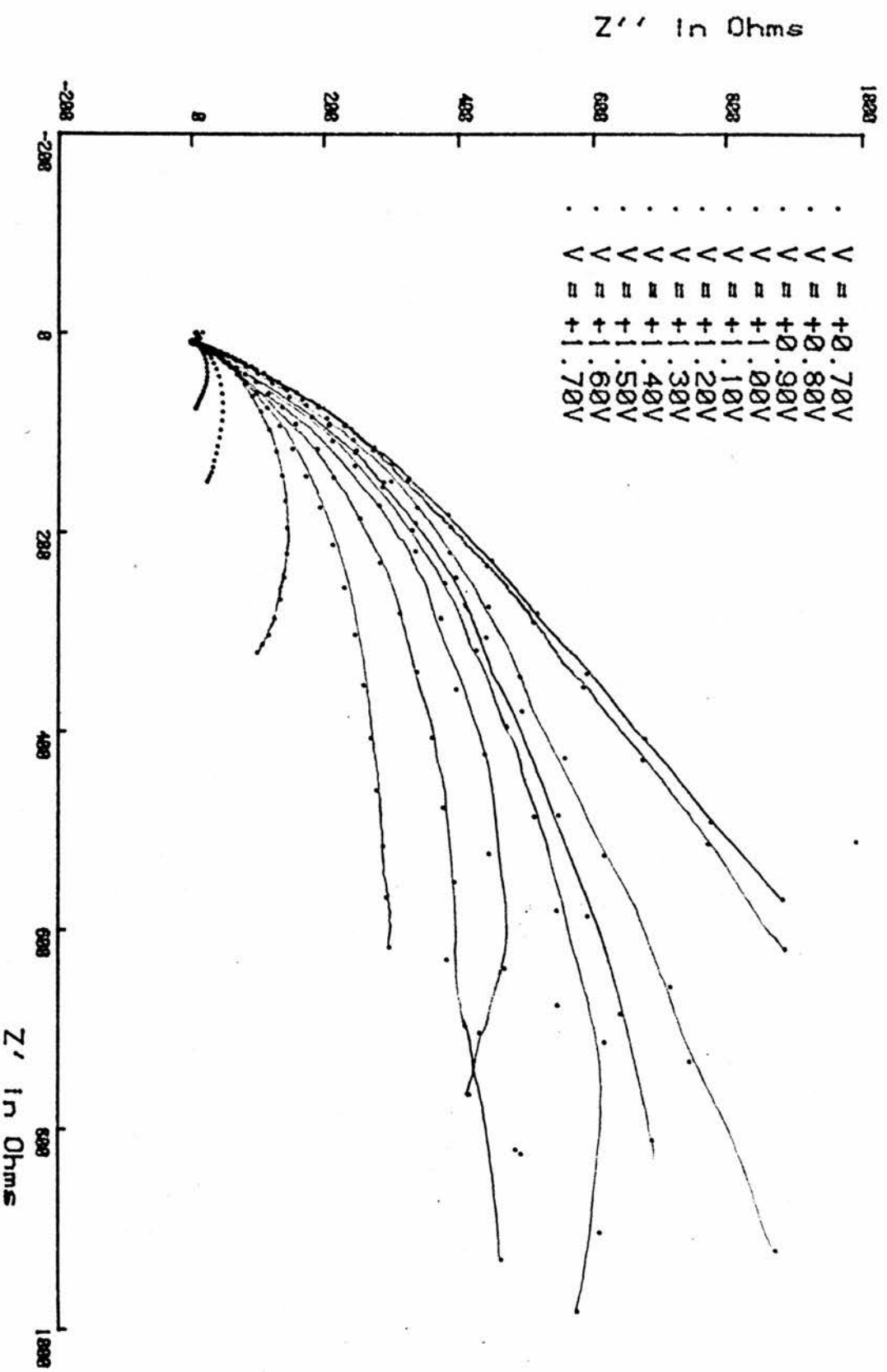

Fig.6.3 Potential Dependence of HM-U 2M207 B/10 Fibres. Anodic Region

Fig.6.4 Potential Dependence of HM-U 2M207 B/10 Fibres. Cathodic Region

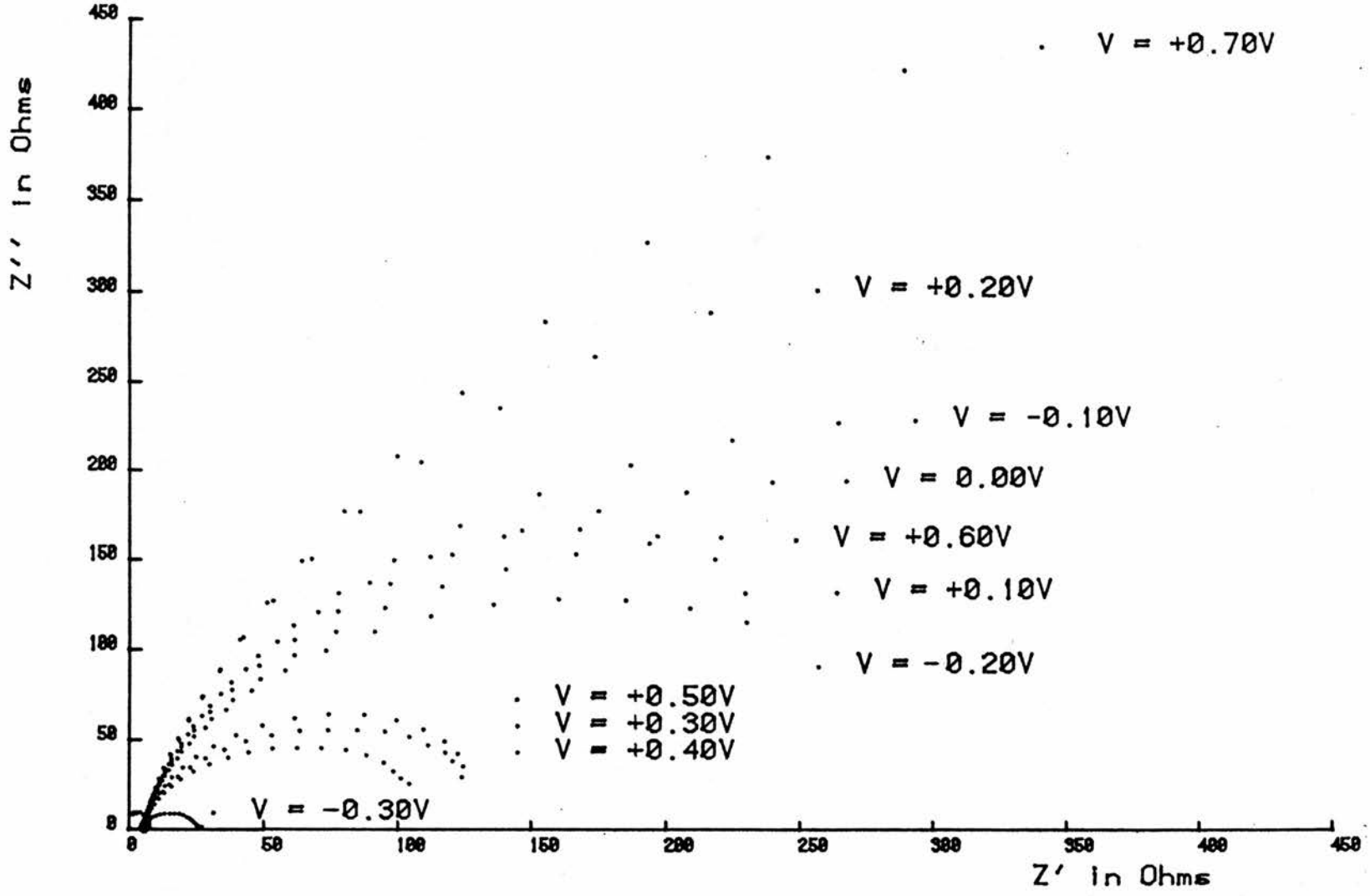

Fig.6.5 Potential Dependence of HM-U 2M371 E/10 Fibres. Anodic Region

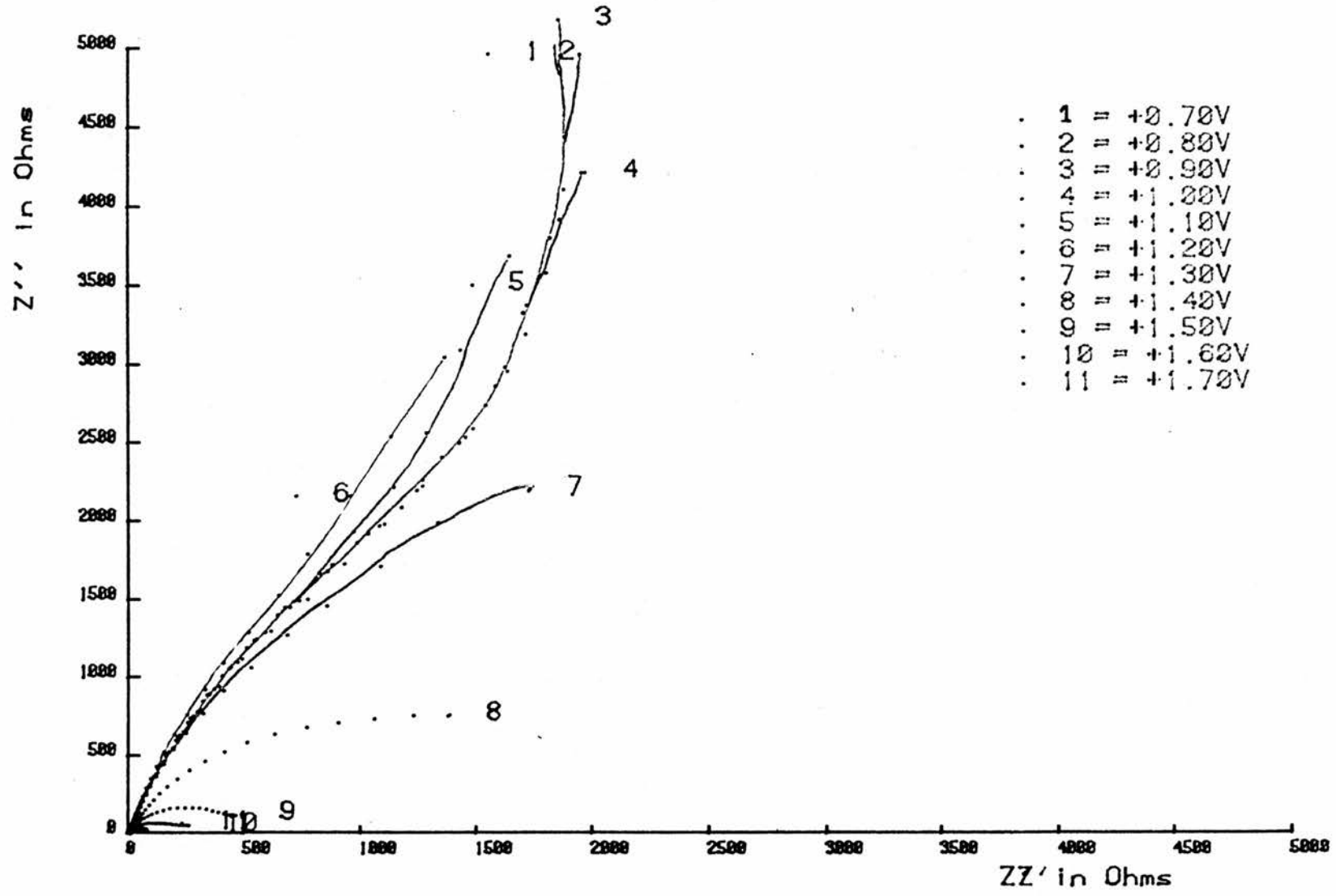

Fig.6.6 Potential Dependence of HM-U 2M371 E/10 Fibres. Cathodic Region

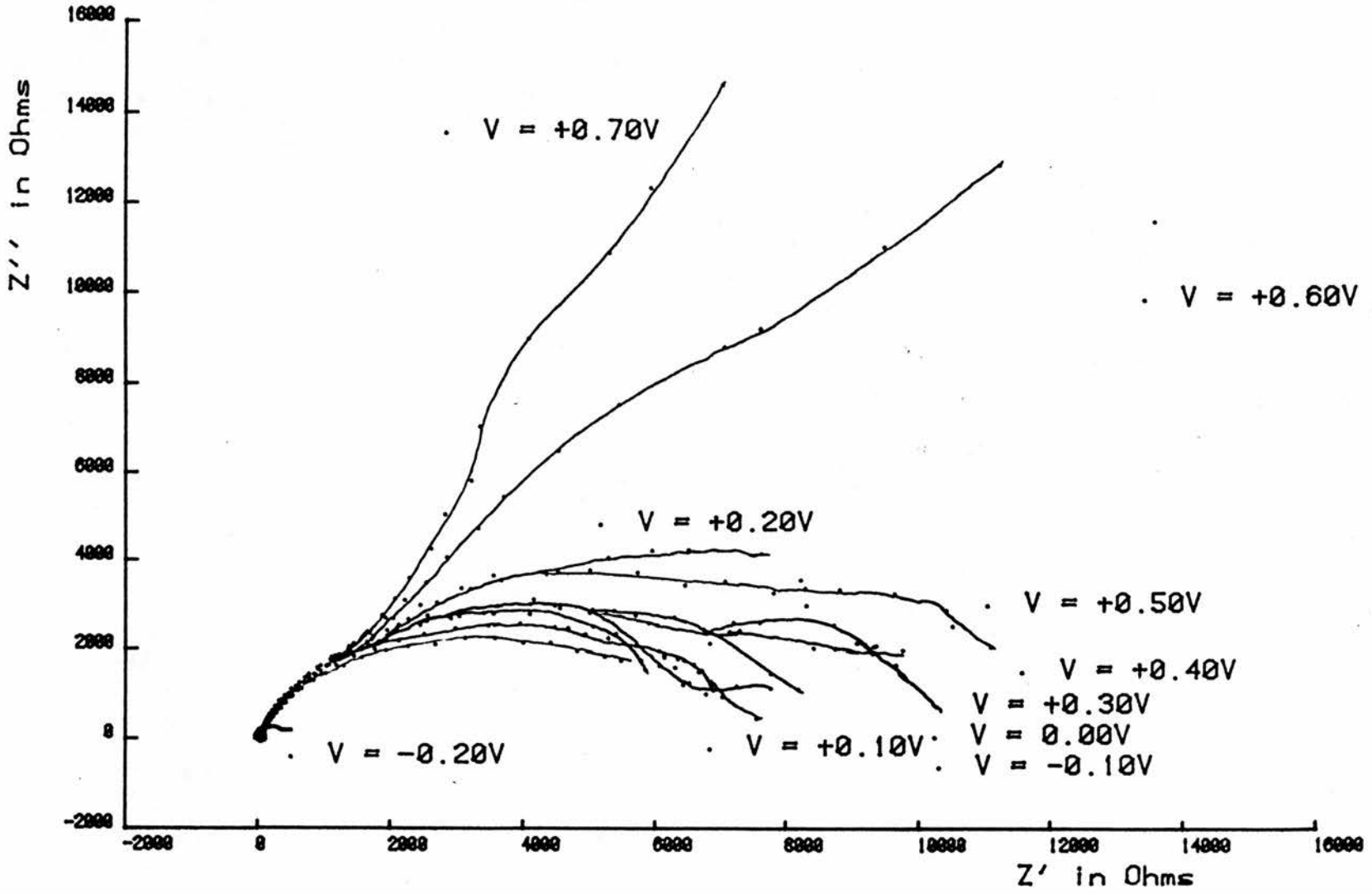

Fig.6.7 Potential Dependence of HM-U 2M307 D/10 Fibres. Anodic Region

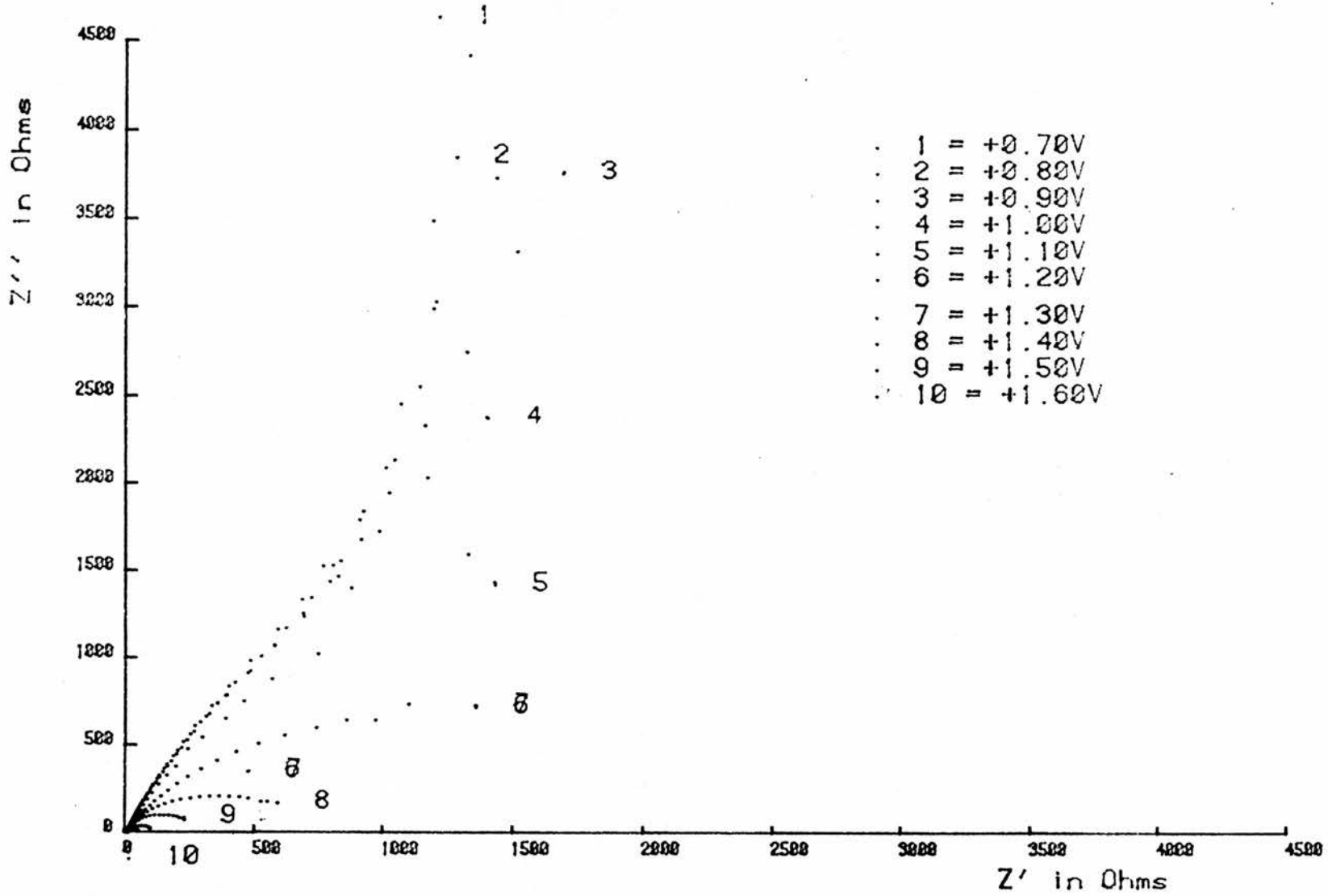

Fig.6.8 Potential Dependence of HM-U 2M307 D/10 Fibres. Cathodic Region

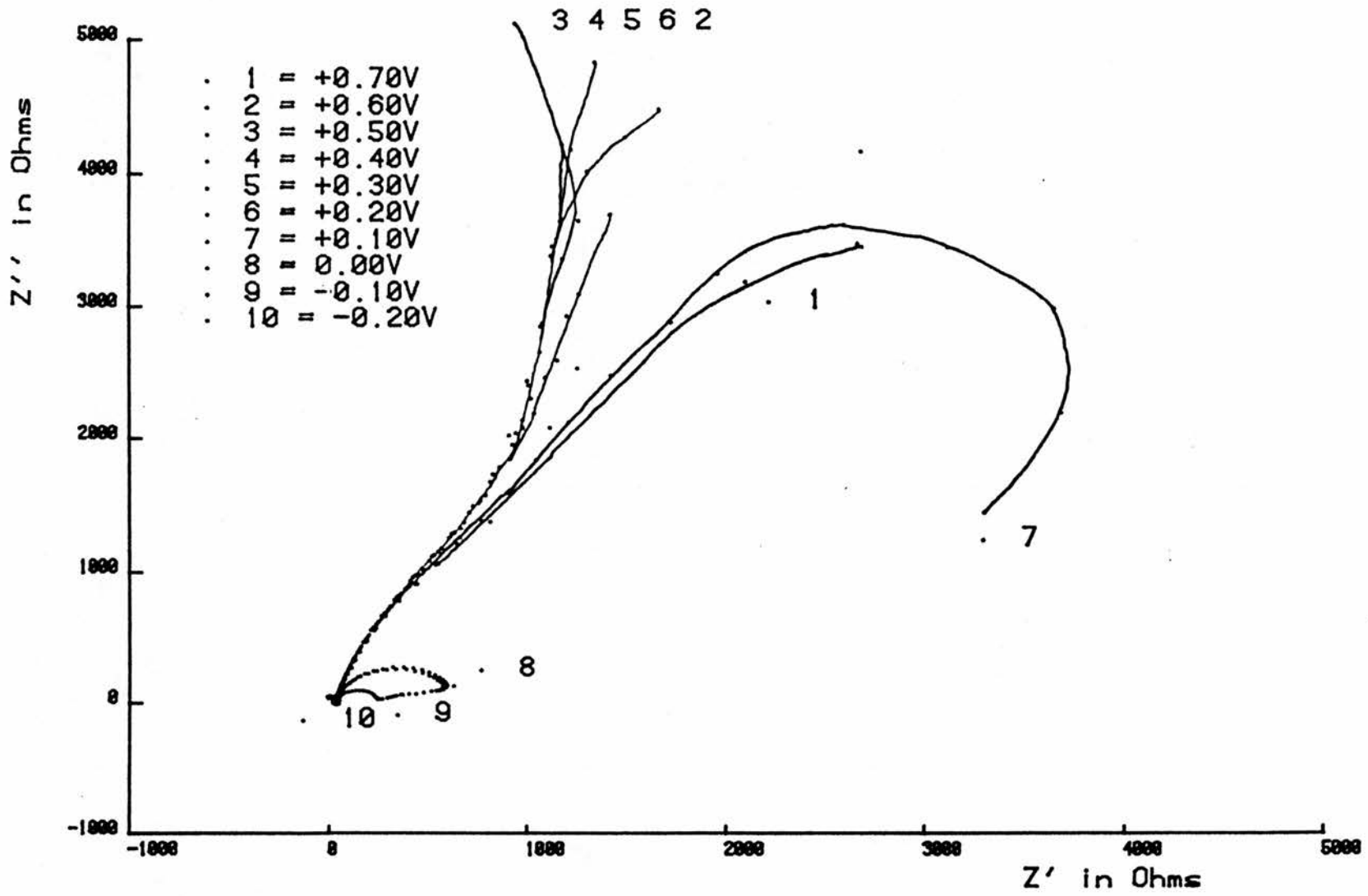

and cathodic potential regions. The resultant diagrams can be seen in figures 6.9-6.16. It must be noted that the potential limits are different between treated and untreated fibres.

6.2.3 The Effect of d.c. Potential Value on Increased Oxidation of HM-U Fibres

The aim of this experiment was to find a suitable anodic polarisation potential for use in the study into the effects of galvanic oxidation on untreated fibres. Three anodic potentials were chosen and a series of increased oxidations were performed. The resultant argand diagrams can be seen in figures 6.17-6.19.

6.2.4 Effect of Increased Galvanic Oxidation on HM-U Fibres

Initial experiments showed that the effect of increased oxidation was much more satisfactorily observed when the galvanic oxidation time was large and that the optimum polarisation potential values were just below the potential limits in both the anodic and cathodic cases. Therefore the range of oxidation times was increased from 0s to 3000s. The resultant plots can be seen in figures 6.20-6.21.

On observation of Fig. 6.20 it was felt that in the case of the anodic experiment that the fibre could be further oxidised by increasing the oxidation duration maximum to 7000s. The results of this can be seen in Fig. 6.22.

Fig.6.9 Potential Dependence Comparison Between HM-U and HM-S Fibres. HM-U 2M307 D/10. Anodic Region Part 1.

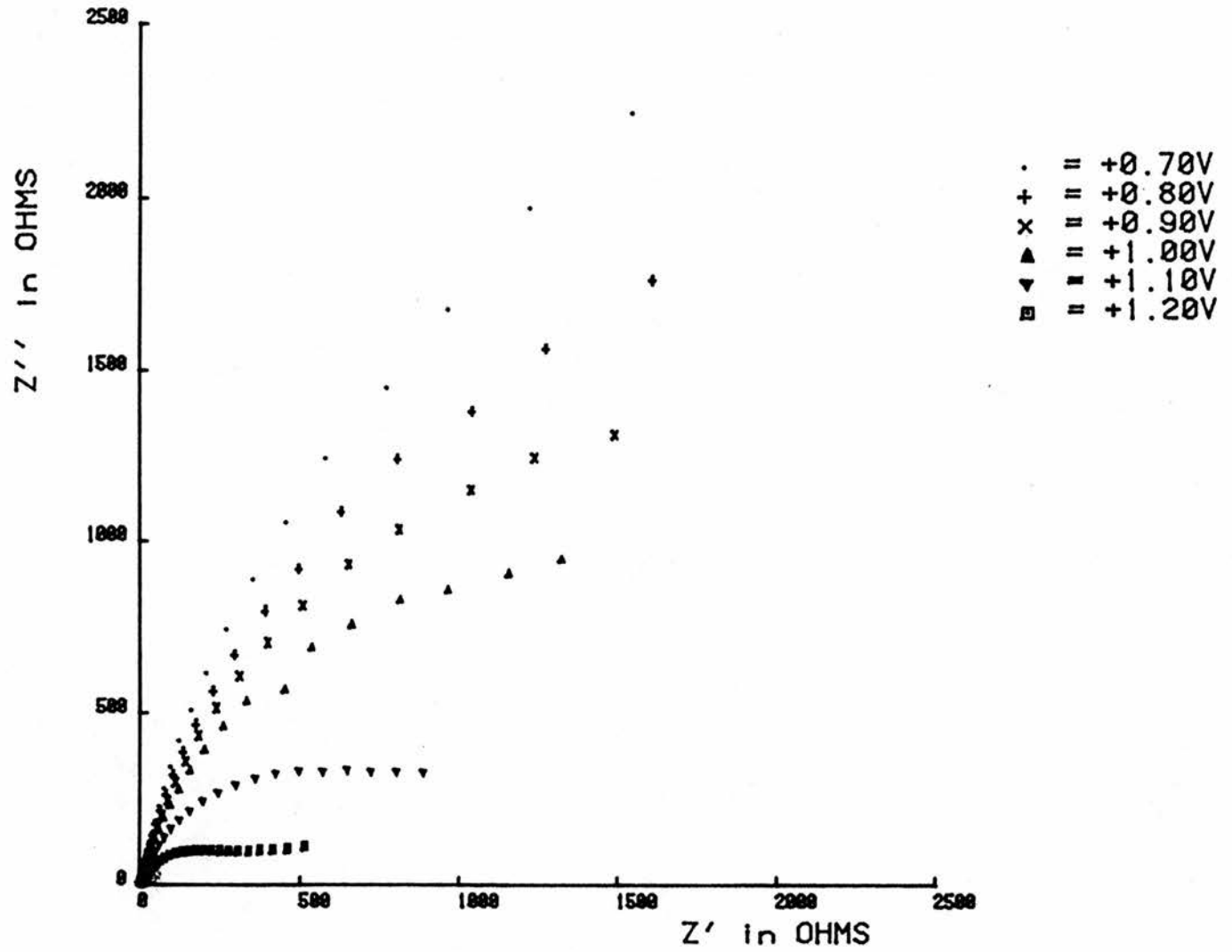

Fig.6.10 Potential Dependence Comparison Between HM-U and HM-S Fibres. HM-U 2M307 D/10. Anodic Region Part 2.

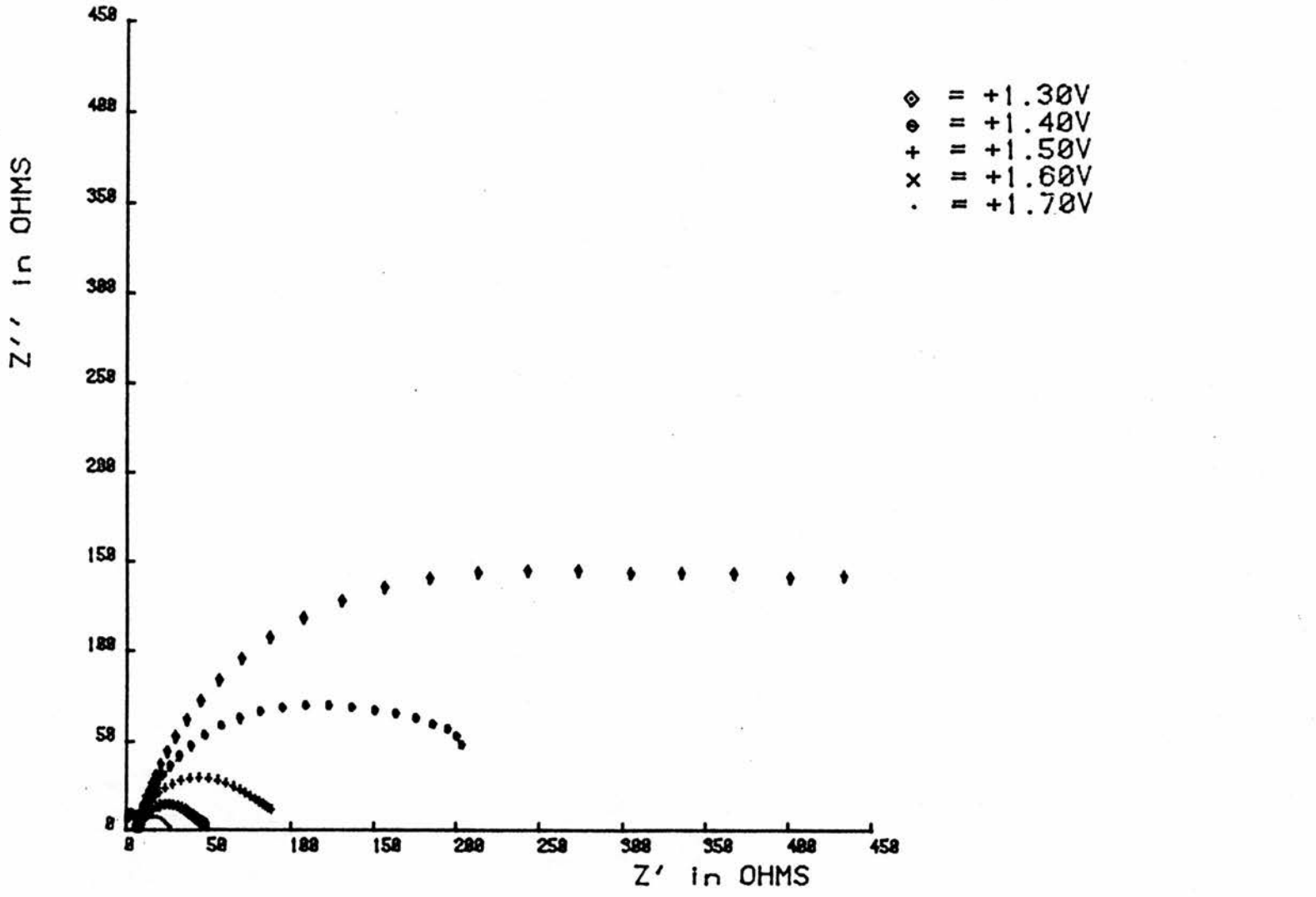

Fig.6.11 Potential Dependence Comparison Between HM-U and HM-S Fibres. HM-U 2M307 D/10. Cathodic Region Part 1.

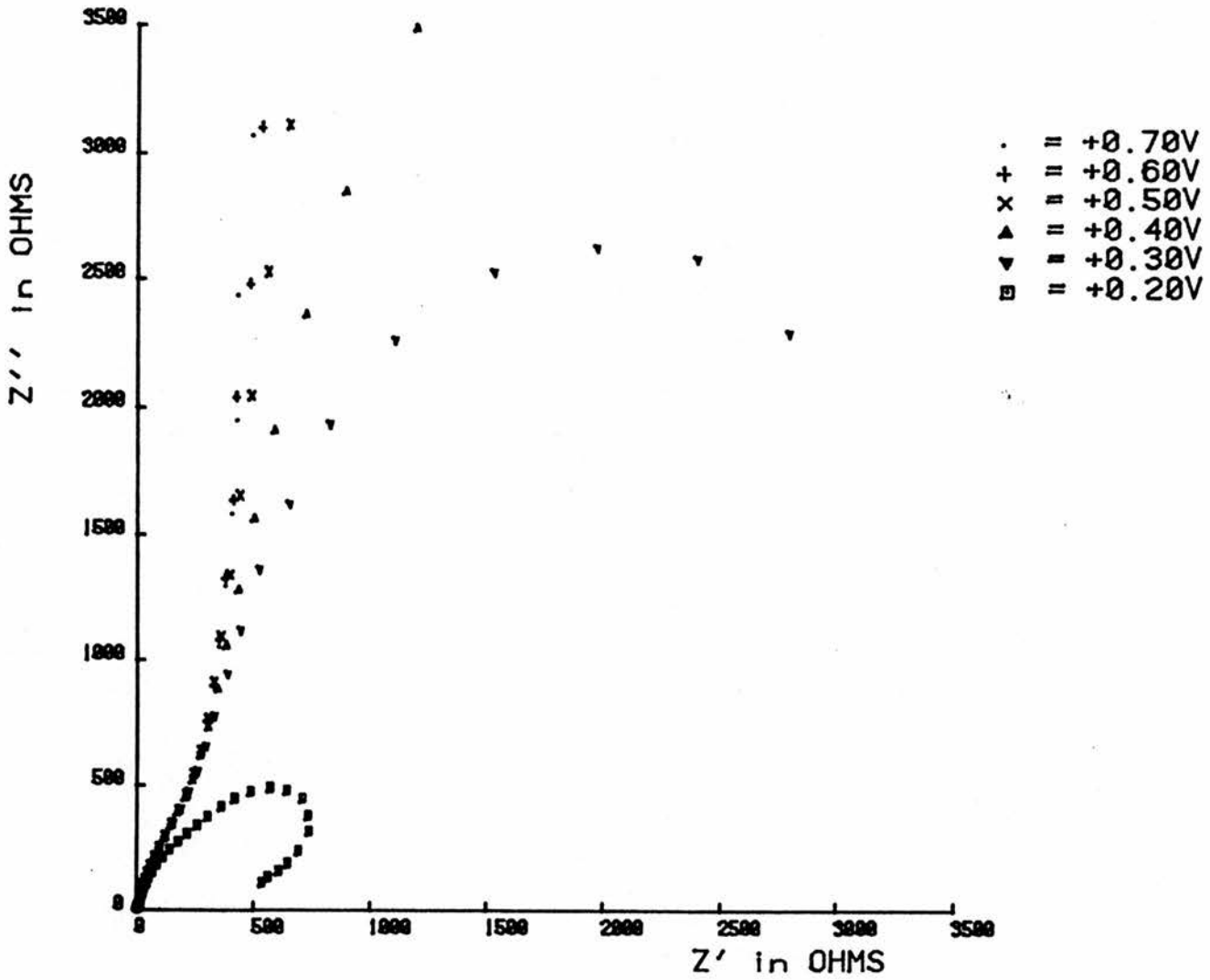

Fig.6.12. Potential Dependence Comparison Between HM-U and HM-S Fibres. HM-U 2M307 D/10. Cathodic Region Fig 6.2

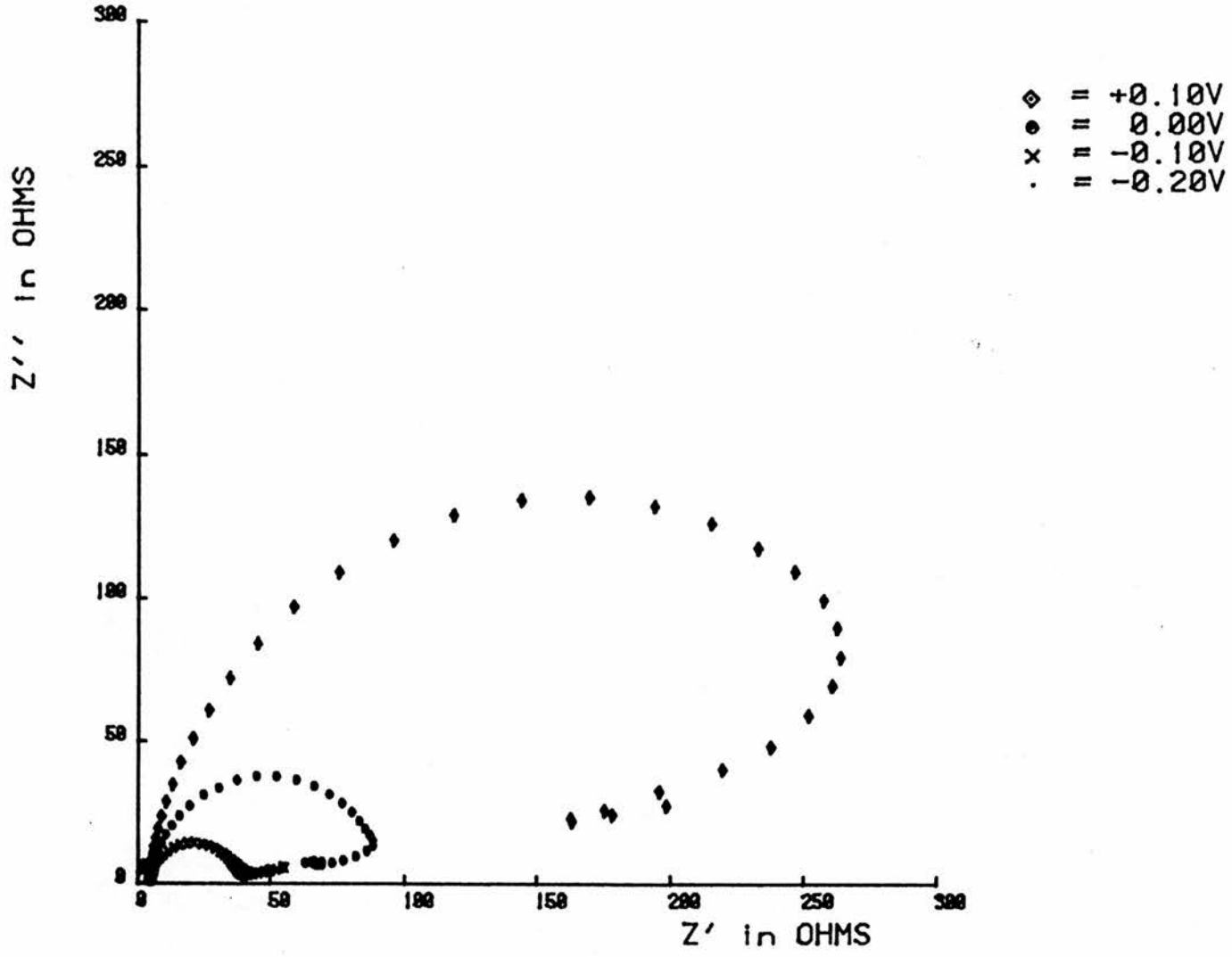

Fig.6.13 Potential Dependence Comparison Between HM-U and HM-S Fibres. HM-S 2M307 F/10. Anodic Region Part 1

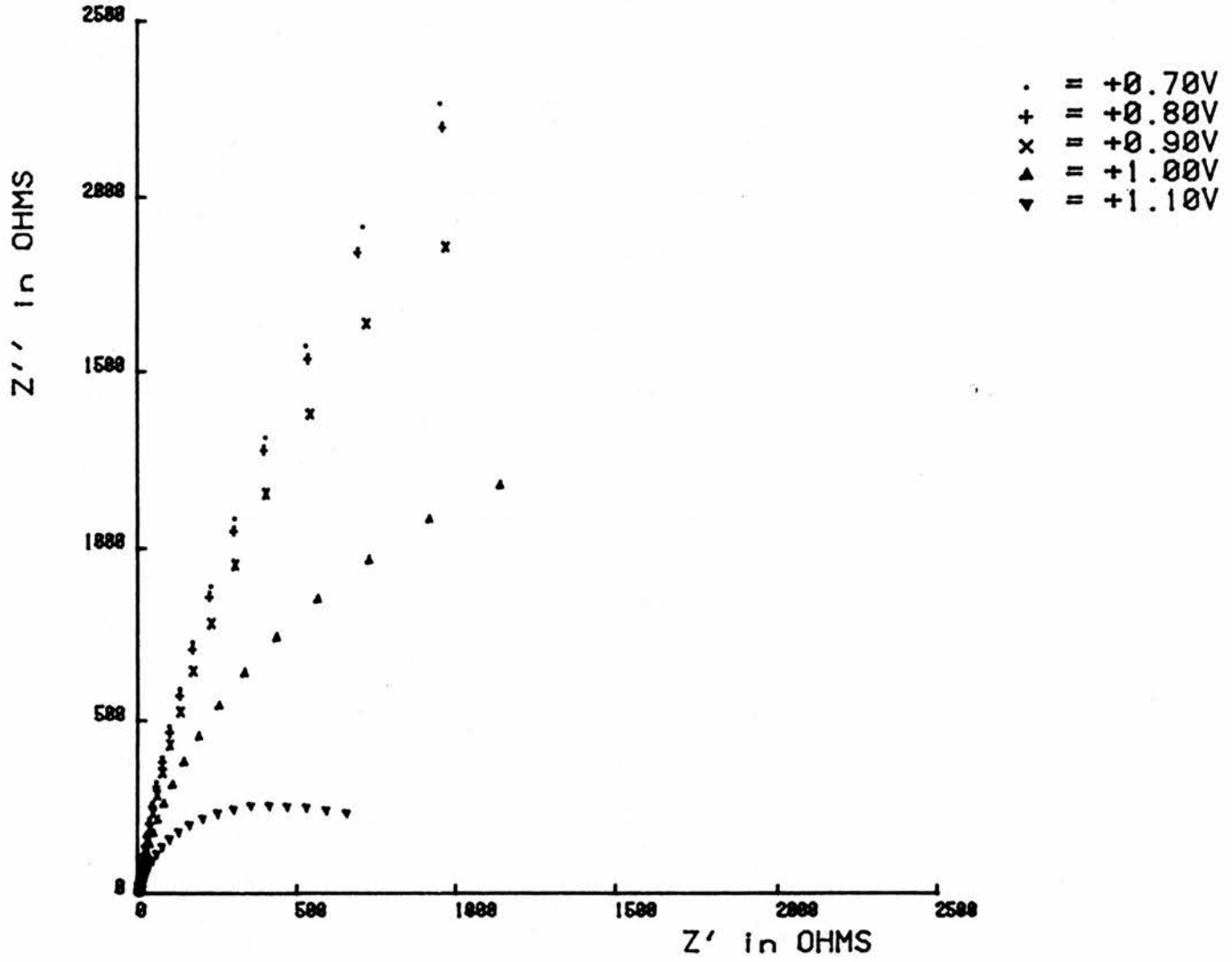

Fig.6.14 Potential Dependence Comparison Between HM-U and HM-S Fibres. HM-S 2M307 F/10. Anodic Region Part 2

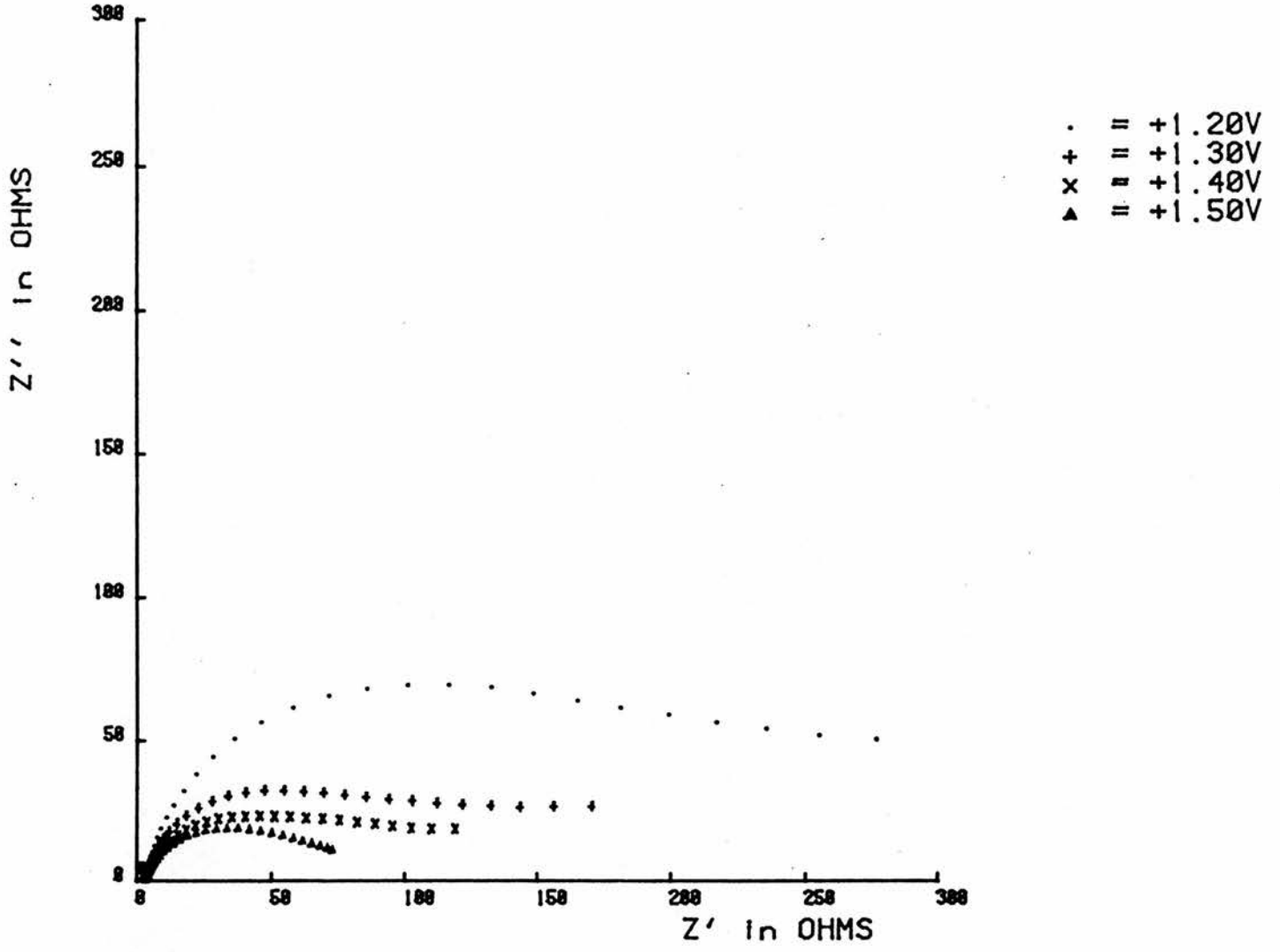

Fig.6.15 Potential Dependence Comparison Between HM-U and HM-S Fibres. HM-S 2M307 F/10. Cathodic Region Part 1

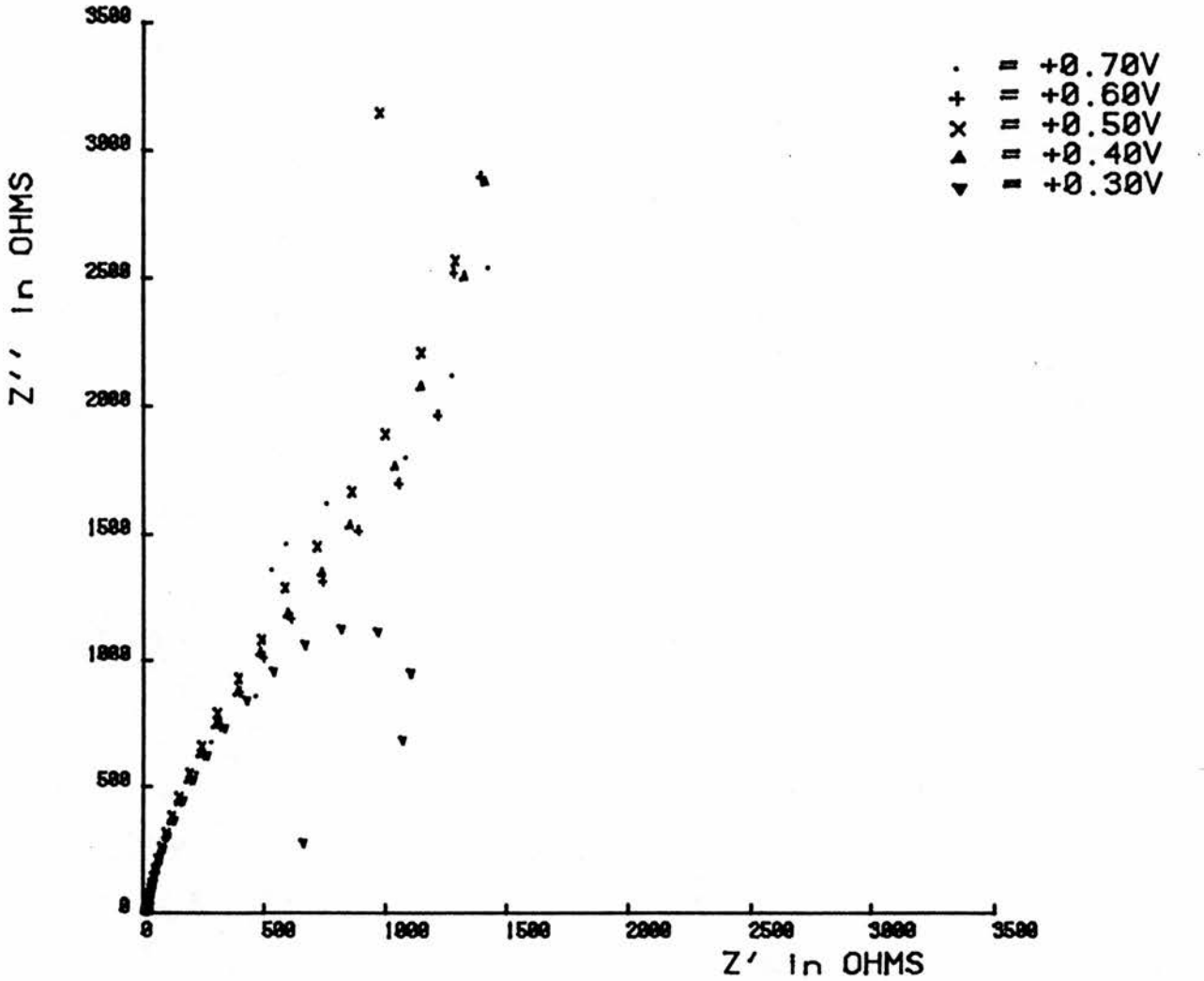

Fig.6.16 Potential Dependence Comparison Between HM-U and HM-S Fibres. HM-S 2M307 F/10. Cathodic Region Part 2

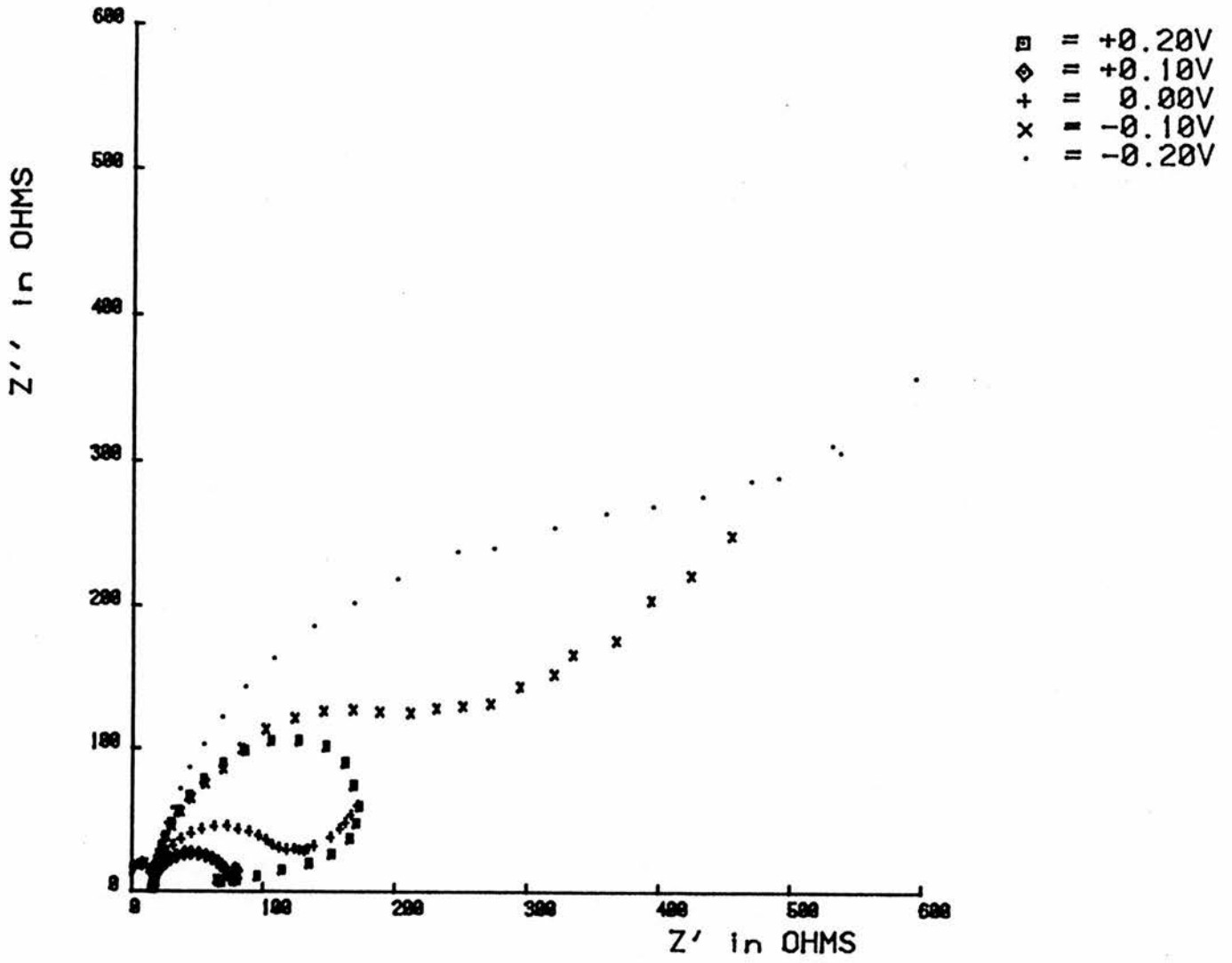

Fig.6.17 The Effect of Polarisation Potential Value on Increased Galvanic Oxidation of HM-U 2M307 D/10 Fibres.

Potential = + 0.70 V

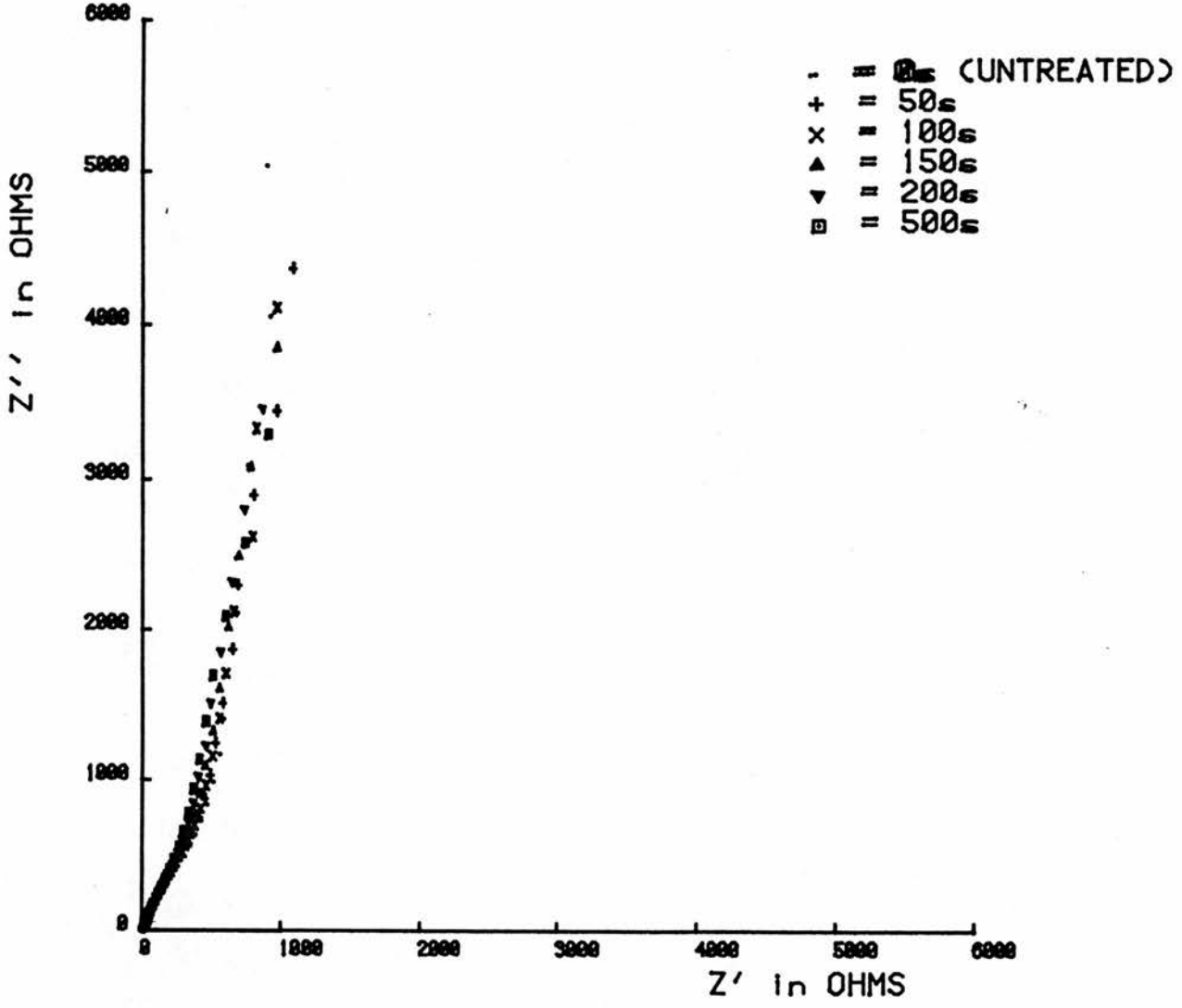

Fig.6.18 The Effect of Polarisation Potential Value on Increased Galvanic Oxidation of HM-U 2M307 D/10 Fibres

Potential = + 1.00 V

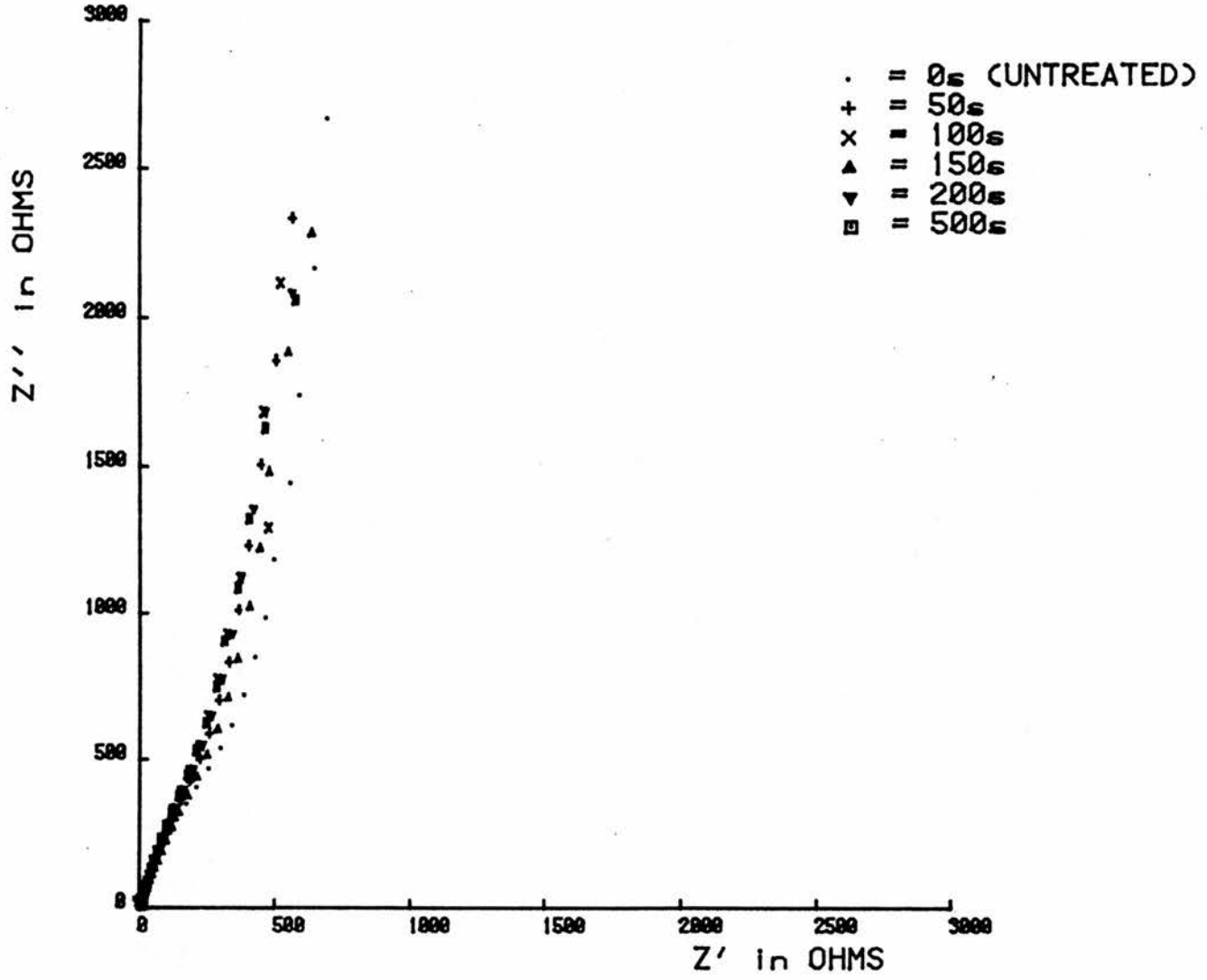

Fig.6.19 The Effect of Polarisation Potential Value on Increased Galvanic Oxidation of HM-U 2M307 D/10 Fibres

Potential = + 1.30 V

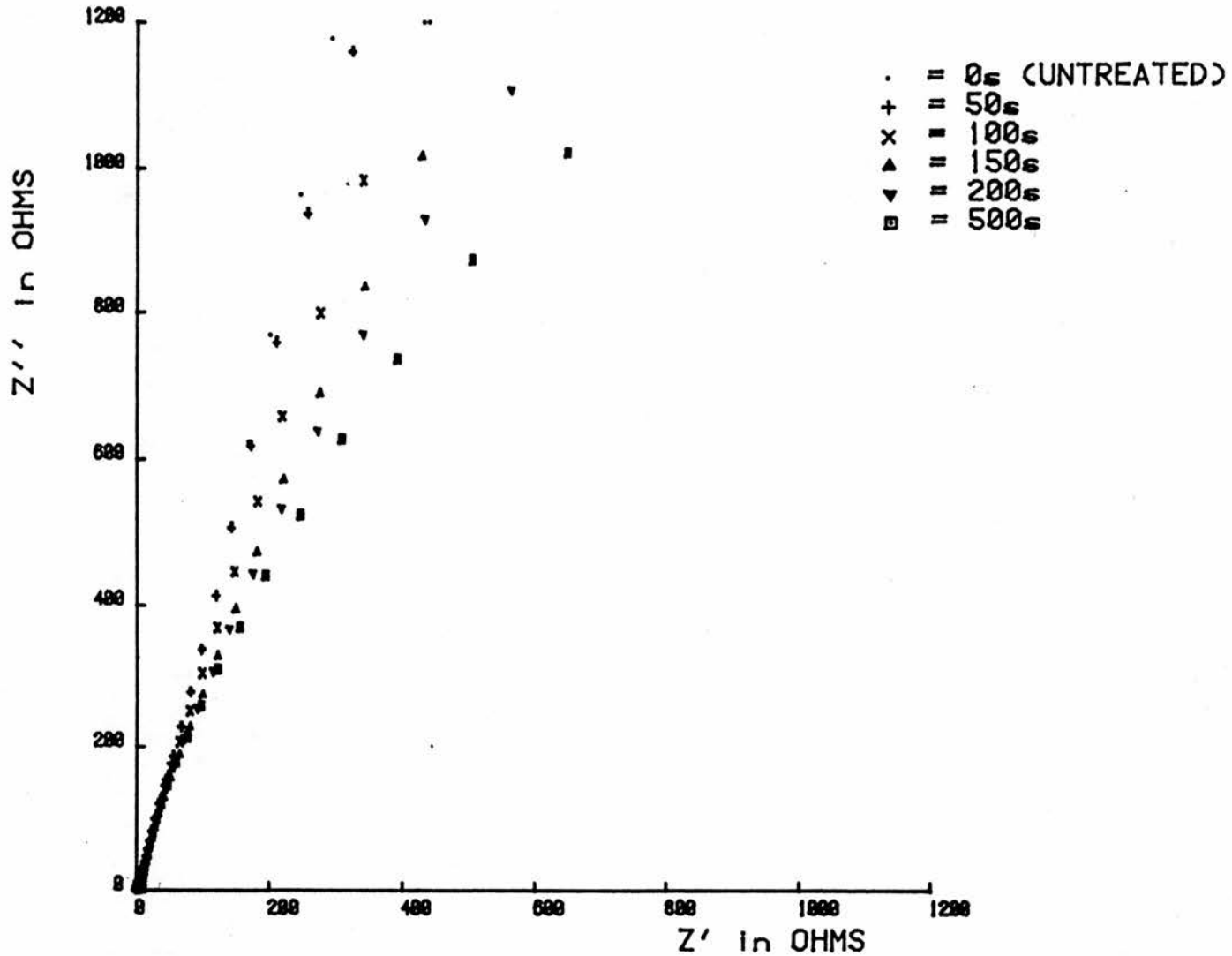

Fig.6.20 The Effect of Increased Galvanic Oxidation of HM-U 2M307 D/10 Fibres. Potential = + 1.30 V

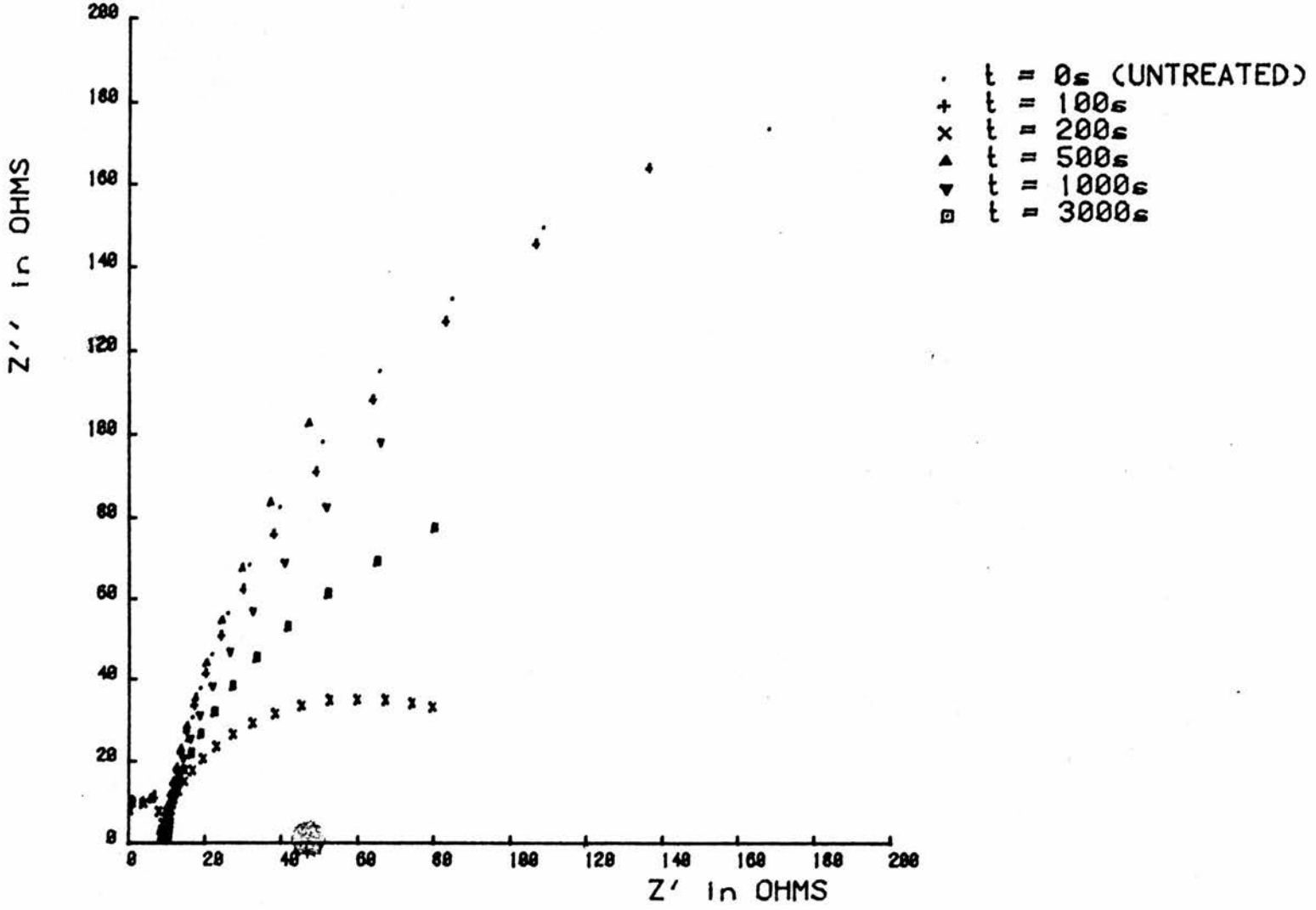

Fig. 6.21 The Effect of Increased Galvanic Reduction of HM-U 2M307 D/10 Fibres. Potential = 0.00 V

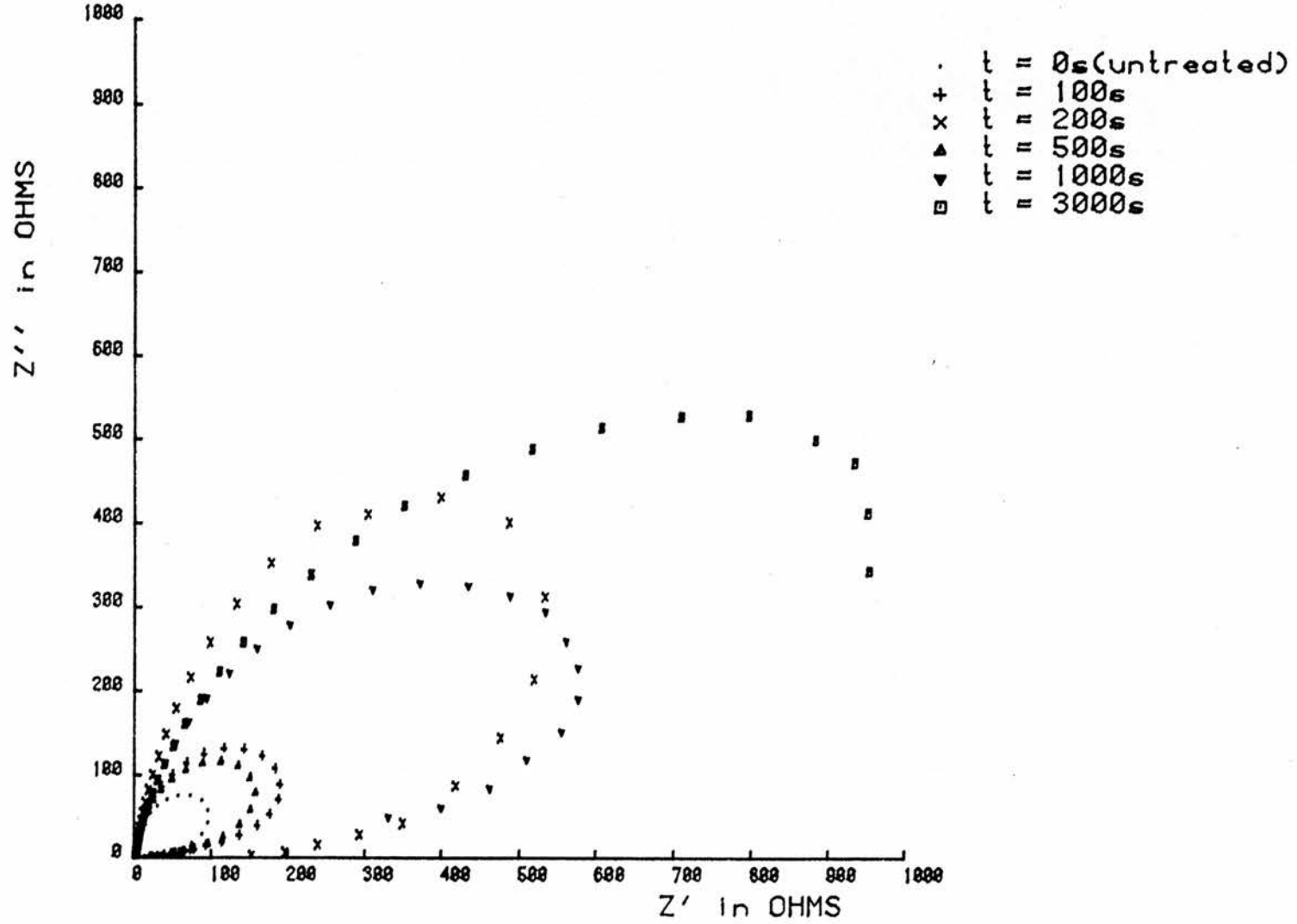

Fig.6.22 Effect of Further Oxidation on HM-U 2M307 D/10 Fibres. Potential = + 1.30 V

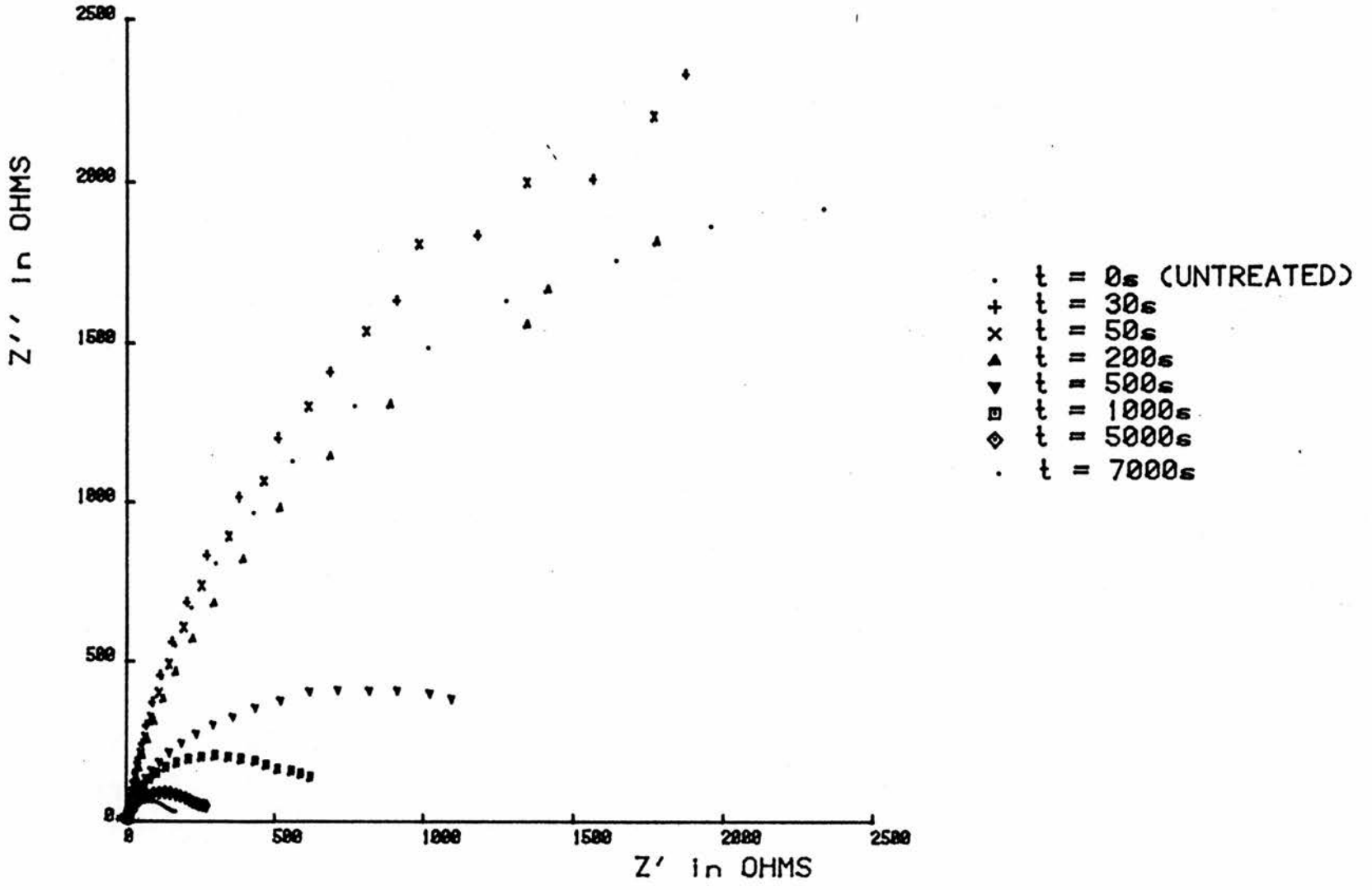

6.2.5 The Effect of Time on the Impedance Response of Galvanically Oxidised HM-U Fibres

As discussed in Chapter 4, it was observed that in previous galvanostatic oxidation experiments the a.c. impedance response of oxidised HM-U fibres seemed to be susceptible to variation due to the effects of time. This observation was thought important enough to warrant further investigation. Therefore a series of experiments were designed to monitor the effect of time on variously oxidised fibres. These oxidised fibres were monitored over a period of 11 days. The resultant argand diagrams can be seen in figures 6.23-6.32.

Fig.6.23 Effect of Time on HM-U 2M307 D/10 Fibres Part 1

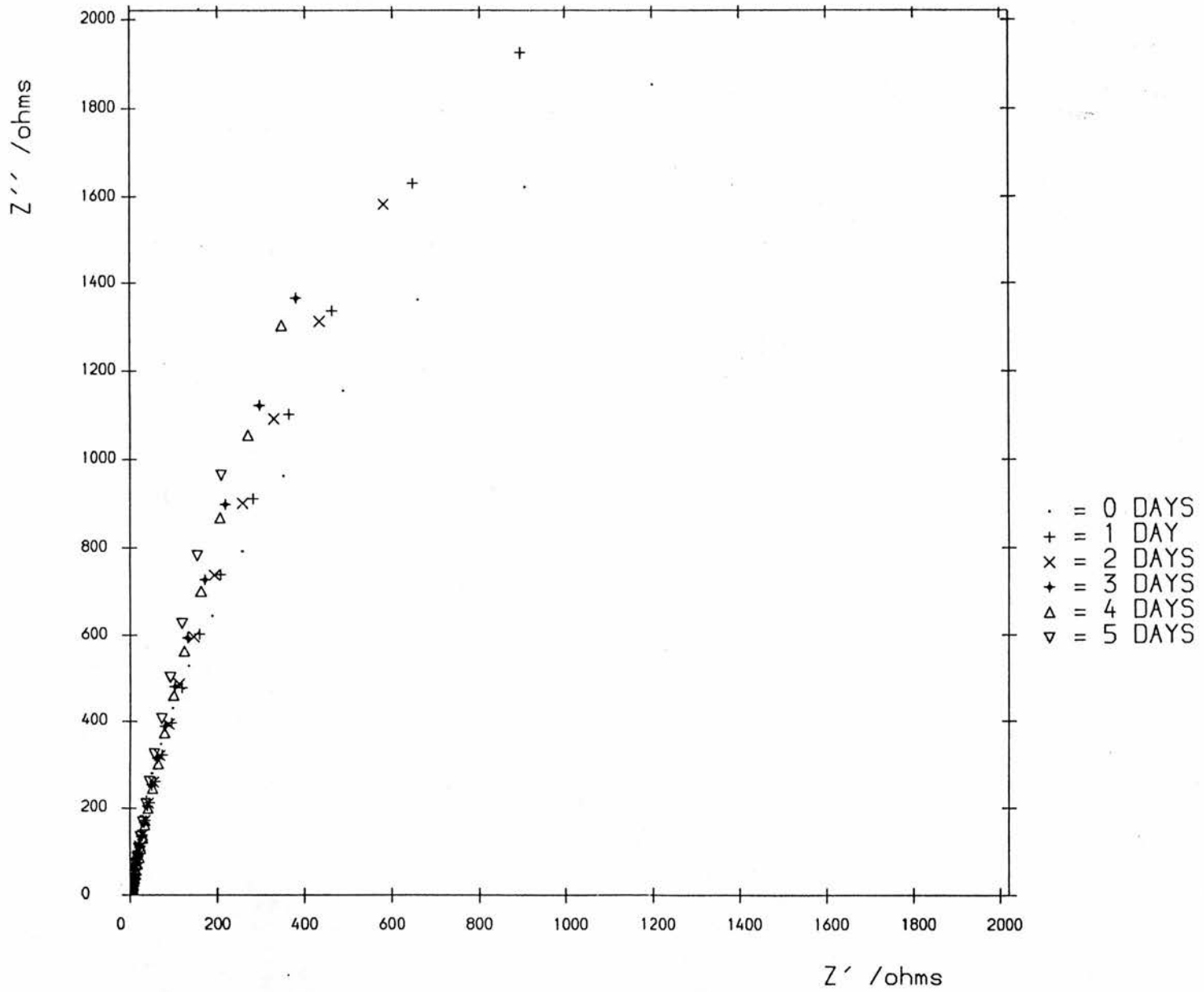

Fig.6.24 Effect of Time on Hm-U 2M307 D/10 Fibres. Part 2

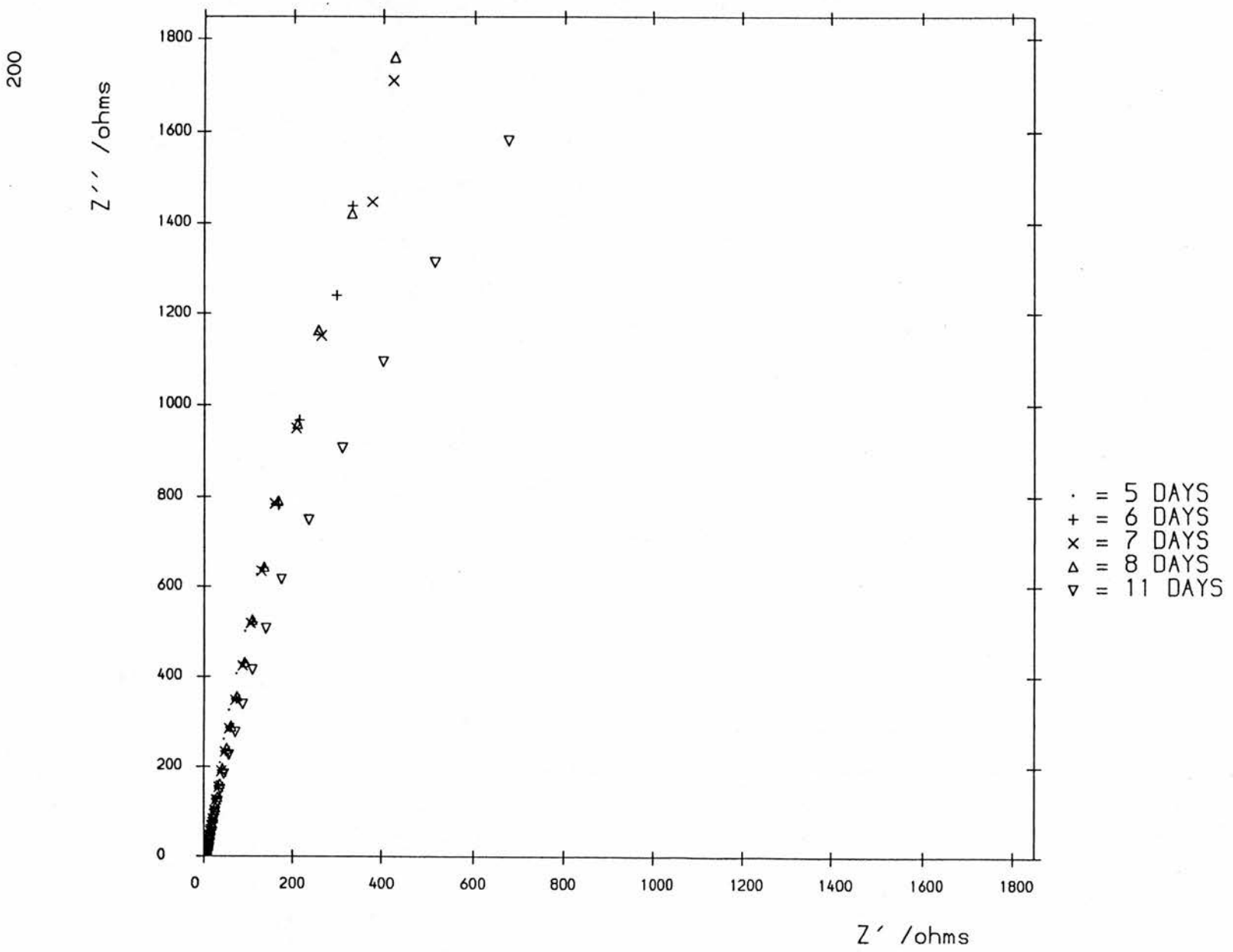

Fig.6.25 Effect of Time on Oxidised HM-U 2M307 D/10 Fibres. Oxidation Time = 500s. Part 1

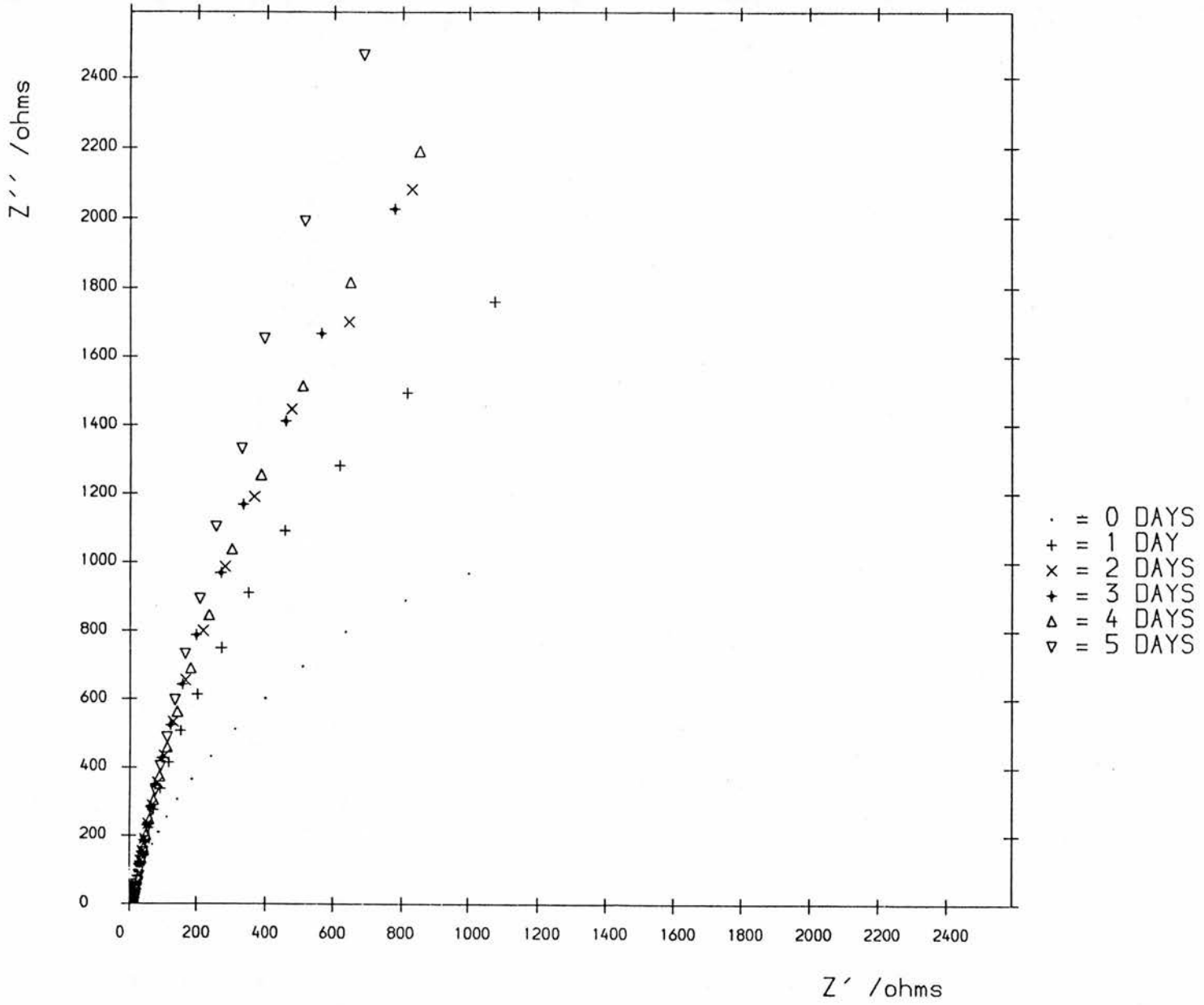

Fig.6.26 Effect of Time on Oxidised HM-U 2M307 D/10 Fibres. Oxidation Time = 500s. Part 2

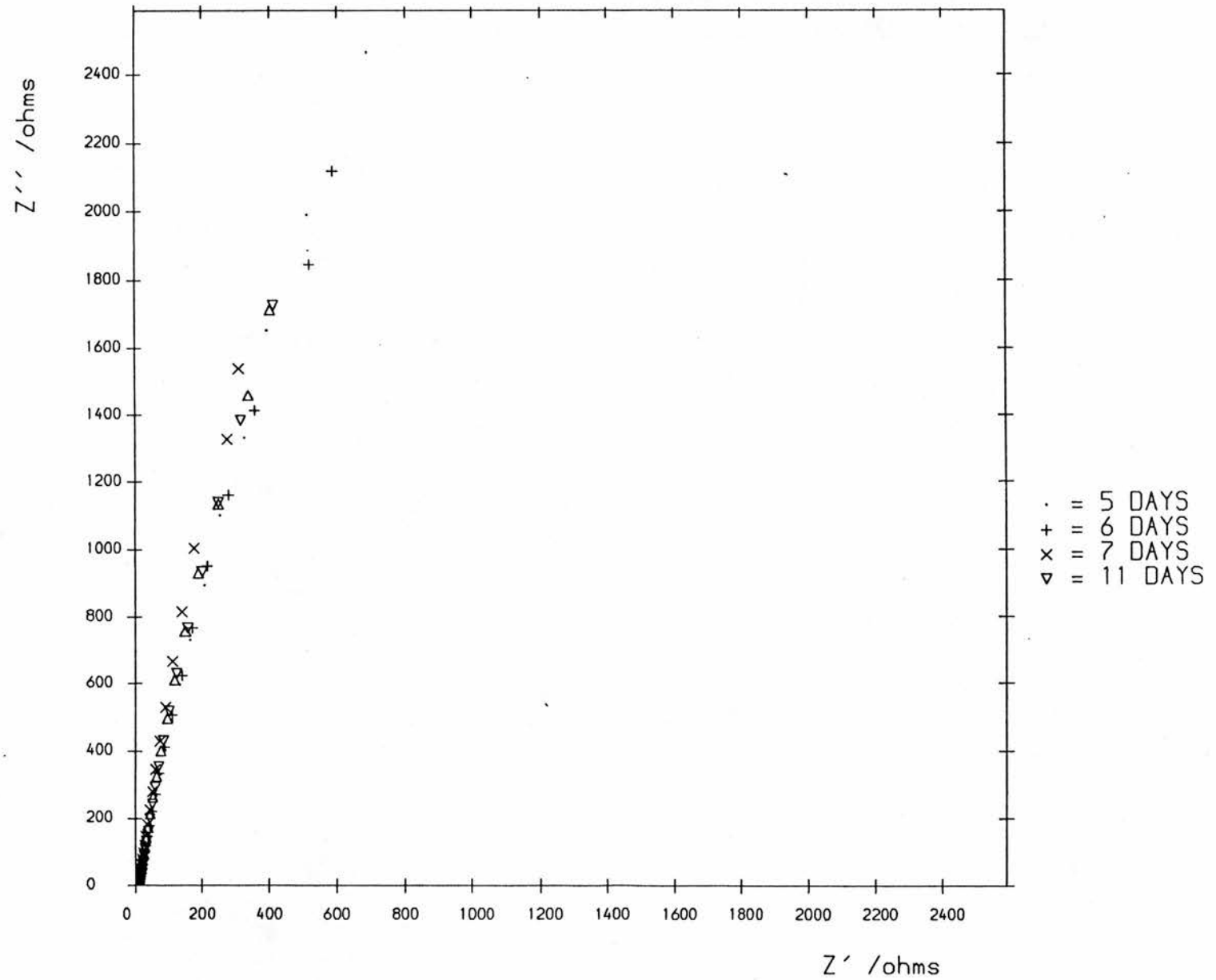

Fig.6.27 Effect of Time on Oxidised HM-U 2M307 D/10 Fibres. Oxidation Time = 1000s. Part 1

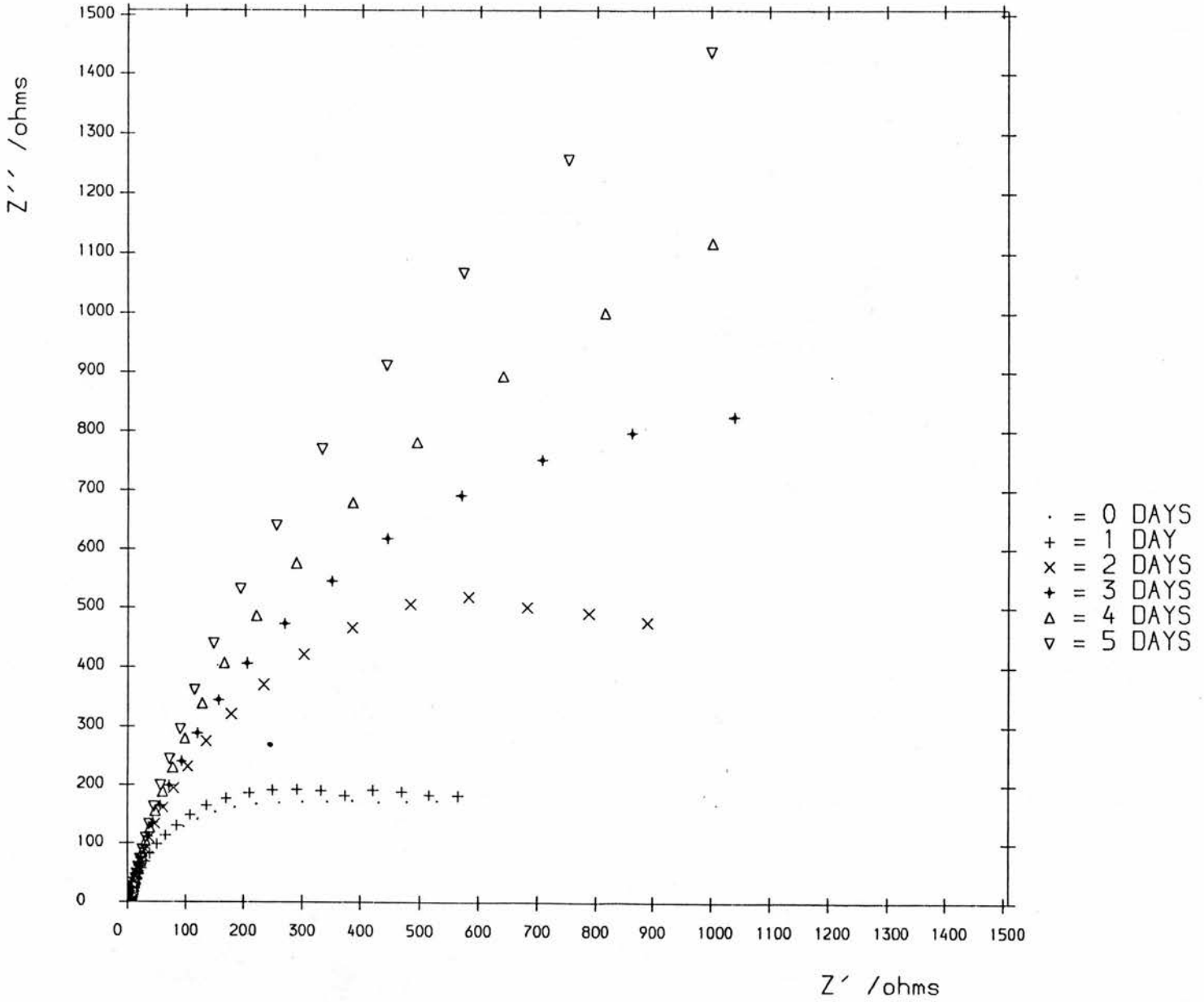

Fig.6.28 Effect of Time on Oxidised HM-U 2M307 D/10 Fibres. Oxidation Time = 1000s. Part 2

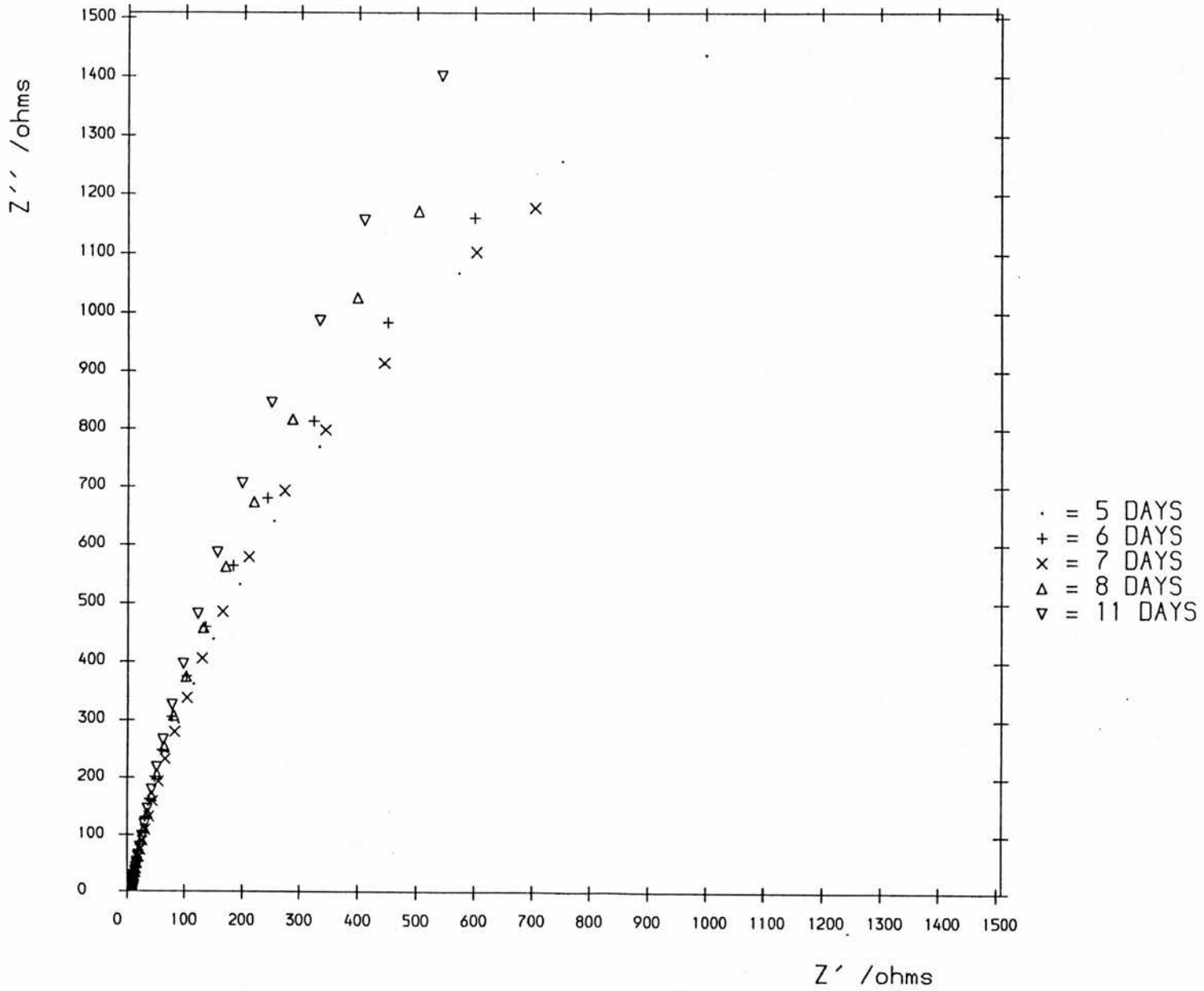

Fig.6.29 Effect of Time on Oxidised HM-U 2M307 D/10 Fibres. Oxidation Time = 3000s. Part 1

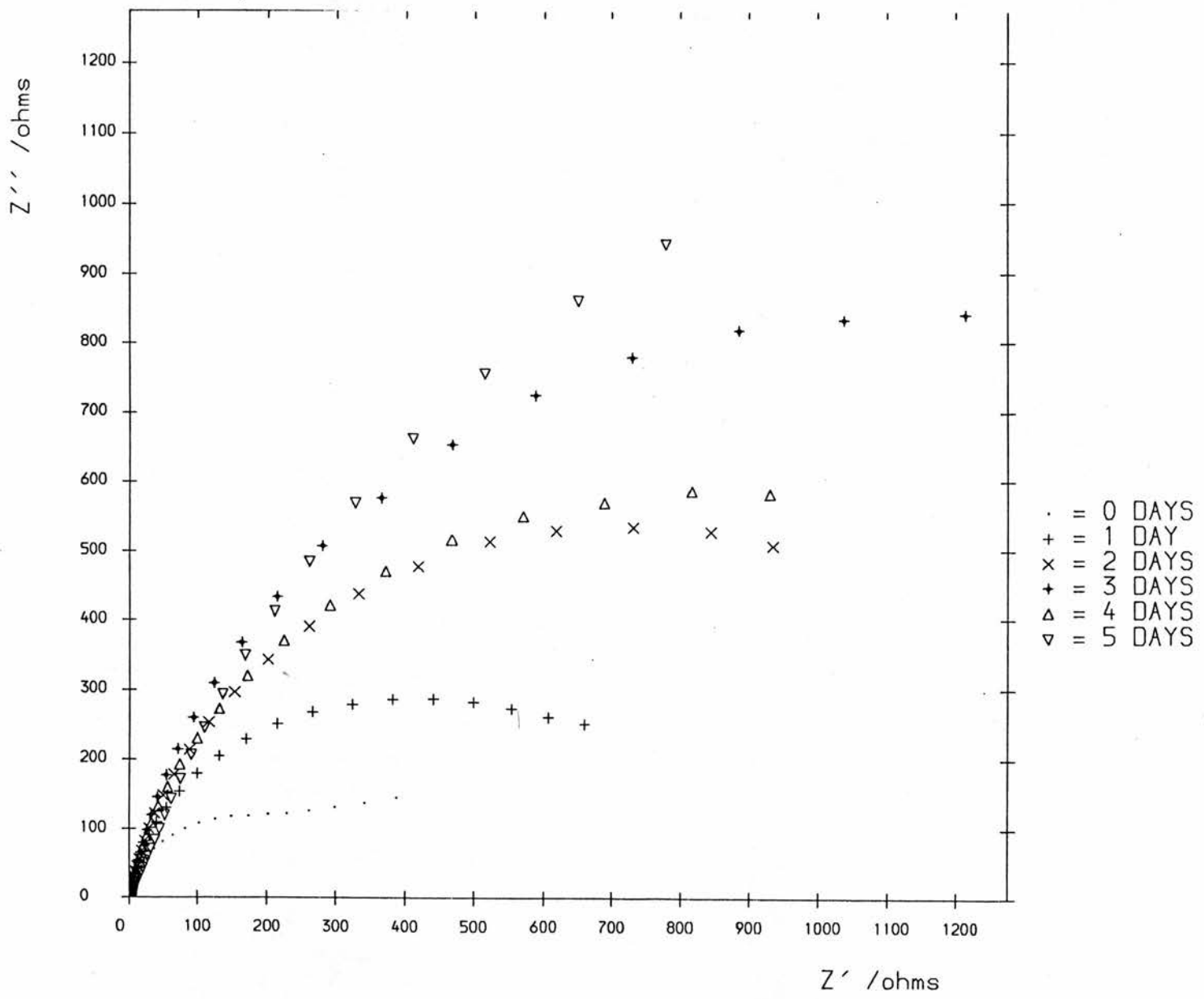

Fig.6.30 Effect of Time on Oxidised HM-U 2M307 D/10 Fibres. Oxidation Time = 3000s. Part 2

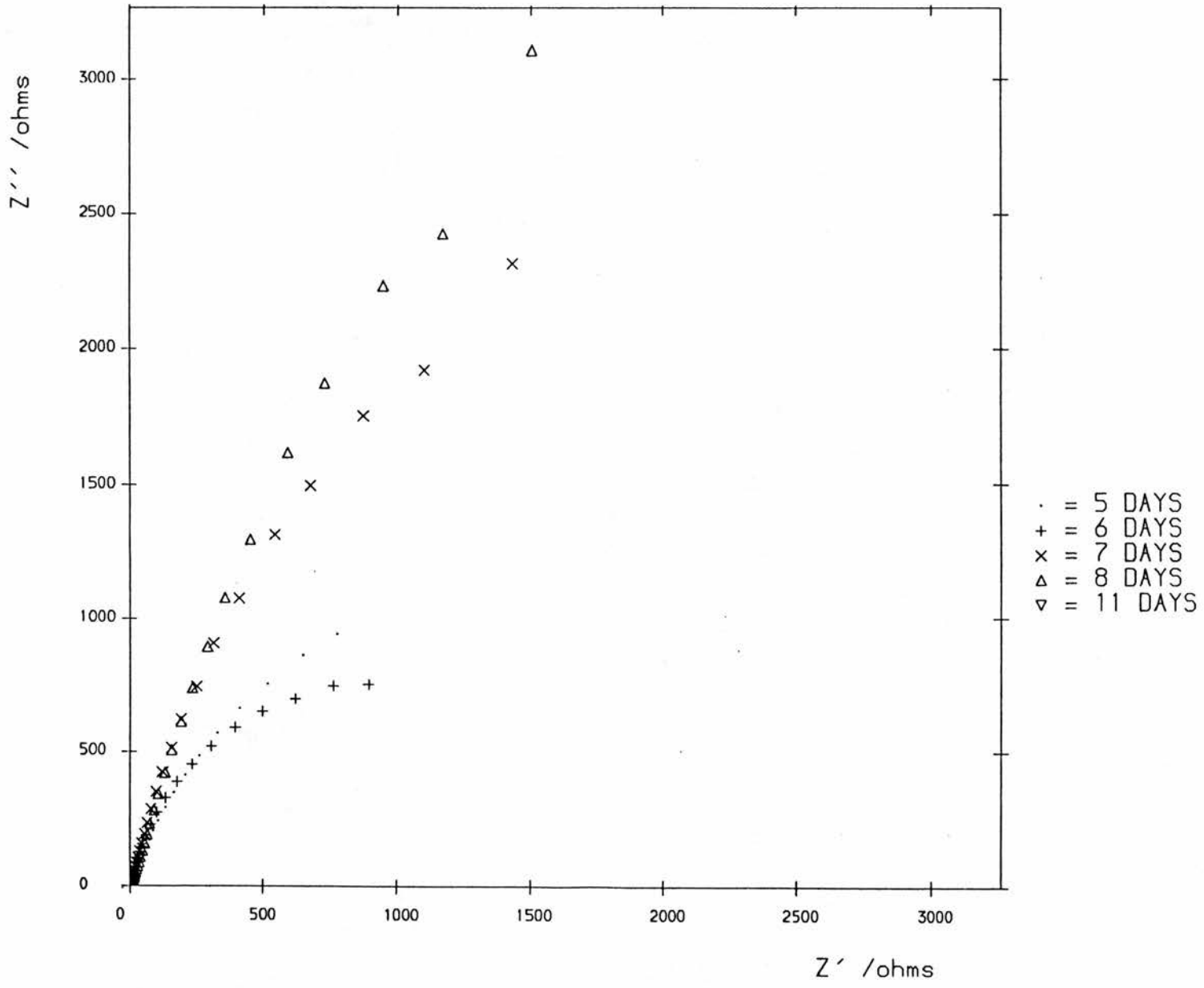

Fig.6.31 Effect of Time on Oxidised HM-U 2M307 D/10 Fibres. Oxidation time = 5000s. Part 1

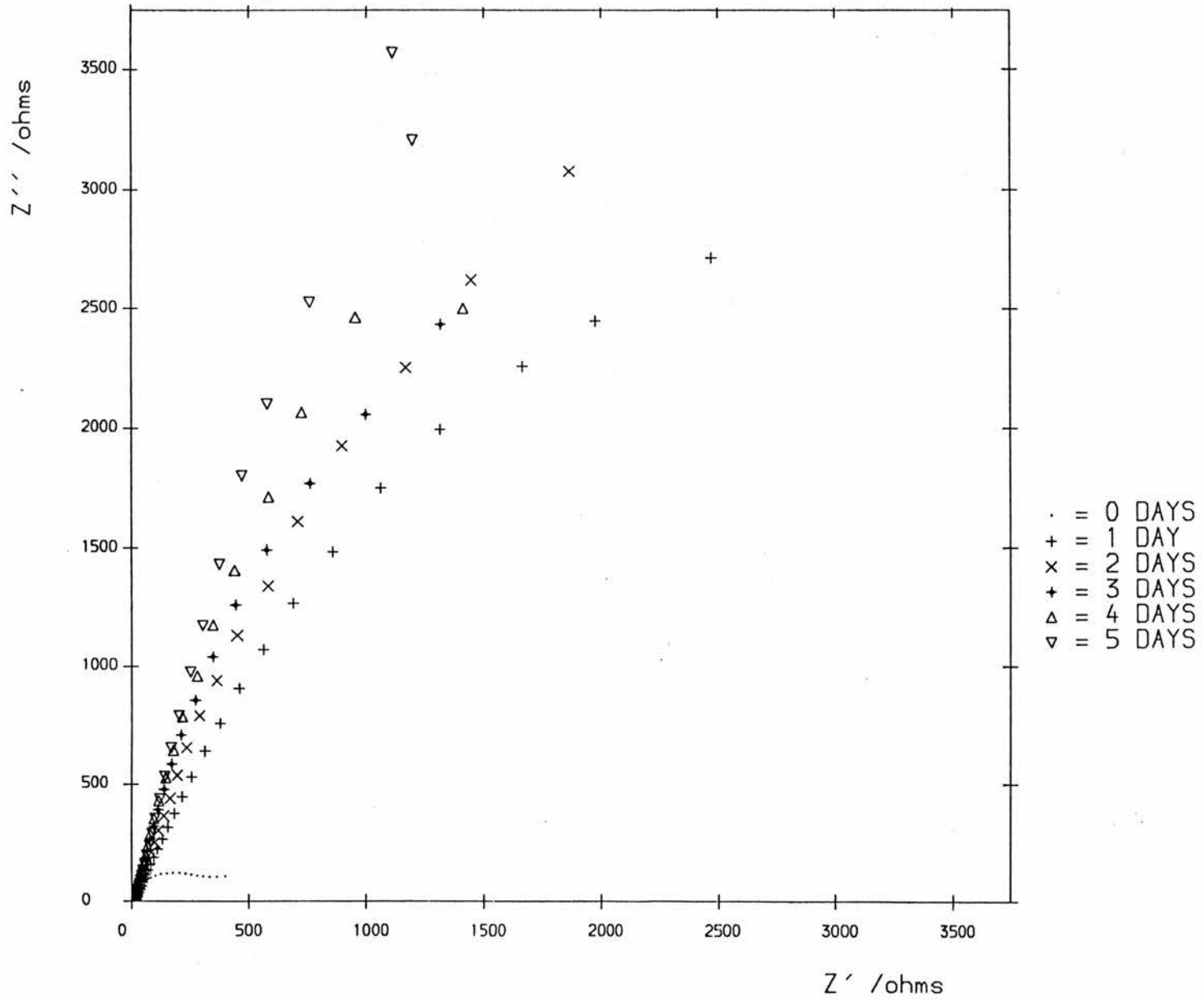

Fig.6.32. Effect of Time on Oxidised HM-U 2M307 D/10 Fibres. Oxidation Time = 5000s. Part 2

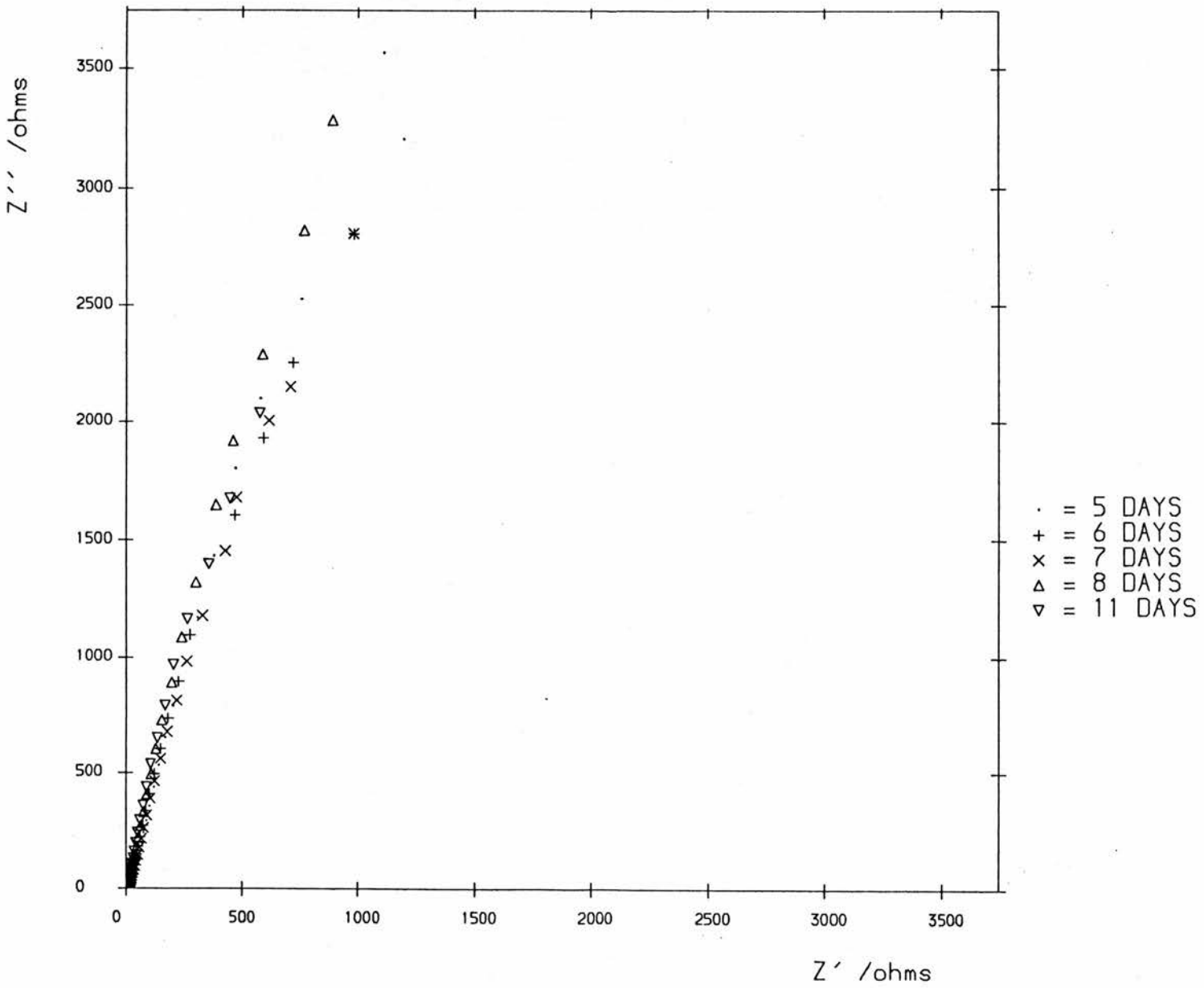

6.3 A.C. Impedance Data Analysis

6.3.1 Development of the Interface Equivalent Circuit

As previously mentioned, it was thought the interface was much more complex and therefore the circuit shown in fig.3.13 was insufficient. These thoughts are borne out on examination of the a.c. impedance plots of the preliminary studies on HM-U 2M207 B/10 fibres. These diagrams show two distinct semi-circles plus an indecipherable high frequency element. It must be noted that there is drastic disintegration of impedance spectra beyond the potential limit. The two semi-circular features indicate that a suitable starting equivalent circuit for analysis could be that shown in Fig.6.33.

Fig.6.33

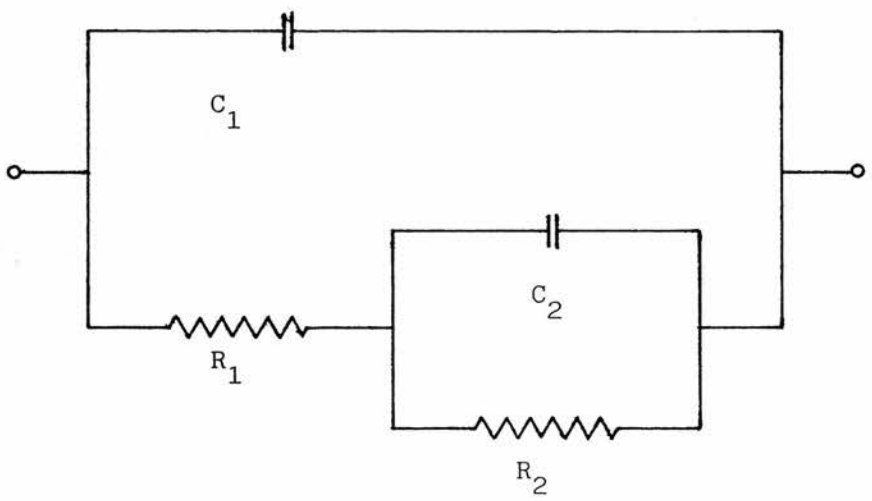

The values for these components were produced using the graphical analysis method shown in Section 3.8.4. The results of this analysis for both the anodic and cathodic regions can be seen in Tables 6.1 and 6.2 respectively.

Table 6.1 Effect of Anodic Potential on the Interface Parameters for HM-U 2M207 B/10 Fibres

POTENTIAL (V)	R_1 (Ω)	C_1 (μF)	R_2 (Ω)	C_2 (μF)
+ 0.70	9.3	8.3	70	2.96×10^4
+ 0.90	11.0	14.5	1778	1.12×10^3
+ 1.10	13.6	7.4	2150	2.35×10^3
+ 1.30	10.0	9.0	1050	1.50×10^3
+ 1.50	10.0	6.4	976	3.26×10^3
+ 1.70	7.7	11.6	86	3.70×10^3
+ 2.00*	6.8	11.7	61	1.00×10^3

Table 6.2 Effect of Cathodic Potential on the Interface Parameters for HM-U 2M207 D/10

POTENTIAL (V)	R_1 (Ω)	C_1 (μF)	R_2 (Ω)	C_2 (μF)
+ 0.70	8.3	10.1	70	3.00×10^4
+ 0.50	6.8	11.1	10.1	2.43×10^3
+ 0.30	8.9	9.2	115	438
+ 0.10	5.7	10.4	124	1.60×10^3
0.00	9.3	8.4	204	572
- 0.20	9.1	8.8	282	376
- 0.40*	10.0	9.0	36	122

*values for the components are somewhat unsure due to disintegration beyond the limits.

As can be seen from the argand diagrams, assessment of component values, particularly R_2 and C_2, by the graphical analysis method can be very difficult. Therefore, since for any useful conclusions to be drawn the component values must be reasonably accurate, it was felt necessary to apply a more accurate circuit analysis method.

The method chosen was a non-linear least squares (NLSS) fitting method for equivalent circuit analysis known as "EQIVCT". This program was devised by Boukamp[2]. The details of its operation have already been discussed in Section 3.8.6. The key to its application is the Circuit Description Code (CDC) which allows the input of any electrical circuit, except those of transmission line type. The program will then fit the experimental a.c. impedance data to that circuit and produce values for the components. In addition, it generates percentage error values and produces residual error plots.

For the development of an accurate equivalent circuit representation for the interface using the Boukamp analysis, it was thought that a suitable starting circuit would be that used previously for the graphical analysis. Initial trials were performed using the data from + 0.30 V plot of the preliminary study into the potential dependence of HM-U 2M207 B/10 fibres. The results of this analysis can be seen in Table 6.3.

Table 6.3 C.D.C. = (C(R(RC)))

COMPONENT	VALUE	ERROR (%)
R_1	6.24 Ω	2.93
C_1	0.119 μF	36.25
R_2	492 Ω	45.80
C_2	126.4 μF	6.36

This circuit was seen to produce a poor fit with the experimental data. It was concluded, after closer examination of the argand diagram, that the circuit was too simple.

Initial thoughts were that the high frequency element previously neglected was in fact another semi-circle and that there seemed to be a degree of overlap between the other two semi-circles. This overlap was thought to indictave the presence of an inductive loop. Therefore by a series of intuitive guesses the possible equivalent circuits were reduced to a choice between those shown in Fig. 6.34. In the case of circuit B) the capacitance C_3 has been replaced by a variable capacitive element known as a Constant Phase Element (CPE)[1,5,7]. This was suggested by the distortion of the low frequency capacitive loop.

Fig. 6.34

A)

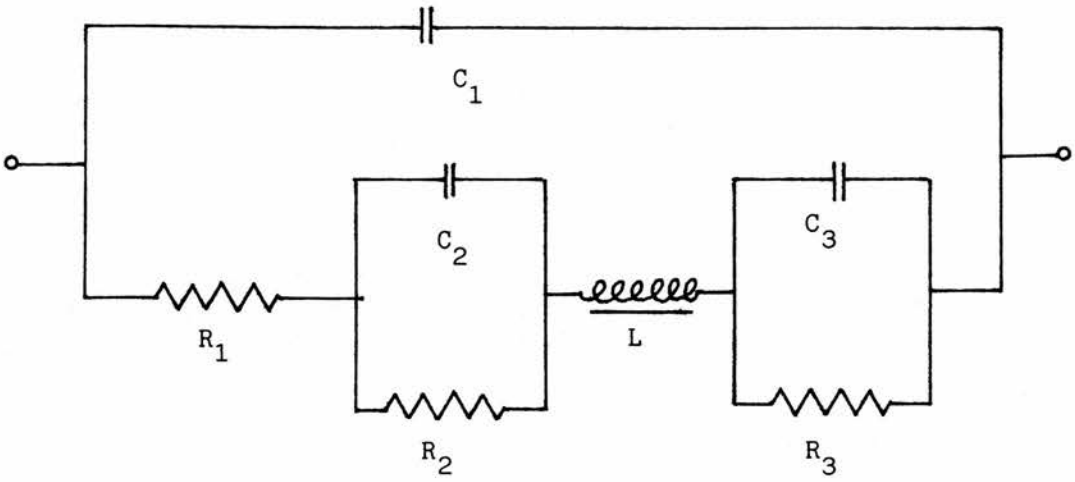

C.D.C. = (C(R(RC)L(RC)))

B)

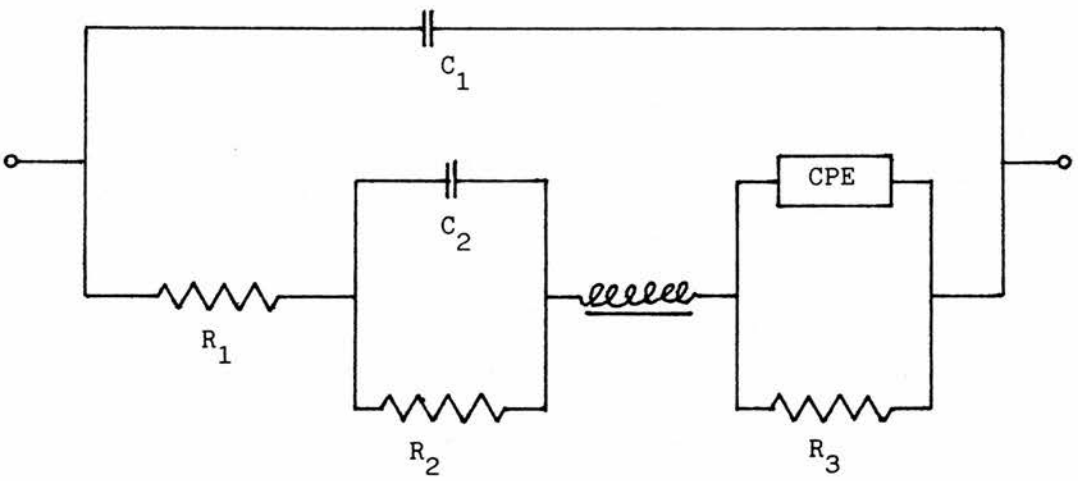

C.D.C. = (C(R(RC)L(RP)))

Boukamp analysis was performed on both circuits and the results are shown in Table 6.4.

Table 6.4

	CIRCUIT A)		CIRCUIT B)	
COMPONENT	VALUE	ERROR %	VALUE	ERROR %
R_1	3.27Ω	8,26	3.23 Ω	8.56
C_1	1.49 μF	5.92	1.50 μF	5.92
R_2	6.59 Ω	11.94	5.99 Ω	16.64
C_2	8.97 μF	19.45	8.89 μF	20.81
L	6.94 μH	20.77	6.9 μH	20.56
R_3	83 Ω	34,00	107 Ω	54.58
C_3	381 μF	17.68		
Y_o) CPE			733 μF	68.44
n)			0.871	15.02

Table 6.4 suggests that circuit A) provides the best fit but on comparison of the fitted data diagrams, shown in Fig.6.35, with the experimental argand diagram, shown in Fig. 6.36, it was concluded that circuit B) actually provided the more accurate fit. This was confirmed by Boukamp analysis over a range of cathodic potentials below the limiting potential, the results of which are shown in Table 6.5.

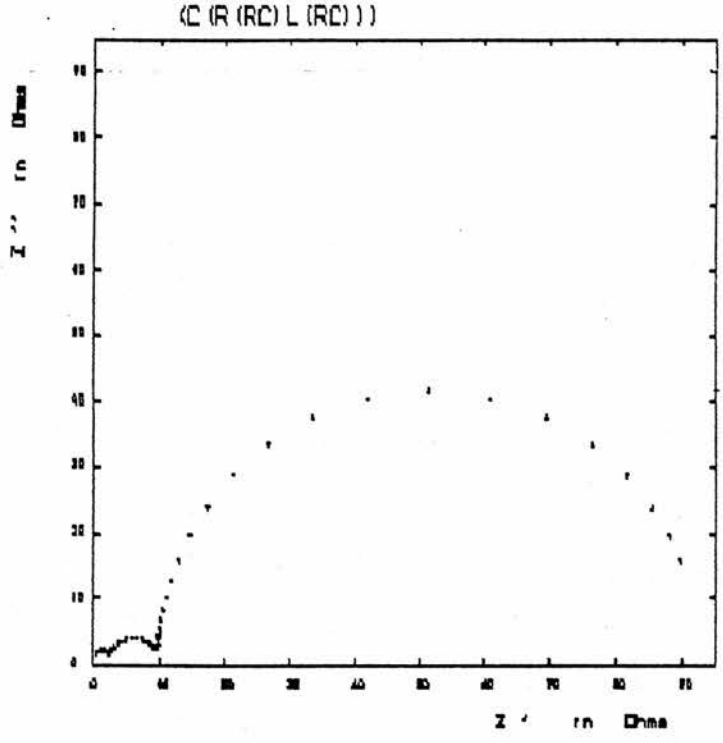
(C (R (RC) L (RC)))

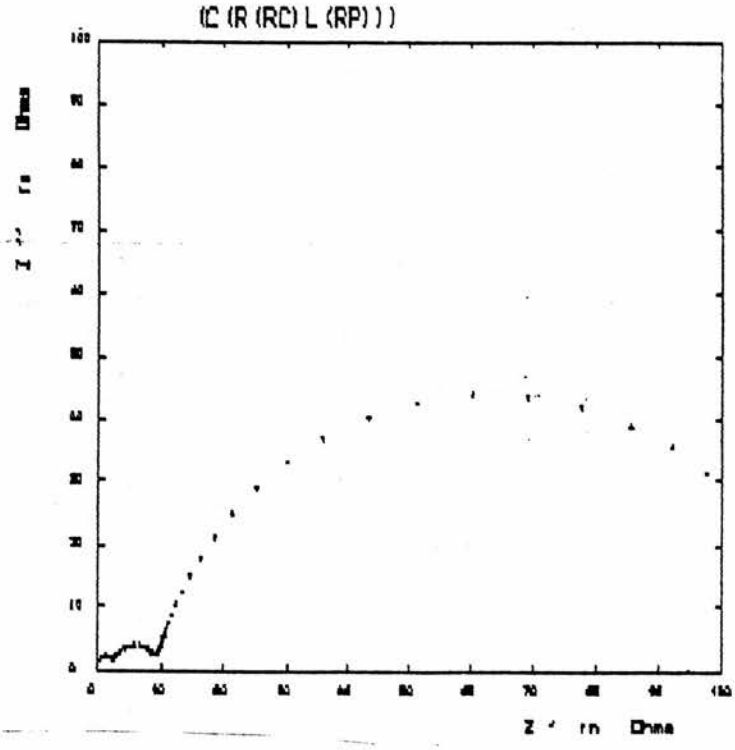
(C (R (RC) L (RP)))

Figure 6.36 Experimental a.c. Impedance Data

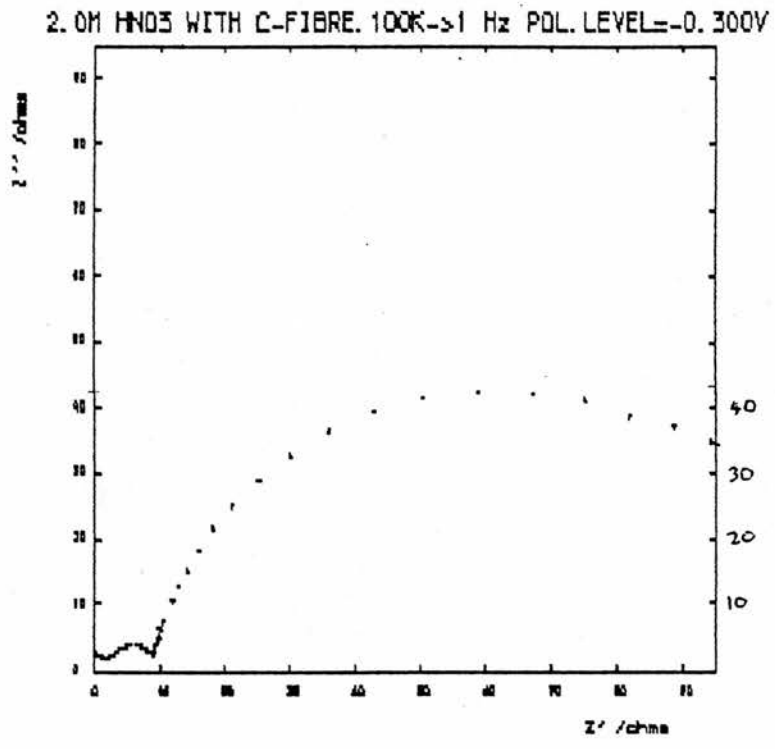

Table 6.5 Initial Investigations in the Potential Dependence of HM-U 2M207 B/10 Fibres. Cathodic Region

POTENTIAL (V)	C_1 (μF)	R_1 (Ω)	R_2 (Ω)	C_2 (μF)	L (μH)	R_3 (Ω)	Y_o (μF)	n
+ 0.70	0.097	0.205	0.382	0.583	0.437	4.46	1910	0.91
+ 0.50	0.097	0.205	0.385	0.579	0.442	0.622	252.2	0.93
+ 0.30	0.095	0.206	0.381	0.566	0.446	6.85	46.7	0.87
+ 0.10	0.095	0.203	0.350	0.580	0.451	9.79	65.6	0.77
0.00	0.095	0.206	0.368	0.557	0.456	10.39	40.1	0.84
- 0.20	0.096	0.206	0.364	0.567	0.454	16.27	30.3	0.84

All component values except the phase angle n are given per mg of fibre.

Beyond the cathodic limiting potential it was found that circuit A) produced the best fit.

- 0.40 V

C_1 (μF)	R_1 (Ω)	R_2 (Ω)	C_2 (μF)	L (μH)	R_3 (Ω)	C_3 (μF)
0.095	0.210	0.413	0.554	0.453	1.41	9.74

This analysis was repeated for the anodic region and in this case circuit A) was found to provide the more accurate fit below the anodic limit. The results of the Boukamp analysis using circuit A) over a range of anodic potentials are shown in Table 6.6.

Table 6.6

POTENTIAL (V)	C_1 (μF)	R_1 (Ω)	R_2 (Ω)	C_2 (μF)	L (μH)	R_3 (Ω)	C_3 (μF)
+ 0.70	0.096	0.205	0.391	0.557	0.452	4.49	1897
+ 0.90	0.095	0.217	0.442	0.560	0.455	18.28	14.49
+ 1.10	0.096	0.210	0.439	0.562	0.450	15.99	19.42
+ 1.30	0.095	0.215	0.435	0.553	0.451	7.08	41.22
+ 1.50	0.096	0.214	0.441	0.565	0.447	5.88	69.87
+ 1.70	0.097	0.209	0.400	0.561	0.443	3.03	128.2

Beyond the anodic limiting potential the circuit giving the best fit was found to be neither A) nor B) but circuit A) with R_1 element removed.

+ 2.00 V

C_1 (μF)	R_2 (Ω)	C_2 (μF)	L (μH)	R_3 ( )	C_3 (μF)
0.104	0.515	0.808	0.745	0.249	0.037

It is thought that the various components represent the following interfacial parameters:-

C_1 = geometric capacitance of the cell

R_1 = solution resistance

R_2 = adsorption resistance

C_2 = adsorption capacitance

L = interfacial inductance

R_3 = charge transfer resistance

C_3 = double layer capacitance

CPE = diffusional element of the double layer

These circuits were thought to provide a reasonable representation of the electrode/electrolyte interface. However, it was discovered when analysing the future experimental results, where adequate de-gassing of the cell was carried out, that the $R_2 - C_2$ parallel element was removed. This confirms the thought that these components were due to adsorption of unrequired gases on the fibre surface. Therefore the basic equivalent circuit used in further analysis is shown in fig. 6.37.

Fig.6.37 Equivalent Circuit Representation of the Electrode/Electrolyte Interface

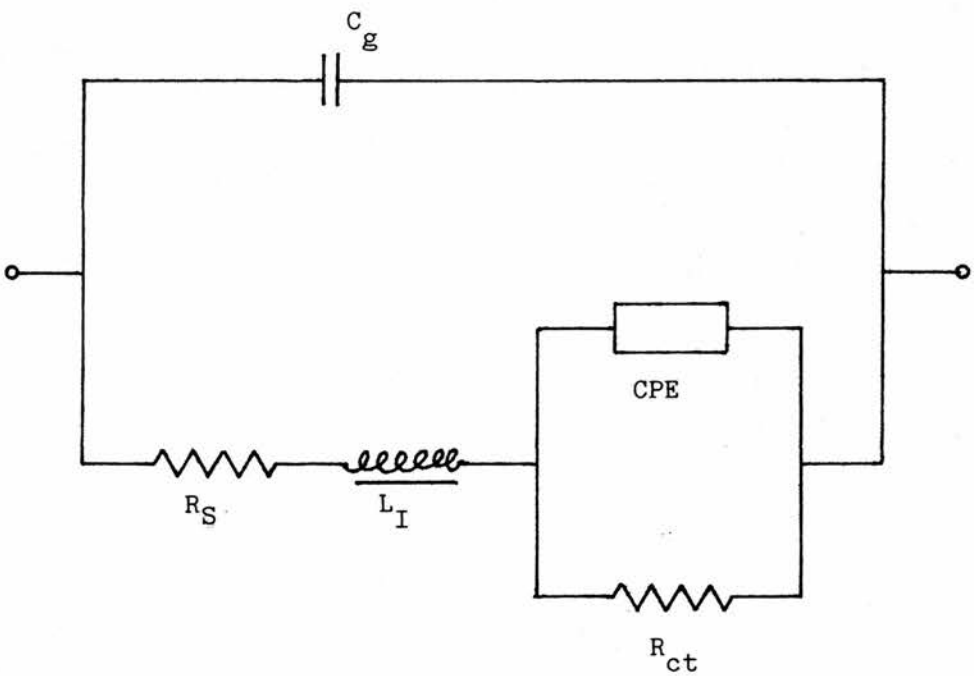

C.D.C. = (C(RL(RP)))

The presence of the inductive component in the equivalent circuit representing the electrode/electrolyte interface was unexpected. As already mentioned, initial thoughts were that it was an interfacial phenomenon. However, it was possible that the inductance was an intrinsic property of the fibre itself. This was checked by using a section of carbon fibre in series with a resistor as the electrical cell and performing an a.c. impedance study. The resultant argand diagram only showed a single dot on the Z' axis at the value of the resistor used, there was no sign of an inductance being present. It was therefore concluded that the inductance was not an intrinsic feature of the carbon fibre but an interfacial phenomenon, as was first thought.

Epelboin and Keddam[2] found that interfacial inductances were seen to be connected to the passivation of Fe solid electrodes in sulphuric acid electrolytes, particularly with the formation and dissolution of $(FeOH)_{ads}$ on the suface of the electrode. Keddam et al[3] further found similar inductive loops at low frequencies using Fe electrode in phosphoric acid, again thought to be related to the passivation of the Fe electrode by $Fe(OH)_{ads}$ film. Macdonald and Urquidi-Macdonald[4] reported inductive behaviour at medium frequencies using A1 electrodes in KOH electrolyte, again thought to be due to dissolution reactions.

However, Meng et al[6] found inductive behaviour at high frequencies, in the case the inductance appeared as a horizontal line on the argand diagrams. These features were produced using Bi_2O_3-based oxygen conductor/porous electrode system at high temperatures. The equivalent circuit provided for this system is very similar to that found for mg carbon fibre/acidic electrolyte system except

that the CPE is replaced by a capacitance. The inductance is thought to be due to the nature of oxygen ion motion in these materials. It is thought to be somewhat like a screw motion instead of linear transport and to be related to crystal structure.

All things considered, the interfacial inductance in the carbon fibre system is thought to be related to the formation and dissolution of an oxide layer on the porous carbon fibre electrode.

6.3.2 Potential Dependence of Untreated HM Fibres

It was felt that, due to the disintegration of the Argand diagrams beyond the limiting potentials, the potential dependence studies should be kept within these limits. The Boukamp analysis of figures 6.3-6.32 are now presented.

2M207 B/10 Fibres in the Anodic Potential Regions

Table 6.7 Model Circuit (C(RL(RP)))

POTENTIAL (V)	C_1 (μF/mg)	R_1 (Ω/mg)	L(H/mg)	R_2 (Ω/mg)	Y_o (μF/mg)	n
+ 0.70	0.222	0.591	1.32×10^{-6}	200	20.2	0.87
+ 0.80	0.021	0.594	1.31×10^{-6}	190	25.8	0.86
+ 0.90	0.022	0.594	1.35×10^{-6}	141	29.4	0.86
+ 1.00	0.023	0.599	1.46×10^{-6}	105	33.5	0.87
+ 1.10	0.024	0.601	1.58×10^{-6}	98	41.8	0.87
+ 1.20	0.024	0.602	1.48×10^{-6}	85	51.0	0.86
+ 1.30	0.025	0.594	1.51×10^{-6}	76	57.8	0.81
+ 1.40	0.025	0.594	1.50×10^{-6}	50	62.4	0.82
+ 1.50	0.025	0.592	1.49×10^{-6}	26	65.3	0.86
+ 1.60	0.025	0.591	1.49×10^{-6}	9.4	78.6	0.86
+ 1.70	0.025	0.592	1.50×10^{-6}	4.5	58.2	0.86

2M207 B/10 Fibres Cathodic Potential Region

Table 6.8 Model Circuit (C(RL(RP)))

POTENTIAL (V)	C_1 (μF/mg)	R_1 (Ω/mg)	L (μH/mg)	R_2 (Ω/mg)	Y_o (μF/mg)	n
+ 0.70	0.029	0.481	0.88	78	21.8	0.89
+ 0.60	0.031	0.479	0.95	33	23.6	0.90
+ 0.50	0.031	0.479	0.93	12	26.4	0.91
+ 0.40	0.032	0.477	0.93	9.3	32.0	0.90
+ 0.30	0.032	0.475	0.95	11	31.9	0.90
+ 0.20	0.031	0.477	0.97	60	31.2	0.90
+ 0.10	0.033	0.478	0.98	28	28.5	0.90
0.00	0.033	0.478	0.99	34	26.9	0.91
- 0.10	0.033	0.478	1.00	39	25.6	0.91
- 0.20	0.034	0.478	1.02	24	24.4	0.91

2M371 E/10 Fibres in the Anodic Region

In this case it was found that two equivalent circuits were required to represent the interface over the anodic potential region. The basic circuit was accurate for the potentials close to the OCV and to the anodic limit however the intermediate potentials required a new circuit where component R_2 becomes infinite in value reducing the equivalent circuit to (C(RLP)) shown in Fig. 6.38. This can be seen on the Argand diagrams as linearity of the low frequency section.

Fig. 6.38

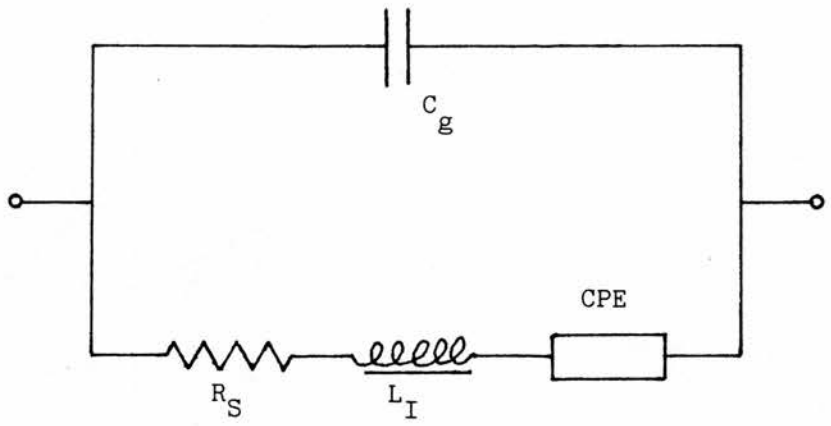

C.D.C. = (C(RLP))

Table 6.9 Model Circuit (C(RL(RP)))

POTENTIAL (V)	C_1 (μF/mg)	R_1 (Ω/mg)	L (μH/mg)	R_2 (Ω/mg)	Y_o (μF/mg)	n
+ 0.70	0.017	0.94	1.51	666	9.1	0.91
+ 0.80	0.018	0.96	1.66	640	10.8	0.90
+ 0.90	0.019	0.98	1.80	626	13.3	0.90
+ 1.00	0.020	1.00	1.93	602	16.5	0.89
+ 1.10*	0.020	1.01	1.98	840	25.4	0.86
+ 1.40	0.021	1.00	2.11	208	55.0	0.78
+ 1.50	0.021	1.02	2.10	46.9	60.0	0.80
+ 1.60	0.020	1.02	2.06	19.9	76.8	0.82
+ 1.70	0.020	1.02	2.07	7.5	120.1	0.87

Table 6.10 Model Circuit (C(RLP))

POTENTIAL	C_1 (μF/mg)	R_1 (Ω/mg)	L (μH/mg)	Y_o (μF/mg)	n
+ 1.10*	0.020	1.01	1.98	26.1	0.86
+ 1.20	0.020	1.03	2.00	43.9	0.84
+ 1.30	0.021	1.00	2.08	57.8	0.78

*In the case of + 1.10 V, both analyses are presented but circuit (C(RLP)) shows the lower percentage errors.

2M371 E/10 Fibres in the Cathodic Potential Region

Table 6.11 Model Circuit (CRL(RP)))

POTENTIAL (V)	C_1 (μF/mg)	R_1 (Ω/mg)	L (μH/mg)	R_2 (Ω/mg)	Y_o (μF/mg)	n
+ 0.70	0.028	6.32	18.7	6027	6.12	0.81
+ 0.60	0.030	6.35	19.6	4278	5.00	0.82
+ 0.50	0.031	6.38	20.4	2354	4.63	0.81
+ 0.40	0.032	6.42	20.9	1695	5.12	0.82
+ 0.30	0.032	6.41	20.7	1668	5.20	0.80
+ 0.20	0.032	6.45	21.7	2156	4.73	0.80
+ 0.10	0.033	6.47	20.8	2407	5.10	0.80
0.00	0.032	6.46	19.6	1705	5.73	0.83
- 0.10	0.031	6.42	18.5	1751	6.15	0.84
- 0.20	0.033	6.27	19.5	90	16.8	0.76

2M307 D/10 Fibres in the Anodic Potential Region

Table 6.12 Model Circuit (C(RL(RP)))

POTENTIAL (V)	C_1 (nF/mg)	R_1 (Ω/mg)	L (μH/mg)	R_2 (Ω/mg)	Y_o (μF/mg)	n
+ 0.70	18.7	0.84	1.92	548	15.6	0.84
+ 0.80	17.2	0.86	1.87	469	18.3	0.84
+ 0.90	17.0	0.87	1.87	410	19.8	0.85
+ 1.00	12.8	0.97	1.69	523	30.5	0.83
+ 1.10	13.8	0.94	1.80	549	46.7	0.77
+ 1.20	14.7	0.91	1.82	120	38.9	0.78
+ 1.30	16.9	0.81	1.62	48.8	50.0	0.79
+ 1.40	15.9	0.92	1.94	19.4	115	0.88
+ 1.50	16.2	0.93	2.00	7.2	156	0.88
+ 1.60	16.5	0.94	2.08	3.0	201	0.87

2M307 D/10 Fibres in the Cathodic Potential Region

Table 6.13 Model Circit (C(RL(RP)))

POTENTIAL (V)	C_1 (nF/mg)	R_1 (Ω/mg)	L (μH/mg)	R_2 (Ω/mg)	Y_o (μF/mg)	n
+ 0.70	7.0	3.33	6.69	836	19.3	0.86
+ 0.60	6.8	3.35	6.54	988	15.1	0.87
+ 0.50	7.3	3.33	7.00	1274	12.3	0.87
+ 0.40	7.8	3.35	7.62	1377	10.3	0.88
+ 0.30	8.0	3.35	7.84	1371	9.5	0.88
+ 0.20	7.8	3.36	7.59	1295	9.1	0.88
+ 0.10	7.9	3.35	7.73	659	8.3	0.88
0.00	7.9	3.37	7.74	62	6.3	0.90
- 0.10	7.7	3.37	7.51	56	5.4	0.92
- 0.20	7.9	3.36	7.70	24	7.0	0.90

6.3.3 Comparison Between Untreated and R.A.E. Treated Fibres

2M307 D/10 HM-U Fibres in the Anodic Potential Region

Table 6.13 Model Circuit (C(RL(RP)))

POTENTIAL (V)	C_1(nF/mg)	R_1(Ω/mg)	L(μH/mg)	R_2(Ω/mg)	Y_o(μF/mg)	n
+ 0.70	31.9	0.573	1.38	557	40.3	0.87
+ 0.80	31.0	0.572	1.34	339	42.3	0.87
+ 0.90	32.4	0.571	1.39	246	44.3	0.87
+ 1.10	36.8	0.568	1.42	73.5	50.1	0.86
+ 1.20	33.6	0.569	1.42	24.6	56.2	0.84
+ 1.30	32.7	0.572	1.39	31.8	79.7	0.84
+ 1.40	36.2	0.570	1.40	15.8	105	0.84
+ 1.50	37.6	0.569	1.44	6.6	130	0.85
+ 1.60	36.4	0.570	1.40	3.2	107	0.86
+ 1.70	37.4	0.573	1.44	1.6	81.8	0.85

It must be noted that the results for + 1.00 V were deleted from the data tapes.

2M307 D/10 HM-U Fibres in the Cathodic Potential Region

Table 6.14 Model Circuit (C(RL(RP)))

POTENTIAL (V)	C_1 (nF/mg)	R_1 (Ω/mg)	L (μH/mg)	R_2 (Ω/mg)	Y_o (μF/mg)	n
+ 0.70	29.3	0.213	0.53	276	17.6	0.86
+ 0.60	29.8	0.213	0.54	283	13.0	0.87
+ 0.50	32.5	0.214	0.58	278	9.6	0.89
+ 0.40	33.0	0.215	0.58	268	8.1	0.90
+ 0.30	32.0	0.216	0.57	204	7.5	0.91
+ 0.20	32.2	0.216	0.58	45.6	6.6	0.91
+ 0.10	31.0	0.216	0.56	15.6	5.6	0.92
0.00	32.3	0.215	0.57	6.4	6.4	0.90
- 0.10	32.9	0.214	0.58	1.8	9.6	0.88
- 0.20	32.3	0.210	0.56	2.0	34.1	0.79

2M307 F/10 HM-S Fibres in the Anodic Potential Region

Table 6.15 Model Circuit (C(RL(RP)))

POTENTIAL (V)	C_1(nF/mg)	R_1(Ω/mg)	L(μH/mg)	R_2(Ω/mg)	Y_o(μF/mg)	n
+ 0.70	30.8	0.132	0.35	240	21.4	0.94
+ 0.80	29.1	0.132	0.33	244	22.8	0.93
+ 0.90	29.4	0.132	0.34	201	25.1	0.92
+ 1.00	29.8	0.132	0.34	86.2	27.5	0.92
+ 1.10	30.0	0.132	0.34	21.4	30.6	0.91
+ 1.20	29.9	0.132	0.34	6.5	40.7	0.89
+ 1.30	29.9	0.132	0.34	3.2	50.8	0.87
+ 1.40	30.0	0.132	0.34	2.3	75.3	0.85
+ 1.50	29.8	0.132	0.34	2.0	129	0.80

2M307 F/10 HM-S Fibres in the Cathodic Potential Region

Table 6.16 Model Circuit (C(RL(RP)))

POTENTIAL (V)	C_1 (nF/mg)	R_1 (Ω/mg)	L (μH/mg)	R_2 (Ω/mg)	Y_o (μF/mg)	n
+ 0.70	22.3	1.854	4.71	305	33.4	0.91
+ 0.60	24.7	1.883	4.90	377	28.4	0.92
+ 0.50	25.2	1.872	4.95	400	26.8	0.92
+ 0.40	25.4	1.868	4.98	382	28.0	0.92
+ 0.30	25.4	1.872	5.00	312	33.6	0.92
+ 0.20	25.1	1.862	4.86	26.0	35.8	0.95
+ 0.10	23.4	1.867	4.99	7.0	41.6	0.93
0.00	22.6	1.860	4.81	11.9	40.8	0.93
- 0.10	22.5	1.859	4.82	31.2	40.9	0.92
- 0.20	24.4	1.862	4.78	58.0	41.0	0.92

6.3.4 The Effect of Anodic Polarisation Potential Value on Increased Galvanic Oxidation of HM-U Fibres

On examination of the argand diagrams, it appears as if the R_2 component tends towards infinity in value. Therefore the modified circuit provided the most accurate fit.

Table 6.17 V = + 0.70 V Model Circuit (C(RLP))

TREATMENT TIME (S)	C_1 nF/mg)	R_1 (Ω/mg)	L(μH/mg)	Y_o (μF/mg)	n
0	41.1	0.338	0.91	10.4	0.87
50	42.3	0.331	0.92	13.1	0.84
100	44.2	0.323	0.89	16.5	0.83
150	42.9	0.334	0.92	18.2	0.82
200	44.4	0.325	0.89	21.9	0.83
500	43.7	0.331	0.89	25.2	0.84

Table 6.18 V = + 1.00 V Model Circuit (C(RLP))

TREATMENT TIME (S)	C_1 (nF/mg)	R_1 (Ω/mg)	L(μH/mg)	Y_o (μF/mg)	n
0	41.5	0.332	0.90	24.9	0.84
50	41.9	0.337	0.89	41.4	0.84
100	43.7	0.328	0.85	44.6	0.84
150	41.7	0.333	0.88	34.9	0.83
200	42.8	0.324	0.84	39.2	0.86
500	41.6	0.330	0.84	42.2	0.87

Table 6.19 V = + 1.30 V Model Circuit (C(RLP)

TREATMENT TIME (S)	C_1(nF/mg)	R_1(Ω/mg)	L(μH/mg)	Y_o(μF/mg)	n
0	41.2	0.332	0.88	177	0.71
50	42.0	0.334	0.87	121	0.80
100	43.3	0.325	0.83	99.5	0.84
150	41.4	0.332	0.86	84.2	0.84
200	42.4	0.322	0.82	88.8	0.86
500	41.4	0.326	0.83	84.7	0.87

6.3.5 Effect of Galvanic Oxidation Duration on HM-U Fibres

Table 6.20 V = + 1.30 V Model Circuit (C(RL(RP))) and (C(RLP))

TREATMENT TIME (S)	C_1(nF/mg)	R_1(Ω/mg)	L(μH/mg)	R_2(Ω/mg)	Y_o(μF/mg)	n
0	18.0	0.593	1.53	35.8	311	0.87
100	19.6	0.532	1.30	44.3	442	0.86
200	25.6	0.470	1.20	5.4	492	0.84
500	24.0	0.511	1.35		942	0.87
1000	21.5	0.536	1.43		874	0.86
3000	20.2	0.538	1,38	9.8	732	0.89

Table 6.21 V = 0.00 V Model Circuit (C(RL(RP)))

TREATMENT TIME (S)	C_1 (nF/mg)	R_1 (Ω/mg)	L (μH/mg)	R_2 (Ω/mg)	Y_o (μF/mg)	n
0	62.3	0.064	0.18	10.8	31.6	0.86
100	53.4	0.074	0.20	16.4	12.3	0.90
200	68.6	0.062	0.19	66.2	20.7	0.79
500	61.8	0.074	0.21	25.8	15.7	0.86
1000	59.8	0.072	0.19	62.4	19.1	0.78
3000	55.7	0.076	0.20	114	34.4	0.73

The effects of further increases in galvanic oxidation are analysed in Table 6.22.

Table 6.22 V = + 1.30 V Model Circuit (C(RL(RP)))

TREATMENT TIME (S)	C_1 (nF/mg)	R_1 (Ω/mg)	L (μH/mg)	R_2 (Ω/mg)	Y_o (μF/mg)	n
0	104	0.646	1.74	679	52.4	0.92
30	89.5	0.818	2.20	1319	70.5	0.88
50	91.8	0.715	1.94	1179	82.2	0.89
200	77.8	0.920	2.44	613	79.9	0.89
500	65.0	1.129	3.01	123	68.3	0.90
1000	74.8	0.980	2.64	70.8	76.8	0.90
5000	99.3	0.998	3.01	34.4	121	0.90
7000	93.2	0.969	2.87	25.0	181	0.89

6.3.6 The Effect of Time on Oxidised HM-U Fibres

Table 6.23 t_o = 0s Model Circuit (C(RLP))

TIME (DAYS)	C_1(nF/mg)	R_1(Ω/mg)	L(μH/mg)	Y_o(μF/mg)	n
0	198	0.327	0.84	86.1	0.90
1	224	0.330	0.96	93.5	0.87
2	175	0.337	0.99	135	0.84
3	172	0.336	0.95	182	0.82
4	166	0.349	0.97	195	0.80
5	176	0.371	1.05	276	0.82
6	170	0.330	0.92	149	0.81
7	159	0.385	1.05	141	0.78
8	193	0.406	1.13	122	0.80
14	200	0.468	1.28	133	0.80

In the case of t_o = 500s it was found that at t = 0 days the best circuit fit was (C(RL(RP))) whereas at longer times the circuit reduced to (C(RLP)).

t = 0 days

C_1 = 170 nF/mg R_1 = 1.102 Ω/mg L = 3.13 μH/mg R_2 = 452 Ω/mg

Y_o = 133 μF/mg n = 0.82

Table 6.24 t_o = 500s Model Circuit (C(RLP))

TIME (DAYS)	C_1(nF/mg)	R_1(Ω/mg)	L(μH/mg)	Y_o(μF/mg)	n
0	202	1.208	2.75	115	0.83
1	121	1.231	4.27	112	0.82
3	91.0	1.227	3.65	112	0.83
4	83.8	1.309	3.75	105	0.83
5	82.4	1.378	3.96	101	0.80
6	89.9	1.366	4.25	118	0.83
7	89.5	1.166	3.45	168	0.84
8	82.5	1.344	3.83	142	0.84
14	101	1.492	5.05	126	0.82

Table 6.25 t_o = 1000s Model Circuit (C(RL(RP)))

TIME (DAYS)	C_1(nF/mg)	R_1(Ω/mg)	L(μH/mg)	R_2(Ω/mg)	Y_o(μF/mg)	n
0	132	0.721	1.78	41.1	73.1	0.93
1	176	0.630	1.41	51.5	70.2	0.89
2	106	0.614	2.06	152	73.3	0.87
3	83.5	0.590	1.84	242	75.4	0.86
4	79.4	0.609	1.84	380	83.2	0.86
5	82.4	0.613	1.86	1116	82.5	0.85

Table 6.26 t_o = 1000s Model Circuit (C(RLP))

TIME (DAYS)	C_1(nF/mg)	R_1(Ω/mg)	L(μH/mg)	Y_o(μF/mg)	n
6	84.0	0.613	1,88	129	0.85
7	75.6	0.653	1.90	95.5	0.79
8	77.4	0.649	1.95	125	0.83
14	105	0.642	2.16	99.8	0.82

A similar situation was found in t_o = 3000s.

Table 6.27 t_o = 3000s Model Circuit (C(RL(RP)))

TIME (DAYS)	C_1(nF/mg)	R_1(Ω/mg)	L(μH/mg)	R_2(Ω/mg)	Y_o(μF/mg)	n
0	255	0.115	0.32	28.6	91.9	0.89
1	262	0.134	0.29	71.6	55.3	0.88
2	198	0.126	0.38	154	57.2	0.85
3	159	0.129	0.38	584	62.2	0.81
4	157	0.130	0.39	188	70.4	0.84
5	137	0.174	0.50	823	88.7	0.75

Table 6.28 t_o = 3000s Model Circuit (C(RLP))

TIME (DAYS)	C_1(nF/mg)	R_1(Ω/mg)	L(μH/mg)	Y_o(μF/mg)	n
6	150	0.146	0.42	96.6	0.78
7	143	0.149	0.44	65.2	0.72
8	138	0.174	0.53	59.9	0.68
14	155	0.220	0.60	61.1	0.68

For t_o = 5000s, only the t = 0 days result could be fitted to (C(RL(RP))), the longer duration experiments seem to fit (C(RLP)) most accurately.

t = 0 days

C_1 = 141 nF/mg R_1 = 0.530 Ω/mg L = 1.48 μH/mg

R_2 = 31.2 Ω/mg Y_o = 71.4 μF/mg n = 0.91

Table 6.29 t_o = 5000s Model Circuit (C(RLP))

TIME (DAYS)	C_1(nF/mg)	R_1(Ω/mg)	L(μH/mg)	Y_o(μF/mg)	n
1	141	0.696	1.26	38.3	0.70
2	107	0.626	2.36	60.6	0.67
3	71.0	0.725	2.01	75.6	0.72
4	61.6	0.816	2.26	66.9	0.74
5	60.9	0.895	2.65	55.9	0.72
6	65.1	0.825	2.43	65.9	0.76
7	58.7	0.860	2.42	58.5	0.74
8	58.4	0.897	2.64	50.7	0.78
14	77.9	0.887	3.02	70.3	0.84

6.4 Discussion of A.C. Impedance Results

6.4.1 The Effect of d.c. Polarisation Potential on Untreated Fibres

On consideration of the equivalent circuits representing the electrode/electrolyte interphase, it was thought that components R_1, C_1 and L would remain constant throughout the potential range. Whereas the values of R_2 and Y_o would vary with potential value. The effect of potential on the phase angle, n, was not known.

Therefore average values of C_1, R_1 and L were calculated for each potentiostatic a.c. impedance experiment and can be seen in Table 6.30. In addition, the variation of R_2, Y_o and n was plotted.

Table 6.30 Average Values of R_1, C_1 and L for Untreated Fibres

HM-U FIBRE	C_1(nF/mg)	R_1(Ω/mg)	L(μH/mg)
2M207 B/10 Anodic	23.7	0.595	1.45
2M207 B/10 Cathodic	31.9	0.478	0.96
2M371 E/10 Anodic	19.7	0.998	1.94
2M371 E/10 Cathodic	31.4	6.40	20.04
2M307 D/10 Anodic	16.0	0.90	1.86
2M307 D/10 Cathodic	7.6	3.35	7.40

It can be seen from Table 6.30 that no conclusions can be made about the effect of fibre batch on the values of components

R_1, C_1 and L in the equivalent circuit representation for the interface. The variation in component value between the anodic and cathodic regions may be explained by the use of two electrodes and the difficulty of placing the working electrode at a set distance from the Luggin capillary.

The effect of d.c. polarisation potential on the remaining circuit components for the various batches of untreated fibres can be seen in figures 6.39-6.44.

2M207 B/10 Fibres

On examination of Fig. 6.39, it can be seen that the component R_2, representing the charge transfer resistance at the interface, shows a continual decrease with increasing anodic potential. This decrease could be linear or even an exponential decay but which is correct it is not possible to conclude. The opposite effect is seen for the potential dependence of Y_o since it increases with increasing potential. The phase angle n is thought to be independent of potential for anodic potential region and has an average value of 0.86.

The cathodic region plots shows R_2 decreases, possibly exponentially from the OCV to a minimum value at + 0.40 V and then shows a gradual increase towards the cathodic potential limit. As was found with the anodic region, the component Y_o exhibits inverse behaviour to that of R_2. Again phase angle n is thought to be constant, at a value of 0.90.

The inverse behaviour of R_2 and Y_o in both potential regions was to be expected from their parallel combination in the overall equivalent circuit.

2M371 E/10 Fibres

In both potential regions the potential dependence of R_2, neglecting the infinite values, shows similar trends to that for 2M207 B/10 fibres but is much less defined. The potential dependence of Y_o in the anodic region also shows similarity to the previous fibre, exhibiting the inverse behaviour found previously. However, in the cathodic region the value of Y_o seems approximately constant, at about 5 μF/mg, until approaching the potential limit where there is a drastic increase in value to approximately 17 μF/mg.

The phase angle n shows a definite potential variation in the anodic region but remains approximately constant in the cathodic region until approaching the limit.

2M307 D/10 Fibres

In the anodic potential region, the potential dependence of R_2, Y_o and n is very similar to that found for 2M307 B/10 fibres. However, in the cathodic region R_2 was found to increase to a maximum of 1400 Ω/mg at about + 0.40 V and then to exponentially decay to a minimum approaching the cathodic limit. Y_o showed a continual decrease to the cathodic limit. The phase angle n could be constant but more probably shows a continual, possibly linear, increase with increasing cathodic potential. In this case Y_o and n in the cathodic region seem to have an inverse relationship.

Fig.6.39 The Effect of d.c. Potential on the Equivalent Circuit Component Value for 2M207 B/10 HM-U Fibres. Anodic Region

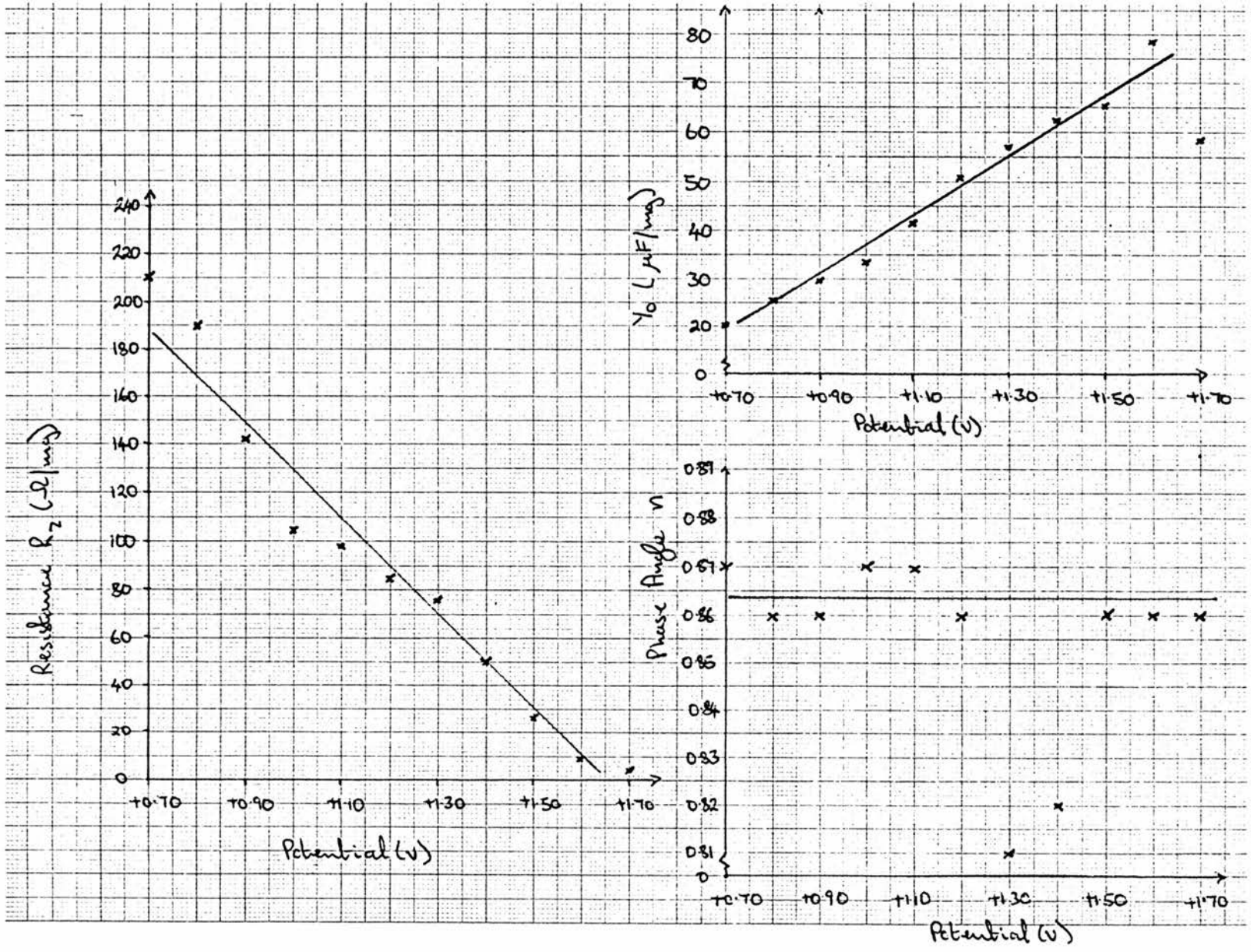

Fig.6.40. The Effect of d.c. Potential on the Equivalent Circuit Component Value for 2M307 B/10 HM-U Fibres. Cathodic Region

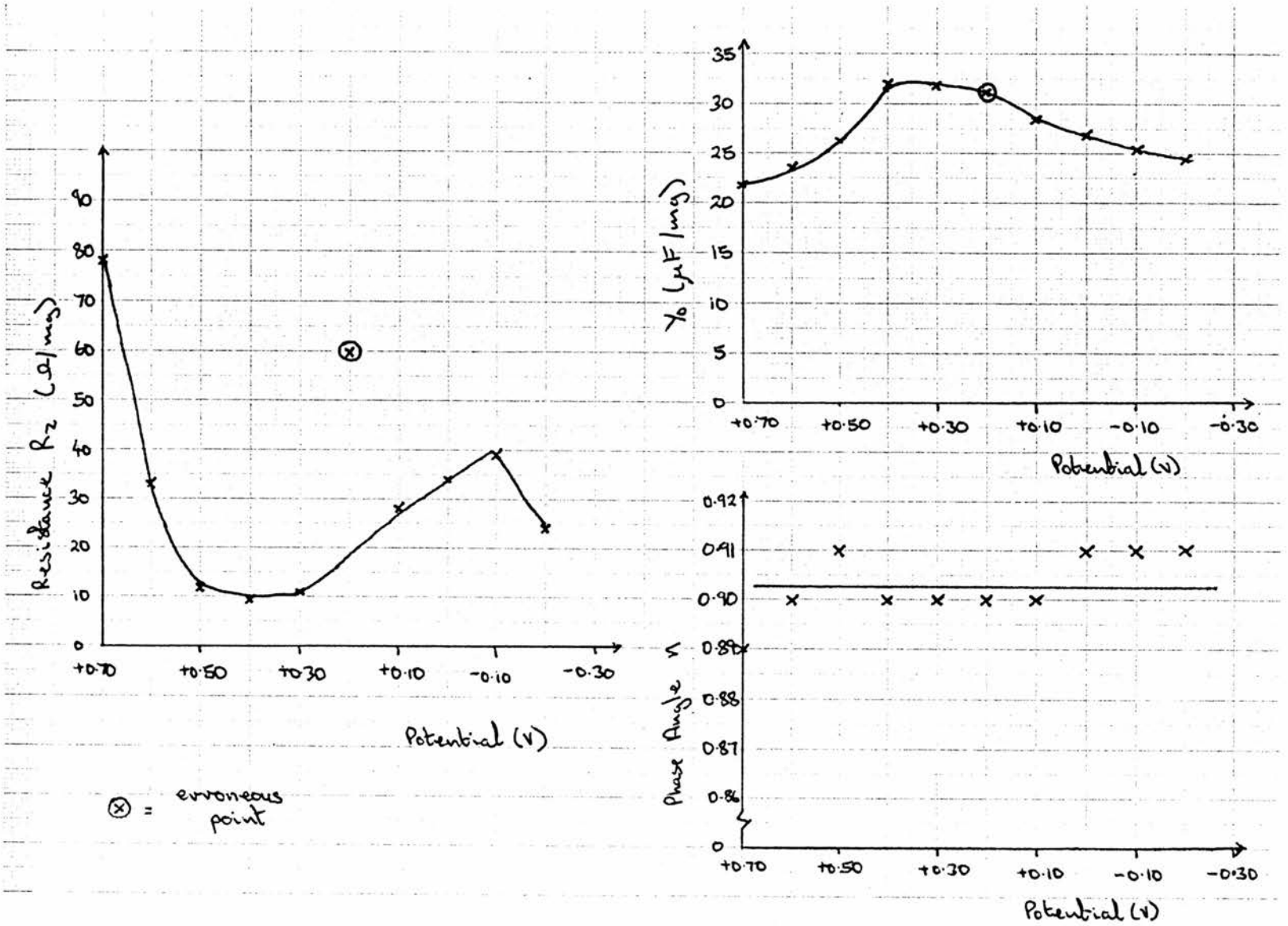

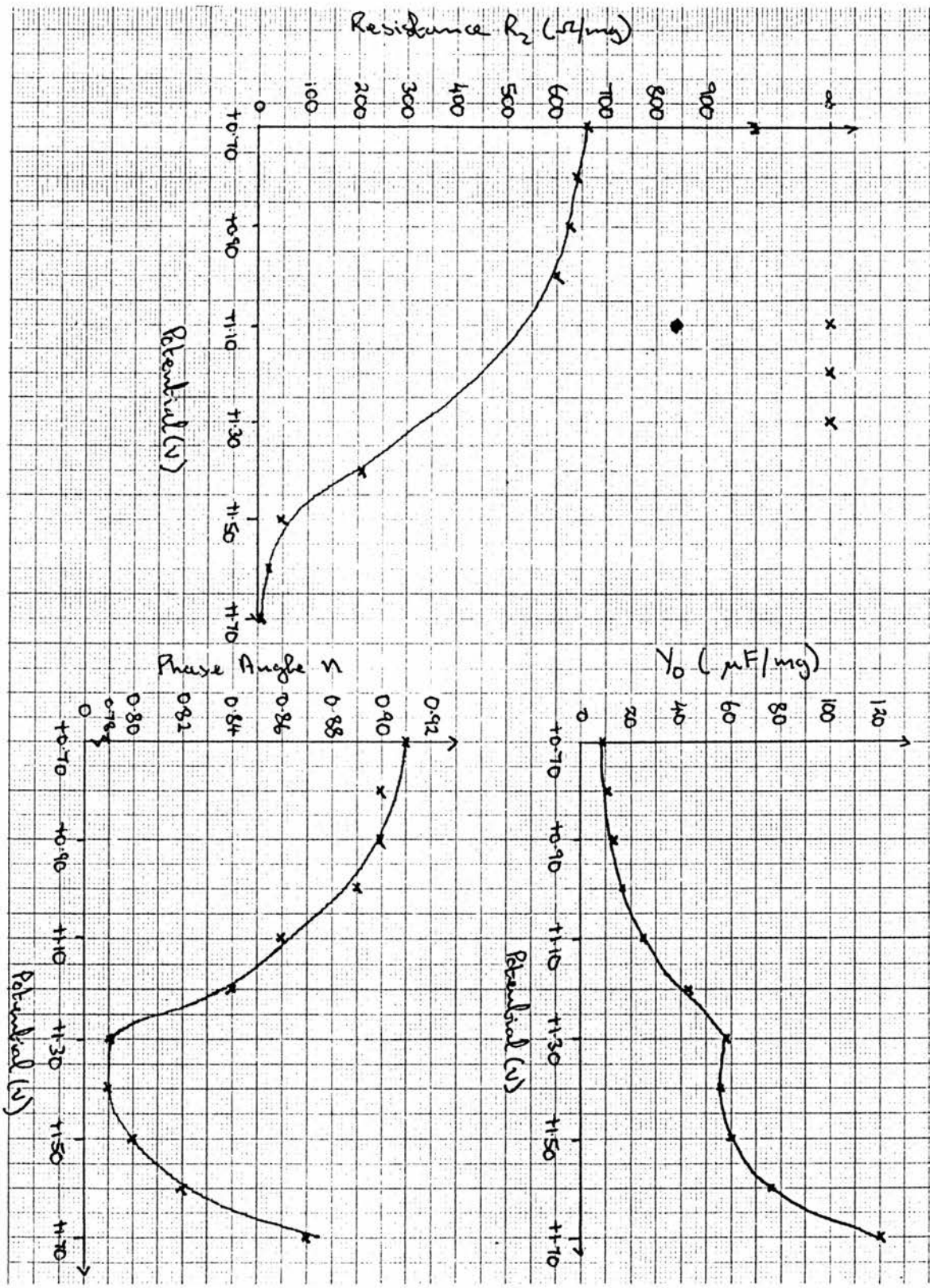

Fig.6.41 The Effect of d.c. Potential on the Equivalent Circuit Component Value for 2M371 E/10 HM-U Fibres. Anodic Region

Fig.6.42. The Effect of d.c. Potential on the Equivalent Circuit Component Value for 2M371 E/10 HM-U Fibres. Cathodic Region

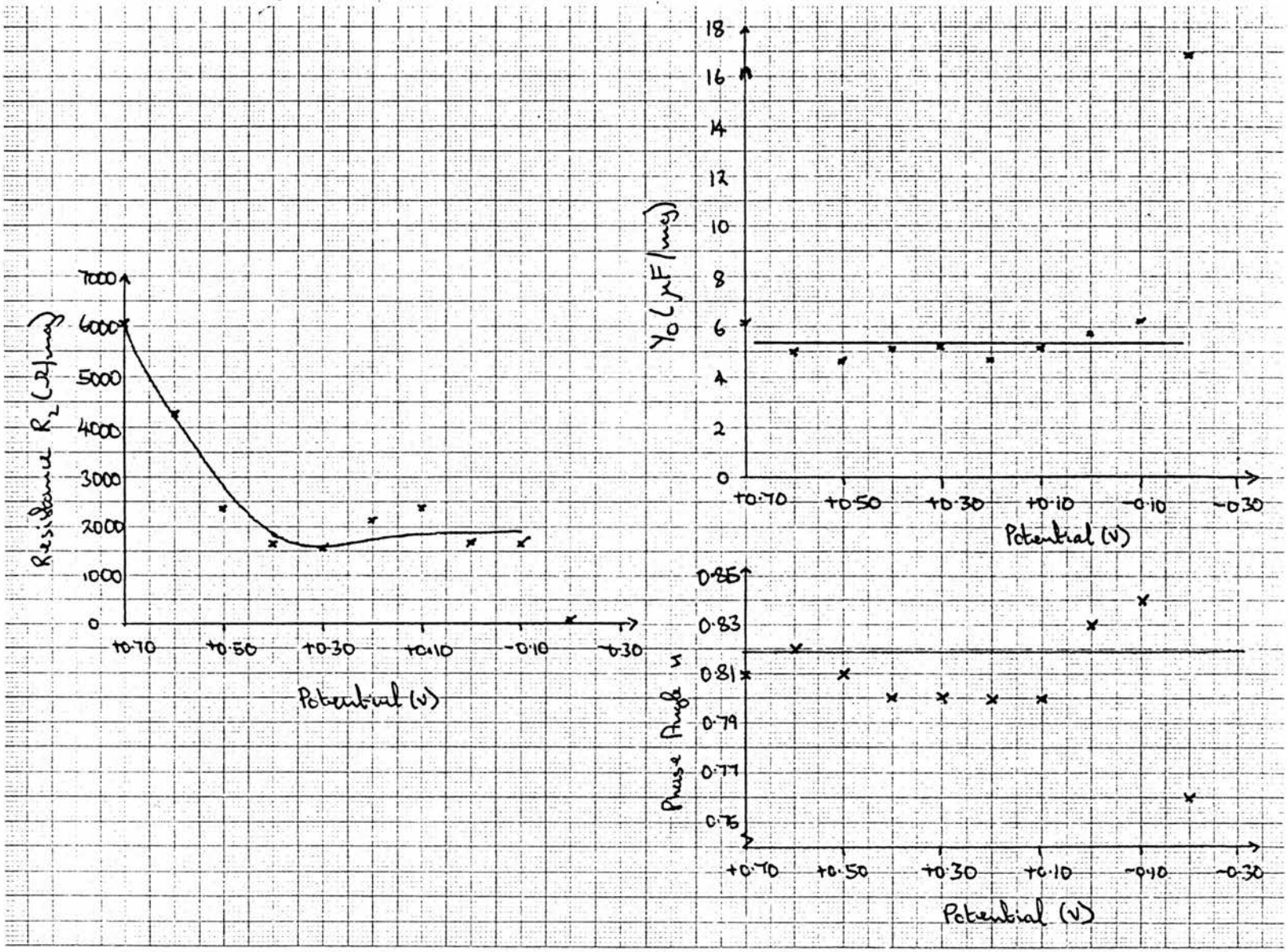

Fig.6.43 The Effect of d.c. Potential on the Equivalent Circuit Component Value for 2M307 D/10 HM-U Fibres. Anodic Region

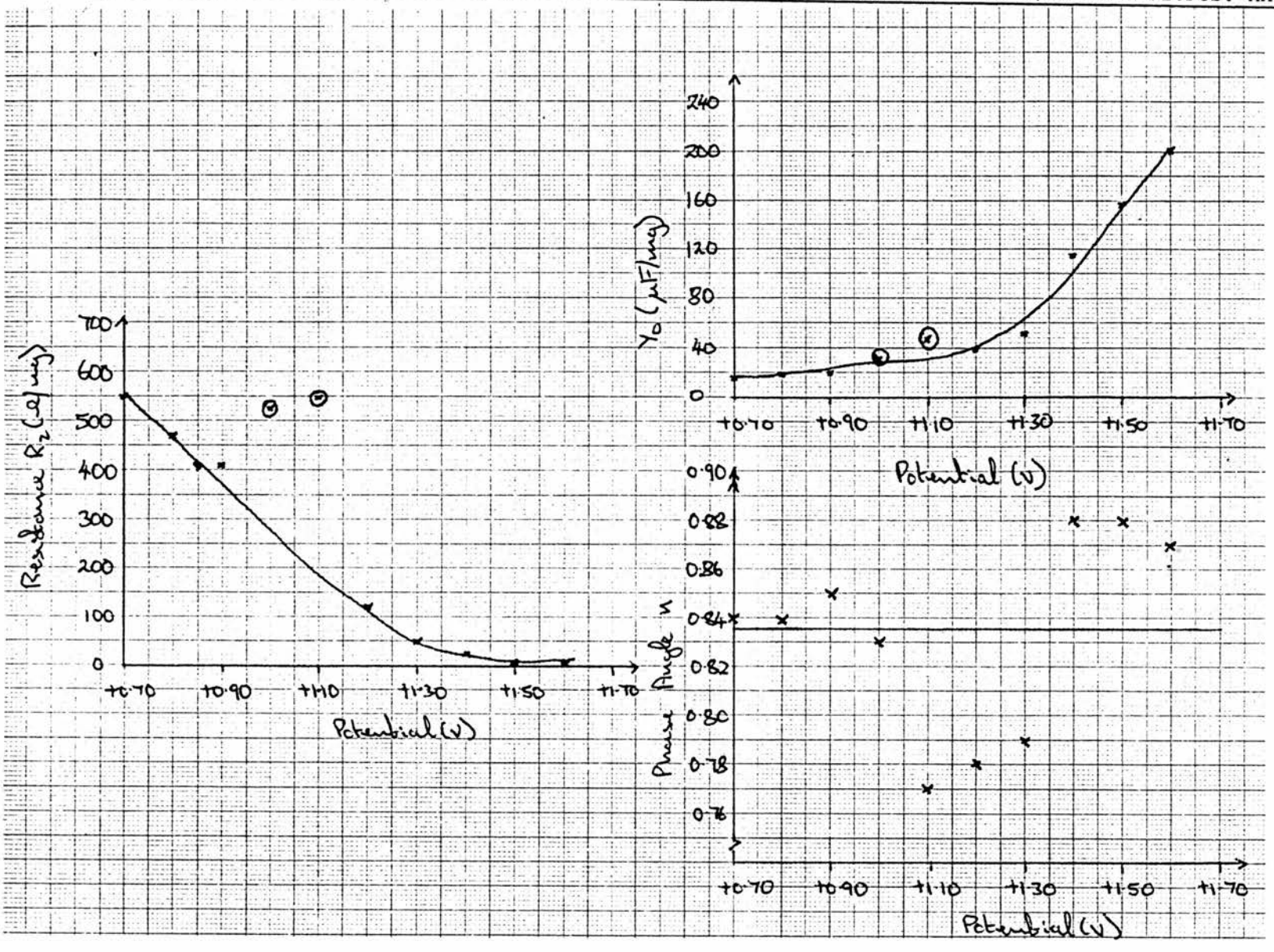

Fig.6.44 The Effect of d.c. Potential on the Equivalent Circuit Component Value for 2M307 D/10 HM-U Fibres. Cathodic Region

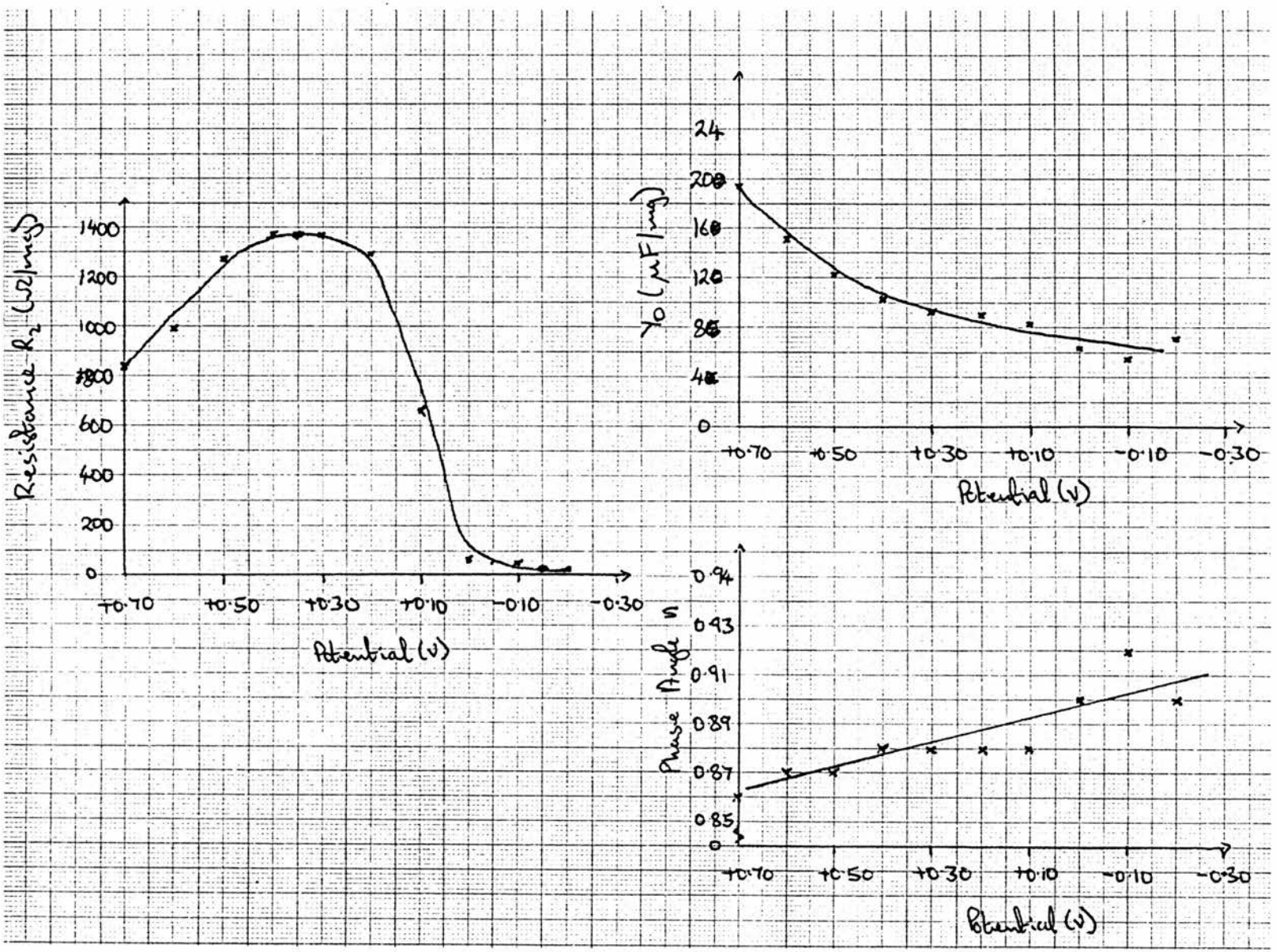

It is possible to conclude that the potential dependence of the various batches of untreated fibres is very similar in the anodic potential region. The only possible variation between the fibre batches in this region could be the actual values of R_2 and Y_o but this was not conclusive due to the problems of generating the actual weight of active fibre electrode.

In the cathodic potential region however, similarities exist between 2M207 B/10 and 2M371 E/10 fibres for the components R_2 and n but are none for the potential variation of Y_o.

6.4.2 Comparison of the Potential Dependence of HM-U and R.A.E. Treated Fibres

It was hoped that it would be possible to distinguish between untreated and treated fibres by considering the potential dependence of their equivalent circuit components.

As was found with the previous potential dependence experiments, the components R_1, C_1 and L were found to be approximately constant for both HM-U and HM-S fibres. The average values for these components can be seen in Table 6.31.

Table 6.31 Average Value of Components R_1, C_1 and L

FIBRE	C_1(nF/mg)	R_1(Ω/mg)	L(μH/mg)
HM-U Anodic	35.3	0.571	1.40
HM-U Cathodic	31.7	0.241	0.56
HM-S Anodic	29.9	0.132	0.34
HM-S Cathodic	24.1	1.866	4.88

As was found with the different batches of HM-U fibres, there was no discernible difference between the values of the components for HM-U and HM-S fibres.

The potential dependence of the remaining circuit components can be seen in figures 6.45-6.48.

The potential dependence of the circuit components of HM-U fibres was as described previously for 2M307 D/10 fibres, except that on reaching the cathodic potential limit Y_o and n show a drastic change in value.

For HM-S fibres, the potential dependence of R_2 and Y_o in the anodic potential region was very similar to that found with HM-U fibres, except for the reduction in the value of the anodic potential limit. However, the potential dependence of n shows inverse behaviour to Y_o, unlike HM-U fibres where n seems to be independent of potential.

Fig.6.45 Comparison Between Treated and Untreated HM Fibres. Untreated Fibres. Anodic Region

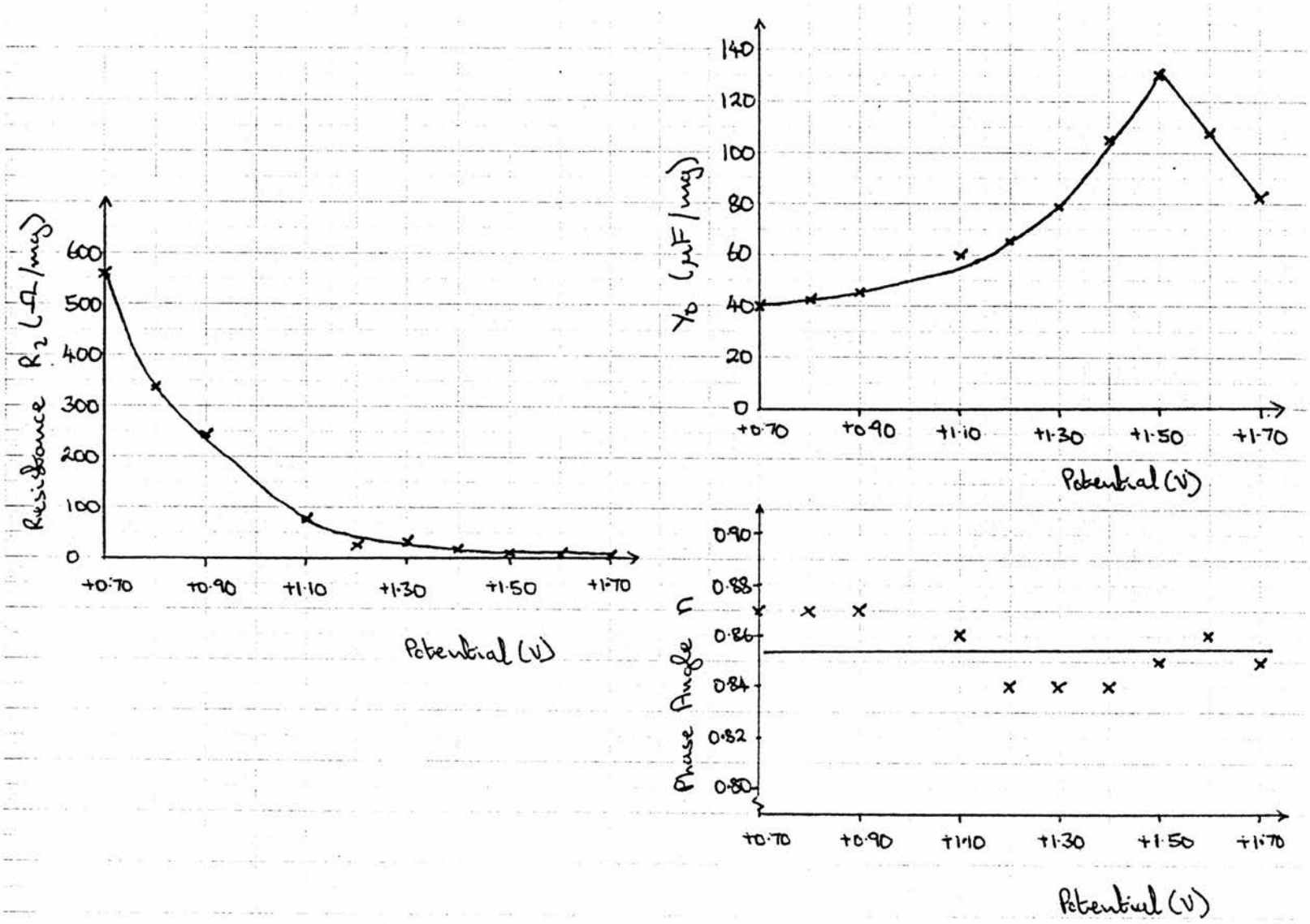

Fig.6.46 Comparison Between Treated and Untreated HM Fibres. Untreated Fibres. Cathodic Region

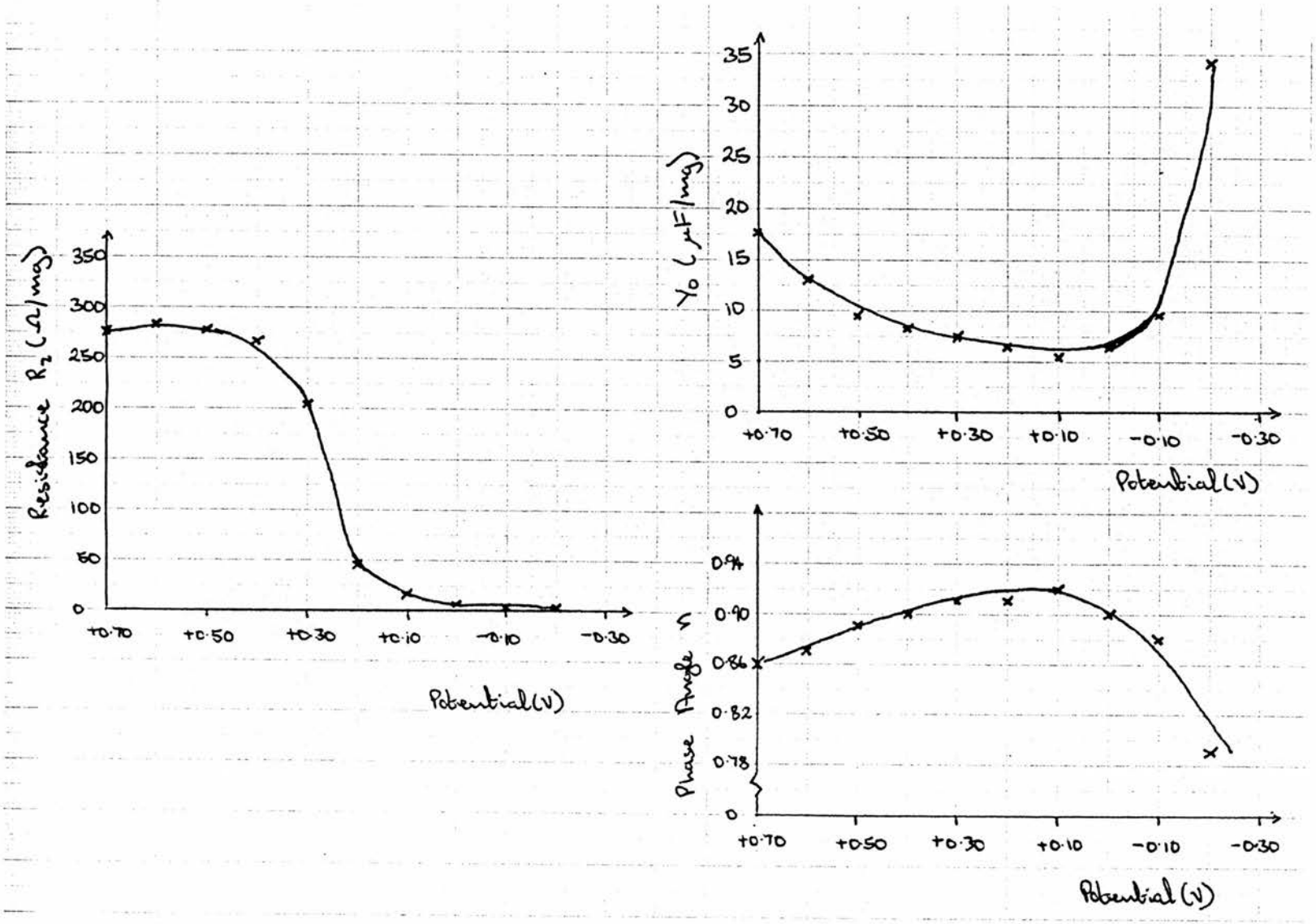

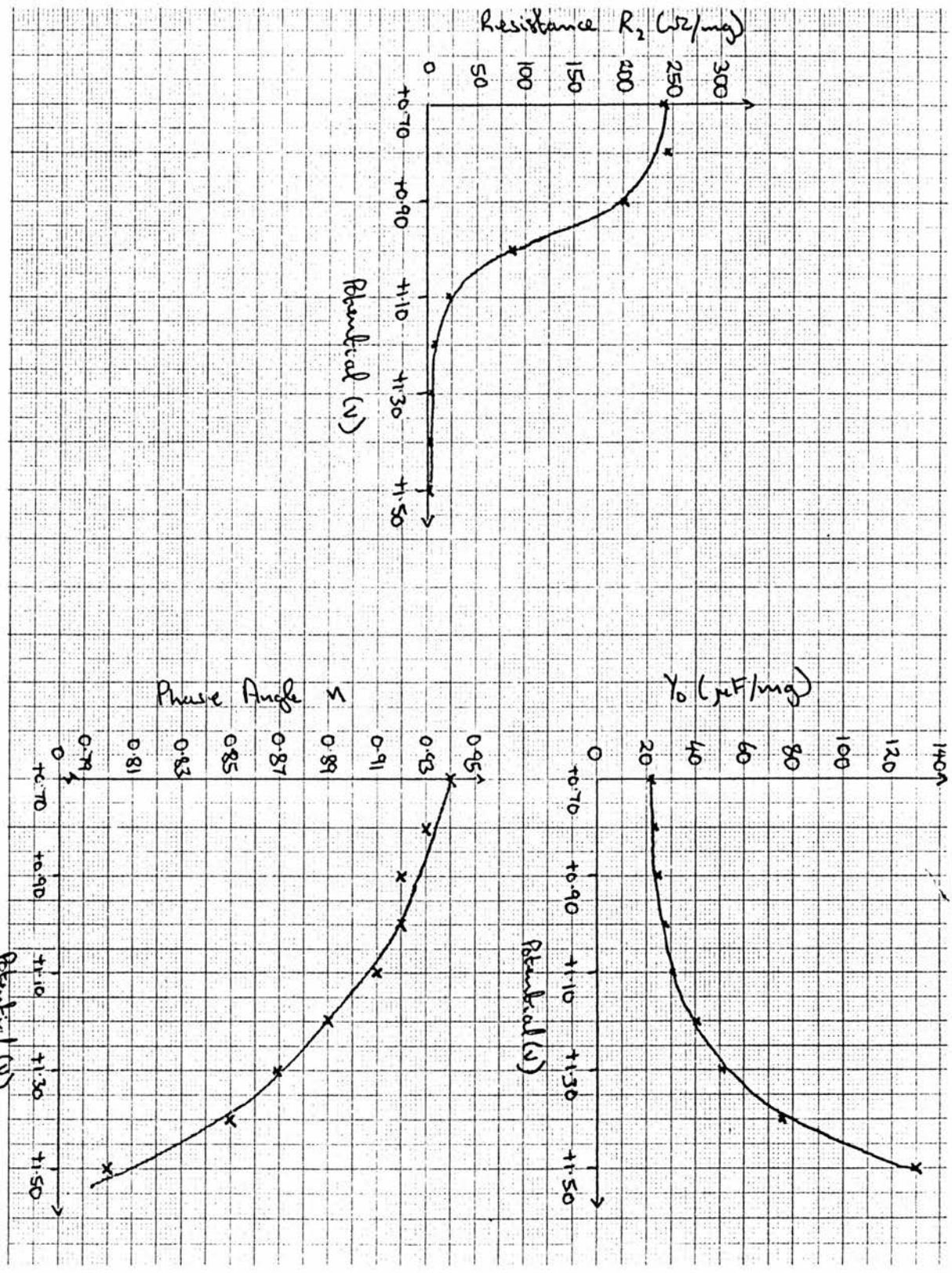

Fig.6.47 Comparison Between Treated and Untreated HM Fibres. Treated Fibres. Anodic Region

Fig.6.48 Comparison Between Treated and Untreated HM Fibres. Treated Fibres. Cathodic Region

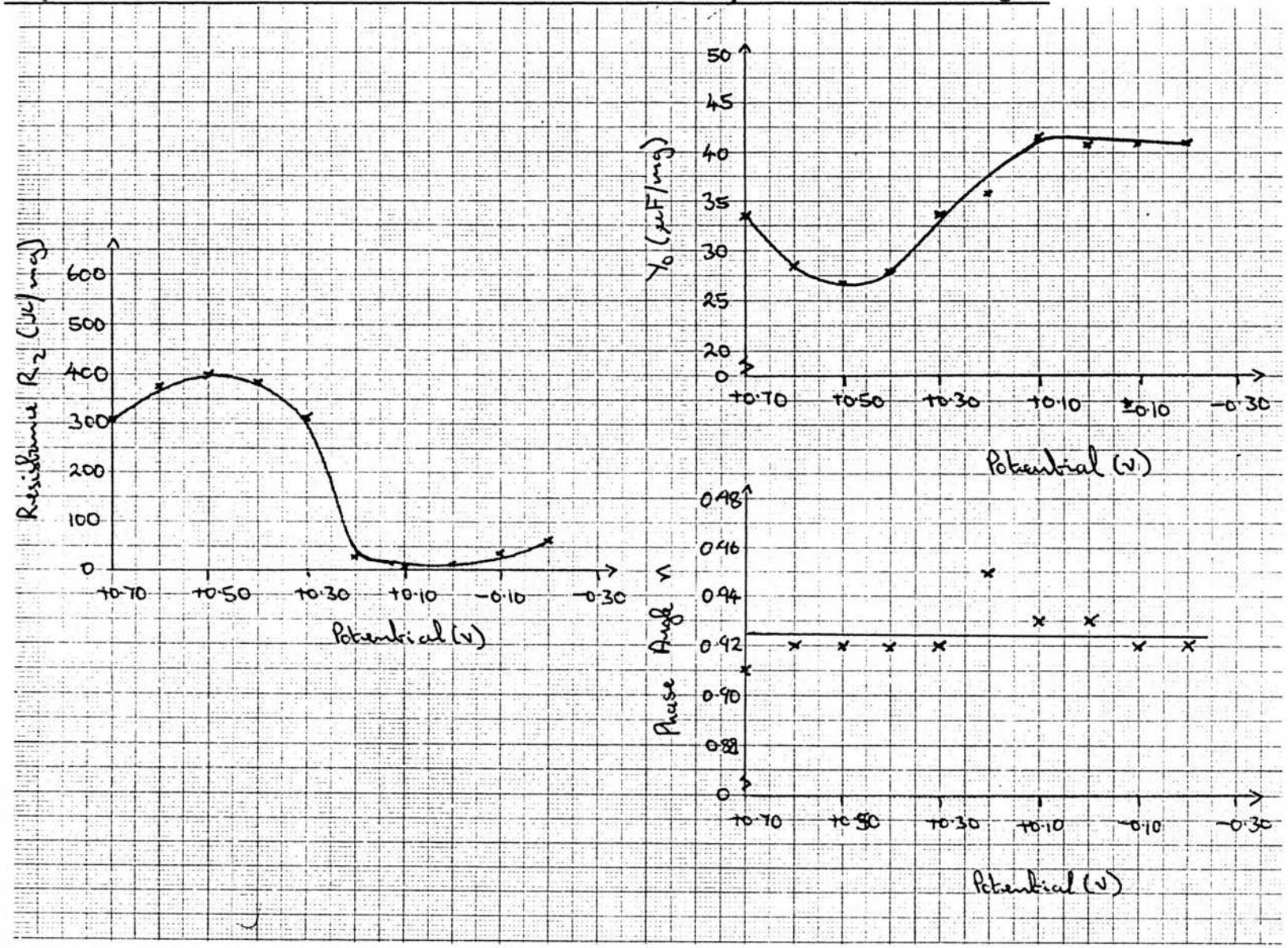

The variation in potential dependence of the circuit components between HM-U and HM-S seems to be more distinct in the cathodic potential region. The potential dependence for HM-S fibres of component R_2 is similar to HM-U but Y_o shows an inverse relationship to R_2, unlike HM-U fibres. Y_o decreases to a minimum value at + 0.50V and then increases to a constant value at + 0.10 V. The component n seems to be constant and does not exhibit the inverse relationship to Y_o found with HM-U fibres.

It may be concluded that it seems possible to distinguish between untreated and treated fibres by considering the potential dependence of their equivalent circuit components. In the anodic potential region differences can be seen in the potential dependence of the phase angle n component and in the value of the anodic potential limit. In the cathodic potential region differences can be observed in the potential dependence of components Y_o and n.

6.4.3 The Effect of Anodic Polarisation Potential Value on Galvanic Oxidation of HM-U Fibres

As discussed in Section 6.2.3, it was felt that the observed effects of galvanic oxidation on HM-U fibres could vary depending on the d.c. anodic potential value used to record the a.c. impedance plots. Therefore three values of potential were selected, one at the OCV, one mid-range anodic potential and one at a value approaching the anodic limit, to determine a suitable anodic potential to observe future investigations into the effects of galvanic oxidation on HM-U fibres.

As before with the potential experiments, the effects of oxidation on the values of R_1, C_1 and L were minimal and the constant

values produced for all three potentials are shown in Table 6.32.

Table 6.32 Average Values of R_1, C_1 and L

POTENTIAL (V)	C_1(nF/mg)	R_1(Ω/mg)	L(μH/mg)
+ 0.70	43.1	0.330	0.90
+ 1.00	42.2	0.331	0.87
+ 1.30	42.0	0.328	0.85

The effect of galvanic oxidation on the values of the other equivalent circuit components for the three potentials can be seen in figures 6.49 and 6.50.

It can be seen that all three anodic potentials produce different results for the effects of galvanic oxidation. However, they all show an inverse relationship between circuit components Y_o and n.

At + 0.70 V, the component Y_o increases in value to a maximum with increasing oxidation whereas n decreases to a minimum. For + 1.00 V, there is an initial rapid increase in the value of Y_o at the onset of galvanic oxidation but then the value seems independent of increased oxidation. Using + 1.30 V however, the value of Y_o exhibits exponential decay with increasing oxidation.

These results show the importance of the d.c. potential value in observing the effects of galvanic oxidation. From consideration of the above results and the argand diagrams, shown in figures 6.17-6.19, it was concluded that the best anodic d.c.

Fig.6.49 The Effect of Anodic Potential Value Used in Monitoring Changes in Component Value of Galvanically Oxidised Fibres

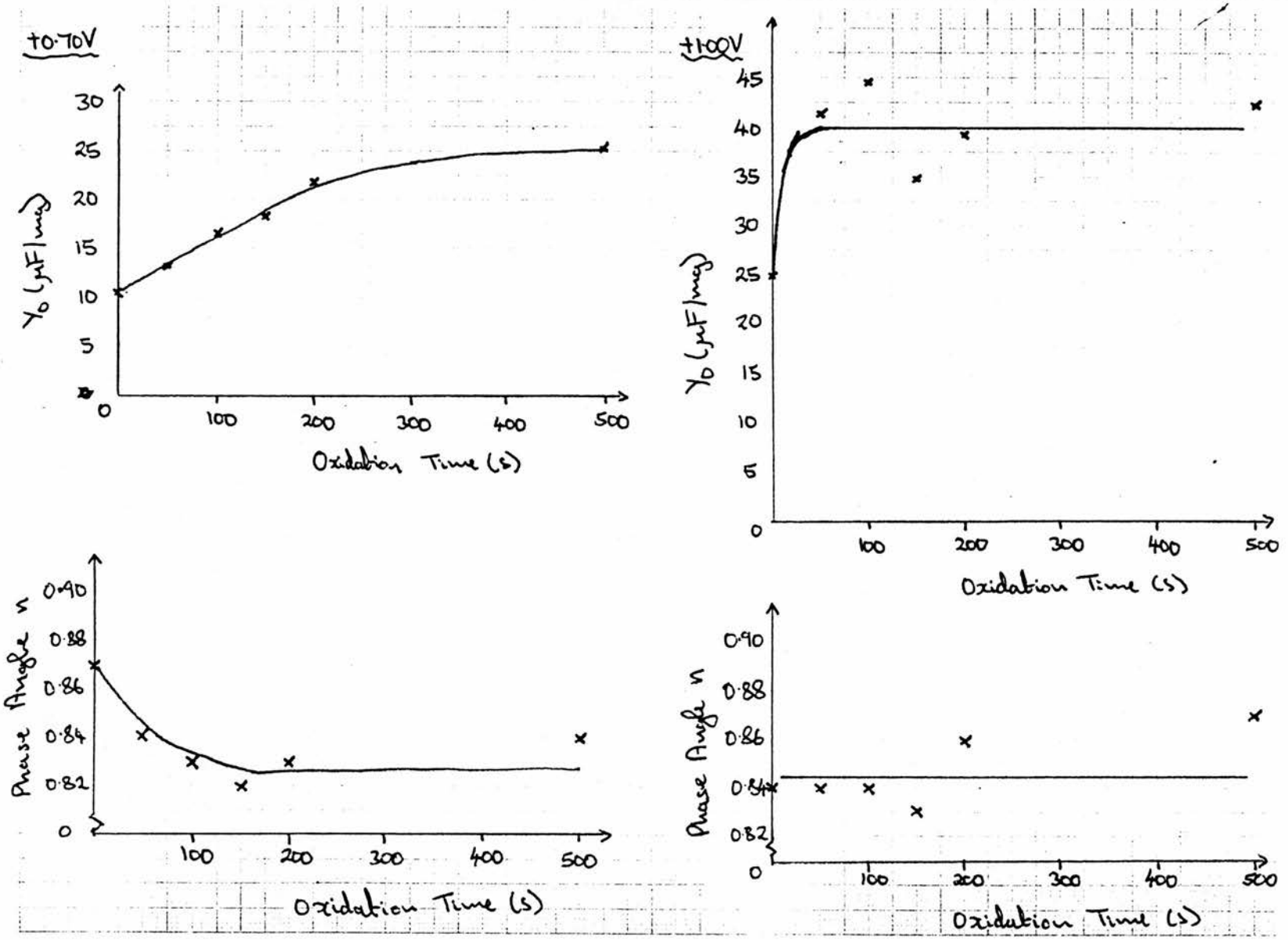

Fig.6.50 The Effect of Anodic Potential Value Used in Monitoring Changes in Component Value of Galvanically Oxidised Fibres

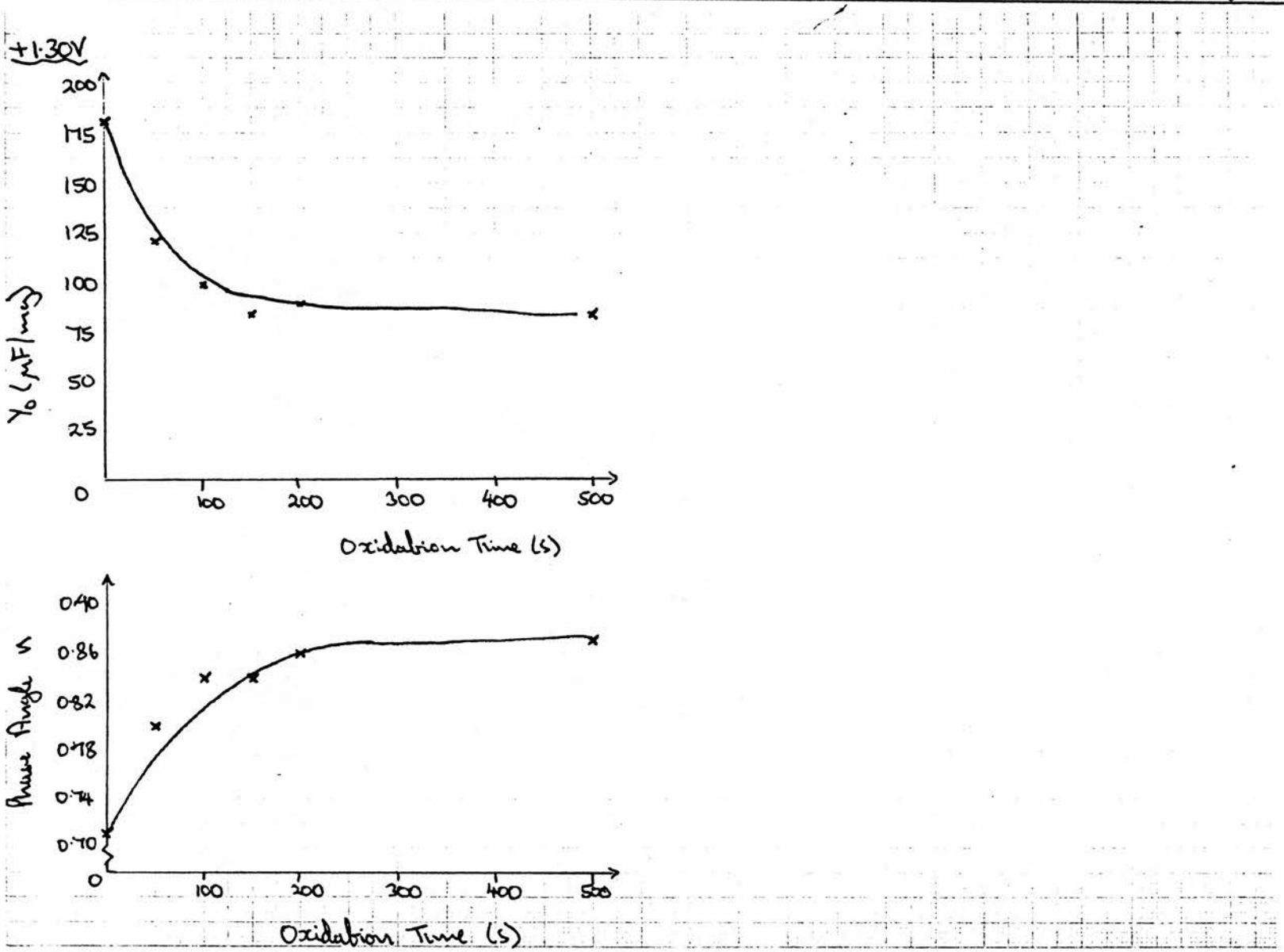

potential value to observe the effects of galvanic oxidation was + 1.30 V.

Similar experiments were conducted in the cathodic region and the optimum potential value in this case was found to be 0.00 V.

6.4.4 The Effects of Galvanic Oxidation on Untreated Fibres

Having obtained suitable d.c. potential values, the effects of galvanic oxidation on untreated fibres were investigated using a.c. impendance methods.

As was found with previous experiments, galvanic oxidation had little effect on the equivalent circuit components R_1, C_1 and L when observed at either potential value. Average values for each component were calculated and are shown in Table 6.33.

Table 6.33 Average Values of R_1, C_1 and L

POTENTIAL (V)	C_1(nF/mg)	R_1(Ω/mg)	L(μH/mg)
+ 1.30 ($t_{o_{max}}$ = 3000s)	21,4	0.530	1.36
+ 1.30 ($t_{o_{max}}$ = 7000s)	86.9	0.899	2.48
0.00 ($t_{o_{max}}$ = 3000s)	60.3	0.070	0.20

The effects of galvanic oxidation on the remaining circuit components can be seen in figures 6.51 and 6.52. It can be seen that there are two sets of data shown in Fig. 6.51. This was necessary since the initial data, on examination, was found to be inaccurate for values t_o = 500 and 1000s and therefore no conclusions could be made about the effects of oxidation on the remaining components. Therefore this experiment was repeated with the addition of a longer t_o max.

The effects of oxidation observed at + 1.30 V showed that component R_2 showed an initial rapid increase in value at the onset of oxidation and then an exponential decay with increasing oxidation. Y_o showed a similar rapid increase but also increased, possibly linearly, beyond this point with increasing oxidation. The component n showed an intial decrease but then seemed unaffected by increasing oxidation, remaining at a constant value of approximately 0.89.

Observations in the cathodic region at 0.00 V showed that component R_2 showed a linear increase wtih increasing oxidation. After an initial reduction in the value of Y_o on the onset of oxidation, Y_o also showed an approximately linear increase with increasing oxidation. As expected, the phase angle n showed inverse behaviour to Y_o with a linear decrease in value with increasing oxidation.

It may be concluded that the effect of galvanic oxidation on untreated fibres could be observed by monitoring the variation in the equivalent circuit components using a.c. impedance techniques.

Fig.6.51 The Effect of Galvanic Oxidation on Untreated Fibres. $\mathcal{V}$ = + 1.30 V

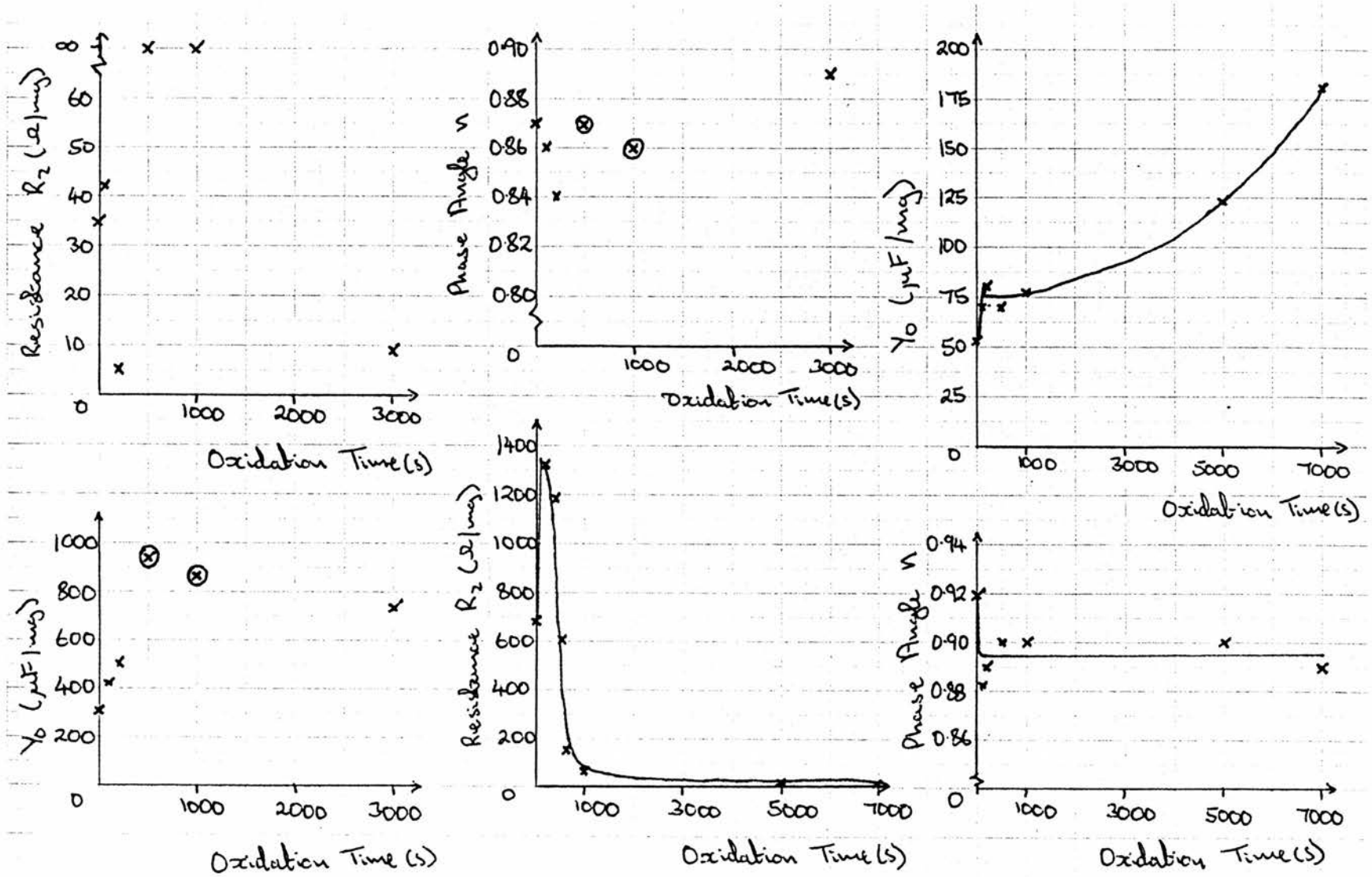

Fig.6.52 The Effect of Galvanic Oxidation on Untreated Fibres. V = 0.00 V

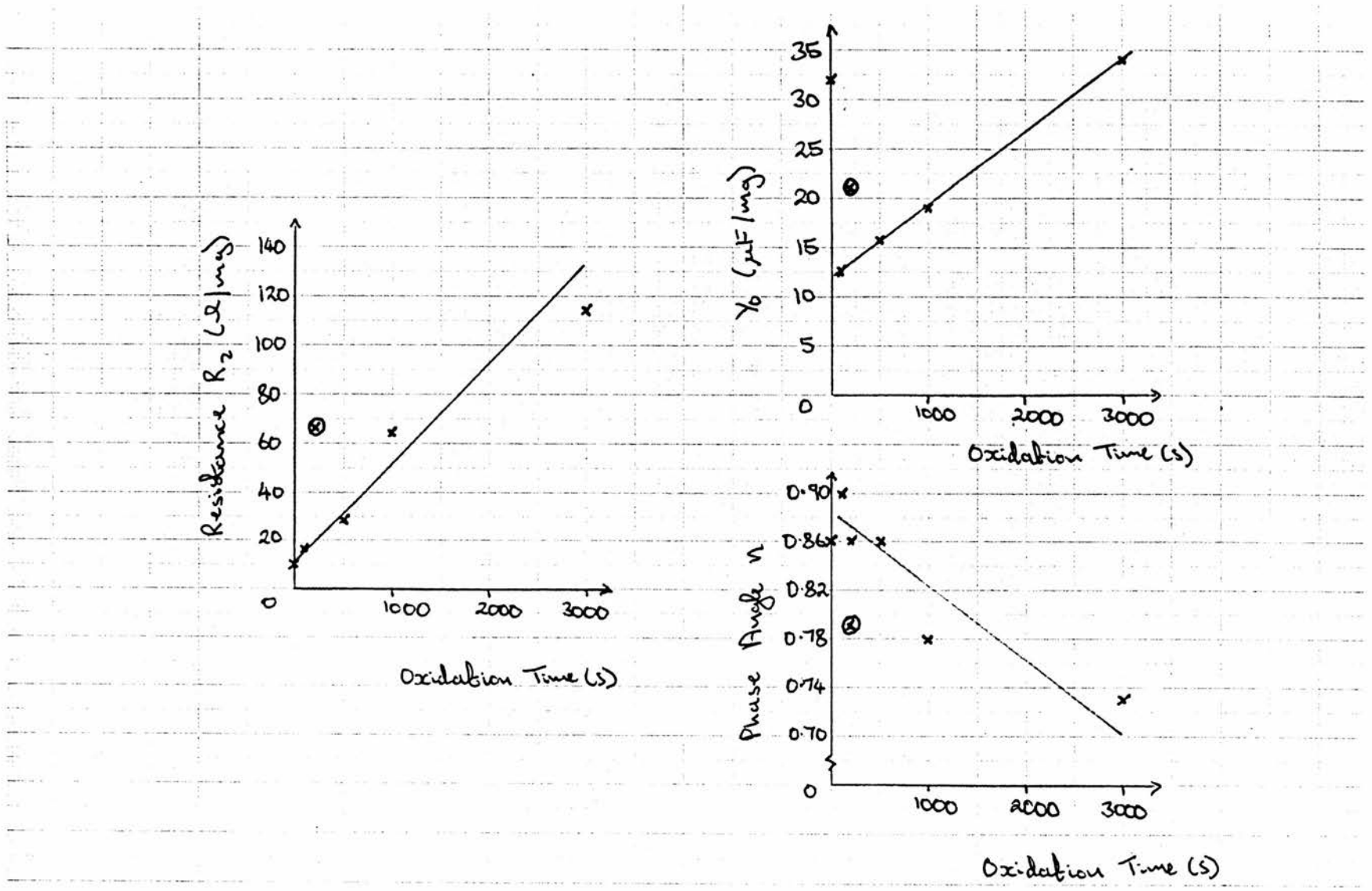

6.4.5 The Effect of Time on Oxidised HM-U Fibres

It was noticed in previous oxidation experiments that the a.c. impedance diagrams of oxidised HM-U fibres seemed to be affected by time. For example, if one recorded an argand diagram of a oxidised fibre and then left it for a period of 2 days and then repeated the argand diagram, these two diagrams were found to be different. This was felt to be an important observation and therefore a detailed study into the effects of time was initiated. Several carbon fibre electrodes were oxidised for various lengths of time and then the effects of time were investigated over a period of 14 days.

As was observed with other experiments, the ciruit components R_1, C_1 and L were unaffected and seem to be independent of time, allowing for electrode placement inaccuracies. Average values were calculated for these components and are shown in Table 6.34

Table 6.34 Average Values for Components R_1, C_1 and L

t_o(s)	C_1(nF/mg)	R_1(Ω/mg)	L(μH/mg)
0	183	0.364	0.92
500	111	1.382	3.81
1000	100	0.633	1.87
3000	175	0.150	0.42
5000	76.6	0.786	2.25

Fig.6.53 The Effect of Time on Oxidised HM-U Fibres

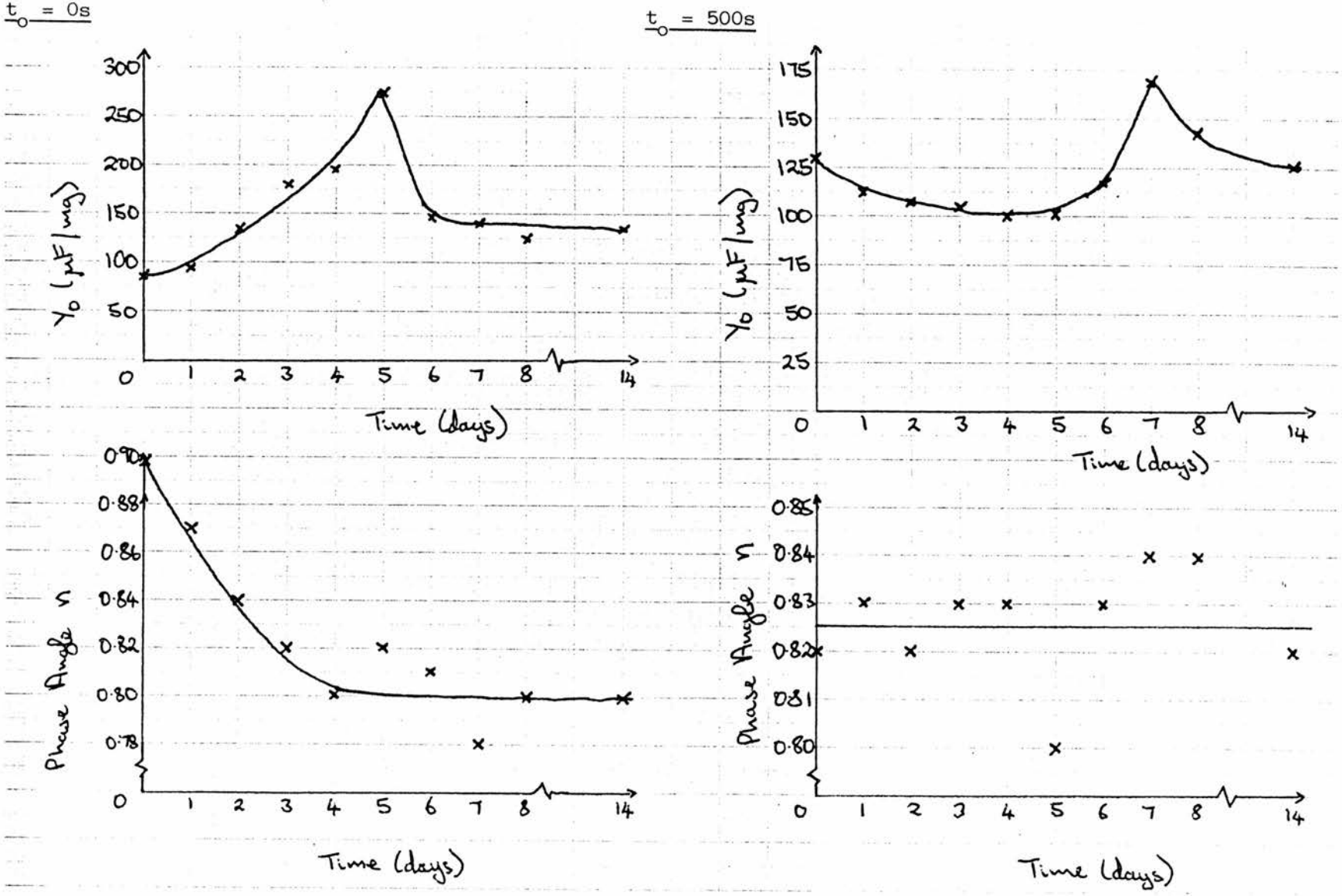

Fig.6.54 The Effect of Time on Oxidised HM-U Fibres

t_o = 1000s

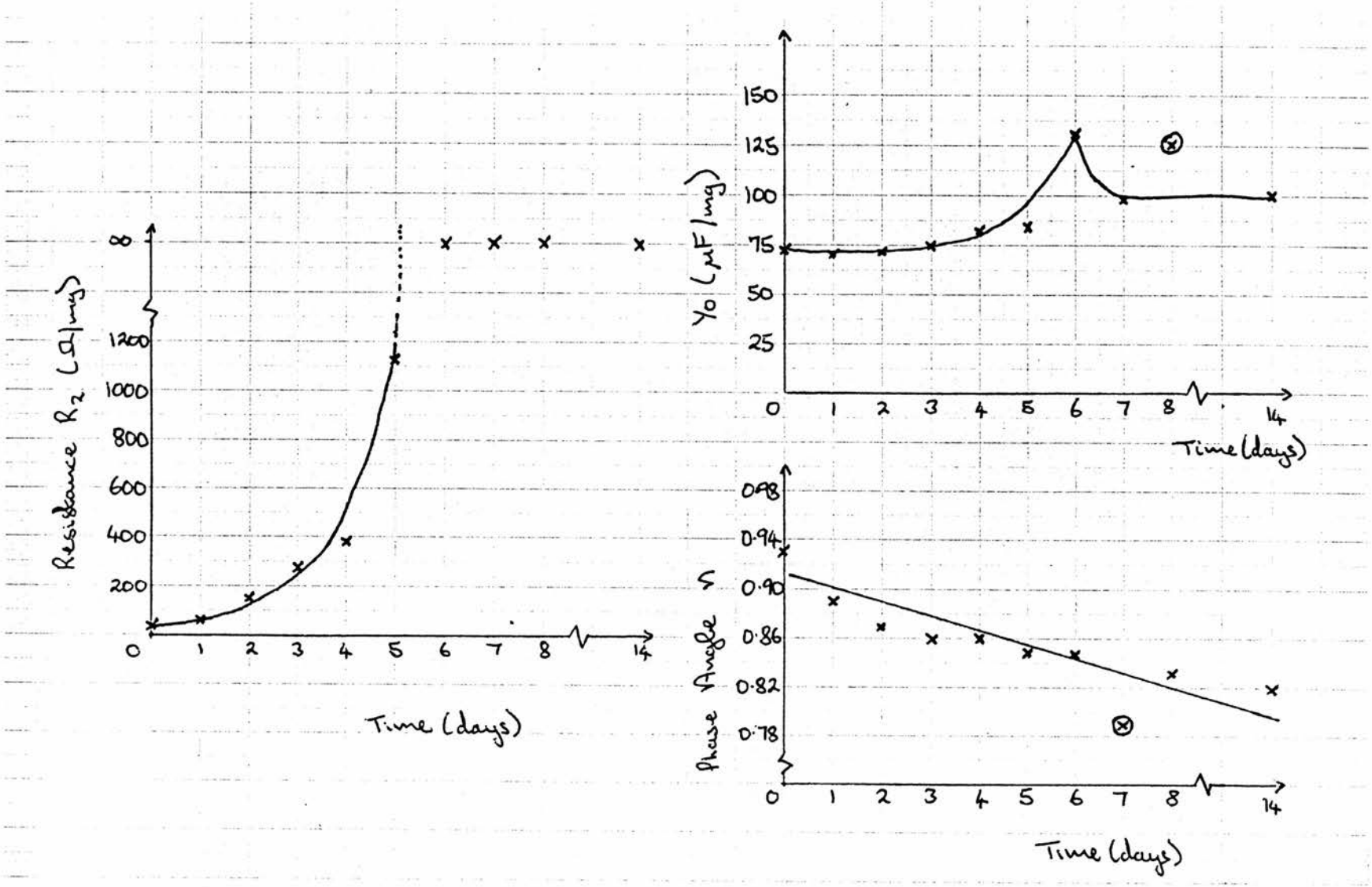

Fig.6.55 The Effect of Time on Oxidised HM-U Fibres

t_o = 3000s

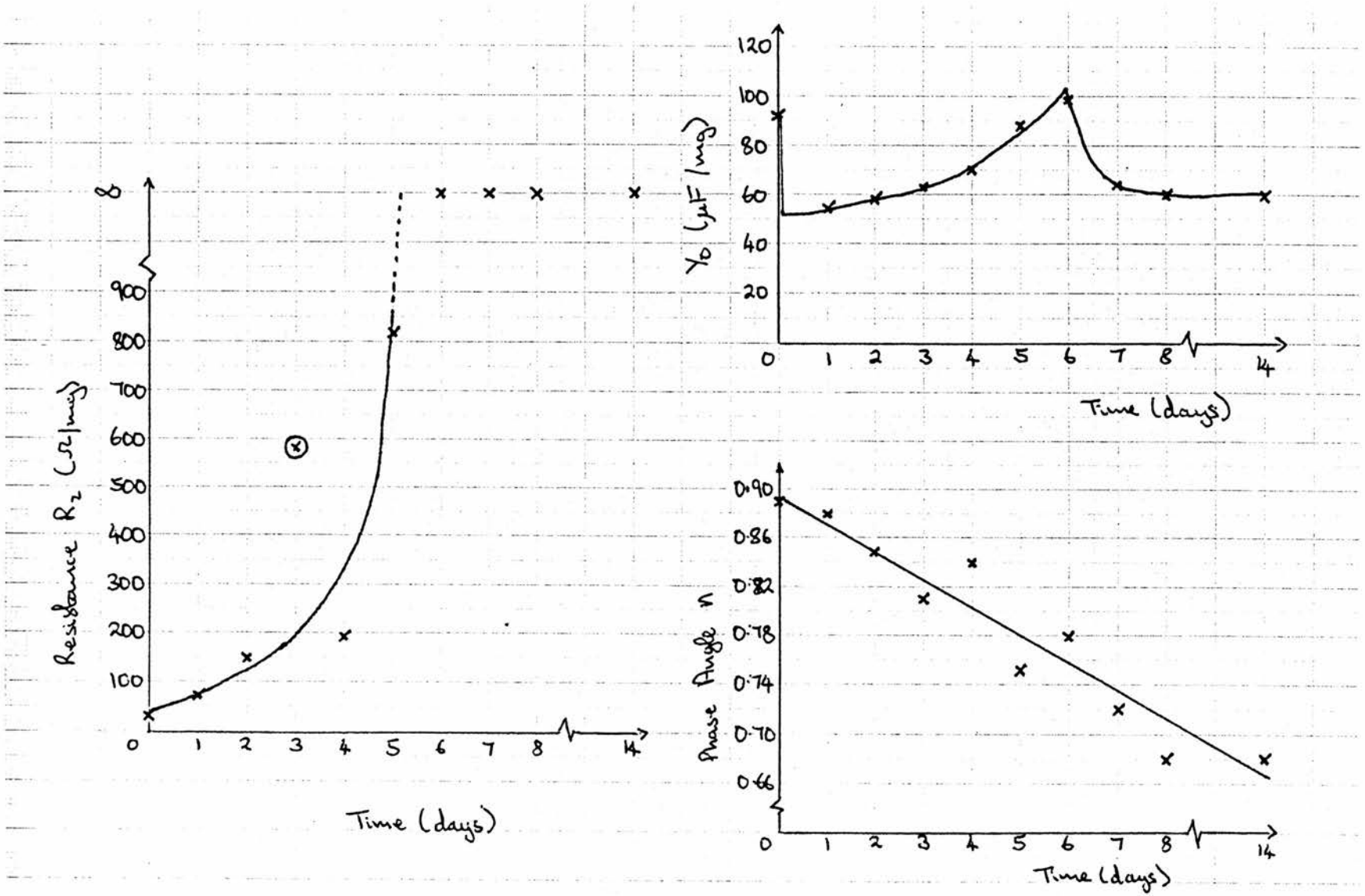

Fig.6.36 The Effect of Time on Oxidised HM-U Fibres

t_o = 5000s

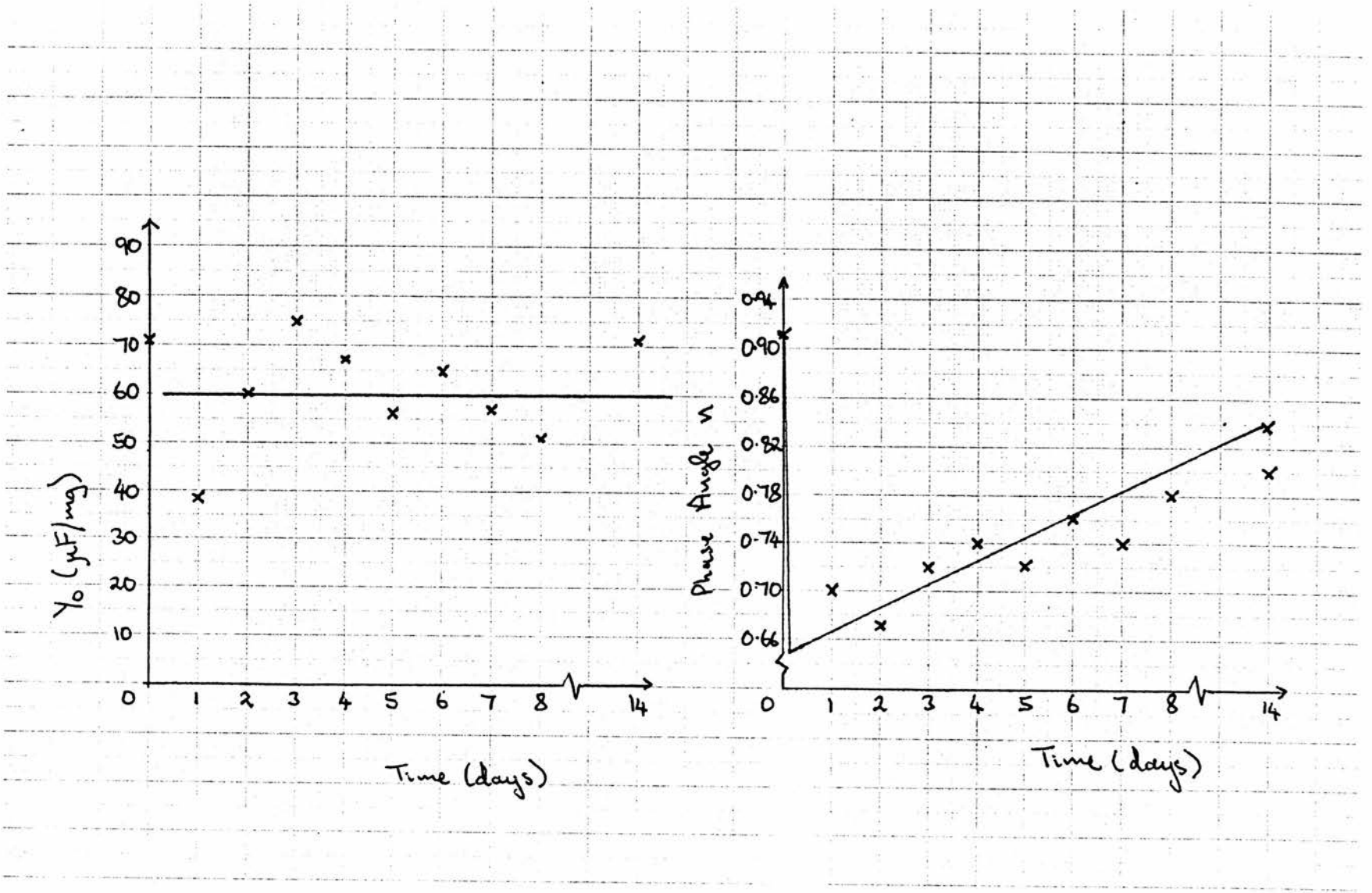

The effect of time on the remaining components can be seen in figures 6.53-6.56.

t_o = 0s

In this case component R_2 was found to be infinite. The value of Y_o increased to a maximum of 270 μF/mg at t = 5 days, the value then rapidly decreased to a constant value of approximately 135 μF/mg. The phase angle n showed an exponential decay to a constant value of 0.80 with increasing time.

t_o = 500s

Beyond t = 0 days R_2 was infinite, as for t = 0s. Y_o showed a slight decrease to a minimum at 4 days then a rapid increase to a maximum value of 165 μF/mg at 7 days. Beyond t = 7 days there is a gradual decrease to a value approaching the inital t = 0 days value. Component n seems to be unaffected by time.

t_o = 1000s

In this case a value for R_2 can be found for the first 5 days. R_2 shows an exponential increase until becoming infinite at t = 6 days. Y'_o shows a continual increase to a maximum value of 130 μF/mg at t = 6 days and then shows a gradual decrease to a constant value of about 100 μF/mg. Phase angle n shows a linear decrease with increasing time.

t_o = 3000s

As with t_o = 1000s, the component R_2 shows an exponential

increase until it reaches infinity at t = 6 days. Y_o also behaves similarly to t_o = 1000s except for the reduction in value between t = 0 and t = 1 day. In this case Y_o max occurs at a value of 100 μF/mg and reduces to 60 μF/mg after 14 days. The phase angle n shows a linear decrease with increasing time.

t_o = 5000s

As for t_o = 5000s, beyond t = 0 days R_2 was infinite. Y_o however seems to be independent of time. The phase angle n, after an initial reduction between t = 0 and t = 1 day, showed a linear increase with increasing time.

On consideration of both the argand diagrams and the component dependence plots, it is possible to tentatively conclude that time has a significant effect on the a.c. impedance diagrams, hence the interface, of galvanically oxidised HM-U fibres. It seems that for treatment levels below t_o = 5000s, the oxidised fibres revert back towards a state approaching the untreated fibre over a prolonged period of time. However, at or above this level the component values seem unaffected by time, beyond an initial stabilisation period.

6.5 Conclusions

In conclusion, application of the a.c. impedance characterisation technique for carbon fibre surfaces has met with some degree of success.

It was found possible to distinguish between untreated high modulus fibres and those which had undergone electrochemical surface treatment by studying the d.c. potential dependence of the equivalent circuit components, used to represent the solution electrolyte/carbon fibre electrode interface in an electrochemical cell. However, it was not possible to distinguish between different batches of the same untreated fibres.

The effects of galvanic oxidation, carried out in the laboratory, on untreated fibres could also be monitored by the oxidation level dependence of the various equivalent circuit components.

Lastly, the effects of time on oxidised fibres were studied and it is thought that below oxidation times of 5000s that the oxidised fibre could revert towards a state approaching that of the untreated fibre. At and above this treatment level the oxidation is thought to produce permanent changes in the fibre surface since they are unaffected by time, after an initial period of stabilisation.

It seems that it could be possible to apply a.c. impedance methods to characterise carbon fibre surfaces. However, these studies are only a preliminary step towards production of an accurate characterisation technique applicable commercially for carbon fibre surfaces.

CHAPTER 6

REFERENCES

1. B A Boukamp: Solid State Ionics 20 31 (1986).

2. I Epelboin; M Keddam: Electrochimia 17 177 (1972).

3. M Keddam; J-F Lizee; C Pallotta; H Takenouti: J.Electrochem. Soc. 131 2016 (1984).

4. D D Macdonald; M Urquidi-Macdonald: J.Electrochem. Soc. 132 2316 (1985).

5. R L Hurt; J R Macdonald: Solid State Ionics 20 111 (1986).

6. G Meng; M Zhou; D Peng: Solid State Ionics 18 and 19 756 (1986).

7. J R Macdonald; L D Potter, Jnr: Solid State Ionics 23 61 (1987).

APPENDIX 1

Trap Preparation Reactions

1. $2\ NH_4^+\ VO_3^- \xrightarrow{HCl} V_2O_5 + 2\ NH_3 + H_2O$

2. $V_2O_5 \xrightarrow{H_2O} 2(VO_2(H_2O)_4)^+$

3. $(VO_2(H_2O)_4)^+ \xrightarrow[HCl]{Zn} (VO(H_2O)_5)^{2+}$

4. $(VO(H_2O)_5)^+ \xrightarrow[Hg]{Zn} (V(H_2O)_6)^{3+}$

5. $(V(H_2O)_6)^{3+} \xrightarrow[Zn]{O_2/N_2} (V(H_2O)_6)^{2+}$